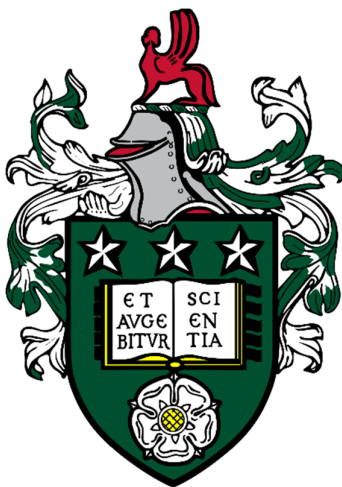


# Towards the design of quasihomogeneous catalytic particles



Thomas Howell

School of Chemical and Process Engineering

University of Leeds

A thesis submitted for the degree of

*PhD and Master of Science*

May 2021



---

The candidate confirms that the work submitted is her own. The candidate confirms that appropriate credit has been given within the thesis where reference has been made to the work of others.

ICP-OES assays of iridium content were provided by Medac Ltd. The use of SEM and TEM equipment was done with training by LEMAS. TGA training and theory was done with the assistance of ERI.

This copy has been supplied on the understanding that it is copyright material and that no quotation from the thesis may be published without proper acknowledgement.

©2021 The University of Leeds and Thomas Howell.

The right of Thomas Howell to be identified as Author of this work has been asserted by her in accordance with the Copyright, Designs and Patents Act 1988

# Acknowledgements

---

My thesis would not be possible without the long-suffering efforts of my Supervisors Dr. Olivier Cayre, Dr. Nicholas Warren and Professor John Blacker. Despite many travails they have helped me get to this point for which I am eternally grateful.

I would like to thank the post-doctoral and post-graduate researchers in The Blacker and Cayre Groups as well as the Technical Staff in the Energy Research Institute for their help and calm guidance; as a veritable nomad between multiple departments it was a boon to have people willing to help and guide me within the labs.

In particular I would like to thank Professor Philip Kocienski, who was an indispensable guide in the synthesis of several novel compounds and RAFT agents; without his many years of experience much of the practical synthesis would have been difficult if not impossible to achieve in the timeframe needed.

I would like to thank the EPSRC for funding the Centre for Doctoral Training Program along with Professor Andrew Mullis who made my entry back into academic life, and into a new and exciting area of research, a true adventure. As hesitant as I was to begin with the program enabled me to grow and expand my knowledge base incalculably.

Finally I would like to thank my family, my wife and children, and friends who shared this journey with me with much forbearance; without them coming home exhausted each day would not seem worth it.

# Abstract

In Chemistry, a catalyst is defined as any substance that increases the rate of a reaction without itself being consumed. They achieve this by providing a thermodynamic pathway of lower energy than the standard required to convert the reactants into products. Chemists have developed an arsenal of catalyst systems for an array of compounds to produce desirable materials in many conditions and at many scales of production.

Catalysts can be largely categorized into 2 sub-categories: homogeneous and heterogeneous; homogeneous catalysts are defined as being in the same phase as the reactant whilst heterogeneous catalysts are defined as being in a separate phase to the reactants. These properties inform how they are used, and particularly whether they can be recycled for future use with more reactants. In general, heterogeneous catalysts, such as solid catalysts in liquid media, are better for larger scale, bulk reactions, capable of many uses before mechanical attrition and chemical change render it less efficacious or potentially changes what products it produces; homogeneous catalysts by comparison lend themselves to smaller scale, batch reactions producing specific compounds where catalyst recovery is less important than the results of that reaction.

Designing a catalyst with the benefits of both homogeneous and heterogeneous systems poses an interesting and rewarding challenge. We attempted to tether an organometallic iridium catalyst, used in transfer-hydrogenation reactions, to organomodified silica nanoparticles.

Several approaches were investigated: catalyst attachment directly to silica nanoparticles using a silica coating agent; monomers functionalized with a chain-transfer agent, attached and brush polymers grown out of the silica nanoparticle resulted in sub-optimal results. Ultimately, functional brush polymers grown on silica particles using functional oligomers yielded the most consistent, reproducible and ultimately promising results, including demonstration of quantitative attachment of the catalyst to the brush polymer.

## i. Abbreviations

ACVA	4,4'-Azobis(4-cyanopentanoic acid)
AIBN	Azobisisobutyronitrile
APTES	3-aminopropyl triethoxysilane
ATR	Attenuated Total Reflection (used in conjunction with FTIR)
CTA	Chain-transfer agent
DCM	Dichloromethane
EDC.HCl	N-(3-Dimethylaminopropyl)-N'-ethylcarbodiimide hydrochloride
EtOAc	Ethyl Acetate
em	Electrophoretic Mobility
FTIR	Fourier Transform Infrared Spectroscopy
GC	Gas Chromatography
GMA	Glycidyl Methacrylate
GPC	Gel Permeation Chromatography
HOBt	Hydroxybenzotriazole
HPLC	High Performance Liquid Chromatography
HPMA	Hydroxypropyl methacrylate
ICP-OES	Inductively coupled plasma atomic emission spectroscopy
IrCp*	Iridium Cyclopentadienyl tethered complex.
LED	Light Emitting Diode
MAPTMS	Methacryloxypropyl-trimethoxysilane
MMA	Methyl methacrylate
MMPAA	Mono-methyl trithio-2-phenylacetic acid
NMP	Nitroxide Mediated

NMR	Nuclear Magnetic Resonance
<i>o</i>	(prefix) “oligo” as in “oligomer”
OrMoSils	Organically Modified Silicas
<i>p</i>	(prefix) “poly” as in “polymer”
PMAA-PBzMA	Poly(methacrylic acid)-poly(benzyl methacrylate)
PETTC	4-cyano-4-(2-phenylethane sulfanylthiocarbonyl) sulfanylpentanoic acid
RAFT	Reversible Addition-Fragmentation chain-Transfer
SCA	Silane Coupling Agent
SEC	Size Exclusion Chromatography
SELECT	Safety, Environment, Legal, Economics, Control and Throughput
SEM	Scanning Electron Microscopy
SiP	Silica Particle
TEM	Transmission Electron Microscopy
TFEMA	2,2,2-trifluoroethyl methacrylate
TGA	Thermogravimetric Analysis
TOF	Turnover Frequency
TON	Turnover Number
UV-Vis	Ultraviolet-Visible

## ii. Contents

Acknowledgements.....	iv
i. Abbreviations.....	vi
ii. Contents.....	viii
iii. List of Figures .....	xiii
iv. List of Tables.....	xxiv
1 Introduction.....	2
1.1 Green Chemistry.....	2
1.2 Turnover Number (TON) and Turnover Frequency (TOF) .....	2
1.3 Types of Catalysis .....	3
1.4 Background to the Project.....	4
1.5 Project Aims.....	3
2 Literature Review .....	1
2.1 From Bench to Plant-scale.....	1
2.1.1 Green Chemistry and SELECT Criteria in Chemical Engineering	3
2.1.2 Heterogeneous Systems .....	4
2.1.3 Homogeneous Systems .....	5
2.1.4 The Pros and Cons of Homogeneous and Heterogeneous Catalysts.....	6
2.1.5 Quasi-homogeneous Catalyst Systems .....	7
2.2 Other Catalyst Immobilisation/Recovery Strategies.....	9
2.2.1 Inclusion Catalyst Immobilisation Strategies .....	9
2.2.2 Association Catalyst Immobilisation Strategies .....	12
2.2.3 Attachment Catalyst Immobilisation Strategies .....	14
2.3 Background To The Current Research .....	16
2.3.1 Hydrogenation: mass transfer limitations .....	16
2.3.2 Iridium and transfer-hydrogenation catalysts.....	17
2.3.3 Cp* Immobilized Catalysts .....	18

2.4	Research Direction .....	19
3	Areas of Study.....	20
3.1	Project Aims.....	20
3.2	Organically Modified Silicas (OrMoSils).....	20
3.2.1	Silica.....	20
3.2.2	Silane Coupling Agents (SCAs) .....	20
3.2.3	Organically Modified Silicas: Design Principles.....	21
3.3	Brush Polymers .....	22
3.3.1	RAFT Polymerization .....	22
3.3.2	RAFT on Silica .....	24
3.3.3	Brush Polymers via CTA-SCA compounds: Design Principles...26	
3.3.4	Brush Polymers via CTA-active SCA oligomers: Design Principles 28	
3.4	Other Routes Investigated.....	29
3.4.1	Latex Nanoparticles.....	29
3.4.2	Electrospinning.....	30
4	Materials and Methodology .....	31
4.1	Materials .....	31
4.2	Characterization Methods .....	32
4.2.1	Transmission electron microscopy (TEM) .....	32
4.2.2	Scanning electron microscopy (SEM) .....	32
4.2.3	UV-Vis spectroscopy .....	32
4.2.4	Fluorescence Spectroscopy .....	32
4.2.5	NMR spectroscopy .....	32
4.2.6	FTIR spectroscopy .....	33
4.2.7	Dynamic Light Scattering and Zeta Potential Measurement.....	33
4.2.8	Size Exclusion Chromatography .....	33
4.2.9	Thermogravimetric Analysis .....	34

4.3	RAFT agent synthesis .....	34
4.3.1	Synthesis of Mono-methyl trithio-2-phenylacetic acid (MMTPAA) 34	
4.3.2	Synthesis of 4-cyano-4-(2-phenylethane sulfanylthiocarbonyl) sulfanylpentanoic acid (PETTC) .....	36
4.3.3	Attachment of MMTPAA to APTES .....	37
4.3.4	Oligomerization of PETTC onto MAPTMS. ....	38
4.4	Methodology: Organofunctionalisation of Silica .....	39
4.4.1	Chapter 5: Condensation of APTES to silica to create Organically Modified Silicas (OrMoSils) .....	39
4.4.2	Chapter 6: Condensation of SCA-CTA to silica to create CTA- functionalised Organically Modified Silicas (OrMoSils).....	40
4.4.3	Chapter 7: Condensation of oligo-SCA-CTA to silica to create oCTA-functionalised Organically Modified Silicas (OrMoSils) .....	40
4.5	Methodology: Free and Brush Polymerization .....	41
4.5.1	Brush polymerization: polymer growth onto the CTA-SiP .....	41
4.5.2	Brush polymerization 2.0: polymer growth onto the oPETTC-SiP 42	
4.6	Catalyst synthesis & attachment.....	43
4.6.1	Iridium Cyclopentadienyl complex synthesis .....	43
4.6.2	Triflation of IrCp* complex, in-situ attachment.....	44
5	Results: Organically Modified Silicas (OrMoSils).....	46
5.1	Determination of surface chemistry of the silica particle .....	46
5.1.1	Silica Hydroxyl-content titration .....	46
5.2	Electrophoretic Mobility .....	47
5.2.1	Determination of best conditions for APTES condensation to 250nm silica particles using Electrophoretic mobility over a pH range. ...	48
5.2.2	Determination of Electrophoretic Mobility across a wide pH range and %-AP-silica Condensation to 250nm Silica.....	52

5.3	Fluorescamine Assay of AP-SiPs .....	57
5.4	Characterisation of IrCp*-tethered AP-SiPs .....	60
5.4.1	Benzaldehyde assay .....	62
5.5	Concluding Remarks .....	63
6	Results: Creating Brush Polymers via Growth of pGMA on silica.....	64
6.1	Thermogravimetric Analysis.....	64
6.2	Addition of Glycidyl Methacrylate into an AP-SiP shell .....	69
6.3	Creation of Brush Polymers via the formation of Chain-transfer Agent-coated Silicas (CTA-SiPs). .....	72
6.3.1	Synthesis of a CTA-functionalised silane coupling agent (SCA) .....	72
6.3.2	Discussion of TGAs of iterations 1-4 .....	77
6.3.3	Discussion of FTIR results of iterations 1-4.....	78
6.3.4	Polymerization at the surface .....	78
6.3.5	Kinetic Studies of pGMA .....	86
6.4	Concluding Remarks .....	91
7	Results: Creating Brush Polymers via oligomerization of MAPTMS, subsequent growth of pHPMA polymers; observed attachment of iridium catalyst.....	92
7.1	Improved Brush Polymers.....	93
7.2	oPETTC-SiP synthesis and polymerization .....	96
7.3	Synthesis of oPETTC-SCA.....	96
7.3.1	Condensation of oPETTC-SCA onto Silica. ....	97
7.3.2	Polymerization to the modified surface of oPETTC-SiP .....	98
7.4	Iteration 1: 3-hour hold, purification testing, 18-hour condensation, and Polymerization of methyl methacrylate at DP = 100. ....	99
7.4.1	FTIR comparison of PETTC, oPETTC-SiP <sub>1a</sub> , and oPETTC-SiP <sub>1b</sub> . ....	99
7.4.2	Thermogravimetric analysis comparison of oPETTC-SiP <sub>1a</sub> , oPETTC-SiP <sub>1b</sub> , and untreated silica particles.....	100

7.4.3	Polymerization of methyl methacrylate using oPETTC-SiP <sub>1a</sub> and oPETTC-SiP <sub>1b</sub> , unpurified and purified oligomer-coated silica. ....	100
7.5	Iteration 2: 3-hour hold oligomerization, 18 hours condensation, polymerization of hydropropyl methacrylate at multiple degrees of polymerization of 50, 100, 200 and 500, and hold times. ....	102
7.5.1	FTIR Comparisons of PETTC and oPETTC-SiP <sub>2</sub> .....	102
7.5.2	Thermogravimetric analysis of oPETTC-SiP <sub>2</sub> .....	102
7.5.3	Polymerization of oPETTC-SiP <sub>2</sub> .....	103
7.6	Iteration 3: 3-hour hold oligomerization, 18 hours condensation, polymerization of hydroxypropyl methacrylate at multiple degrees of polymerization of 50, 100, 200 and 500, with 18-hour hold times.....	104
7.6.1	FTIR Comparisons of oPETTC-SiP <sub>2</sub> with oPETTC-SiP <sub>3</sub> .....	105
7.6.2	Thermogravimetric analysis of oPETTC-SiP <sub>3</sub> .....	105
7.6.3	Polymerization of oPETTC-SiP <sub>3</sub> .....	105
7.7	Iteration 4: 7-hour hold oligomerization & UV-Vis study of 2 weight ratios, 20 hours condensation, followed by polymerization of hydroxypropyl methacrylate with 18-hour hold times. ....	106
7.7.1	UV-Vis Spectroscopy monitoring monomer consumption of MAPTMS.....	108
7.7.2	FTIR comparison of oPETTC-SiP <sub>4a</sub> and oPETTC-SiP <sub>4b</sub> .....	112
7.7.3	Thermogravimetric analysis of of oPETTC-SiP <sub>4a</sub> and oPETTC-SiP <sub>4b</sub>	113
7.7.4	Polymerization of oPETTC-SiP <sub>4</sub> particles.....	113
7.8	Conclusions .....	118
7.8.1	Polymer Chain Length and HPMA Molarity of .....	118
8	Addition of Iridium-Cyclopentylidienyl to pHPMA-SiPs.....	121
8.1	Addition of Iridium-Cyclopentylidienyl to pHPMA-SiPs .....	122
8.1.1	FTIR comparisons of IrCp*-SiP to its component parts.....	122
8.1.2	Inductively coupled plasma atomic emission spectroscopy.....	124

8.1.3	Transmission Electron Microscopy & Dynamic Light Scattering	125
8.1.4	Conclusions.....	130
	References .....	132
	Appendices .....	147
i.	List of Appendices Figures .....	147
ii.	List of Appendices Tables .....	150
A.1	Accompanying Figures and Tables to Chapter 5: Organically Modified Silicas (OrMoSils). .....	152
A.2	Accompanying Figures and Tables to Chapter 6.3: Creation of Brush Polymers via the formation of Chain-transfer Agent-coated Silicas (CTA-SiPs).155	
A.3	Accompanying Figures and Tables to Chapter 7.4. Iteration 1: 3-hour hold, purification testing, 18-hour condensation, and Polymerization of methyl methacrylate at DP = 100. ....	170
A.4	Accompanying Figures and Tables to Chapter 7.5. Iteration 2: 3-hour hold oligomerization, 18 hours condensation, polymerization of hydropropyl methacrylate at multiple degrees of polymerization of 50, 100, 200 and 500, and hold times. ....	178
A.5	Accompanying Figures and Tables to Chapter 7.6. Iteration 3: 3-hour hold oligomerization, 18 hours condensation, polymerization of hydroxypropyl methacrylate at multiple degrees of polymerization of 50, 100, 200 and 500, with 18-hour hold times.....	187

### iii. List of Figures

Figure 1-1: IrCp\*-immobilised transfer hydrogenation catalyst: a). Immobilisation of hydroxyl tethered dimers onto a Wang resin via an in-situ formation of a reactive triflate intermediate; b). Reaction profiles showing the reuse of catalyst 4c after washing with 7.4mol% Ir loading in the transfer

hydrogenation of benzaldehyde; c). Reaction profiles of 4c and 4d (different tether lengths) compared to $[\text{IrCp}^*\text{Cl}_2]_2$ .....	5
Figure 1-2: Benzaldehyde reduction by the immobilised n-5 IrCp* catalyst species on Wang Resin to Benzyl alcohol. The exchange of one chloride ligand with an alkoxide is thought to generate the active “precatalyst”; however, the exchange of the second chloride ligand leads to a potassium alkoxide-iridate species which is deactivated to further catalysis.....	2
Figure 1-3: Schematic describing the overall Polymer Brush approach that forms the basis of this thesis.....	3
Figure 2-1: Heterogeneous catalysis of hydrogenation of an alkene. Reactants adsorb to the catalyst surface which alters the state of both the catalyst and the reactants so that the available energy of the system is more likely to initiate the reaction to product based on a lower energy of activation of the catalytic intermediate species. The absorbed product species is then desorbed from the surface changing both the catalyst to its original state and the reactants into products. ....	4
Figure 2-2: Wesselbaum et. al. use a ruthenium-phosphine system to hydrogenate CO <sub>2</sub> . Catalyst was suspended in super-critical CO <sub>2</sub> with hydrogen gas to produce methanol in an autoclave at lower temperature and pressure conditions than currently utilised in industrial methanol production. ....	6
Figure 2-3: Figures and graphs from the catalyst system from Stasiak et. al.: a.) Imino aldol and an aza-Diels-Alder model reaction systems; b.) poly-p-xylylene (PPX) deposition scheme. ....	10
Figure 2-4: TPAP@OrMoSil inclusion complex design principles, showing catalytic oxidation of benzaldehyde; a hydrophobic silane coupling agent is reacted with tetraethyl orthosilicate in the presence of TPAP to form porous silica particles with hydrophobic surface groups, encapsulating the catalyst but enabling reactant to pass through.....	11
Figure 2-5: Takaya et. al. cross-linked star polymer particles with diphenylphosphinostyrene functionality for the binding of ruthenium salts; core ruthenium-complexes oxidise secondary alcohols to ketones with an isopropanol feedstock. ....	12

Figure 2-6: Pandarus and Pagliaro et. al. SiliaCat catalyst systems. a) SiliaCat TEMPO new oxidizing catalyst for oxidation of alcohols or aldehydes ; b) SiliaCat DPP-Pd used for Suzuki/Heck reactions. c) SiliaCat S-Pd used for Suzuki/Heck reactions. ....	13
Figure 2-7: Moore et. al. MacMillan recyclable polymer organocatalysts; the <i>R</i> -endo-enantiomer was the predicted favourite (overall enantioselectivity: 74-80% ee for major product, yield: >70% for all cycles) .....	15
Figure 3-1: Simplified scheme for addition of IrCp* to silica via the triflation mechanism. ....	21
Figure 3-2: The over-arching design principles for building brush polymers with silica core which both the first and second generation followed: some mechanism was found for attaching a RAFT agent to a silane coupling agent (via X) which itself was attached to the silica core and from which functional polymer could be grown, with a view to attaching the organometallic iridium (via Y). ....	22
Figure 3-3: The RAFT Chain Transfer Mechanism: the core of all RAFT chain-transfer agents (CTAs) is the thiocarbonylthio moiety [ZC(=S)SR]; this groups forms a radical species which controls the growth of polymer chains until they reach an equilibrium where the growth in molecular weight is retarded by continual exchange of the chain-transfer moiety and the availability of monomer is reduced significantly.....	23
Figure 3-4: Synthesis Route for RAFT-SCA (EHT, Scheme 1) and free-RAFT agent used (ECPMT, Scheme 2) .....	26
Figure 3-5: Simplified reaction scheme leading to supported IrCp* catalyst via a RAFT-grown pGMA brush particle with a silica core: A reversible addition-fragmentation chain-transfer (RAFT) agent is attached to a silane coupling agent (SCA) to form a combination CTA-SCA. This in turn is condensed to the silica particle (CTA-SiP) to enable polymer brush growth from the particle surface. Glycidyl methacrylate (GMA) can then be grown in the presence of the CTA-SiP. The poly(glycidyl methacrylate), contains an epoxy ring through which our IrCp*Cl <sub>2</sub> group, in this instance functionalized with an amine tether, can attach via epoxy-ring opening. ....	27

Figure 3-6: The simplified route to synthesis of oligomeric .....	28
Figure 3-7: Proposed scheme for attaching IrCp* moieties to PS/Latex nanoparticles. ....	29
Figure 3-8: SEM images of (i). cellulose acetate powder; (ii). Electrospun cellulose-acetate coated fibres; (iii). Free fibre used in the deposition process with CA. SEM was done using a Hitachi TM3030 Bench Top SEM. A solution of CA was prepared as a 7.5w/v% in a mixture of DMF, treated with 0.1w/v% lithium bromide, ethanol and acetone. ....	30
Figure 4-1: Reaction scheme for MTPAA: Sodium methanthiolate (1) in a solution of ethyl acetate (3) was placed under nitrogen. To this carbon disulphide (2) in ethyl acetate (20mL) was added slowly before the mixture is left to stir for 2 hours. The yellow precipitation was evaporated before being re-suspended in ethyl acetate, yielding a white precipitate and yellow solution; the suspension was passed through celite to remove the precipitate was washed with additional ethyl acetate. To this DL- $\alpha$ -Bromophenylacetic acid (5) was added slowly before the ethyl acetate solution was washed with saturated NaHCO <sub>3</sub> solution. The dried, filtered and evaporated oil was triturated with petroleum ether and recrystallized in a 1:1 mix of petroleum ether and benzene to produce a yellow solid.....	35
Figure 4-2: Reaction Scheme for PETTC synthesis: 2-Phenylethanethiol (1) was added to a suspension of sodium hydride (2) in diethyl ether (3). The reaction mixture was cooled and carbon disulfide (4) was added to produce sodium 2-phenylethanetrithiocarbonate, which was collected by filtration. Solid iodine (5) was gradually added to the suspension in diethyl ether. This reaction mixture was then stirred and the insoluble white precipitate of sodium iodide was removed by filtration. The yellow–brown filtrate was washed with an aqueous solution of sodium thiosulfate to remove excess iodine, dried over sodium sulfate, and then rotovapped to yield bis(2-phenylethanesulfanylthiocarbonyl) disulfide. A solution of 4,4'-azobis(4-cyanopentanoic acid) (6) and bis(2-phenylethane sulfanylthiocarbonyl) disulfide in ethyl acetate was degassed and heated to reflux under a dry nitrogen atmosphere for 18 h. The crude was evaporated, before being dissolved in ethyl	

acetate, washed with water, saturated brine solution, then dried, filtered and rotovapped. The crude product was recrystallized in a minimum of ethyl acetate before being cooled to -20°C overnight, then evaporated under high-vacuum to a waxy solid .....36

Figure 4-3: Reaction scheme for MMTPAA-APTES amide coupling: APTES, MMTPAA, EDCI.HCl, and HOBt were combined in DMF and stirred. The reaction is monitored using TLC and once the MMTPAA peak has disappeared the reaction mixture is immediately transferred into the dispersed silica. ....38

Figure 4-4: Oligomerization of PETTC with MAPTMS: Methacryloxypropyl-trimethoxysilane was dissolved in ethanol with 4-cyano-4-(2-phenylethane sulfanylthiocarbonyl) sulfanylpentanoic acid (PETTC), and initiator 4,4'-Azobis(4-cyanopentanoic acid) (ACVA) before the solution was sparged with nitrogen gas. The mixture was then heated under nitrogen for 3 hours before being quenched in an ice bath before being used for silica condensation. ....38

Figure 4-5: APTES condensation onto silica in ethanol, showing presumed condensation parameters of 3 silylic acid moieties to one APTES molecule. Typically silica was dispersed mechanically in ethanol for 10 minutes before APTES was added. The dispersed silica and APTES was then stirred at room temperature for 24 hours before being collected and centrifuged at 3000rpm for 5 minutes, and solvent exchanged with fresh ethanol. This was repeated 3 times, then repeated 3 times more in water, before the solid precipitate was dried in a vacuum oven overnight at 80°C. ....39

Figure 4-6: Typically, silica was dispersed mechanically in toluene or ethanol for 10 minutes before the recovered crude SCA-CTA oil was added in excess to the silica surface hydroxyl groups. The dispersed silica and SCA-CTA was then refluxed at 90°C for 18 hours before being centrifuged at 10,000rpm for 10 minutes, and solvent exchanged with fresh ethanol. This was repeated 3 times then repeated before the solid precipitate was dried in a vacuum oven overnight at 25°C..... 40

Figure 4-7: Typically, silica was dispersed mechanically in ethanol for 10 minutes before the recovered crude SCA-CTA oil in ethanol was added along with trimethylamine before being sparged with nitrogen. Under nitrogen, the

mixture was refluxed at 80-90°C for 18-24 hours before being centrifuged at 10,000rpm for 10 minutes, and solvent exchanged with fresh ethanol. This was repeated 4 times then once with water before the solid precipitate was dried in a vacuum oven overnight at 50°C. ....41

Figure 4-8: CTA-SiP (1) is mechanically dispersed in DMF (2). The methacrylate monomer (2, glycidyl or methyl methacrylate), MMTCAA (3) and AIBN (4) are added, the mixture was sealed and sparged with nitrogen for 10 minutes. The mixture is then kept under nitrogen and heated to 65°C for a set hold time dependent on the experiment. The mixture is then cooled and the solid centrifuged at 8000rpm for 10 minutes, decanted and repeated with fresh ethanol and re-dispersed 3 times, before being dried in a vacuum oven. ....42

Figure 4-9: *o*PETTC-SiP (1) is dispersed in ethanol (15mL) solvent. Hydroxypropyl methacrylate (2), PETTC (3) and ACVA (4) are added, the mixture sealed and sparged with nitrogen for 10 minutes. The mixture is then kept under nitrogen and heated to 70°C for a set hold time dependent on the experiment. The mixture is then cooled and the solid centrifuged at 8000rpm for 10 minutes, decanted and repeated with fresh ethanol and re-dispersed 3 times, before being dried in a vacuum oven. ....42

Figure 4-10: Synthesis of IrCp\*Cl<sub>2</sub>. Under a nitrogen atmosphere, iridium trichloride hydrate (2) and sodium bicarbonate (3) were added to degassed methanol (4) in a 10ml capacity microwave tube and the suspension was sparged with nitrogen for 10 minutes. After adding 1-(5-hydroxypentyl)-2,3,4,5-tetramethylcyclopentadiene (1), the suspension was sparged for a further 5 minutes. The tube was then sealed and microwave heating was applied at 150°C for 10 minutes. After effervescence from the solution had subsided, the tube was opened and the solution was diluted with DCM, washed with water, brine, dried over Na<sub>2</sub>SO<sub>4</sub> and the solvent removed using a rotary. The resulting oily red residue was dissolved in DCM, precipitated with hexane and left overnight in a fridge-freezer to yield an orange powder. ....43

Figure 4-11: Triflation of IrCp\*Cl<sub>2</sub>: Under nitrogen, a solution of 2,6-Lutidine (3) in dichloromethane (4) was added to trifluoromethanesulfonic anhydride (2) in dichloromethane at -10°C. A solution of (1) in dichloromethane was slowly

added over 30 minutes. After stirring for 2 hours the solution was rotovapped to dryness under vacuum before being used immediately in the attachment step.....44

Figure 5-1: Silica hydroxyl content for 500 and 250nm commercial silica. Legend ■ : 500nm silica; ● : 250nm silica. ....47

Figure 5-2: (A) Electrophoretic mobility of 500nm silica particles with and without APTES in ethanol. Inset (B): Figures 4 & 5 combined. Base: ammonium hydroxide (NH<sub>4</sub>OH) catalyst (0.9mL in 5mL solvent) Key: ■ : Blank silica; ▲ : Ethanol, base catalyst; ◆ : Ethanol, no base catalyst; ● : Toluene, base catalyst; ▼ : Toluene, no base catalyst..... 49

Figure 5-3: (A) Electrophoretic mobility of 500nm silica particles with and without APTES in toluene. Inset (B) is Figures 4 & 5 combined. Base: ammonium hydroxide (NH<sub>4</sub>OH) catalyst (0.9mL in 5mL solvent) Key: ■ : Blank silica; ▲ : Ethanol, base catalyst; ◆ : Ethanol, no base catalyst; ● : Toluene, base catalyst; ▼ : Toluene, no base catalyst..... 50

Figure 5-4: Electrophoretic mobility for 250nm silica nanoparticles reacted with increasing %-APTES as a function of pH; The suspension at original pH X was divided in half and concentrated HCl and NaOH solutions were added to gradually change the pH, decreasing and increasing it respectively. Measurements of APTES to silanol content are made in equivalents of 3[Si-OH]; legend: ■ : 0.0 equivalents to silica (blank, untreated silica); ● : 0.01; ▲ : 0.10; ▼ : 0.20; ◆ : 0.60; ◀ : 1.00; ▶ : 1.50..... 53

Figure 5-5: (i): low APTES content; (ii): high APTES content; Electrophoretic mobility for organically modified 250nm silica nanoparticles with increasing %-APTES content across a wide pH range; The suspension at original pH X was divided in half and concentrated HCl and NaOH solutions were added to gradually change the pH, decreasing and increasing it respectively. Measurements of APTES to silanol content are made in equivalents of 3[Si-OH]; legend: ■ : 0.0 equivalents to silica (blank, untreated silica); ● : 0.01; ▲ : 0.10; ▼ : 0.20; ◆ : 0.60; ◀ : 1.00; ▶ : 1.50..... 54

Figure 5-6: Electrophoretic mobility values vs increasing APTES content at 3 different pH ranges: ■ : pH 2.5-3.5; ● : pH 6.0-7.5; ▲ : pH 10-11 ..... 55

Figure 5-7: Average diameter of modified 250nm silica nanoparticles with increasing %-APTES content as a function of pH; The suspension at original pH X was divided in half and concentrated HCl and NaOH solutions were added to gradually change the pH, decreasing and increasing it respectively. Legend: ■: 0% equivalents to silica (blank, untreated silica); legend: ■: 0.0 equivalents to silica (blank, untreated silica); ●: 0.01; ▲: 0.10; ▼: 0.20; ◆: 0.60; ◀: 1.00; ▶: 1.50..... 56

Figure 5-8: Mode of action for Fluorescamine when reacting with a primary amine moiety. Primary amines react irreversibly with fluorescamine, The secondary-aminated molecule then produces characteristic fluorescence under a UV light source of 390nm as opposed to the unreacted form, producing light around the 487nm region. This can be quantitatively measured to create an assay system. .... 58

Figure 5-9: Mechanism for Fluorescamine Assay: 1. A known concentration of Fluorescamine is introduced to a known weight of AP-treated silica; 2. The sample is agitated and then centrifuged to remove solid, treated OrMoSil; 3. A sample of known volume of the eluent is taken and treated with a known excess of propylamine. The samples UV fluorescence is then measured and compared against a calibration curve. .... 59

Figure 5-10: Fluorescamine assay of organically modified silica. Predicted assay results are based on the predicted amine content assumed from the conditions used to create the OrMoSil in question, in this case this is linked to silica. This is discussed in greater detail in the section in Chapter 4 on Fluorescence Spectroscopy..... 60

Figure 5-11: SEM Images comprising: a. 250nm silica (untreated); b. Silica from the 20% APTES regimen; c. Silica post-route A to IrCp\*-APTES-Silica (copper mount); d. Silica post-route B to IrCp\*-APTES-Silica. .... 61

Figure 5-12: SEM-EDX cross section of route A silica (AP-silica + IrCp\*) and iridium scanning..... 62

Figure 5-13: Benzaldehyde assay of Routes A & B IrCp\*-SiPs vs. unattached IrCP\*. Key: Purple: Test benzaldehyde and benzyl alcohol; Red: free Iridium cyclopentadienyl complex synthesised and utilised in the silica particles; Blue:

IrCp-treated silica particles via route A; Green: IrCp-treated silica particles via route B. ....	63
Figure 6-1: Average AP-SiP TGA values for each AP-SiP sample in Table 6-1 vs AP% ratio to silica (assuming 1 APTES molecule per 3 Si-OH moieties. ▼, ◆, and ◀ are averaged values for the 3-aminopropyl excluding the values in Table 1. ....	67
Figure 6-2: Mechanism of GMA coating onto the surface of APTES-modified silica particles via a methacryloxy-1-β-hydroxy-3-aminopropyl trimethoxysilane. Proposed growth pathway of pGMA is then moderated via RAFT polymerization from the surface AP-GMA moiety whilst growing as a free polymer in solution. ....	70
Figure 6-3: Michael addition of glycidyl methacrylate (GMA) to the aminopropyl-moiety of the silica particle (AP-SiP). Reaction is via the double bond with the amine resulting in deactivation for further polymerization from the double bond. ....	71
Figure 6-4: Synthesis of mono-methyl trithio-2-phenylacetic acid (MMTPAA) with 3-aminopropyl triethoxysilane (APTES) using amide-coupling agents to create the CTA-functionalised silane coupling agent (SCA). HOBt: Hydroxybenzotriazole; DMF: dimethyl formamide. ....	73
Figure 6-5: <sup>1</sup> H-NMR of the SCA-CTA recovered oil. Samples were dissolved in CDCl <sub>3</sub> . Proton-signal attribution did not correspond directly to the intended compound but key signals did and are colour-coded. ....	74
Figure 6-6: Proposed chemical reorganisation of the SCA-CTA compound. The lower left indicates a proposed mechanism for the formation of a heterocycle, the right, the formation of an oligomerised SCA-CTA. ....	75
Figure 6-7: Simplified anticipated reaction scheme of the SCA-CTA compound with silica surface. ....	76
Figure 6-8: Recovered CTA-SiP from iteration 1 following multiple washes in toluene (x3) and water (x3) before drying in a vacuum oven overnight. ....	77
Figure 6-9: FTIR spectra from the isolated free pMMA from pMMA-SiP <sub>6</sub> utilising CTA-SiP <sub>3</sub> . ....	83

Figure 6-10: FTIR spectra of pMMA-SiP <sub>7</sub> utilising CTA-SiP <sub>4</sub> at DP = 100. ....	84
Figure 6-11: Scheme for kinetic behavior for the 3 potential scenarios of polymerization with or without a chain-transfer agent. ....	87
Figure 6-12: Schema for determining the extent of polymerization of pGMA. Red and blue germinal hydrogens on the epoxy ring have NMR signals that shift with polymerization. The alkene geminal hydrogens become indistinguishable from the methyl peak. ....	88
Figure 6-13: Kinetic studies of pGMA in 3 scenarios; ▲: PETTC as CTA; ◆: MMTCAA; ■: no CTA, initiator only. ....	90
Figure 7-1: (i) Synthesis of oligomers (5:1) of MAPTMS with PETTC to create oligo-CTA-SCAs (oCTA-SCAs); (ii) Condensation of oCTA-SCA to silica to create oCTA-SiPs. X and Y groups are as indicated above. The MAPTMS chain number, n, is indicated as aiming for a 5:1 molar ratio of MAPTMS:PETTC in this initial stage. ....	94
Figure 7-2: Polymer growth from an oligomer-treated silica particle, oCTA-SiP. Hydroxypropyl methacrylate (HPMA) were used in the block-polymerization step. The HPMA polymer chain number, m, is given by the free monomer molar ratio to free CTA. ....	95
Figure 7-3: Functionalisation of the pHPMA-SiP with Iridium Cyclopentadienyl complex functionalised with a hydroxyl group. The carbon chain length of the IrCp* complex, o, represents the number of carbons in the linking chain and was synthesised with a 5- and 12-carbon chain backbone; however, only the 5-carbon chain was investigated at this stage. ....	95
Figure 7-4: MAPTMS was dissolved in DMF at a molar ratio of 5:1 to PETTC before polymerization is initiated with AIBN at 70°C for 3 hours. ....	96
Figure 7-5: Schematic showing the condensation of oPETTC-SCA to silica particles used throughout; individual conditions described in each section for each iteration. ....	97
Figure 7-6: Polymer growth from the oligomer-coated active-silica, utilizing free-polymerization of monomer in the presence of ACVA initiator and free chain-	

transfer agent. Specific conditions are discussed for each iteration, as is the monomer used.....	98
Figure 7-7: Schematic showing the oligomerization process and highlighting the chemical moieties and absorbance regions observable using UV-Visible Spectroscopy. ....	109
Figure 7-8: UV-Vis absorbance at 210nm. The value for MAPTMS absorbance attribution was determined by discounting the PETTC signal in comparison to its absorbance at 300nm and can be seen in the legend.....	110
Figure 7-9: MAPTMS monomer content over time during oligomerization. Values are derived from the absorbance spectra in Figure 7-8 and compared to the calibration curve for MAPTMS. ....	111
Figure 7-10: Infrared spectra of the <i>o</i> PETTC-SiP <sub>4</sub> samples. Legend: (i): <i>o</i> PETTC-SiP <sub>4a</sub> ; (ii): <i>o</i> PETTC-SiP <sub>4b</sub> .....	112
Figure 7-11: Thermogravimetric analysis of <i>o</i> PETTC-SiP <sub>4</sub> samples. Legend: (i): <i>o</i> PETTC-SiP <sub>4a</sub> ; (ii): <i>o</i> PETTC-SiP <sub>4b</sub> .....	113
Figure 7-12: FTIR spectra comparison between (i) <i>o</i> PETTC-SiP <sub>4a</sub> and (ii) pHPMA-SiP <sub>4a</sub> . Peak region below 1500 omitted for clarity.....	115
Figure 7-13: FTIR spectra comparison between (i) <i>o</i> PETTC-SiP <sub>4b</sub> and (ii) pHPMA-SiP <sub>4b</sub> . Peak region below 1500 omitted for clarity.....	115
Figure 7-14: Thermogravimetric analysis of pHPMA-SiP <sub>4a-b</sub> . The TGA protocol used the new method as per that of the blank, untreated silica as in Figure A-21. Legend: (i) pHPMA-SiP <sub>4a</sub> ; (ii) pHPMA-SiP <sub>4b</sub> . ....	118
Figure 8-1: Addition of Iridium-Cyclopentylidienyl complex to pHPMA-SiP <sub>2a</sub> via triflation of the alkoxide-IrCP complex.....	121
Figure 8-2: Comparison of FTIR spectra of IrCp* <sup>-</sup> -SiP with it's constituent parts. Legend: (i) IrCp* free-catalyst; (ii) IrCp* <sup>-</sup> -SiP; (iii) pHPMA-SiP <sub>2a</sub> .....	123
Figure 8-3: TEM imaging of pHPMA-SiP <sub>2a</sub> .....	126
Figure 8-4: TEM imaging of IrCp* <sup>-</sup> -SiPs.....	127
Figure 8-5: pHPMA-SiP <sub>2a</sub> TEM image showing polymer layer thickness at the uniform regions. ....	129

Figure 8-6: Schematic describing the overall Polymer Brush approach that forms the basis of this thesis..... 130

#### iv. List of Tables

Table 2-1 : The advantages (+) and disadvantages (-) of homogeneous and heterogeneous catalysts. ....7

Table 4-1: Conditions for attachment of the triflated iridium complex in each instance of its use, including the Chapter/Section it can be found. ....44

Table 6-1: Sample Cohorts of AP-SiPs, with the %-weight loss range given as the difference between untreated silica and the AP-SiP. Average  $\text{mmols}_{\text{AP}} \text{g}_{\text{SiP}}^{-1}$  values given based on the average %-weight loss range. ....66

Table 6-2: Conditions for CTA-SCA condensation to silica particles. EDCI coupling of the chain-transfer agent (CTA) to the silane coupling agent (SCA) is as per Figure 6-4 in all instances.....77

Table 6-3: %-organic mass loss, taken as the difference in mass loss between the untreated silica (mass loss due to water, silica-surface dehydration and calcination) and the organically treated silica.....78

Table 6-4: Polymerisation conditions; standard conditions throughout: Temperature hold: 64°C, Total volume: less than 6mL; hold time: 24 hours. CTA-SiP mass: 40mg; nitrogen sparge time: 5 minutes prior to temperature bath. Molar ratio of CTA to initiator,  $n_{\text{CTA}}/n_{\text{initiator}}$  ratio = 10.....80

Table 6-5: SEC-HPLC results for Molecular weight of the free pMMA polymer produced in-situ CTA-SiP<sub>1</sub> .....81

Table 6-6: SEC-HPLC results for Molecular weight of the free polymer produced in-situ CTA-SiP<sub>2</sub> .....82

Table 6-7: SEC-HPLC results for Molecular weight of the free polymer produced in-situ with CTA-SiP<sub>3</sub>.....83

Table 6-8: SEC-HPLC results for Molecular weight of the free poly(glycidyle methacrylate) polymer produced in-situ with CTA-SiP<sub>4</sub>. Chart includes details of the Peak Molecular Weight Report for %Area of the peak, with main weights

being shown. All remaining individually detected at a maximum account for less than 3% of the peak area respectively. .... 85

Table 6-9: Kinetic study scenarios for GMA polymerization: all studies were conducted with the same amount of monomer and molar equivalents of CTA when used and initiator. Reactions are sparged with N<sub>2</sub> for 5 minutes before being heated to 70°C, aliquots taken on an hourly basis are immediately cooled in an ice bath and <sup>1</sup>H-NMR is used to determine the extent of the reaction... 89

Table 7-1: Summary of the production of *o*PETTC-SiP<sub>4</sub> and pHPMA-SiP<sub>4</sub> particles. .... 107

Table 7-2: polymer SEC-GPC profiles for each pHPMA-SiP<sub>4</sub> created. Bound polymer values in parenthesis shows the actual DP values for the free polymer and the %-equivalent of that for the bound polymer in bold). Molar Ratio, M:CTA = 100; Theoretical Mn: 14,756. .... 114

Table 7-3: Dynamic Light Scattering (DLS) studies of *o*PETTC-SiP<sub>4a-b</sub> and pHPMA-SiP<sub>4a-b</sub> particles. Particles were dispersed in ethanol at <0.5 wt%. Legend: (i): *o*PETTC-SiP<sub>4a</sub>; (ii): *o*PETTC-SiP<sub>4b</sub>; (iii): pHPMA-SiP<sub>4a</sub>, DP = 100; (iv): pHPMA-SiP<sub>4b</sub>, DP = 100; (v): free polymer from pHPMA<sub>4a</sub>; (vi): free polymer from pHPMA<sub>4b</sub>. Particle diameter derived from size distribution by number values. .... 116

Table 7-4: %-mass loss for the 125-540°C region determined through thermogravimetric analysis for pHPMA-SiP<sub>4</sub> samples and their constituent parts, collated from previous graphs. Legend: (i) Silica Particles, SiP<sub>250nm</sub> used in preparation of the rest; (ii) *o*PETTC-SiP<sub>4a</sub>; (iii): *o*PETTC-SiP<sub>4b</sub>, (iv): pHPMA-SiP<sub>4a</sub>, DP = 100; (v): pHPMA-SiP<sub>4b</sub>, DP = 100; (vi): pHPMA-SiP<sub>3d</sub>, DP = 500. Mass loss differences between the pHPMA-SiP<sub>4</sub> samples, the SiP<sub>250nm</sub> and their respective *o*PETTC-SiP<sub>4</sub> samples are shown in the second and third column respectively. .... 117

Table 8-1: ICP-OES analysis of IrCp\*-SiP in comparison to the original IrCp\*-wang ..... 124

Table 8-2: Dynamic Light Scattering Size Distribution by Number values for IrCp\*-SiP, with pHPMA-SiP<sub>2a</sub> shown for comparison. Both were dispersed in ethanol at <0.5%w/w in line with previous particle samples..... 128

# 1 Introduction

## 1.1 Green Chemistry

There are 12 principles that identify chemistry as “green” (i.e. chemistry which optimizes itself and limits the use of hazardous components; Anastas and Eghbali, 2010). Green chemistry principle #9 states that catalysts are superior to stoichiometric reagents. They influence many of the other principles: from atom economy, safer processes and pollution to waste mitigation. Both research and process chemists have an incentive to develop new catalysts and catalytic processes that:

1. Improve reactivity and the rate of a desired reaction.
2. Are versatile; being insensitive to an array of chemical environments.
3. Are selective; displaying specific reactivity towards a limited number of chemical moieties.
4. Are cost effective; demonstrating an evident reduction in costs, waste and side products and itself being either cheap to replace or recyclable.

The definition of “Catalyst” as “a substance that changes the velocity of a reaction without itself being changed in the process” is at best misleading: catalysts undergo many transformations throughout the reaction, only reverting back to its original or an “active” but recognizably discrete state at the end of a reaction profile. Within any particular reaction scheme there are several stages when the trajectory of the reaction can change and by extension the outcome for both the reaction and the catalyst.

## 1.2 Turnover Number (TON) and Turnover Frequency (TOF)

Catalytic activity is defined by two terms: turnover number (TON) and turnover frequency (TOF). TON is the number of moles of substrate a mole of catalyst can convert before becoming deactivated (Bligaard et al., 2016) – it is unitless; The term TON was first used in heterogeneous catalysis to compare the rate of reaction to the number of active catalytic sites which is difficult in practice to evaluate; in homogeneous catalysts it refers to the moles of product formed per

mole of catalyst. TOF describes the number of revolutions of the catalytic cycle per unit time; it is effectively the TON per a given time period.

### 1.3 Types of Catalysis

Catalysts can be placed into 2 broad categories: homogeneous and heterogeneous catalysts. Homogeneous catalysts are present in the same phase as the reactants; commonly they are co-dissolved in the solvent with the reactants and encompass chemical species as diverse as metal salts, acids, organometallics and enzymes. They are ubiquitous with smaller scale reactions as work-up regimens are a lot more complex and require isolation of the desired product(s); routinely the catalyst and waste products are not recoverable/recyclable, recovery being a secondary concern to pure, clean product.

Heterogeneous catalysts are present in a different phase to the reactants, usually in the solid state to a gaseous or liquid environment. Reactants are adsorbed onto the surface or interface where the reaction then takes place before the product desorbs into the media. They are mostly associated with reactions producing bulk compounds either of one simple chemical structure, such as an inorganic salt or a blend of products such as hydrocarbons produced whilst cracking crude oils into petroleum products (Levenspiel, 1999). In general heterogeneous catalysts are less selective but more stable, meaning more extreme conditions can be used; they are also easier to separate from the product and can be recycled or used multiple times, making them more amenable to scaled up and bulk reactions.

For more complex organic chemicals, homogeneous catalysts can be more selective, producing high-value target molecules of high purity; however, the catalysts used are often less stable, prone to decomposition or breakdown under more severe conditions as you would expect in bulk reactions, and difficult to separate from the product, resulting in limits being placed on the scalability of reactions utilizing them. To combine the qualities of both types of catalyst is a desirable goal.

## 1.4 Background to the Project

Platinum-group metals, a cluster of 6 noble precious metallic elements consisting of ruthenium, rhodium, palladium, osmium, iridium, and platinum have been shown to form a number of organometallic compounds with an array of properties, particularly catalytic (Lucas et al., 2013). They have been shown to have utility in generating novel compounds and applications, such as in the development of Light Emitting Diodes (LEDs, Page et al., 2017).

However, some of these metallic elements, such as iridium, are non-terrestrial; being the least abundant metals on earth, with refinement and production amounting to a few thousand kilos, this also makes it an extremely expensive metal to obtain (John R. Rumble, 2021). In order to harness the potential benefits of such a metal mechanisms for recovery, recycling and reuse would have to be developed, particularly to make it a viable compound in process chemistry beyond lab scale.

Lucas *et al* developed a method for immobilising hydroxyl-tethered iridium/rhodium organometallic compounds on a Wang resin, a material used in the commercial production of biopolymers and proteins (Lucas et al., 2013) (Figure 1-1).

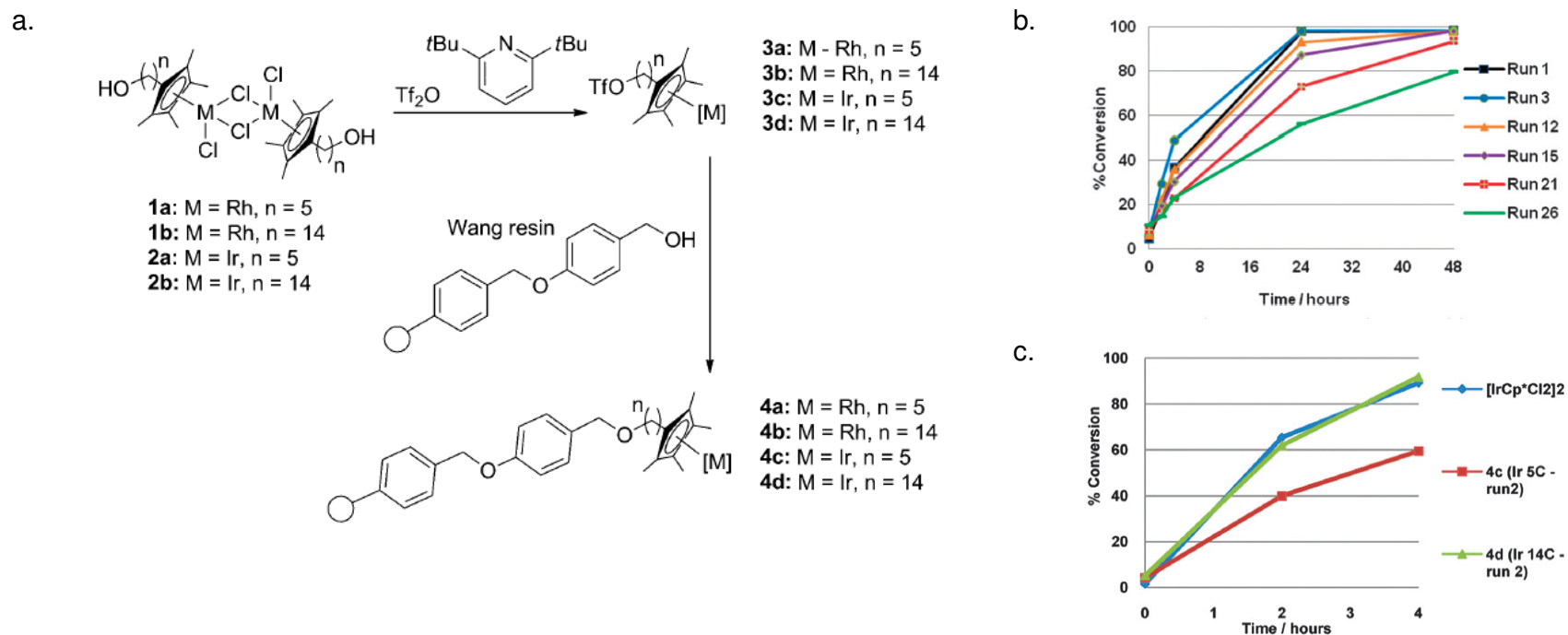


**Figure 1-1: IrCp\*<sup>\*</sup>-immobilised transfer hydrogenation catalyst: a). Immobilisation of hydroxyl tethered dimers onto a Wang resin via an in-situ formation of a reactive triflate intermediate; b). Reaction profiles showing the reuse of catalyst 4c after washing with 7.4mol% Ir loading in the transfer hydrogenation of benzaldehyde; c). Reaction profiles of 4c and 4d (different tether lengths) compared to [IrCp\*Cl<sub>2</sub>]<sub>2</sub>**

This followed earlier work to develop a racemisation catalyst with the same organometallic compound immobilised on an polyethylene glycol scaffold in the asymmetric transformation of racemic sertraline (Blacker et al., 2009). The materials could be used as effective catalysts for transfer hydrogenation reactions and recycled with limited evidence of leaching. Increasing the tether length increases the short term activity in comparison with shorter chain versions of the catalysts; however it also decreases the number of uses before the catalyst deactivates.

In one example the immobilised IrCp\* complex was shown to be effective and recyclable in the transfer hydrogenation of benzaldehyde over 25 runs at an effective catalyst concentration of 0.3 mol%/reaction (Figure 1-2); however, a slow and partial deactivation of the catalyst was observed over 26 runs (giving it an effective TON > 350); the replacement of chlorine with alkoxide ligands was identified as the primary reason for this; treatment with dilute aqueous HCl restored catalytic activity for 3 runs before losing it again, suggesting another form of Cl inclusion in the organometallic complex (Sherborne et al., 2015).

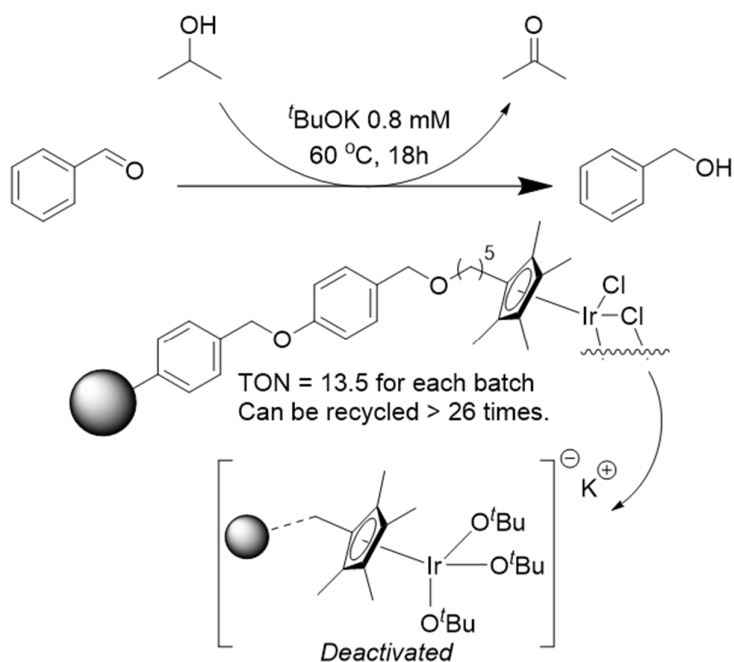


**Figure 1-2: Benzaldehyde reduction by the immobilised n-5 IrCp\* catalyst species on Wang Resin to Benzyl alcohol. The exchange of one chloride ligand with an alkoxide is thought to generate the active “pre-catalyst”; however, the exchange of the second chloride ligand leads to a potassium alkoxide-iridate species which is deactivated to further catalysis.**

Another problem associated with this type of immobilisation strategy is that Wang resins are designed to be cleaved in the presence of strong acids such as trifluoroacetic acid, restricting the range of reaction conditions they can operate under.

As a proof of concept this represents a useful touchstone in generating novel catalyst systems, capable of harnessing elements of complexity that many homogeneous catalysts systems offer; simultaneously, developing an element of recyclability and reuse more at home with heterogeneous catalyst systems would improve the utility of such a platform.

Development of “scaffold” systems could show a great deal of utility in developing chemical processes that use more complex chemistry at a larger scale of production using this and other catalysts.

## 1.5 Project Aims

Initially the project aims were to investigate alternative scaffolding materials capable of providing a proof of concept for further development of organometallic iridium catalyst scaffolding systems. Organically modified silicas (OrMoSils) were chosen as the initial source of investigation issues of attachment and loading became apparent. Following this it was decided we would try and growth outward by creating silica-core brush polymers: silica particles with polymer chain-transfer agents (CTAs) based on reversible addition-fragmentation chain-transfer agents (RAFT agents) were condensed onto their surface in 2 tranches (the schematic in Figure 1-3 encapsulates the overall approach and will be repeated throughout):

1. Single-unit 3-aminopropyl triethoxy silane (APTES) functionalized with a RAFT agent before condensation to silica and subsequent polymer growth.

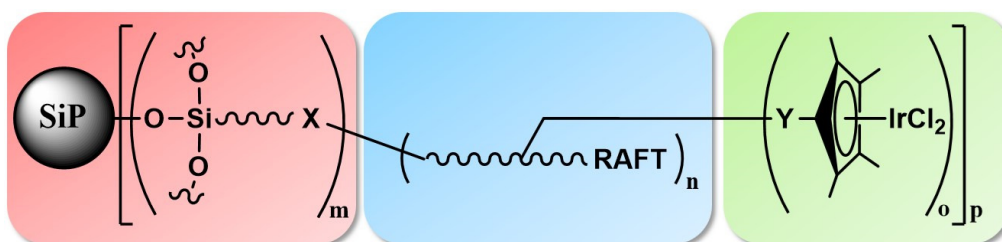


**Figure 1-3: Schematic describing the overall Polymer Brush approach that forms the basis of this thesis.**

Once a suitable scaffold-particle had been developed that could be well characterized, modified and reproduced at scale we could then test it for catalyst loading and efficacy against the benchmark homogeneous catalyst and the original immobilized version illustrated in Figure 1-1.

## 2 Literature Review

### 2.1 From Bench to Plant-scale

A catalyst is a substance that increases the rate of a reaction without modifying the overall standard Gibbs energy change in the reaction; the process is called catalysis (McNaught and Wilkinson, 1997). Catalysis can be sub-grouped into 2 distinct categories: heterogeneous, in which the catalyst is in a separate phase to the medium (e.g. a catalytic converter converting toxic exhaust emissions into carbon dioxide, nitrogen and water), and homogeneous, in which the catalyst exists in the same phase and media (e.g. esterification of an alcohol and a carboxylic acid promoted by a mineral acid catalyst such as sulphuric acid). Both sub-groups and the catalysts that fall into them can offer an array of uses but usually offer consistent trade-offs depending on the type of catalyst ultimately used.

Catalyst use in bulk-scale production is dominated by heterogeneous catalysts, particularly “supported” species (Satterfield and N, 1991; Liu and Corma, 2018); the degree of complexity and degree of change during the reaction scheme of the product is limited. Most simple compounds, both organic and inorganic in nature, as well as reactions where the desired outcome is to lower the presence of one constituent in the product and its associated phase (Argyle and Bartholomew, 2015) fall into this category. These kind of compounds have a low E-factor (equating to kilo of waste/kilo of product) compared to more complex compounds (Sheldon, 1997).

Conversely, in areas like pharmaceutical manufacture complex chemical synthesis is required, carried out by complex catalyst species, predominantly homogeneous at all scales of production, from lead-research to process development and even to full-scale production (Muller and Latimer, 2009).

Homogeneous catalysts used in creating research quantities of a desired product are not always suitable for producing larger quantities of that material, therefore it becomes necessary to adapt, replace or revise reactions or a reaction scheme to produce the desired material in bulk (>1kg). This has an impact on process development and clinical testing timeframes.

In the past the chemical industry has treated process development with lower priority as the higher marginal costs of drugs more than accounted for inefficiencies; however, profitability of large-scale processing operations and the high failure rate during clinical testing, means that improvements in process development are becoming more important (Butters et al., 2006; Blacker and Williams, 2011).

Good drug design invites insight into the process development stage at an earlier stage to speed up the drug development process; methodologies for investigating, evaluating and adapting processes for scale-up suitability have been developed (Singh et al., 2012) and where possible the trend is to replace bench-scale processes such as:

- Multiple-phase, multi-stepped washing and work up procedures.
- Single-use Homogeneous catalysis.
- Low concentration, high dilution reactions.
- Batch synthesis.

To processes suitable for scale-up such as:

- Recrystallization.
- Reusable heterogeneous catalysis (or a recycling methodology for homogeneous catalysts)
- High concentration/low dilution reactions.
- Continuous flow synthesis methods.

Moreover, economic and safety factors are paramount to successful, large-scale process design: fewer reagents and less solvent, shorter/simpler workup techniques and less energy, wastage and lower disposal requirements all figure earlier in the development process. Minor changes in catalyst design can have a major impact in these areas of process development.

### 2.1.1 *Green Chemistry and SELECT Criteria in Chemical Engineering*

In order to adapt the production of lead chemical compounds discovered at the research and development stage, usually at bench scale (1-100g) chemists and process chemists must identify methods for producing the compound at higher quantities with fewer materials if possible – economies of scale need to be adapted so as to limit pitfalls in drug development in order to get it to market and limiting production costs in terms of financial and environmental.

Anastas listed 12 principles that should be adopted to make a chemical product or process greener (Anastas and Eghbali, 2010); they are:

1. *Prevent waste.*
2. *Maximize atom economy.*
3. *Design less hazardous chemical syntheses.*
4. *Design safer chemicals and products.*
5. *Use safer solvents and reaction conditions.*
6. *Increase energy efficiency.*
7. *Use renewable feedstocks.*
8. *Avoid chemical derivatives.*
9. *Use catalysts, not stoichiometric reagents.*
10. *Design chemicals and products to degrade after use.*
11. *Analyse in real time to prevent pollution.*
12. *Minimize the potential for accidents.*

Design of Green Chemical processes is only half the battle if they cannot be scaled-up to a useful scale for the market for that product. Scale-up routes can also be evaluated against the SELECT criteria, the acronym standing for: Safety, Environment, Legal, Economics, Control and Throughput (Butters et al., 2006; Ambhaikar and Krishnamurthy, 2014). Whilst greener processes can positively affect the SELECT criteria there are some instances where the impact is less clear on route selection; one such area is catalysis. At pilot and bulk scale which tool to select is usually based on the number and type of phases involved in the reaction. The biggest division in systems therefore is the classification between *homogeneous* and *heterogeneous* systems (Levenspiel, 1999). Similarly catalysis can also be defined by these 2 categories.

### 2.1.2 Heterogeneous Systems

A reaction is heterogeneous if it requires the presence of 2 phases to proceed at the rate that it does; usually catalysts in such systems operate in a different phase to the reactants, usually in the solid state to a gaseous or liquid environment. Examples include metal or metal-on-ceramic scaffold materials like catalytic converters. Reactants are adsorbed onto the surface where the reaction then takes place before the product desorbs into the media.

Being in a separate phase to the reactants usually means that there is a rate of adsorption and desorption from the catalyst surface to consider in addition to the reaction rate, meaning the reaction proceeds at a slower rate yet still quicker than if it would occur in the catalysts absence (Mizuno and Misono, 1998). A simple scheme representing this is show in Figure 2-1:

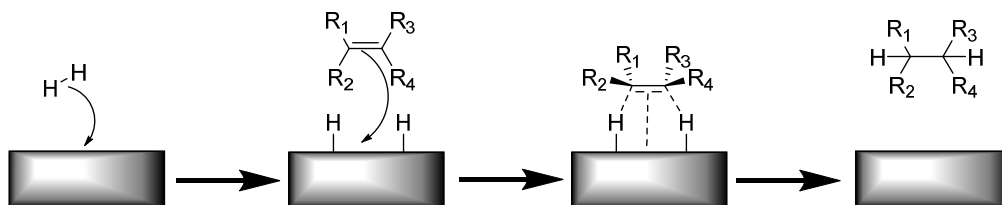


**Figure 2-1: Heterogeneous catalysis of hydrogenation of an alkene. Reactants adsorb to the catalyst surface which alters the state of both the catalyst and the reactants so that the available energy of the system is more likely to initiate the reaction to product based on a lower energy of activation of the catalytic intermediate species. The absorbed product species is then desorbed from the surface changing both the catalyst to its original state and the reactants into products.**

The availability of catalytic surface is important, with more diffuse catalyst with a higher available surface area, as well as a responsive configuration (Piccialli, 2014) leading to greater adsorption/desorption and increasing the observed rate. The crystalline nature of many heterogeneous catalysts usually means they are also relatively simple with little scope for modification – it is for this reason that many examples of heterogeneous catalysts exist in the bulk processing of commodities like ammonia or petroleum fractions, where throughput is more important than specialisation.

Heterogeneous catalysts are a staple in large scale industrial catalytic processes (Satterfield and N, 1991). Materials of this nature are usually

crystalline and as such exhibit different crystal planes on the surface with differing chemisorption energies and affinities; modelling and experimental estimates demonstrate these differences in adsorption of reagents (Somorjai and Li, 2010). Thus we see that, by decreasing the size of the catalyst particle, thereby increasing the surface area, we increase the number of higher-energy planes and chemisorption sites on the catalyst; we see a limiting effect for this once we start to decrease particle size below 100nm in size (Moshfeqh, 2009) as we reach the maximal number of available sites, active planes, defects and similar high activity sites available (Astruc, 2007); as catalyst size becomes molecular and more homogeneous in nature to its reactants we start to see higher activity (Daniel and Astruc, 2004; Corma and Garci, 2008). Paradoxically, a reduction in size confers the potential for loss of catalyst during workup and it is thus an important aspect of heterogeneous nanoparticle catalyst design to develop a suitable scaffolding material for it (Ramarao et al., 2002; Astruc et al., 2005).

### **2.1.3 *Homogeneous Systems***

A reaction can be considered homogeneous if the catalyst is in the same phase as the reactants. Usually this is achieved by both reactant and substrate being present at the molecular level and being free to diffuse through their phase (such as a liquid phase). As both the desired product and the secondary components are in the same phase purity and product recovery can be difficult when compared to heterogeneous systems in which the catalyst can be filtered. This difficulty usually means homogeneous catalysts can be used only once; this fact discourages the use of homogeneous catalysts in large scale reactions unless the economic arguments and product are sufficiently complex and/or the processing technique can work around the inherent recovery and recyclability issues.

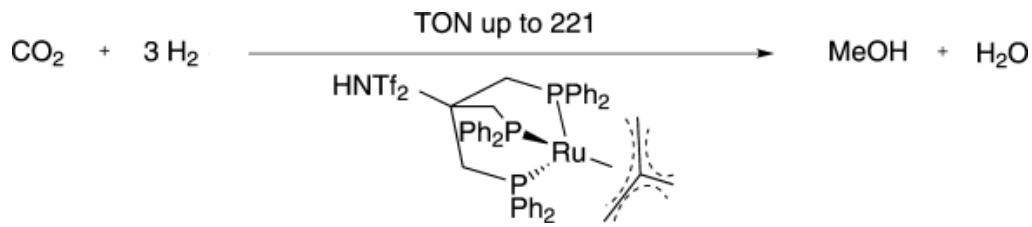


**Figure 2-2: Wesselbaum et. al. use a ruthenium-phosphine system to hydrogenate CO<sub>2</sub>. Catalyst was suspended in super-critical CO<sub>2</sub> with hydrogen gas to produce methanol in an autoclave at lower temperature and pressure conditions than currently utilised in industrial methanol production.**

Wesselbaum et al. (2014) used a homogeneous ruthenium-phosphine catalyst in the hydrogenation of supercritical carbon dioxide to methanol with TONs of up to 221 achieved (Figure 2-2). Experimentally this reaction was achieved with lower temperature and pressure conditions (140°C, autoclave pressurised at room temperature at 80 bar) than methanol's current syngas-derived industrial production (Goeppert et al., 2014) and could lead to more complex products in situ; however, this doesn't deal with the wider problem of catalyst removal.

#### **2.1.4 The Pros and Cons of Homogeneous and Heterogeneous Catalysts**

Table 2-1 Summarises the advantages (+) and disadvantages (-) of homogeneous and heterogeneous catalysts:

**Table 2-1 : The advantages (+) and disadvantages (-) of homogeneous and heterogeneous catalysts.**

Homogeneous	Heterogeneous
<b>high reactivity (+)</b>	(Usually) lower reactivity than homogeneous equivalents where applicable (-)
<b>Normally irrecoverable/non-recyclable, single use (-)</b>	Tend to be recoverable/recyclable, multi-use (+)
<b>More customisation (optical isomerisation, stereo/chemo-selective etc.), complexity adaptation (+)</b>	Normally limited complexity and customisation (e.g. bulk manufacture of non-specific isomers) (-)
<b>Trend towards expensive components/manufacturing processes of the catalyst (-)</b>	Comparatively inexpensive components/manufacturing process to get catalyst (+)
<b>Higher likelihood of contaminating the product, meaning more workup/resource requirements (-)</b>	Lower likelihood of contaminating the product; lower workup/resource requirements (+)

Catalyst technology has improved and delineated down the line of utility and the practical daily use, resulting in the advantages and disadvantages becoming more apparent. With the focus in recent decades in areas such as nanotechnology, process chemistry and chemical engineering there have been more inroads into blending the advantages of both systems whilst limiting the disadvantages.

### **2.1.5 Quasi-homogeneous Catalyst Systems**

If a particle size continuously decreases it will ultimately reach a moiety at either the molecular or the single-atom level; likely at this stage the catalyst will be present in the same phase as the substrate and can be considered homogeneous; but what if we could find a trade-off in which all possible routes

to for chemi-sorption for a particular substrate through which the desired reaction will become occur, whilst encumbering the catalyst sufficiently so as to bestow on it some of the desirable utility of a heterogeneous catalyst? if this has the effect of placing the catalyst in the same phase it can then be considered a homogeneous catalyst with all the benefits and drawbacks of such a system. At this periphery between these 2 classifications exists metal nanoparticles of sufficiently small size so as to have maximal surface area available to substrate (Astruc et al., 2005).

Whilst supported nanoparticle catalysts can suffer from reductions in rates there are many examples of progress towards new support structures and particle morphology modification to enable these to be more amenable to larger-scale process design (Moshfegh, 2009) incorporating unique design principles from magnetic nanoparticles (Mori and Yamashita, 2010; Mori and Yamashita, 2011) to polymer-stabilised dispersions of nanoparticles (Ohtaka et al., 2012); however, nanoparticles can suffer from problems associated with both heterogeneous and homogeneous catalysis including deactivation (Argyle and Bartholomew, 2015), active site obstruction as well separation issues due to their nanometer size (<100nm).

At bulk scale wherever possible, the process chemist will select a heterogeneous catalyst over a homogeneous one; the reduction in reactivity is offset against the lower likelihood of catalyst leaching into the product post work-up and the likely higher TON of the catalyst as a whole; however, there are usually limits to the types of reactions that such catalysts can be involved in.

Creating a catalyst system with high reactivity, capable of incorporating complexity into a product and able to be used in multiple runs of a reaction, increasing its overall turnover number, is a desirable research goal and the theme of many research groups, either by immobilising homogeneous catalysts or by introducing complexity to a heterogeneous catalyst system.

## 2.2 Other Catalyst Immobilisation/Recovery Strategies

There are many examples of immobilisation and complexation strategies for homogeneous catalysis that hope to increase their recyclability and amenability to pilot and plant scale process development; strategies include:

- Inclusion: incorporating a catalyst species within a foreign material such as an inorganic matrix whilst enabling free movement of the product.
- Association: non-covalent binding/tethering of a catalyst to a support through ionic or supramolecular bonding.
- Attachment: covalent binding/tethering of the homogeneous catalyst to a solid support, such as a resin.

Herein, we will present examples of each strategy followed by a discussion of the background to the current research and finally the foundation and risks associated with the current research problem and aims.

### 2.2.1 *Inclusion Catalyst Immobilisation Strategies*

Stasiak et al have also investigated embedding scandium triflate into polystyrene fibres for use in imino aldol and aza-Diels-Alder model reactions (Stasiak, Studer, et al., 2007; Stasiak, Röben, et al., 2007) (Figure 2-3).

The efficacy and recyclability of these catalysts could be modified by the application of a poly-p-xylylene (PPX) deposition scheme to the scandium salt/polystyrene fibres with changes in the amount of leaching experienced.

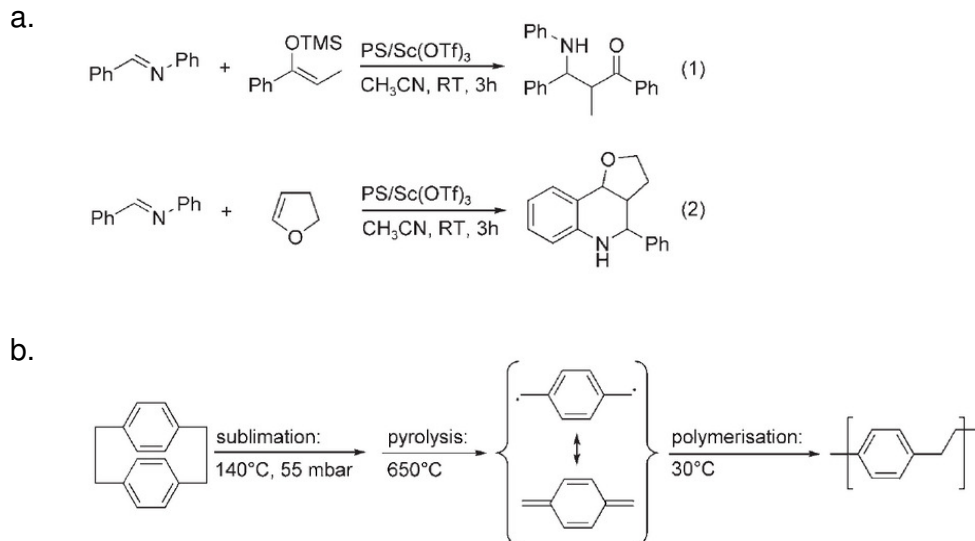


**Figure 2-3: Figures and graphs from the catalyst system from Stasiak *et. al.*: a.) Imino aldol and an aza-Diels-Alder model reaction systems; b.) poly-p-xylylene (PPX) deposition scheme.**

Pagliari *et al.* have reviews (Ciriminna *et al.*, 2011; Ciriminna *et al.*, 2013) and books (Pagliari, 2009) on organosilica catalyst strategies that present inclusion, association and attachment strategies. These illustrate an array of techniques from physically, covalently or ionically trapping catalyst materials within a sol-gel matrix.

Pagliari *et. al.* have looked at various sol-gel catalytic systems including that of the encapsulated ruthenium species tetra-n-propylammonium perruthenate (TPAP) in a sol-gel condensate of TMOS and alkyl trimethoxysilanes (Ciriminna and Pagliaro, 2003) (

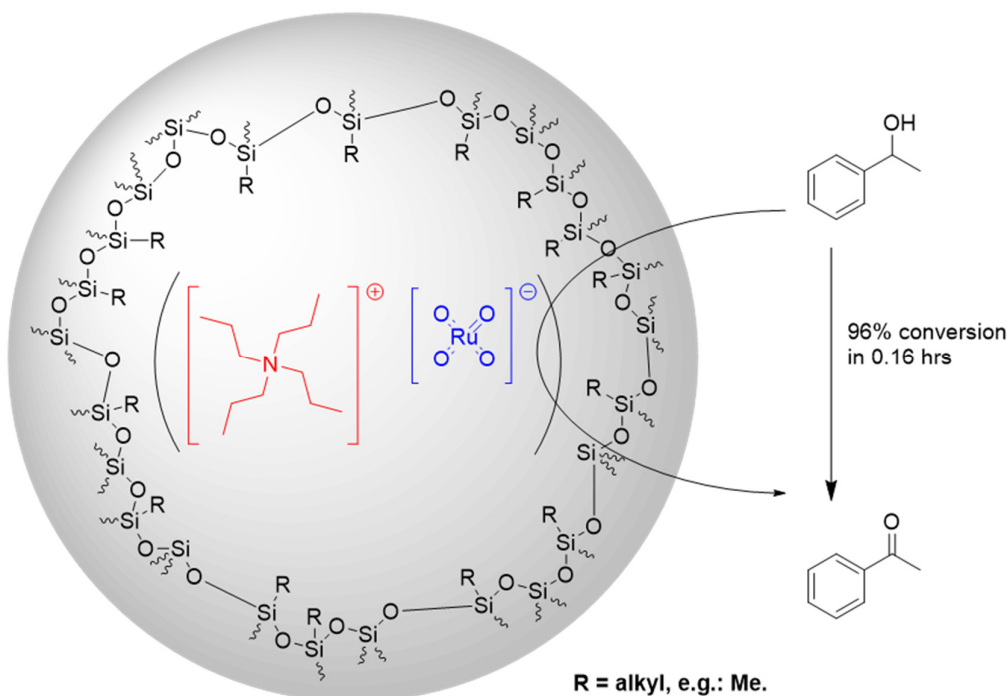


**Figure 2-4: TPAP@OrMoSil inclusion complex design principles, showing catalytic oxidation of benzaldehyde; a hydrophobic silane coupling agent is reacted with tetraethyl orthosilicate in the presence of TPAP to form porous silica particles with hydrophobic surface groups, encapsulating the catalyst but enabling reactant to pass through.**

A category of catalysts that have not been discussed due to their unique position straddling the heterogeneous and homogeneous barriers are enzymes; whilst there are well established methods for immobilising enzymes and proteins (Carette et al., 2007) for biocatalytic purposes (Engelmark Cassimjee et al., 2014) this is still a rich area of study with new techniques being demonstrated all the time; examples include encapsulation of laccase in silica colloidosomes (Zhang et al., 2013), encapsulation of amylase in latex particle-colloidosome with a  $\text{CaCO}_3$  “mortar” (Keen et al., 2014); Xu et al bridged the gap between inorganic/biological catalysis by combining amorphous ruthenium alloy particles and amyloglucosidase enzyme in an mesoporous silica matrix - this combination demonstrated a one-pot method for conversion of dextrin to sorbitol (Wu et al., 2011).

## 2.2.2 Association Catalyst Immobilisation Strategies

Takaya *et. al.* have created microgel core star polymers comprised of cross-polymerised methyl methacrylate (MMA), cross-linker ethylene glycol dimethacrylate and diphenyl-phosphinostyrene with the ruthenium salt  $\text{RuCl}_2(\text{PPh}_3)_3$  (Terashima *et al.*, 2007). This was observed to oxidise 1-phenylethanol to its corresponding ketone, acetophenone at high yield as well as an array of secondary alcohols with aromatic and aliphatic functionality (Terashima *et al.*, 2011). They demonstrated recyclability with no apparent loss in activity over 3 runs and no leaching or oxidation of the ruthenium-star complex over 3 runs at relatively low levels of ruthenium loading (1:1000 substrate) and a turnover frequency of up to  $320 \text{ h}^{-1}$ .

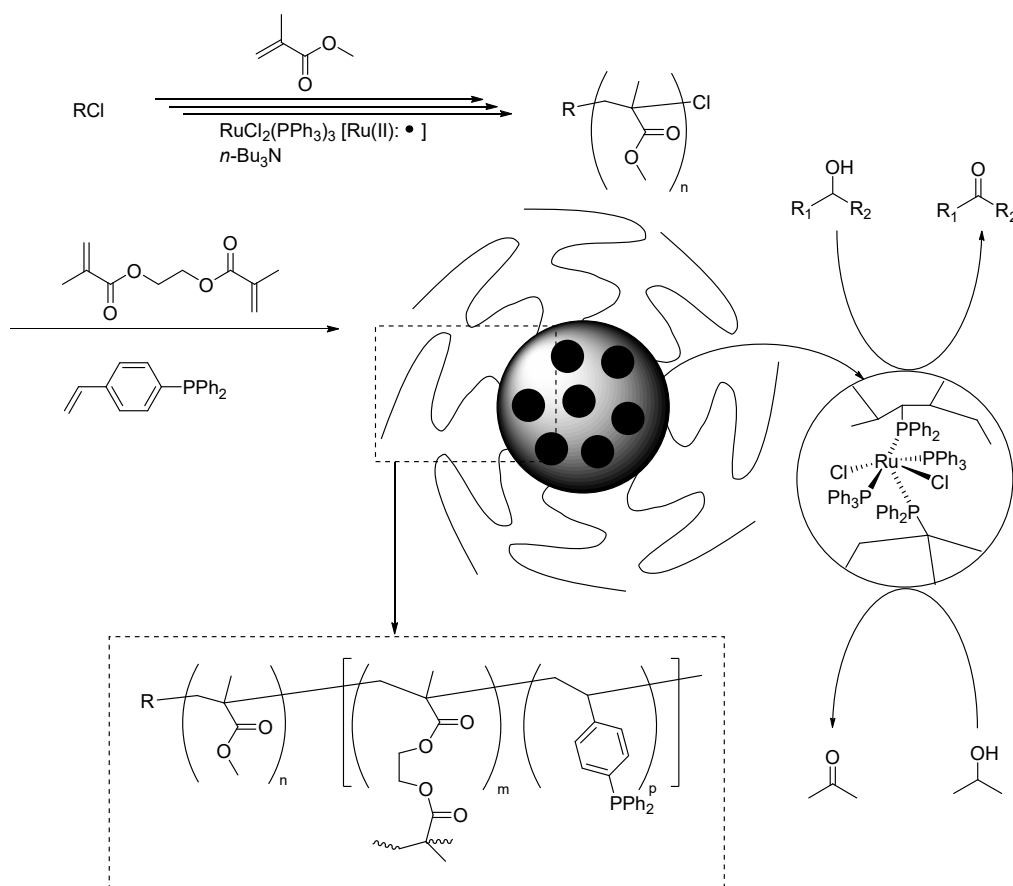


**Figure 2-5: Takaya *et. al.* cross-linked star polymer particles with diphenyl-phosphinostyrene functionality for the binding of ruthenium salts; core ruthenium-complexes oxidise secondary alcohols to ketones with an isopropanol feedstock.**

In a distinctively different strategy Wu *et. al.* manufactured a “tagged” (ammonium salt) organometallic ruthenium-arene complex which remained homogeneous in the asymmetric hydrogenation of 2-methylquinoline but could then be removed by adding magnetic nanoparticles functionalised with crown-8 which formed a reversible complex that could be removed and reactivated for additional runs (Wu *et al.*, 2011). This maintained high conversion and enantioselectivity even after 4 cycles but over activity was low (16 hours to completion at 15°C), not to mention the secondary labour and material intensive procedure for catalyst removal.

Pandarus and Pagliaro *et. al.* have also looked at the organometallic-functionalisation of silica particles in several reviews on the subject (Pagliaro *et al.*, 2009; Pandarus *et al.*, 2013; Ciriminna *et al.*, 2013); palladium-organometallic systems featuring diphenylphosphine (DPP) and sulphur ligand systems have been used in Suzuki coupling reactions (Figure 2-6b and c).

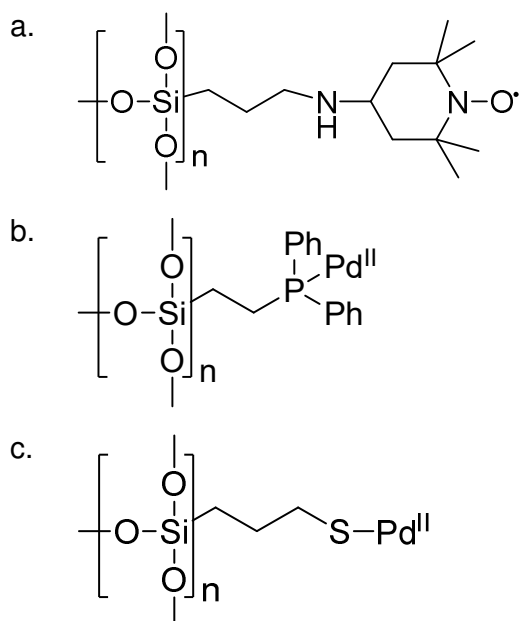


**Figure 2-6: Pandarus and Pagliaro *et. al.* SiliaCat catalyst systems. a) SiliaCat TEMPO new oxidizing catalyst for oxidation of alcohols or aldehydes ; b) SiliaCat DPP-Pd used for Suzuki/Heck reactions. c) SiliaCat S-Pd used for Suzuki/Heck reactions.**

### 2.2.3 Attachment Catalyst Immobilisation Strategies

Dickerson et al have reviewed several approaches using soluble mono-methoxy-terminated polyethylene glycol polymer scaffolds for an array of reactions ranging from asymmetric transfer-hydrogenations to Sharpless AD reactions; these ranged bound complexes ranging from bis(phosphine) ruthenium complexes for hydrogenation to chiral (salen)-Mn complexes for epoxidation reactions. The polymer was easily extracted by adding methanol and water (Dickerson et al., 2002).

Outside of traditional organic-based catalysts such as enzymes we have also seen the emergence of organocatalysts; Schmidt *et al* have demonstrated their asymmetric hydrogenation using a polymer network of thiophene-functionalized binaphthyl phosphoric acids (Schmidt et al., 2014).

Moore *et. al.* have designed a novel MacMillan organocatalysts-functionalised monomer (**M1**, Figure 2-7) that was polymerised with diethylene glycol methyl ether methacrylate (DEGMA) to form linear polymeric materials that could be used in a Diels-Alder reaction between cyclopentadiene and *trans*-hexen-1-al; this could be recycled through several runs by extraction of product from the polymer/MeOH/H<sub>2</sub>O solution into organic solvent in a “pseudo-continuous method” (Moore et al., 2013).

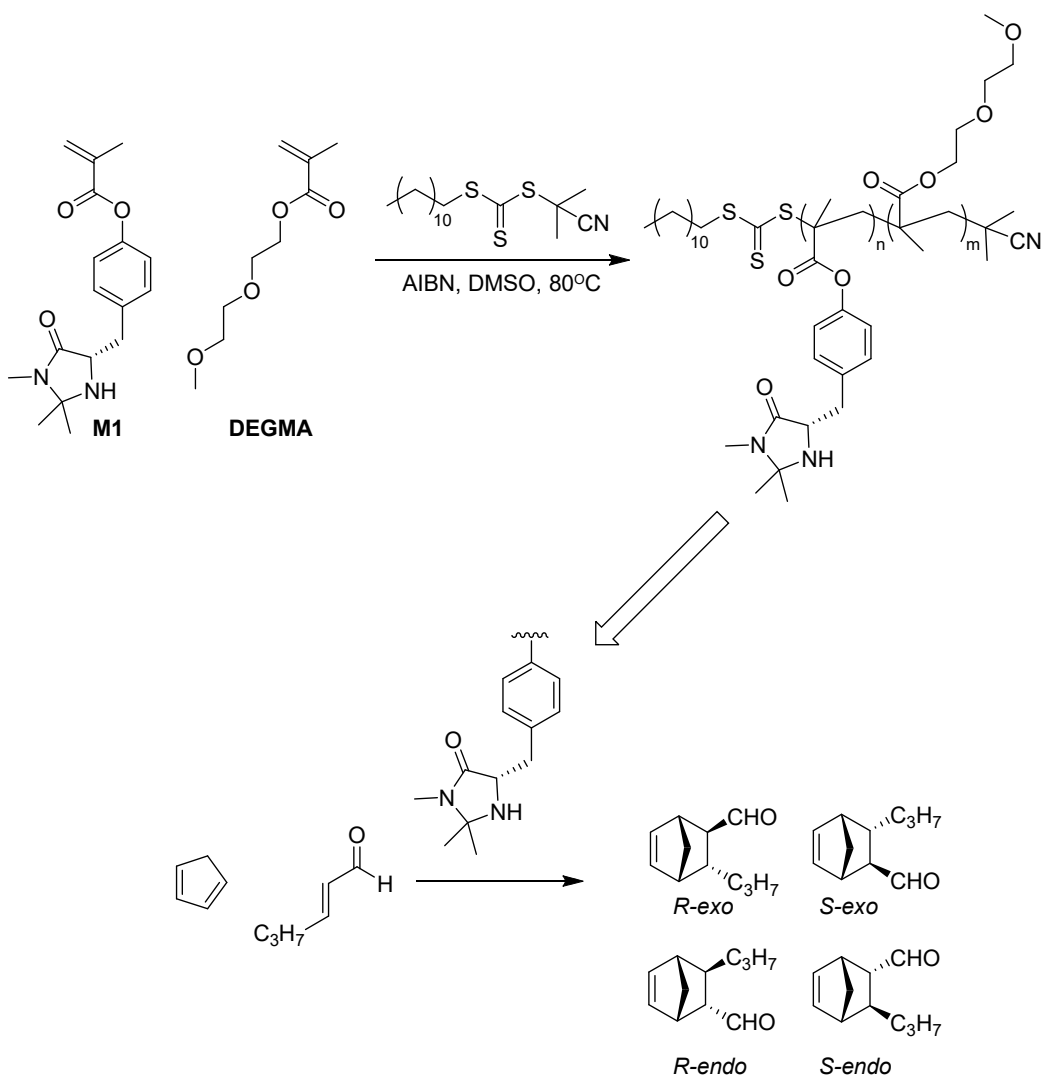


**Figure 2-7: Moore et. al. MacMillan recyclable polymer organocatalysts; the *R-endo*-enantiomer was the predicted favourite (overall enantioselectivity: 74-80% ee for major product, yield: >70% for all cycles)**

They went further with **M1** by incorporating it into polymeric core-shell nanogels featuring hydrophobic cores (Moore et al., 2014); these exhibited a “hydrophobic/concentrator effect” and similar traits in terms of conversion and enantioselectivity as TONs between 5-24. O’Reilly and Lu explored the concept of “nanoreactors” in a review on the subject (Lu and O’Reilly, 2013).

Elsewhere we see organo-modified silica networks of amines capable of catalysing aldol condensation (Brunelli, Didas, et al., 2012). Pandarus and Pagliaro *et. al.* have also looked at the organofunctionalisation and organometallic-functionalization of silica particles in several reviews on the

subject (Pagliaro et al., 2009; Pandarus et al., 2013; Ciriminna et al., 2013); in addition to nanoparticulate incorporation they have also incorporated a 2,2,6,6-tetramethylpiperidine-1-oxyl nitroxyl (TEMPO) radical species which can engage in selective oxidation reactions (Michaud et al., 2007) (Figure 2-6a).

The breadth and scope of techniques employed underlines the general trend towards greener catalyst chemistry and processing (Luo et al., 2004; Busacca et al., 2011).

### **2.3 Background To The Current Research**

Iridium, a non-terrestrial transition metal in the platinum group (Becker, 2002), has a long, storied history going back several decades in catalysis with the discovery of several organometallic variants showed diverging reaction mechanisms (Crabtree, 1979). Initial work showed the iridium analog of Wilkinson's Catalyst,  $\text{IrCl}(\text{PPh}_3)_3$ , failed to engage in catalytic hydrogenation in the same way as its rhodium variant; however, advances in ligand development showed it had strongly directing properties for diastereoselectivity in catalyzed reactions such as hydrogenation (Andersson, 2011). This was expanded to other reactions such as allylic substitution (Madrahimov et al., 2009) and 1,3 dipolar cycloadditions (Carmona et al., 2007).

#### **2.3.1 Hydrogenation: mass transfer limitations**

In conventional hydrogenation reactions low solubility of hydrogen leads to a scarcity of hydrogen at the catalyst surface leading to inefficiencies in the mass transfer to the desired compound; this is overcome with high temperatures and pressures of hydrogen and inert atmospheres in heterogeneously catalysed reactions.

It has been demonstrated by Singh et al that careful modification of the reactor and catalyst makeup can have a positive effect on hydrogenation of soy bean oil (Singh et al., 2011); in their experiment they used a metal-sputtered polymeric fluid bed through which hydrogen gas was bubbled through, similar to fluidised bed reactor design (Werther et al., 2014), utilised elsewhere to improve a multitude of reactor technologies (Ayyadurai et al., 1988).

To do away with the more complex and problematic aspects of hydrogenation whilst overcoming issues associated with mass transfer is an area of significant research and development.

### **2.3.2 Iridium and transfer-hydrogenation catalysts**

Transfer-hydrogenation is the process by which a molecule of hydrogen is transferred from a feedstock compound (i.e. isopropanol, forming acetone) to a recipient compound (i.e. benzaldehyde); it has been shown that some platinum-group metals, such as iridium and ruthenium, converted to organometallic compounds are capable of performing this type of reaction. Whilst not as atom efficient as direct combination of molecular hydrogen to a recipient compound the significantly milder and safer conditions to that of conventional hydrogenation and the potential degree of control that can be exerted in terms of enantioselectivity and yield make this an active field of study.

Using these types of catalyst Li *et al.* demonstrated asymmetric transfer hydrogenation of ketones in water (2006). Wu *et al.* demonstrated hydrogenation of N-heterocycles (2013) and hydrogenation of imines (2014). Talwar *et al.* used cyclometalated iridium compounds in reductive amination of ketones to primary amines using ammonium formate as both the nitrogen and hydrogen source (2014). Similar catalysts and activity has been reported by Campos *et al.* (2014), alongside novel uses in CO<sub>2</sub> fixation and water oxidation in flow systems (Wesselbaum *et al.*, 2014; Sheehan *et al.*, 2015). Iridium is therefore a versatile candidate for an array of useful chemical reactions and potentially a useful green catalyst, if we can overcome limitations such as the ability to recycle and reuse.

### 2.3.3 Cp\* Immobilized Catalysts

Lucas *et al.* demonstrated a method for immobilising hydroxyl tethered iridium-rhodium complexes onto Wang resin (Lucas *et al.*, 2013), a solid, polymeric resin developed for use in solid-state synthesis of peptides (Wang, 1973). The synthesis of this catalyst can be seen in Figure 1-1. The group demonstrated the effective and recyclable use of the immobilised IrCp\* complex in the transfer hydrogenation of benzaldehyde up to 25 runs, at an effective catalyst concentration of 0.3 mol%/reaction (Figure 1-2), as well as determined the effect of chain-length variability in its reactivity, namely that a longer tether (C14) was more reactive than the shorter (C5).

The novel iridium organometallic is leach-resistant in part due to the stability of the  $\eta^5$ -cyclopentadienyl ligand system; bonding is fluxional across the whole 5-membered ring, preventing it from completely dissociating. The changing hapticity of the ligand system through the course of a reaction and how it accommodates alternate ligands is important for the transition state needed for effective transfer hydrogenation; however, as Sherborne *et al.* demonstrated, it also leads to the replacement of chloride ion ligands attached to the iridium with alkoxide ions and the gradual deactivation of the catalyst (2015). This explained observations made by Lucas *et al.* that there was no observed leaching of the iridium whilst an eventual reduction in efficacy across multiple runs. It is thought to be due to the subsequent precatalyst formation with an alkoxide ligand exchange with a chloride, activating the catalyst initially, but ultimately deactivating the catalyst with a second chloride/alkoxy exchange forming the potassium alkoxide-iridate species which is non-catalytic.

## 2.4 Research Direction

As described in the next chapter, the project aimed at creating and characterizing organically modified silica particles with an array of different tethering systems; initially, we looked at silica-core particles with amine groups at the surface for organometallic iridium attachment (discussed in Chapter 5). We then looked to building “upward”; the core-silica was coated in chain-transfer agent so that polymer could be grown from the silica surface, colloquially known as a “polymer brush”. The initial attempts at polymer brushes and improvements are discussed in Chapters 6 and 7 respectively.

## 3 Areas of Study

### 3.1 Project Aims

The wider goal of my thesis was to investigate new materials for the “loading” of catalytic species to improve recyclability, efficacy in comparison to the heterogeneous species and manipulation of the end species to improve its adaptability. By better understanding and manipulating the surface chemistry of the parent particle it was hoped improvements to, or at least control of, the efficacy of the catalysis could be demonstrated.

### 3.2 Organically Modified Silicas (OrMoSils)

#### 3.2.1 Silica

By itself silica is a useful starting point for investigation as a potential scaffold material, due to its long history of links with organic synthesis and purification; its synthesis and properties can be manipulated to form an array of structures and functionalized compounds with relative ease (Stöber et al., 1968; Schmidt, 1992; Ng et al., 1995; Tudor and O’Hare, 1997; Zhuravlev, 2000; Alvaro et al., 2004; Soleimani Dorcheh and Abbasi, 2008; Schmidt et al., 2014). There have been many examples and methods established for using organosilica and organometallic silica compounds (Satterfield and N, 1991; Macquarrie et al., 2002; Bautista et al., 2006; Mori et al., 2008; Pagliaro et al., 2009; Kuschel et al., 2010; Brunelli, Venkatasubbaiah, et al., 2012; Kluwer et al., 2013; Li et al., 2014). With readily controllable surface chemistry and properties as well as a benign interaction with many solvents and reaction conditions it makes an ideal starter point.

#### 3.2.2 Silane Coupling Agents (SCAs)

Silane coupling agents (SCAs) are compounds whose molecules contain functional groups that bond with both organic and inorganic materials. At their core they consist of a carbon-silicon bond with reactive leaving groups on the silicon atom capable of exchanging and condensing it to an inorganic surface, such as a ceramic or silicate material like glass or silica particles. The organic component can be varied so that it was an array of functional groups capable bonding covalently or through intermolecular forces such as hydrogen bonding

or electrostatic interactions (Brunel et al., 2000). Both elements of the silane coupling agent can be modified to affect the degree of bonding and parameters.

### 3.2.3 Organically Modified Silicas: Design Principles

To this end we initially focused on building organically modified silica particles (OrMoSils) with a view to functionalizing the organic surface coating with catalyst (Figure 3-1).

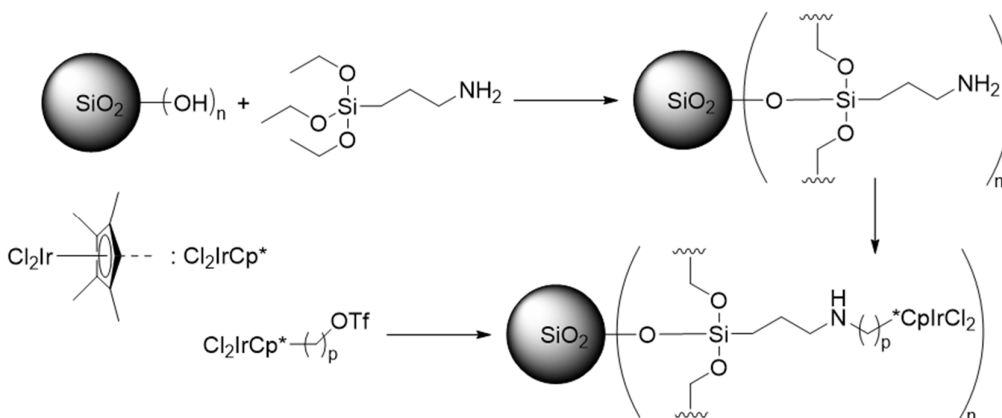


**Figure 3-1: Simplified scheme for addition of IrCp\* to silica via the triflation mechanism.**

This theme's methodology is developed in Chapter 4 and the results in Chapter 5; however, the surface constraints associated with a simple silica particle proved insufficient for the required catalyst loading so Brush Polymers, with a silica core, and polymers grown from the organic coating on it, became the primary focus.



growth in molecular weight is retarded by continual exchange of the chain-transfer moiety and the availability of monomer is reduced significantly. This technique enables very precise control of the polymer weight and polydispersity index (PDI) reported at or below 1.1 (Chiefari et al., 1998).

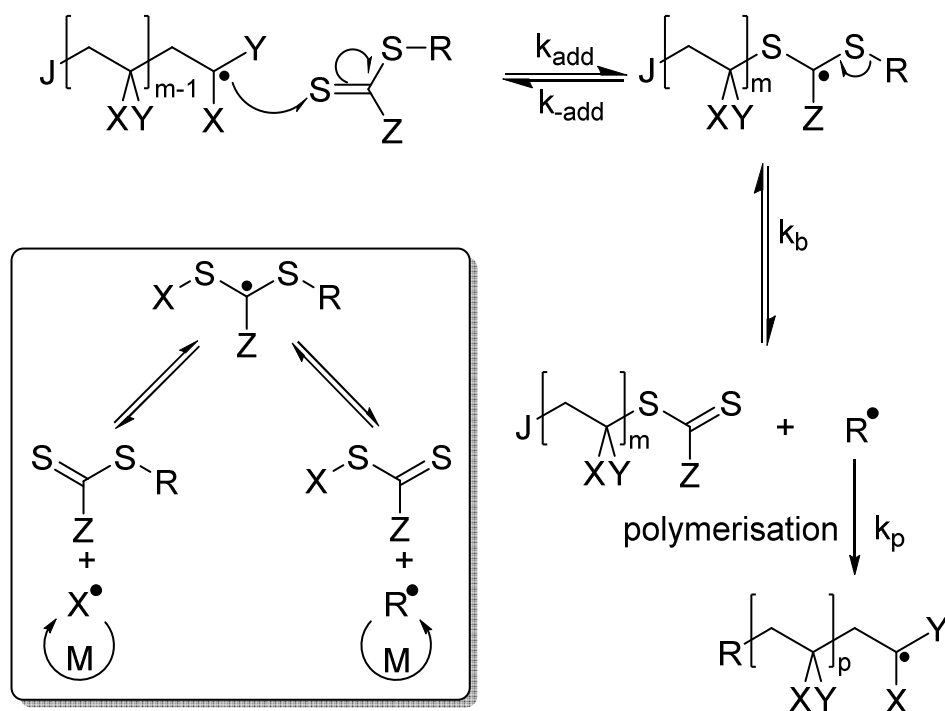


**Figure 3-3: The RAFT Chain Transfer Mechanism: the core of all RAFT chain-transfer agents (CTAs) is the thiocarbonylthio moiety [ZC(=S)SR]; this groups forms a radical species which controls the growth of polymer chains until they reach an equilibrium where the growth in molecular weight is retarded by continual exchange of the chain-transfer moiety and the availability of monomer is reduced significantly.**

Another useful feature of RAFT polymerization is that the thiocarbonylthio moiety is retained at the end of the process; it should be possible then to isolate the manufactured polymer and change the conditions and monomer for further polymerisation; it is feasible to generate block co-polymers with divergent properties and behaviours. Semsarilar et al demonstrated the power of this technique through the preparation of AB and ABC block copolymers of poly(methacrylic acid)-poly(benzyl methacrylate) (PMAA-PBzMA) and the same with a 2,2,2-trifluoroethyl methacrylate (TFEMA) block respectively (2014). This versatility has found uses in the development of novel architectures

such as star polymers and dendrimers (Chiefari et al., 1998; Gregory and Stenzel, 2012); more importantly it has proven possible to create polymer architectures which can interact with other materials such as gold nanoparticles (Feng et al., 2013), latex nanoparticles (Semsarilar et al., 2014), cotton and fabrics (Perrier et al., 2004) and silica nanoparticles (C. Li et al., 2006; Ohno et al., 2011; Gao et al., 2013).

### **3.3.2 RAFT on Silica**

Combination RAFT-SCA agents are a good example of combining the techniques of living radical polymerisation with “click-chemistry” (Kolb et al., 2001), click-chemical reactions being a broad term for simple, high-yielding “spring-loaded” chemical reactions with easily removed wastes and solvents. Several groups have synthesized combination RAFT-SCA agents, demonstrating several approaches to pre- and post-functionalization of both moieties via:

- Condensation to an inorganic particle such as silica or iron oxide via the silane coupling agent moiety.
- Polymerisation with an array of monomers via the RAFT moiety.

The Perrier group have illustrated several techniques for the combination of RAFT-SCA and RAFT-Polymer-SCA agents to silica particle and polymer growth (Moraes et al., 2013):

#### **3.3.2.1 Grafting To**

Polymer chains are grown on the RAFT-SCA agents and the finished polymer-SCA can be condensed to the silica particle; in this method the coupling reaction needs to be highly efficient to overcome steric hindrance inherent in solvated polymer chains – Ranjan and Brittain utilised the click-chemical reaction between an azide-functionalised OrMoSil and a RAFT polymerized polystyrene and polyacrylamides with an alkyne termination to achieve a high density polymer brush particle (2007). Huang *et al.* created a RAFT agent with a trimethoxysilane end-group which they subsequently polymerized to and attached to a silica particle, albeit with a lower chain density than Ranjan and Brittain (Huang et al., 2009).

The above literature examples are sometimes referred to as “sequential” techniques as they first involves a polymerization step followed by a coating step (as opposed to the reverse process of the *grafting from* methodology); another approach entirely is known as the “Z-group” approach –the RAFT agent is attached by the Z-group to the particle; Perrier et al showed that this technique eliminates the need for free RAFT agent (Perrier et al., 2005), but creates subsequent hurdles for block-copolymerization were a second block to be added.

### 3.3.2.2 *Grafting From*

Using conventional techniques like nitroxide-mediated (NMP) and atom-transfer radical-polymerisation (ATRP) techniques equates to binding an initiator to the silica surface; this potentially places constraints on the conditions used to couple the initiator to the surface; however, using the RAFT approach the CTA agent can be attached to the surface via the SCA and the polymer grown from the surface. Tsujii *et al.* pioneered the use of grafting-from RAFT agents on silica, first attaching an oligomeric polystyrene group to the silica particle using conventional ATRP, then post-functionalising it with a RAFT agent and growing a further styrene block to it (2001). Simplification and improvements in versatility and synthesis were made by Ohno et al in which the RAFT-SCA synthesised could be applied to the silica particle direct and grown using conventional RAFT polymerisation techniques (Figure 3-4, Ohno et al., 2011). In both the earlier Tsujii and later Ohno papers it was identified that a free RAFT agent (route 2 in Figure 3-4) used in conjunction with the bound-RAFT agent significantly increased the control over polymerisation; this is because free RAFT agent in solution allows a more efficient exchange between surface bound radicals and free (where the Z-group wasn't an OrMoSil surface) chains, resulting in better polydispersity and grafted chain yield. Post-modification of the brush-polymer particle with a biomarker tag, intravenous injection into a tumor-bearing mouse and particle accumulation and identification at the tumour site was also demonstrated (Ohno et al., 2012).

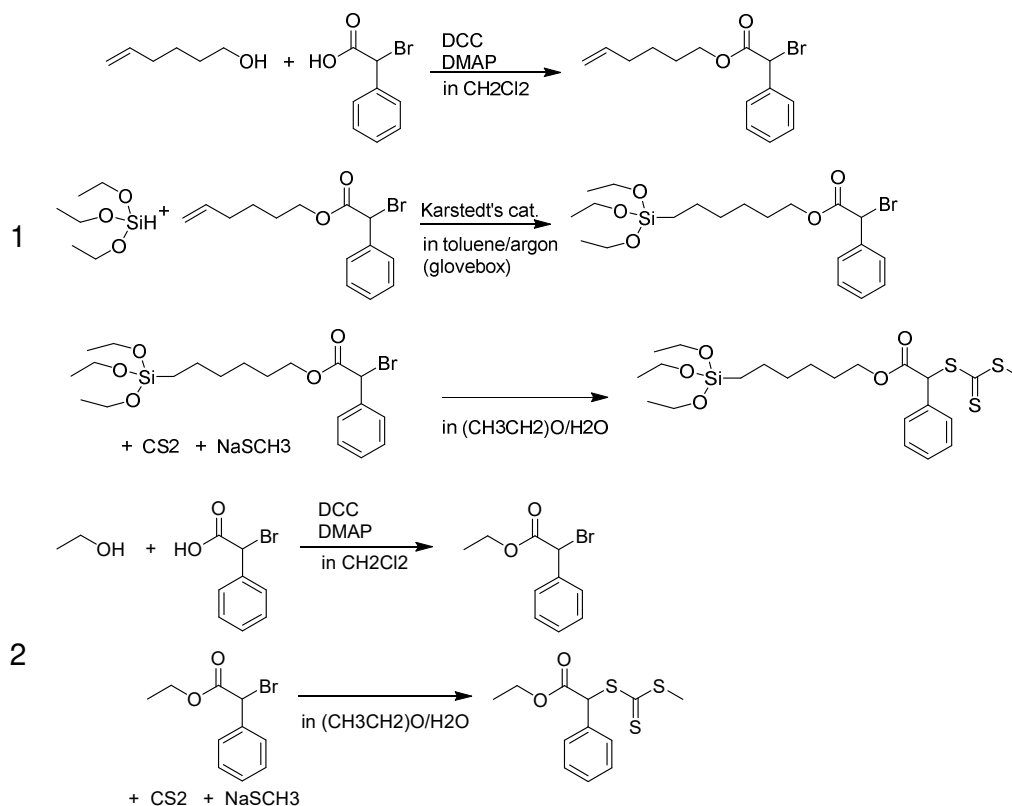


**Figure 3-4: Synthesis Route for RAFT-SCA (EHT, Scheme 1) and free-RAFT agent used (ECPMT, Scheme 2)**

Li and Benicewicz reported synthesis and attachment of a RAFT-SCA to SiPs and growth of a di-block copolymer of styrene and n-butyl acrylate (Li and Brian C. Benicewicz, 2005). A kinetics study in which the RAFT agent was attached to an amine-bearing OrMoSil demonstrated growth of poly-(methyl methacrylate) (pMMA) and polystyrene (pS) demonstrated greater control than would be apparent with just free RAFT agent (C. Li et al., 2006); subsequent work on block-copolymer-grafted SiP nanoparticles demonstrated significant improvements in the ductility, tensile-toughness and modulus values in treated epoxy Bisphenol A diglycidyl ether (DGEBA) resins (Gao et al., 2012, 2013).

### 3.3.3 Brush Polymers via CTA-SCA compounds: Design Principles

The limited loading potential and attachment efficiency of IrCp\* complex led us to build “upwards”: the synthesis of silane coupling agents (SCAs) attached to chain-transfer agents (CTA-SCA) made up of Reversible Addition-Fragmentation chain Transfer (RAFT) agents was attempted and subsequently attached to the silica surface of the 250nm silica particle (CTA-SiPs).

Following this, polymer growth using methyl methacrylate (MMA) as a test material, and glycidyl methacrylate (GMA) to create bound-polymer was then tried in the presence of these CTA-SiPs (Figure 3-5), and if successful to attach an amine-functionalized IrCp\* to the pGMA-SiP via epoxide ring-opening of its R-group.

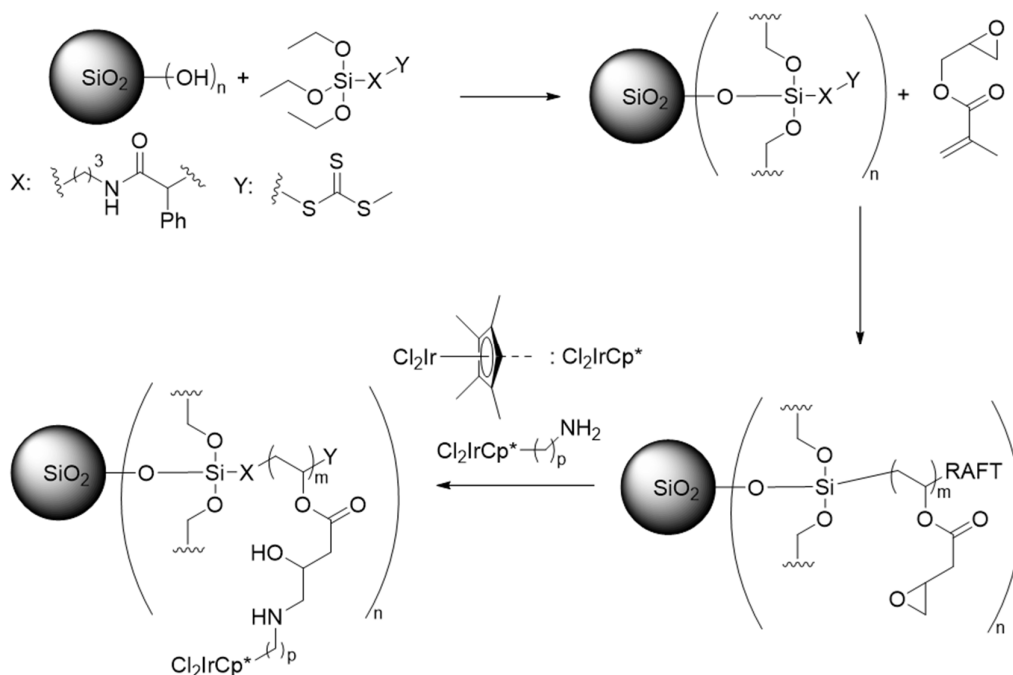


**Figure 3-5: Simplified reaction scheme leading to supported IrCp\* catalyst via a RAFT-grown pGMA brush particle with a silica core: A reversible addition-fragmentation chain-transfer (RAFT) agent is attached to a silane coupling agent (SCA) to form a combination CTA-SCA. This in turn is condensed to the silica particle (CTA-SiP) to enable polymer brush growth from the particle surface. Glycidyl methacrylate (GMA) can then be grown in the presence of the CTA-SiP. The poly(glycidyl methacrylate), contains an epoxy ring through which our IrCp\*Cl<sub>2</sub> group, in this instance functionalized with an amine tether, can attach via epoxy-ring opening.**

The first generation of CTA-SiPs ran into 2 issues:

1. The condensation of the CTA-SCA onto the silica particle (SiP) resulted in significant loss of the active CTA-moiety, resulting in limited subsequent polymer growth when polymerized with methyl methacrylate in the testing phase.
2. Glycidyl methacrylate proceeded to form a gel in the presence of silica, which prevented extraction of the solid material from the free polymer and solution.

A new approach to Brush Polymers was sought in the form of creating oligomeric silane coupling agents via RAFT polymerization which had the combined use of making a “stickier” silane compound and an incorporated chain-transfer agent added at condensation.

### 3.3.4 Brush Polymers via CTA-active SCA oligomers: Design Principles

Methacryloxypropyl trimethoxysilane (MAPTMS) was polymerized using a chain-transfer agent to form a short-chain oligomer with the RAFT agent incorporated into it. This was then condensed to the silica surface. Polymerization with hydroxypropyl methacrylate (HPMA) was attempted at the silica surface.

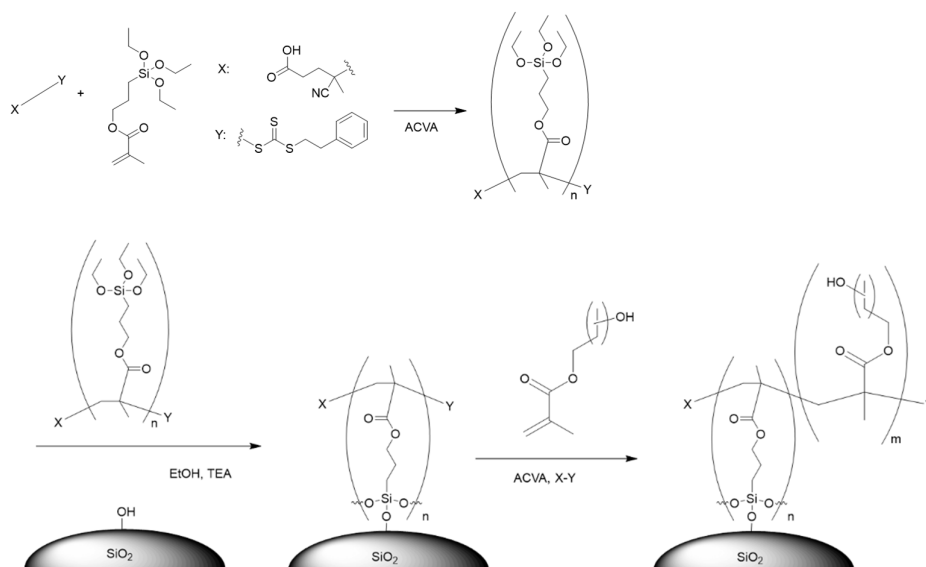


**Figure 3-6: The simplified route to synthesis of oligomeric**

Several areas of control were evaluated and the output characterized at multiple stages above, and ultimately an attempt at organometallic iridium attachment via the hydroxyl R-group.

### 3.4 Other Routes Investigated.

#### 3.4.1 Latex Nanoparticles

Latex nanoparticles, consisting of charged surface polymer anchored into a polystyrene/latex core formed using aqueous emulsion polymerization of styrene with diblock copolymers (Ganeva et al., 2007; Hunter and Armes, 2020), was first looked at as a potential scaffold system for its potential to form self-assembled spheres, “worms” and vesicles with a functionalised anchor-polymer that could be adjusted and modified to meet a wide array of needs in catalyst support-development. Initially latex nanoparticles, consisting of block-copolymers of polyacrylic acid and poly(glycidyl methacrylate (PAA/PGMA) attached to a block of poly(trifluoroethyl methacrylate) (pTFEMA), anchored into a polystyrene/latex core, were investigated to determine how much organometallic iridium could be anchored onto the functionalised coating polymer surface (via glycidyl-initiated epoxide opening, following the proposed scheme in Figure 3-7).

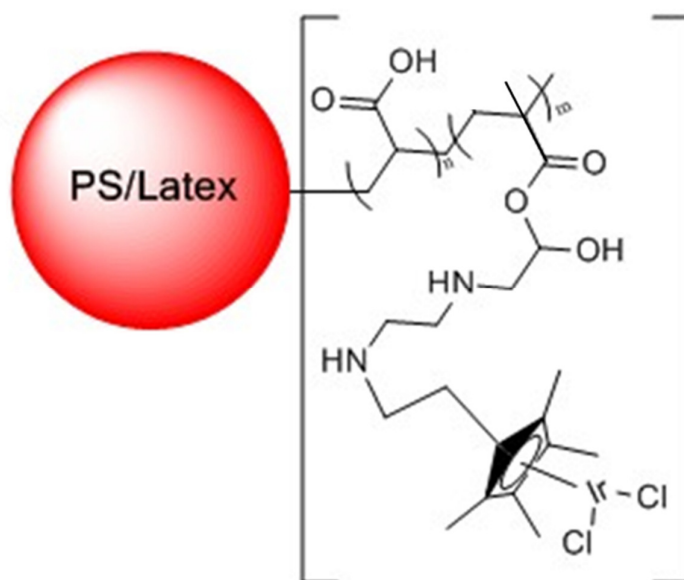


**Figure 3-7: Proposed scheme for attaching IrCp\* moieties to PS/Latex nanoparticles.**

However, difficulties in effectively resolving the exact amount of available chemical moieties on the latex surface, and the availability of methods of analysis for resolving this issue with OrMoSils and the ensuing brush polymer development, resulted in efforts being directed towards this goal.

### 3.4.2 *Electrospinning*

Electrospinning is used to generate a non-woven web of nanofibers. High voltage electricity is applied to a liquid solution of polymer (in this case cellulose acetate, or CA) and a collector, which lets the solution extrude from a nozzle forming a jet of polymer that is deposited on the collector as nanofibers. It was hoped that these fibres could be reacted with organometallic iridium via triflation to form functionalized catalytic “fibres”.

However, many of the early attempts to create CA fibers that could be dried and suspended in anhydrous solvents for the triflation process proved to be insufficiently robust to withstand the conditions presented; efforts were already well ahead in developing effective mechanisms for the creation of improved brush polymers.

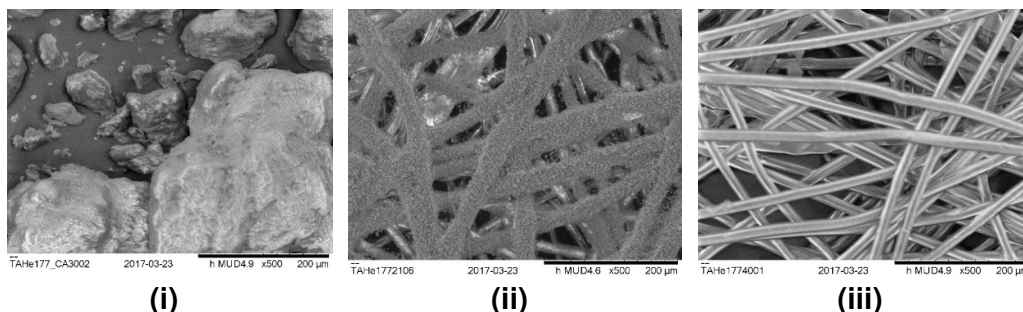


**Figure 3-8: SEM images of (i). cellulose acetate powder; (ii). Electrospun cellulose-acetate coated fibres; (iii). Free fibre used in the deposition process with CA. SEM was done using a Hitachi TM3030 Bench Top SEM. A solution of CA was prepared as a 7.5w/v% in a mixture of DMF, treated with 0.1w/v% lithium bromide, ethanol and acetone<sup>1</sup>.**

<sup>1</sup> At a ratio of 2:1:1. CA was dissolved in this mixture with mild agitation at 60°C for one hour until fully dissolved.

## 4 Materials and Methodology

### 4.1 Materials

The following components used in RAFT-agent synthesis were used as supplied unless otherwise indicated in the reaction scheme: Sodium methanethiolate (Sigma Aldrich, CAS Number: 5188-07-8); carbon disulphide (Sigma Aldrich, CAS Number: 75-15-0); DL- $\alpha$ -Bromophenylacetic acid (ACROS Organics, 97%, CAS Number: 4870-65-9); 2-Phenylethanethiol (Sigma Aldrich, CAS Number: 4410-99-5); Sodium Hydride (60% in oil, ACROS Organics, CAS Number : 7646-69-7); Solid iodine (ACROSS Organics, CAS: 7553-56-2); 4,4'-azobis(4-cyanopentanoic acid) (ACVA, 98%, Sigma Aldrich, CAS Number: 2638-94-0); N-(3-Dimethylaminopropyl)-N'-ethylcarbodiimide hydrochloride (EDC.HCl, Sigma Aldrich, CAS Number: 25952-53-8); 1-Hydroxybenzotriazole (HOBt, Sigma Aldrich, CAS Number: 123333-53-9); Hydrochloric acid (fuming HCl, Merck, 37% HCl, CAS (water): 7732-18-5, (HCl): 7647-01-0), Sodium hydroxide (reagent grade, >98%): CAS Number 1310-73-2. Solvent grades, unless otherwise stated, are ACS reagent grade.

250nm.d Silica particles were gifted to me from the Cayre Group and used throughout when referring to silica particles (AngstromSphere, CAS Number: 7631-86-9)

1-(5-hydroxypentyl)-2,3,4,5-tetramethylcyclopentadiene (Cp\*) was gifted to me by the Blacker group research team and used as presented.

Hydrochloric acid and sodium hydroxide solutions were prepared from the following diluted to specification with Milli-Q water.

Water used in these experiments was purified Millipore Milli-Q water (18.2 M  $\Omega$  cm resistivity at 25°C).

## 4.2 Characterization Methods

### 4.2.1 *Transmission electron microscopy (TEM)*

Samples were analyzed using a FEI Tecnai TF20 with a field emission transmission gun electron microscopy (FEGTEM) operating at 200kV fitted with a HAADF detector and Gatan Orius SC600A CCD camera. All samples were dispersed in acetone before being deposited on a TEM grid (carbon film, 400 Cu Mesh from Agar Scientific) and allowed to dry. ImageJ software was used to determine particle and coating sizes.

### 4.2.2 *Scanning electron microscopy (SEM)*

Samples were analyzed using a Hitachi SU8230 scanning electron microscope (SEM) operating at 15kV. EDX elemental mapping was employed using the associated module for this. Dried samples were applied to a carbon film and a sputter coat of gold was applied analysis under vacuum.

Rapid imaging of microcapsules were also attained using a Hitachi TM3030 Tabletop SEM at 15kV using carbon film under normal observation conditions.

### 4.2.3 *UV-Vis spectroscopy*

Trithiocarbonate consumption was analyzed with a Perkin Elmer Lambda 950 UV-Vis spectrophotometer in order to detect characteristic peaks for monomer consumption (210nm) and RAFT agent (300nm). All samples were analyzed in the 190-800nm range.

### 4.2.4 *Fluorescence Spectroscopy*

Fluorescamine assays were conducted using a Horiba FluoroMax-3 Fluorimeter using the excitation spectra for aminated fluorescamine (390nm) and recording the emission spectra (487nm) (Castell et al., 1979). Calibration standards of fluorescamine and propyl amine were used to determine the amine content at the silica surface.

### 4.2.5 *NMR spectroscopy*

<sup>1</sup>H-NMR spectra were recorded on a Bruker DPX 300 spectrometer or a Bruker Avance 500 spectrometer. Unless otherwise stated all samples were dissolved in deuterated chloroform-D (CDCl<sub>3</sub>, 99.8 atom % D) containing 1% v/v tetramethylsilane (TMS, as reference material).

#### **4.2.6 FTIR spectroscopy**

Infrared spectra were collected using a Perkin Elmer Spectrum 100 FTIR equipped with a diamond attenuated total reflectance (ATR) module, and where indicated in the text, a Bruker FTIR Spectrometer with an ATR module. Both spectrometers used an average of 32 scans per spectrum.

#### **4.2.7 Dynamic Light Scattering and Zeta Potential Measurement**

Dynamic Light Scattering (DLS) and Zeta Potential Measurements were collected using a Zetasizer Nano ZS. DLS samples were collected in an array of dispersion media using a glass cuvette. Zeta potential measurements were collected using a zeta potential cuvette with samples in aqueous media of variable pH.

#### **4.2.8 Size Exclusion Chromatography**

Initially a SEC-HPLC set up was used to ascertain free-polymer weight and is described below; near the end of my thesis a SEC-GPC was introduced to the lab and samples were taken on this.

##### **4.2.8.1 Size Exclusion Chromatography (SEC)-High Performance Liquid Chromatography (HPLC) (SEC-HPLC)**

Size Exclusion Chromatography-High Performance Liquid Chromatography (SEC-HPLC) analysis for the determination of molecular weight of polymers was conducted using a Perkin Elmer Series 200 HPLC suite. Sample size was determined using a Phenomenex Phenogel 5 $\mu$ M 100A column and a guard column. The HPLC eluent used was THF. The polymer concentration was typically 1% w/w and a series of PS calibration standards with weight ranges between the weights of 900 and 75,000g mol<sup>-1</sup> were used to determine weight range. Chromatograms were analyzed using the Perkin-Elmer HPLC-SEC software.

##### **4.2.8.2 Size Exclusion Chromatography (SEC)-Gel Permeation Chromatography (SEC-GPC)**

Size Exclusion Chromatography-Gel Permeation Chromatography (SEC-GPC) analysis for the determination of number-average molecular weight ( $M_n$ ), weight average ( $M_w$ ) and polydispersity of an array of pHPMA polymers. The

instrument set-up comprised two Agilent PL gel 5 $\mu$ m Mixed-C columns and a guard column connected in series to an Agilent 1260 Infinity GPC system operating at 60°C. The GPC eluent was HPLC-grade DMF containing a 10mmol Lithium Bromide. The polymer concentration was typically 1% w/w and a series of pMMA calibration standards with weight ranges between the weights of 1,080 and 1,020,000g mol<sup>-1</sup> were used to determine weight range. Chromatograms were analyzed using Agilent GPC-SEC software.

#### **4.2.9 Thermogravimetric Analysis**

Thermogravimetric analysis was obtained using a Mettler Toledo TGA-DSC1 set up. The system was set up with a nitrogen atmosphere and samples were prepared in alumina crucibles. Sample and crucible weights were determined using an ultrafine balance capable of measuring milligram weights down to 4 d.p. Protocol design and set up is discussed in Chapters 6 and 7. Analysis was conducted using the Mettler Toledo software suite.

### **4.3 RAFT agent synthesis**

#### **4.3.1 Synthesis of Mono-methyl trithio-2-phenylacetic acid (MMTPAA)**

The reaction scheme for MMTPAA is presented in Figure 4-1. It was suggested as an initial, easy to make RAFT agent capable of demonstrating controlled-polymerization for methacrylate monomers produced using the synthesis method laid out by Gottharddt et al (1979).

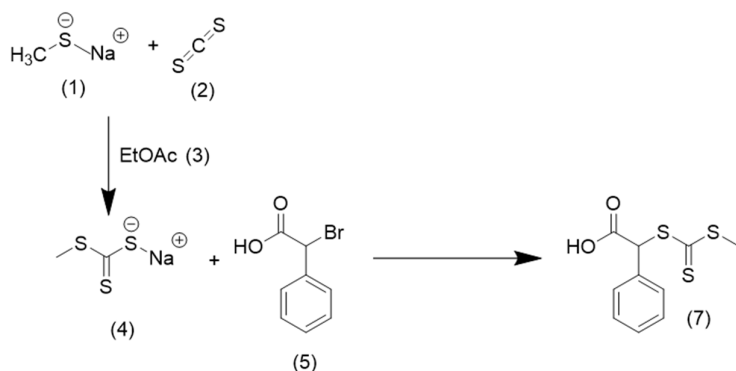


**Figure 4-1: Reaction scheme for MMTCAA: Sodium methanthiolate (1) in a solution of ethyl acetate (3) was placed under nitrogen. To this carbon disulphide (2) in ethyl acetate (20mL) was added slowly before the mixture is left to stir for 2 hours. The yellow precipitation was evaporated before being re-suspended in ethyl acetate, yielding a white precipitate and yellow solution; the suspension was passed through celite to remove the precipitate was washed with additional ethyl acetate. To this DL- $\alpha$ -Bromophenylacetic acid (5) was added slowly before the ethyl acetate solution was washed with saturated NaHCO<sub>3</sub> solution. The dried, filtered and evaporated oil was triturated with petroleum ether and recrystallized in a 1:1 mix of petroleum ether and benzene to produce a yellow solid**

Synthesis was as follows: Sodium methanthiolate (1, 5g, 71.33mmols) in a solution of ethyl acetate (3, ACS reagent grade, 70mL) was degassed with nitrogen. Then carbon disulphide (3, 5.97g, 78.46mmol) in ethyl acetate (20mL) was added slowly to avoid an exotherm (temperature rises 20-25°C) before the mixture was left to stir for 2 hours. The subsequent cloudy, yellow suspension was evaporated before being re-suspended in ethyl acetate, yielding a white precipitate and yellow solution; the suspension was passed through celite to remove the precipitate, which was washed with additional ethyl acetate. Then DL- $\alpha$ -Bromophenylacetic acid (12.27g, 57.06mmols) was added slowly before the ethyl acetate solution was washed with saturated NaHCO<sub>3</sub> solution. The crude solution was dried (Na<sub>2</sub>SO<sub>4</sub>), filtered and rotovapped to oil, which was triturated with petroleum ether (40-60°C) and recrystallized in a ~1:1 mix of petroleum ether and benzene to produce a yellow solid (10.01g, 38.7mmol, 67% yield). Melting point: 116-118°C; <sup>1</sup>H-NMR (*Avanche* 500MHz, CDCl<sub>3</sub>, 298K):  $\delta$  (ppm) = 2.78 (s, 3H, -CH<sub>3</sub>), 5.89 (s, 1H, Ph-H), 7.42 (m, 5H, aromatic).

### 4.3.2 Synthesis of 4-cyano-4-(2-phenylethane sulfanylthiocarbonyl) sulfanylpentanoic acid (PETTC)

PETTC was prepared as per the literature synthesis method (Jones et al., 2012; Penfold et al., 2017) and can be seen in Figure 4-2:

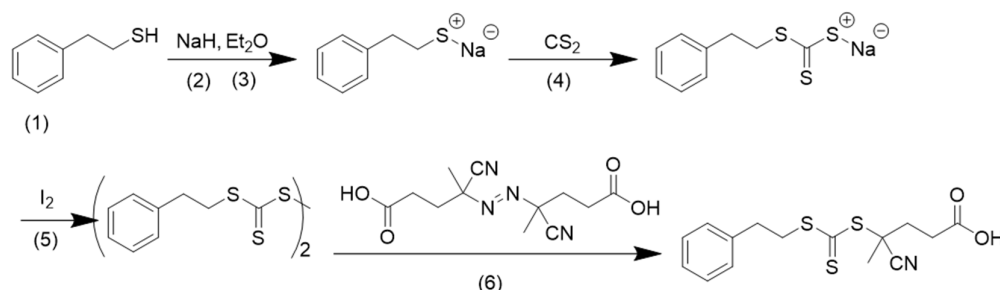


**Figure 4-2: Reaction Scheme for PETTC synthesis: 2-Phenylethanethiol (1) was added to a suspension of sodium hydride (2) in diethyl ether (3). The reaction mixture was cooled and carbon disulfide (4) was added to produce sodium 2-phenylethanetrithiocarbonate, which was collected by filtration. Solid iodine (5) was gradually added to the suspension in diethyl ether. This reaction mixture was then stirred and the insoluble white precipitate of sodium iodide was removed by filtration. The yellow–brown filtrate was washed with an aqueous solution of sodium thiosulfate to remove excess iodine, dried over sodium sulfate, and then rotovapped to yield bis(2-phenylethanesulfanylthiocarbonyl) disulfide. A solution of 4,4'-azobis(4-cyanopentanoic acid) (6) and bis(2-phenylethane sulfanylthiocarbonyl) disulfide in ethyl acetate was degassed and heated to reflux under a dry nitrogen atmosphere for 18 h. The crude was evaporated, before being dissolved in ethyl acetate, washed with water, saturated brine solution, then dried, filtered and rotovapped. The crude product was recrystallized in a minimum of ethyl acetate before being cooled to -20°C overnight, then evaporated under high-vacuum to a waxy solid**

Synthesis was conducted as follows: 2-Phenylethanethiol (**1**, 10g, 72.34mmol) was gradually added over 10 min to a stirred suspension of sodium hydride (60% in oil) (**2**, 2.894g, 72.35mmol) in diethyl ether (**3**, 150 mL) at between 5 and 10 °C. Vigorous evolution of hydrogen gas was observed, and the grayish suspension was slowly transformed into a white viscous slurry of sodium phenylethanethiolate over 30 min. The reaction mixture was cooled to 0 °C (using an acetone/ice bath), and carbon disulfide (**4**, 5.5g, 72.34mmol) was gradually added to produce a thick yellow precipitate of sodium 2-phenylethanetrithiocarbonate, which was collected by filtration after 30 min and

subsequently used in the next step without further purification. Solid iodine (**5**, 9.37g, 0.369mol) was gradually added to the suspension in diethyl ether (100 mL). This reaction mixture was then stirred at room temperature for 1 h, and the insoluble white precipitate of sodium iodide was removed by filtration. The yellow–brown filtrate was washed with an aqueous solution of sodium thiosulfate to remove excess iodine, dried over sodium sulfate, and then rotovapped to yield bis(2-phenylethanesulfanylthiocarbonyl) disulfide (~100% yield). A solution of 4,4'-azobis(4-cyanopentanoic acid) (ACVA) (**6**, 11.02g, 32.23mmol) and bis(2-phenylethane sulfanylthiocarbonyl) disulfide (2.13 g, 0.005 mol) in ethyl acetate (50 mL) was degassed by nitrogen bubbling and heated at reflux under a dry nitrogen atmosphere for 18 h. After removal of the volatiles under vacuum, the crude product was dissolved in ethyl acetate, washed with water (3 x 50 mL), then with a saturated brine solution (50mL), before being dried (Na<sub>2</sub>SO<sub>4</sub>), filtered and rotovapped. The crude product was recrystallized in a minimum of ethyl acetate before being cooled to -20°C overnight, this was then evaporated under high-vacuum to a waxy solid (7.88g, 23.20mmol). <sup>1</sup>H-NMR (*Avanche* 500MHz, CDCl<sub>3</sub>, 298K): δ (ppm) = 1.87 (3H, –CH<sub>3</sub>), 2.36–2.65 (m, 2H, –CH<sub>2</sub>), 2.68 (t, 2H, –CH<sub>2</sub>), 3.00 (t, 2H, –CH<sub>2</sub>), 3.54 (t, 2H, –CH<sub>2</sub>), 7.17–7.32 (m, 5H, aromatic).

#### **4.3.3 Attachment of MMTPAA to APTES**

The reaction scheme for MMTPAA-APTES amide coupling is as presented in Figure 4-3. Isolation of the combined silane coupling agent-chain-transfer agent (SCA-CTA) is discussed in Chapter 5 but proved difficult to characterize, so the SCA-CTA was used as follows: APTES (**1**, 0.91mL, 3.87mmol), MMTPAA (**2**, 1g, 3.87mmol), EDCI.HCl (**3**, 0.89g, 4.65mmol) and HOBt (**4**, 0.59g, 3.87mmol) were combined in DMF (10mL) and stirred. The reaction is monitored using TLC (ethyl acetate w 1%vol acetic acid) and once the MMTPAA peak has disappeared the reaction mixture is immediately transferred into the dispersed silica (Section 4.4.2).



**Figure 4-3: Reaction scheme for MMTCAA-APTES amide coupling:** APTES, MMTCAA, EDCI.HCl, and HOBT were combined in DMF and stirred. The reaction is monitored using TLC and once the MMTCAA peak has disappeared the reaction mixture is immediately transferred into the dispersed silica.

#### 4.3.4 Oligomerization of PETTC onto MAPTMS.

The reaction scheme for oligomerization of MAPTMS and PETTC to create oligo-MAPTMS functionalized with PETTC (*o*PETTC-SCA) can be seen in Figure 4-4. Use of the isolated *o*PETTC-SCA was discussed and investigated in Chapter 7 but was deemed unnecessary, so the iterations typically followed this route: methacryloxypropyl-trimethoxysilane (MAPTMS, 1mL, 4.21mmol) was dissolved in ethanol (1mL) with 4-cyano-4-(2-phenylethanesulfanylthiocarbonyl) sulfanylpentanoic acid (PETTC, 0.286g, 0.84mmol), and initiator 4,4'-Azobis(4-cyanopentanoic acid) (ACVA, 0.014g, 0.084mmol) before the solution was sparged with nitrogen gas. The mixture was then heated for 3-7 hours before being quenched in an ice bath before being used for silica condensation (Section 4.4.3.)

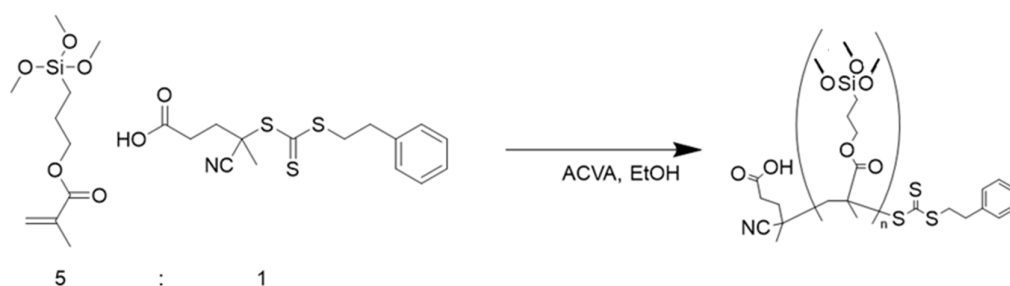


**Figure 4-4: Oligomerization of PETTC with MAPTMS:** Methacryloxypropyl-trimethoxysilane was dissolved in ethanol with 4-cyano-4-(2-phenylethanesulfanylthiocarbonyl) sulfanylpentanoic acid (PETTC), and initiator 4,4'-Azobis(4-cyanopentanoic acid) (ACVA) before the solution was sparged with nitrogen gas. The mixture was then heated under nitrogen for 3 hours before being quenched in an ice bath before being used for silica condensation.

#### 4.4 Methodology: Organofunctionalisation of Silica

Specifics for attachment of various organic components are discussed per each Chapter:

##### 4.4.1 Chapter 5: Condensation of APTES to silica to create Organically Modified Silicas (OrMoSils)

Condensation of silica was determined in Section 5.2.1 in Chapter 5 from several mechanisms as a probe into condensation of 3-aminopropyl triethoxysilane (APTES). Typically silica was dispersed mechanically in ethanol (at a ratio of 1:50 g silica/mL ethanol) for 10 minutes before APTES was added as per the experiment requirement. The molar ratio between APTES, with 3 silane groups, to the silica surface hydroxyl groups, Si-OH, was based on condensation occurring to 3 silylic acid groups per 1 APTES, so the molar ratio of APTES is always measured as a multiple or fraction of 1 APTES molecule per 3 silylic acid groups (3x Si-OH, Figure 4-5). The dispersed silica and APTES was then stirred at room temperature for 24 hours before being collected and centrifuged at 3000rpm for 5 minutes, and solvent exchanged with fresh ethanol. This was repeated 3 times then repeated 3 times more in water, before the solid precipitate was dried in a vacuum oven overnight at 80°C.

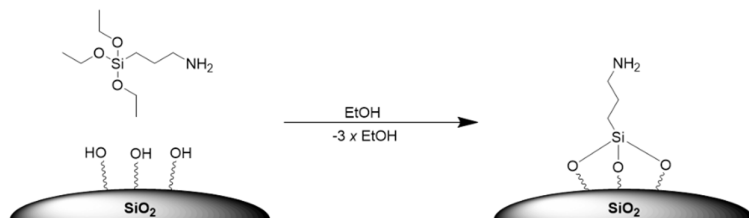


**Figure 4-5: APTES condensation onto silica in ethanol, showing presumed condensation parameters of 3 silylic acid moieties to one APTES molecule. Typically silica was dispersed mechanically in ethanol for 10 minutes before APTES was added. The dispersed silica and APTES was then stirred at room temperature for 24 hours before being collected and centrifuged at 3000rpm for 5 minutes, and solvent exchanged with fresh ethanol. This was repeated 3 times, then repeated 3 times more in water, before the solid precipitate was dried in a vacuum oven overnight at 80°C.**

#### 4.4.2 Chapter 6: Condensation of SCA-CTA to silica to create CTA-functionalised Organically Modified Silicas (OrMoSils)

Typically, silica was dispersed mechanically in toluene or ethanol (at a ratio of 1:50 g silica/mL solvent) for 10 minutes before the recovered crude SCA-CTA oil in DMF was added in excess to the silica surface hydroxyl groups, at a 1:1 molar ratio is 1 SCA-CTA to 1 silylic acid groups (1x Si-OH, Figure 4-6). The dispersed silica and SCA-CTA was then refluxed at 90°C for 18 hours before being centrifuged at 10,000rpm for 10 minutes, and solvent exchanged with fresh ethanol. This was repeated 3 times then repeated before the solid precipitate, the CTA-SiP, was dried in a vacuum oven overnight at 25°C<sup>2</sup>.

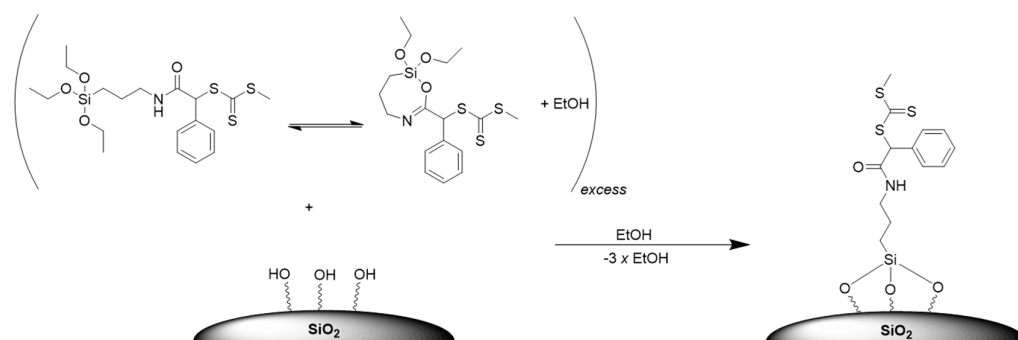


**Figure 4-6: Typically, silica was dispersed mechanically in toluene or ethanol for 10 minutes before the recovered crude SCA-CTA oil was added in excess to the silica surface hydroxyl groups. The dispersed silica and SCA-CTA was then refluxed at 90°C for 18 hours before being centrifuged at 10,000rpm for 10 minutes, and solvent exchanged with fresh ethanol. This was repeated 3 times then repeated before the solid precipitate was dried in a vacuum oven overnight at 25°C.**

#### 4.4.3 Chapter 7: Condensation of oligo-SCA-CTA to silica to create oCTA-functionalised Organically Modified Silicas (OrMoSils)

Typically, silica was dispersed mechanically in ethanol (at a ratio of 1:40 g silica/mL solvent) for 10 minutes before the recovered crude SCA-CTA oil in ethanol (at a ratio of 1:20 g SCA-CTA/mL solvent) was added to the dispersed silica (Figure 4-7) along with trimethylamine (TEA, molar ratio of 18:1 moles<sub>TEA</sub>/moles<sub>SiOH</sub>) before being sparged with nitrogen. Under nitrogen, the mixture was refluxed at 80-90°C for 18-24 hours before being centrifuged at

<sup>2</sup> Originally dried at 80°C; however, sample had likely decomposed based on the smell and the failed tranche of experiments.

10,000rpm for 10 minutes, and solvent exchanged with fresh ethanol. This was repeated 4 times then once with water before the solid precipitate, the *o*PETTC-SiP, was dried in a vacuum oven overnight at 50°C.

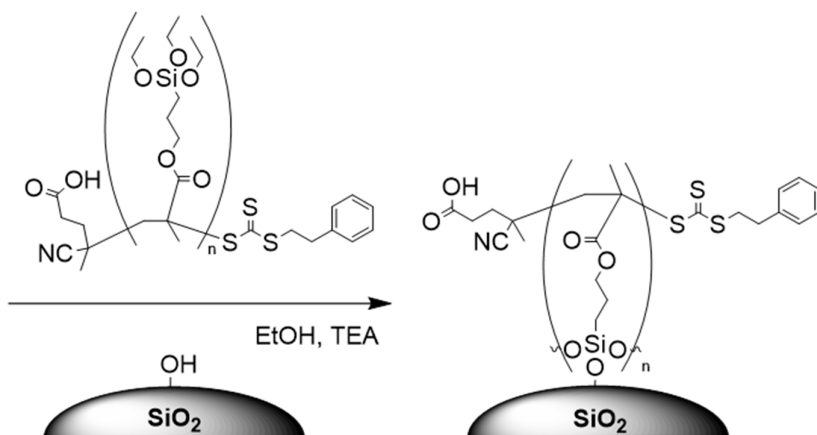


**Figure 4-7:** Typically, silica was dispersed mechanically in ethanol for 10 minutes before the recovered crude SCA-CTA oil in ethanol was added along with trimethylamine before being sparged with nitrogen. Under nitrogen, the mixture was refluxed at 80-90°C for 18-24 hours before being centrifuged at 10,000rpm for 10 minutes, and solvent exchanged with fresh ethanol. This was repeated 4 times then once with water before the solid precipitate was dried in a vacuum oven overnight at 50°C.

#### 4.5 Methodology: Free and Brush Polymerization

##### 4.5.1 Brush polymerization: polymer growth onto the CTA-SiP

Polymerization of monomer in the presence of CTA-SiP was typically carried out in the following fashion: CTA-SiP (**1**, 40-50mg) is mechanically dispersed in DMF (**4**, up to 10mL). The methacrylate monomer (**3**, glycidyl or methyl methacrylate, 10.0mmol), MMTPAA (**3**, 0.10mmol) and AIBN (**3**, 0.01mmol) are added, the mixture was sealed and sparged with nitrogen for 10 minutes. The mixture is then kept under nitrogen and heated to 65°C for a set hold time dependent on the experiment. The mixture is then cooled and the solid centrifuged at 8000rpm for 10 minutes, decanted and repeated with fresh ethanol and re-dispersed 3 times, before being dried in a vacuum oven.

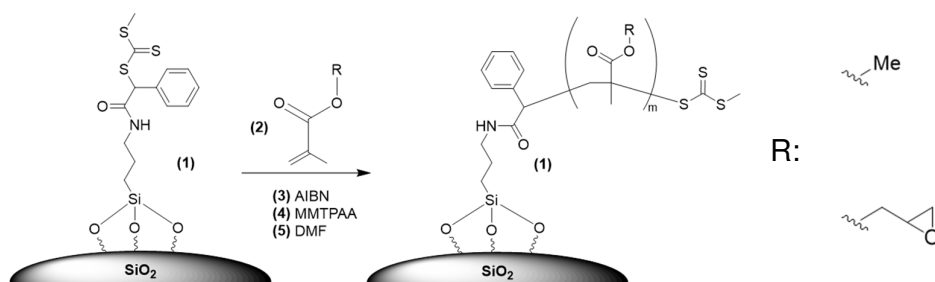


**Figure 4-8:** CTA-SiP (1) is mechanically dispersed in DMF (2). The methacrylate monomer (2, glycidyl or methyl methacrylate), MMTCAA (3) and AIBN (4) are added, the mixture was sealed and sparged with nitrogen for 10 minutes. The mixture is then kept under nitrogen and heated to 65°C for a set hold time dependent on the experiment. The mixture is then cooled and the solid centrifuged at 8000rpm for 10 minutes, decanted and repeated with fresh ethanol and re-dispersed 3 times, before being dried in a vacuum oven.

#### 4.5.2 Brush polymerization 2.0: polymer growth onto the oPETTC-SiP

Polymerization of monomer in the presence of oPETTC-SiP was typically carried out in the following fashion: oPETTC-SiP (1, 150mg) is dispersed in ethanol (15mL) solvent. Hydroxypropyl methacrylate (2, 4.22mL, 31.21mmol), PETTC (3, 106.0mg, 0.312mmol) and ACVA (4, 11.7mg, 0.03mmol) are added, the mixture sealed and sparged with nitrogen for 10 minutes. The mixture is then kept under nitrogen and heated to 70°C for a set hold time dependent on the experiment. The mixture is then cooled and the solid centrifuged at 8000rpm for 10 minutes, decanted and repeated with fresh ethanol and re-dispersed 3 times, before being dried in a vacuum oven.

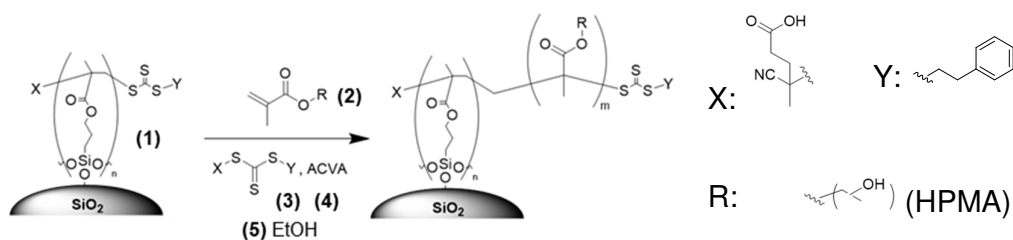


**Figure 4-9:** oPETTC-SiP (1) is dispersed in ethanol (15mL) solvent. Hydroxypropyl methacrylate (2), PETTC (3) and ACVA (4) are added, the mixture sealed and sparged with nitrogen for 10 minutes. The mixture is then kept under nitrogen and heated to 70°C for a set hold time dependent on the experiment. The mixture is then cooled and the solid centrifuged at 8000rpm for 10 minutes, decanted and repeated with fresh ethanol and re-dispersed 3 times, before being dried in a vacuum oven.

## 4.6 Catalyst synthesis & attachment

### 4.6.1 Iridium Cyclopentadienyl complex synthesis

The IrCp\*Cl<sub>2</sub> complex was prepared as per the literature method (Lucas et al., 2013). The scheme for it can be seen in Figure 4-10:

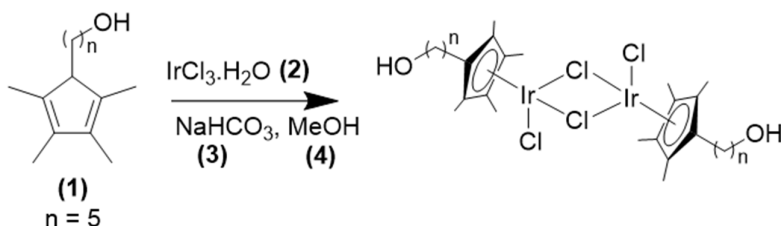


**Figure 4-10: Synthesis of IrCp\*Cl<sub>2</sub>.** Under a nitrogen atmosphere, iridium trichloride hydrate (2) and sodium bicarbonate (3) were added to degassed methanol (4) in a 10ml capacity microwave tube and the suspension was sparged with nitrogen for 10 minutes. After adding 1-(5-hydroxypentyl)-2,3,4,5-tetramethylcyclopentadiene (1), the suspension was sparged for a further 5 minutes. The tube was then sealed and microwave heating was applied at 150°C for 10 minutes. After effervescence from the solution had subsided, the tube was opened and the solution was diluted with DCM, washed with water, brine, dried over Na<sub>2</sub>SO<sub>4</sub> and the solvent removed using a rotary. The resulting oily red residue was dissolved in DCM, precipitated with hexane and left overnight in a fridge-freezer to yield an orange powder.

Under a nitrogen atmosphere, iridium trichloride hydrate (2, 0.10g, 0.28mmol) and sodium bicarbonate (3, 0.02g, 0.24mmol) were added to degassed methanol (4, 3ml) in a 10ml capacity microwave tube and the suspension was sparged with nitrogen for 10 minutes. After adding 1-(5-hydroxypentyl)-2,3,4,5-tetramethylcyclopentadiene (1, 0.118g, 0.57mmol), the suspension was sparged for a further 5 minutes. The tube was then sealed and microwave heating was applied at 150°C for 10 minutes. After effervescence from the solution had subsided, the tube was opened and the solution was diluted with DCM (20 ml), washed with water (10 ml), brine (10 ml), dried over Na<sub>2</sub>SO<sub>4</sub> and the solvent rotovapped. The resulting oily red residue was dissolved in DCM, precipitated with hexane and left overnight in a fridge-freezer to yield an orange powder (0.20g, 0.21mmol, 75%). <sup>1</sup>H NMR (300 MHz, CDCl<sub>3</sub>, 298K) δ (ppm) = 3.64 (t, 4H, 2 × CH<sub>2</sub>OH), 2.12 (t, 4H, -CH<sub>2</sub>-), 1.72-1.51 (m, 12H, 6 × CH<sub>2</sub>), 1.61 (s, 12H, 8 × CH<sub>3</sub>).

## 4.6.2 Triflation of IrCp\* complex, in-situ attachment

### 4.6.2.1 Triflation step of IrCp\* complex.

The IrCp\*Cl<sub>2</sub> complex was prepared as per the literature method (Lucas et al., 2013). The scheme for it can be seen in Figure 4-11:

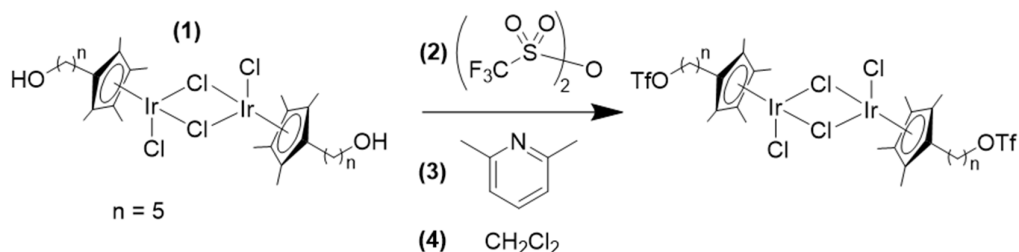


**Figure 4-11: Triflation of IrCp\*Cl<sub>2</sub>: Under nitrogen, a solution of 2,6-Lutidine (3) in dichloromethane (4) was added to trifluoromethanesulfonic anhydride (2) in dichloromethane at -10°C. A solution of (1) in dichloromethane was slowly added over 30 minutes. After stirring for 2 hours the solution was rotovapped to dryness under vacuum before being used immediately in the attachment step.**

Under nitrogen, a solution of 2,6-Lutidine (3, 0.45ml, 3.84mmol) in dichloromethane (4, 2ml) was added to trifluoromethanesulfonic anhydride (2, 0.32 ml, 1.92mmol) in dichloromethane (2ml) at -10°C (dry ice/methanol). A solution of 1 (0.20 g, 0.21mmol) in dichloromethane (2.2 ml) was slowly added over 30 minutes. After stirring for 2 hours the solution was rotovapped to dryness under vacuum before being used immediately in the attachment step.

### 4.6.2.2 Attachment of the triflated Iridium complex, {IrCp\*-Tf}.

In all instances using triflated iridium complex the following step was undertaken in preparation: under nitrogen, the dry, triflated IrCp\* complex was dissolved in fresh, anhydrous dichloromethane. This was added to a solution of the material it was being added to, and the conditions for each instance can be seen in Table 4-1. It was added at a 1.1x excess to whatever moiety it was being attached to, whether amino-group on APTES, or hydropropyl-methacrylate R-group.

**Table 4-1: Conditions for attachment of the triflated iridium complex in each instance of its use, including the Chapter/Section it can be found.**

---

**Chapter    Conditions****Section #**

**5.4A**      The AP-SiP was solvent-exchanged into anhydrous toluene (99.8%) with several repeat washings before being agitated. To this, under nitrogen, the triflated iridium complex in dichloromethane was added and stirred for 22 hours before the particulate matter was centrifuged and solvent exchange into ethanol before being dried in a vacuum oven.

**5.4B**      APTES was dissolved into anhydrous toluene (99.8%). To this, under nitrogen, the triflated iridium complex in dichloromethane was added and stirred for 2 hours before being evaporated. The residual oil was dissolved in ethanol with a dispersion of 250nm silica particles and refluxed at 80°C for 22 hours. Particulate matter was centrifuged and solvent exchange into ethanol before being dried in a vacuum oven.

**8.1**        pHPMA-SiP<sub>2a</sub> is solvent-exchanged into fresh, anhydrous THF before agitation before being sparged with nitrogen. To this, under nitrogen, the triflated iridium complex in dichloromethane was added and stirred for 22 hours before the particulate matter was centrifuged and solvent exchange into ethanol before being dried in a vacuum oven.

---

## 5 Results: Organically Modified Silicas (OrMoSils)

### 5.1 Determination of surface chemistry of the silica particle

Investigating organically modified silicas (OrMoSils) as a potential scaffold for organometallic iridium required scrutinising the degree to which the untreated silica could be modified, starting with understanding the best route to condensation of organic material on to the silica surface.

Once attachment of the catalyst to our well-defined OrMoSil with known chemical structure is demonstrated and conditions are established, adjustments to the silica employed could be explored and form the basis for future efforts.

#### 5.1.1 Silica Hydroxyl-content titration

In order to understand how much catalysts we can load onto our silica it is important we understand the density of silica particle silanol surface groups that will subsequently be chemically modified.

In order to determine how much 3-aminopropyl triethoxy silane (APTES) could be condensed onto the particles, the free hydroxyl content at the surface for 250nm and 500nm diameter silica particles was first determined using a modified version of the titration method used by Kang et al. (2001). For this purpose, different weights of silica ( $W$ ) from 0.5 – 2.5g (in 0.5g increments) were placed in 80mL 0.05M NaOH solution, sealed and stirred for 24hr; the samples were then centrifuged and 10mL of the supernatant was titrated with 0.05M HCl to neutralization ( $B$ ). Equation 1 gives the free-hydroxyl content:

$$X = \frac{k(B - A)}{W} \quad (5.1)$$

Where  $X$  is the free-hydroxyl content, measured in mols of OH groups/gram of silica;  $B$  is the volume of HCl required to neutralise a blank, stock NaOH solution used in the silica consumption,  $A$  the volume of HCl required to neutralise a silica sample,  $k$ , is a conversion constant factoring in for sampling ( $k = 0.05 \text{ mols mL}^{-1} \times 80\text{mL}/10\text{mL} = 0.4\text{mols mL}^{-1}$ ), and  $W$  is the mass of silica. A plot of  $k(B-A)$  vs.  $W$  gives the free-hydroxyl content,  $X$ . Figure 5-1 shows the collected results for silica nanoparticles of 250nm and 500nm diameter.

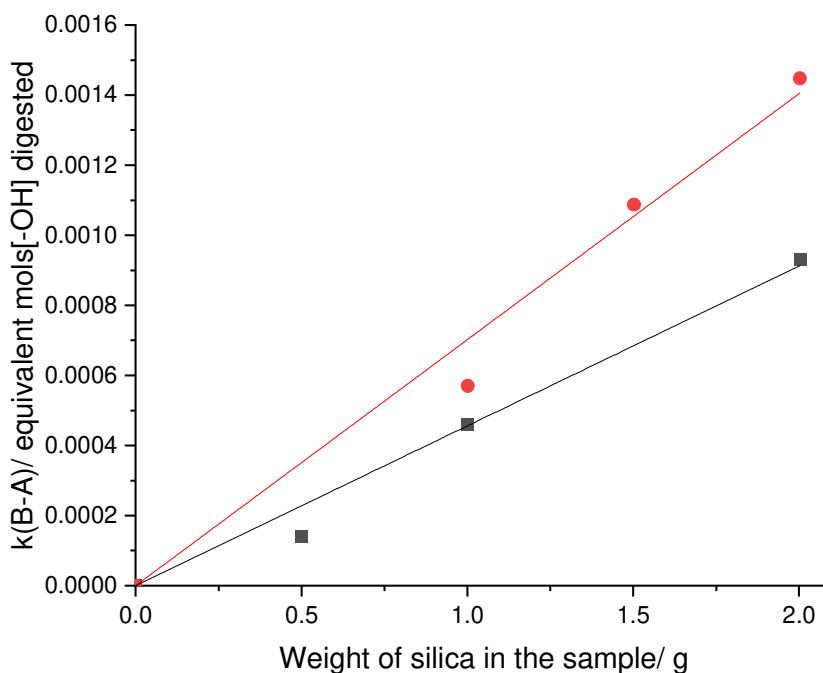


**Figure 5-1: Silica hydroxyl content for 500 and 250nm commercial silica. Legend ■ : 500nm silica; ● : 250nm silica.**

As expected the consumption of silylic acid moiety on the silica surface as a function of the amount of silica present (with constant sodium hydroxide content) follows a linear trend. This allows for the determination of the approximate content of silylic acid moiety as follows:  $0.70 \pm 0.02$  and  $0.46 \pm 0.03 \text{ mmol g}^{-1}$  for the 250nm and 500nm silica nanoparticle samples (NPs), respectively. This is low when compared to the Wang Resin ( $1.5 \text{ mmols g}^{-1}$ ), this is a frame of reference in determining efficacy for OrMoSil and catalytic nanoparticle creation.

## 5.2 Electrophoretic Mobility

3-aminopropyl triethoxysilane (APTES), a silane coupling agent (SCA), was selected to investigate its use as an attachment point for Iridium Cyclopentadienyl ( $\text{IrCp}^*$ )-type catalysts to silica via the amine moiety using triflation. In order to get to this stage it is important to understand the degree of condensation of APTES to the silica nanoparticle.

The addition of an organic-amine group to the silica surface represents a significant change in surface chemistry. This should be discernable in its electrophoretic mobility, which is a measurement of the motion of dispersed particles relative to a fluid under the influence of a uniform electric field. How much APTES we can add to the silica surface can be determined by changing the ratio of APTES to surface hydroxyl groups and looking for a plateau in electrophoretic mobility.

### ***5.2.1 Determination of best conditions for APTES condensation to 250nm silica particles using Electrophoretic mobility over a pH range.***

This experiment aims to produce salinized silica particles by chemically reacting APTES on the surface of the silica particles. The SiPs are first dispersed in an APTES solution in either ethanol or toluene. There is some evidence of incomplete condensation of all available silanes to silica but it is generally regarded as a non-limiting factor (Ma et al., 2007); at maximum condensation, 3 surface hydroxyl groups would react with one APTES molecule, therefore the molar ratio of APTES is always adjusted to 1/3 of with regards to the calculated available surface hydroxyl molar content (so 1 molar equivalent, or 100%, of APTES is  $0.70/3$  mmols  $g^{-1}$  of silica nanoparticles, or  $0.23$  mmols  $g^{-1}$  of SiP-[Si-OH]<sub>3</sub>, see above), be that more, or less, or equal to the surface hydroxyl content. To perform the reaction, the SiPs were stirred in the APTES solution for 24h in the presence or absence of an ammonium hydroxide catalyst. After 24, the samples were washed in fresh solvent repeatedly through centrifugation steps where the particles were spun down and the supernatant removed in between washes. Finally, the sample was dried in a vacuum oven.

The dried samples were then re-dispersed in water, the pH was adjusted, and electrophoretic mobility of the produced samples was determined over a pH range. The corresponding measurements can be seen in Figure 5-2: and Figure 5-3::

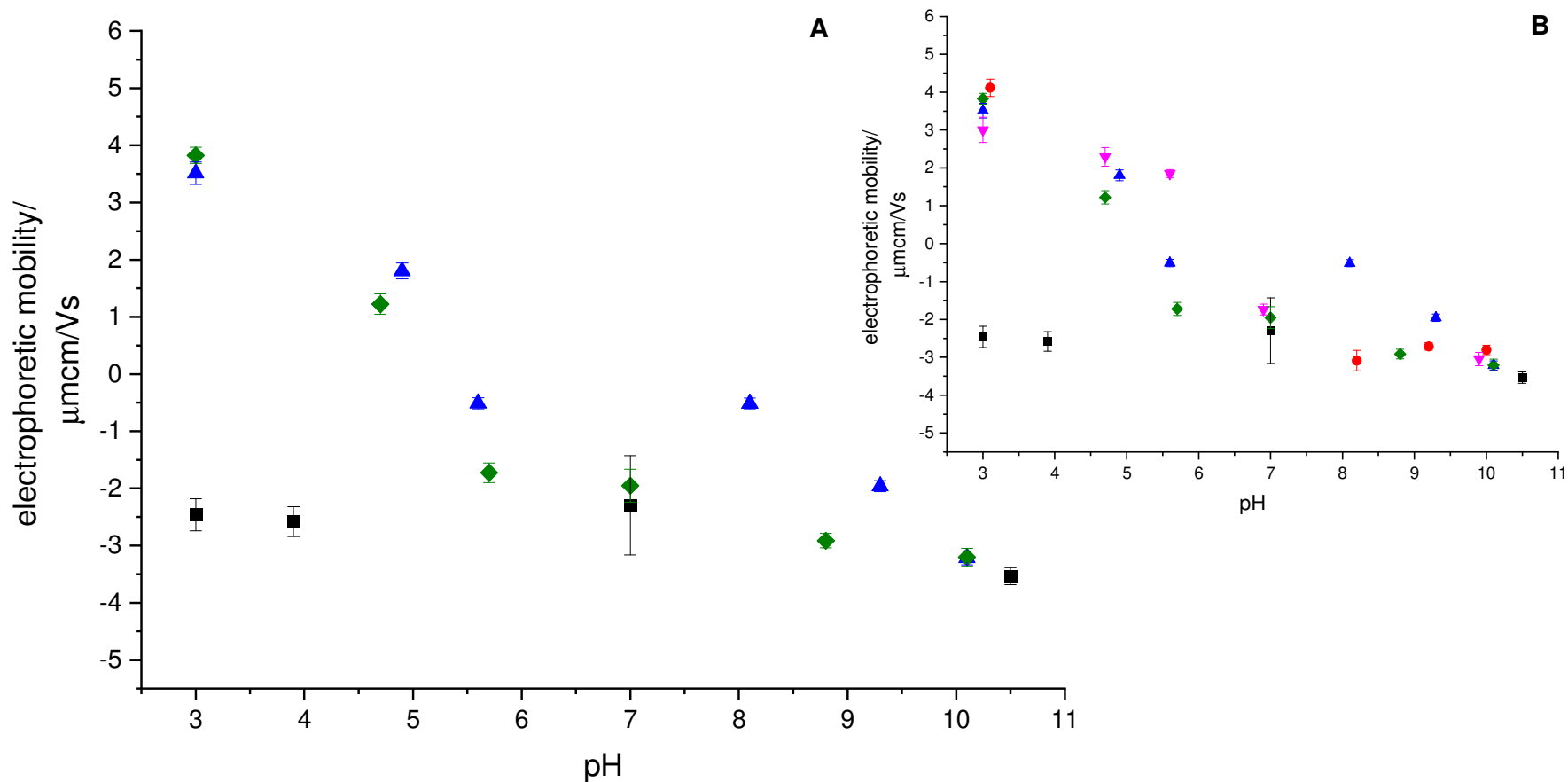


Figure 5-2: (A) Electrophoretic mobility of 500nm silica particles with and without APTES in ethanol. Inset (B): Figures 4 & 5 combined. Base: ammonium hydroxide ( $\text{NH}_4\text{OH}$ ) catalyst (0.9mL in 5mL solvent) Key: ■: Blank silica; ▲: Ethanol, base catalyst; ◆: Ethanol, no base catalyst; ●: Toluene, base catalyst; ▼: Toluene, no base catalyst.

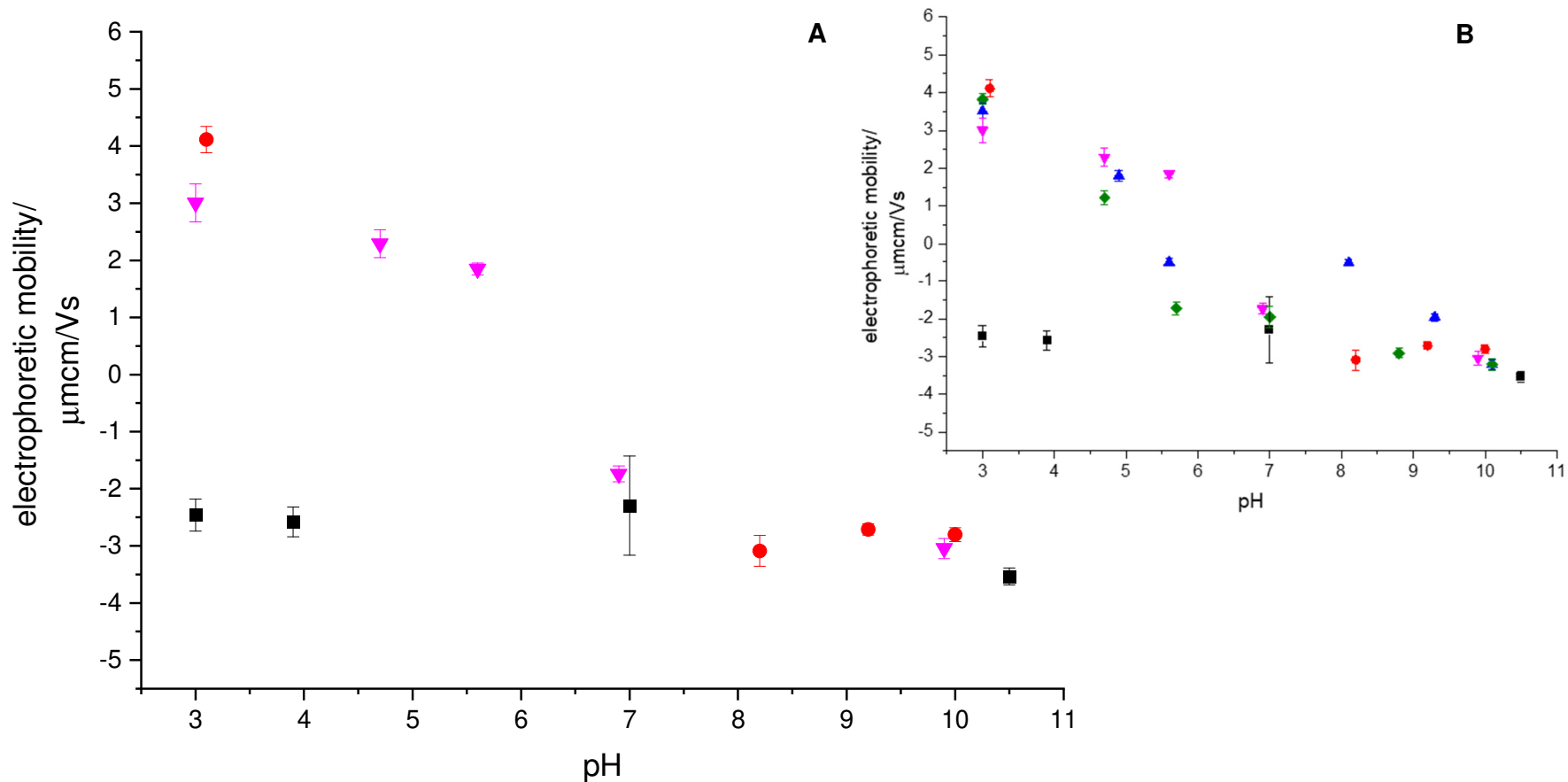


Figure 5-3: (A) Electrophoretic mobility of 500nm silica particles with and without APTES in toluene. Inset (B) is Figures 4 & 5 combined. Base: ammonium hydroxide ( $\text{NH}_4\text{OH}$ ) catalyst (0.9mL in 5mL solvent) Key: ■: Blank silica; ▲: Ethanol, base catalyst; ◆: Ethanol, no base catalyst; ●: Toluene, base catalyst; ▼: Toluene, no base catalyst.

The results demonstrate that surface condensation is occurring in both solvents and when both a catalyst base is used (ammonium hydroxide) or not. This is in line with protocols that indicate the defining step for silyl condensation to the surface is the creation of the intermediate silyl hydroxide species.

With limited difference in output whether ammonium hydroxide was added or not, it was omitted in further studies. Combinations of dispersed silica, solvent and silane coupling agent (APTES) were examined beyond this stage.

The maximum theoretical organic mass added to the silica surface was determined using Equation 2:

$$A_{APS} = \left(\frac{X}{3}\right) x [APS] \quad (5.2)$$

where: *A* is the mass of APS added per gram of silica; *X* is the silica surface hydroxyl content as determined in 5.1; [APS] is the molar weight of the 3-aminopropyl silane moiety condensed to the silica surface<sup>3</sup>.

This becomes:

$$\left(\frac{0.7 \times 10^{-3} \text{ mol}_{SiOH} \text{ g}_{SiP}^{-1}}{\frac{3_{SiOH}}{SCA}}\right) x 83.17 \times 10^3 \text{ mg mol}^{-1} = \mathbf{19.41 \text{ mg}_{AP} \text{ g}_{SiP}^{-1}}$$

The determination of maximum theoretical mass of 3-aminopropyl triethoxysilane assumes 100% total coverage via condensation, to every available silylic acid moiety on the silica surface calculated using the titration method at a ratio of 3 Si-OH groups to every silane coupling agent (SCA). This means that at maximum we can add 1.94% additional organic mass of 3-aminopropyl moiety to the silica surface using this technique.

---

<sup>3</sup> APS molecular weight is adjusted to account for condensation at the surface assuming 3 hydroxyl groups condensate to one AP moiety. Molecular mass of the AP moiety is calculated using a molecular formula of C<sub>3</sub>H<sub>5</sub>NSi which accounts for proton losses from the silica surface when added.

### ***5.2.2 Determination of Electrophoretic Mobility across a wide pH range and %-AP-silica Condensation to 250nm Silica***

Having established a straightforward method for adding APTES to silica we needed to look at how much APTES we could add to the silica surface under these conditions.

In order to determine the degree of chemical change at the surface, samples of AP-coated silicas, at varying ratios of the theoretical maximum upper limit, ranging from 1-150%, were prepared. Electrophoretic mobility measurements were then taken over a wide pH range, the belief being that an upper limit to the degree of electrophoretic mobility would be observed when the maximal quantity of AP on silica had been reached - the "plateau region", indicative of maximal condensation, with no expected increase in electrophoretic mobility above a maximum condensation level, could then be deduced.

Electrophoretic mobility (em) is the response of a colloidal particle to an applied electrical field, and the degree to which cations, anions and neutral particles can move between cathode and anode. Depending on the chemical character of my silica particles, treated to varying degrees with APTES, we would expect to see different degrees of electrophoretic mobility across a pH range, with low or no amine-content silica resulting in a low to negative em at a lower pH than would be observed with the higher amine-content silica.

Samples with an available AP-coverage between 0-1.5 equivalents (0.0, 0.01, 0.10, 0.20, 0.60, 1.00 and 1.50 equivalents) are created by mixing APTES with silica dispersed in ethanol as per conditions settled on in section 5.2.1, cleaning and drying it before the samples were split in 2. The samples pH were then adjusted using 0.1M aqueous HCl & NaOH solutions respectively and their electrophoretic mobility measured across varying pH ranges (Figure 5-4).

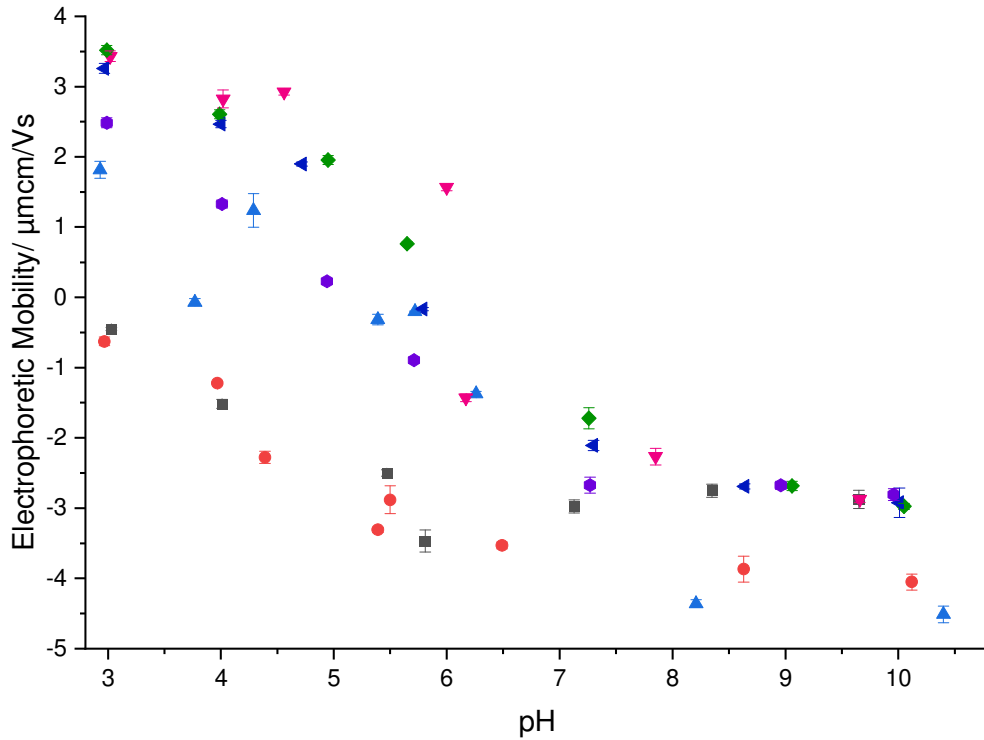


**Figure 5-4: Electrophoretic mobility for 250nm silica nanoparticles reacted with increasing %-APTES as a function of pH; The suspension at original pH X was divided in half and concentrated HCl and NaOH solutions were added to gradually change the pH, decreasing and increasing it respectively. Measurements of APTES to silanol content are made in equivalents of 3[Si-OH]; legend: ■: 0.0 equivalents to silica (blank, untreated silica); ●: 0.01; ▲: 0.10; ▼: 0.20; ◆: 0.60; ◀: 1.00; ▶: 1.50.**

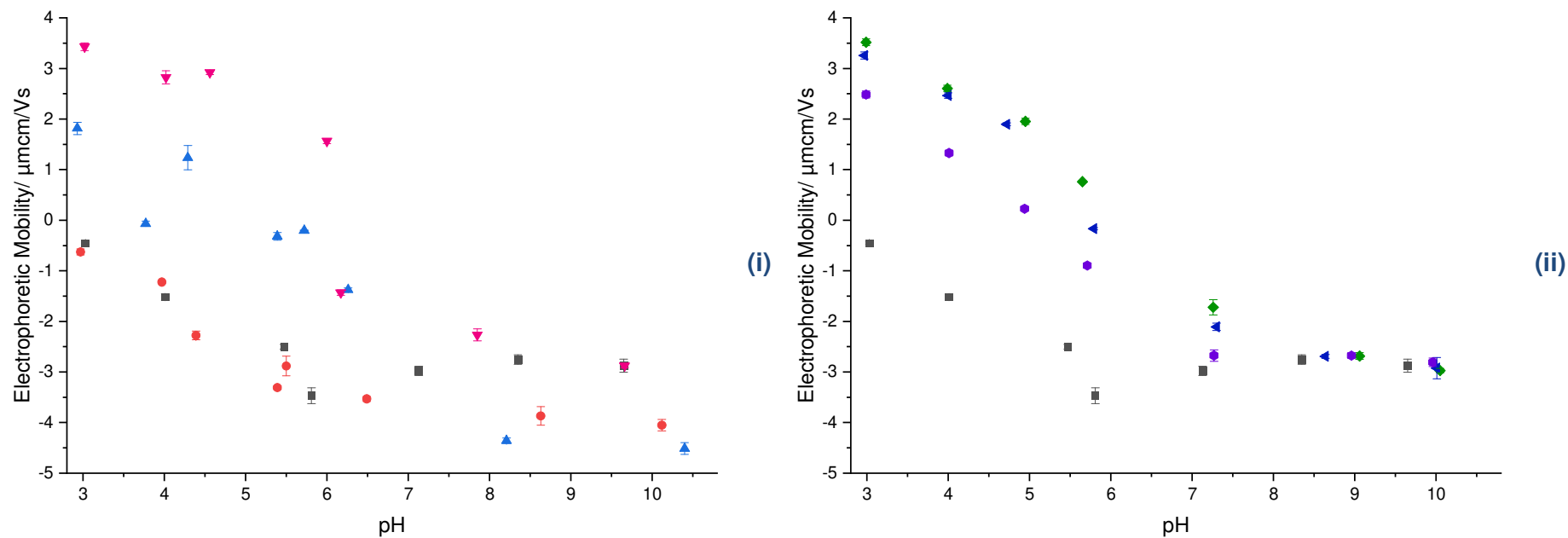
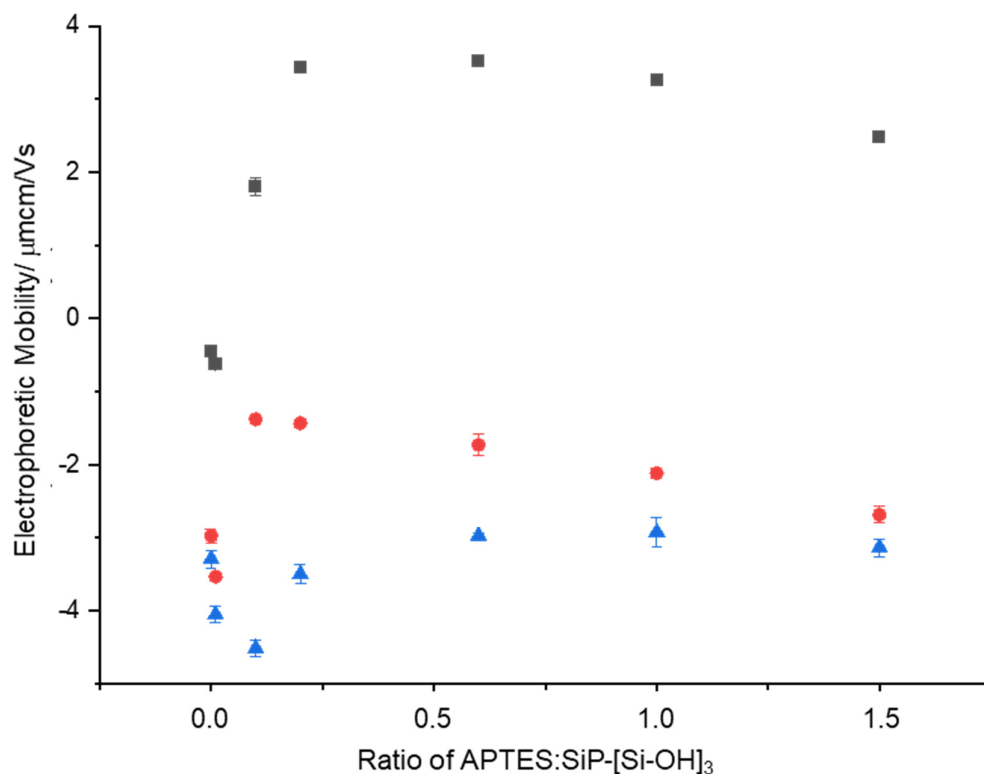


Figure 5-5: (i): low APTES content; (ii): high APTES content; Electrophoretic mobility for organically modified 250nm silica nanoparticles with increasing %-APTES content across a wide pH range; The suspension at original pH X was divided in half and concentrated HCl and NaOH solutions were added to gradually change the pH, decreasing and increasing it respectively. Measurements of APTES to silanol content are made in equivalents of  $3[\text{Si-OH}]$ ; legend: ■: 0.0 equivalents to silica (blank, untreated silica); ●: 0.01; ▲: 0.10; ▼: 0.20; ◆: 0.60; ◀: 1.00; ▶: 1.50.

Figure 5-4 and Figure 5-5 show that at low pH there is a clear point at which there is little to no change in chemistry at the surface; at equivalents of APTES:SiP-[Si-OH]<sub>3</sub> between 0.10 and 0.20 equivalents there is a very clear increase in em at low pH, inferring there is distinct change at the chemical surface, attributable to increased amine content that is completely protonated; however, limited changes are seen above 0.20 equivalents at low pH, indicating it is unlikely APTES content increases above 0.20 equivalents of the APTES:SiP-[Si-OH]<sub>3</sub> ratio using this route.

Figure 5-6 shows electrophoretic mobility at a function of increasing APTES-exposure at 3 pH ranges: pH 2.5-3.5, where we would expect to see full protonation of the amine group on the APTES moiety; pH 6-7.5, where we would expect the amine group to be almost fully deprotonated; and at pH10-11, where the amine group would be completely deprotonated and would not participate in providing charge to the particle surface.



**Figure 5-6: Electrophoretic mobility values vs increasing APTES content at 3 different pH ranges: ■ : pH 2.5-3.5; ● : pH 6.0-7.5; ▲ : pH 10-11**

At pH 2.5-3.5 electrophoretic mobility is seen to plateau for silica particle samples that have been modified with 0.20 equivalent proportions of APTES. Determination of Particle Size as a measure of particle coagulation across a pH range

Particle size measurements were also obtained with the electrophoretic mobility (Figure 5-4, all samples, and Figure 5-5 for low and high APTES-content samples) and can be seen in Figure 5-7 (showing all samples, Figure A-1 in the appendices shows this split into low (i) and high (ii) APTES-content).

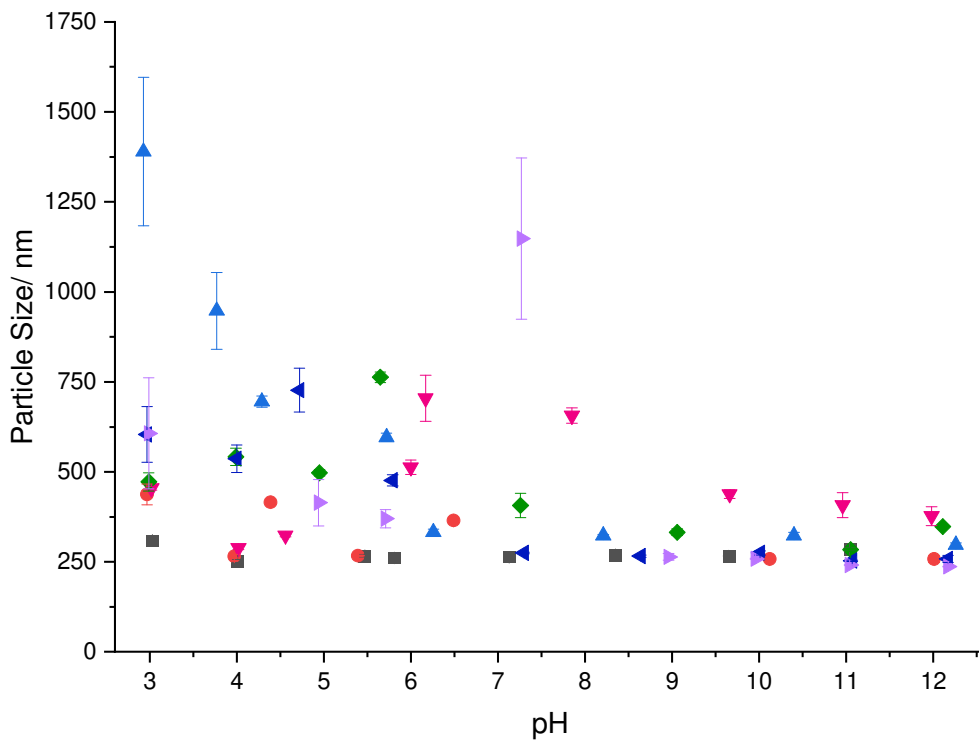


**Figure 5-7: Average diameter of modified 250nm silica nanoparticles with increasing %-APTES content as a function of pH; The suspension at original pH X was divided in half and concentrated HCl and NaOH solutions were added to gradually change the pH, decreasing and increasing it respectively. Legend: ■: 0% equivalents to silica (blank, untreated silica); legend: ■: 0.0 equivalents to silica (blank, untreated silica); ●: 0.01; ▲: 0.10; ▼: 0.20; ◆: 0.60; ◀: 1.00; ▶: 1.50.**

Figure 5-7 and Figure A-1 shows that there is some size variability with the addition of APTES across all examples across the pH range; the lowest pH range, representing the highest amount of HCl solution in Figure 8(i) could potentially be related to the addition of high amount of ionic content, causing a

collapse in the electric double layer with respect to the silica particle and their agglomeration. At pH7, APTES-treated samples start to show evidence of aggregation and particle size increases around pH7 when the samples had not had their pH modified; compared to Figure 5-4 and Figure 5-5 these same samples exhibit low zeta-potential, likely meaning the sample would begin to aggregate at this point, particularly with little to no amine-surface content. 20%-AP-SiP exhibits the greatest stability across pH ranges but a similar phenomenon of marginally increasing particle size can be observed between pH 5-7, the point of inflection to a negative zeta potential occurring around this point.

It is difficult to determine the degree of particle aggregation but the uniformity of zeta potential results above 20%-APTES led us to believe there was likely little increased in amine content at the surface.

### **5.3 Fluorescamine Assay of AP-SiPs**

Quantitative evaluation of the 3-aminopropyl content is sought by exposure to a known excess of fluorescamine before the sample is centrifuged. Fluorescamine exhibits a change in fluorescence in the presence of primary amines by irreversibly binding with the amine (Figure 5-8). This is a very efficient stoichiometric reaction, which allows simple quantification of the presence of amine moieties in a sample (Castell et al., 1979).

A calibration curve was run on propylamine; when the sample is treated, excess fluorescamine to the surface amine could be recouped by centrifugation and analysis of the supernatant for comparison.

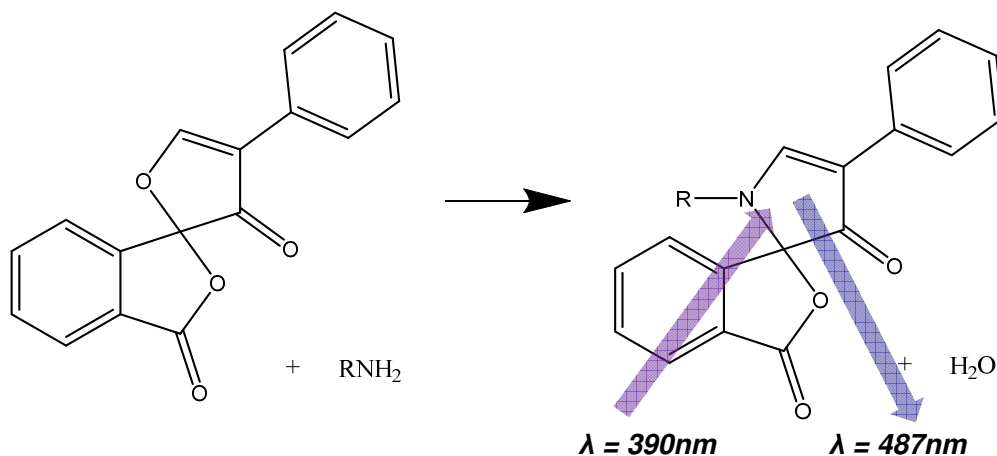


**Figure 5-8: Mode of action for Fluorescamine when reacting with a primary amine moiety. Primary amines react irreversibly with fluorescamine, The secondary-aminated molecule then produces characteristic fluorescence under a UV light source of 390nm as opposed to the unreacted form, producing light around the 487nm region. This can be quantitatively measured to create an assay system.**

The scheme for the assay of AP-treated silica can be seen in Figure 5-9. The calibration curve can be seen in the appendices in Figure A-2: known quantities of propylamine are reacted with an excess of fluorescamine and their fluorescamine pattern is recorded to produce the subsequent calibration curve.

The calibration curve produces a molar absorption coefficient of  $5.27 \times 10^{11} \text{ L mol}^{-1}$ . The amine content of APTES-coated silica particles as discussed in the production of particles in Section 5.2.1 is attempted to be quantitatively ascertained using the fluorescamine assay as described in *Chapter 4*.

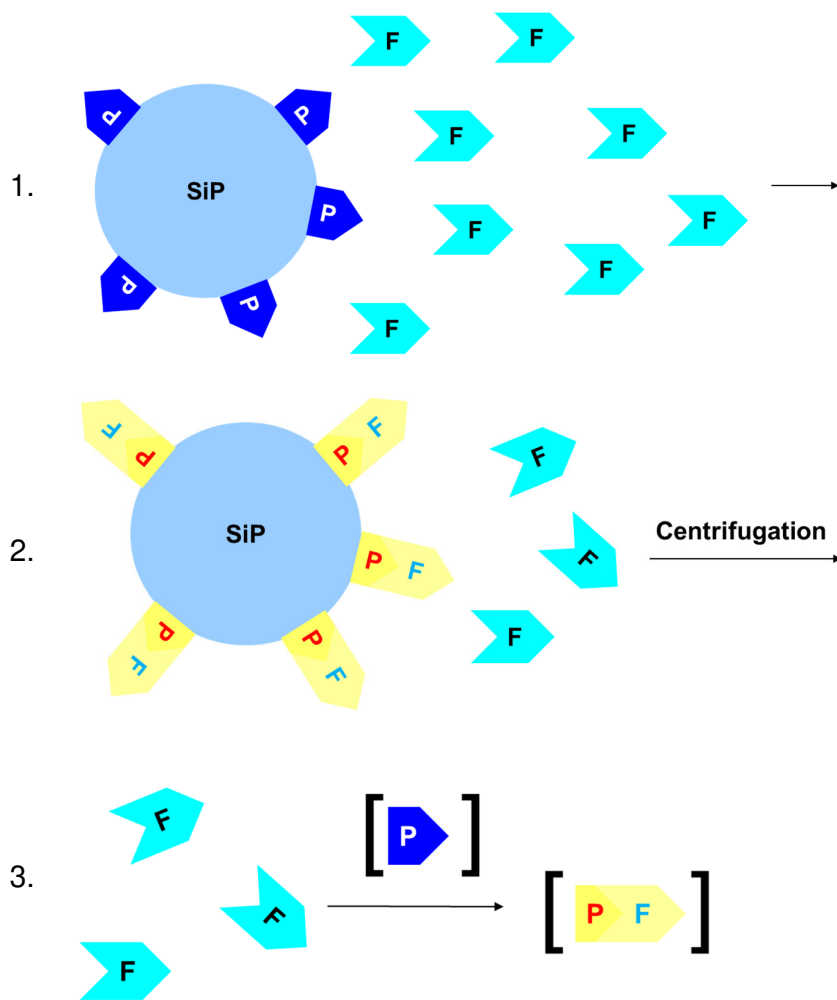


**Figure 5-9: Mechanism for Fluorescamine Assay:** 1. A known concentration of Fluorescamine is introduced to a known weight of AP-treated silica; 2. The sample is agitated and then centrifuged to remove solid, treated OrMoSil; 3. A sample of known volume of the eluent is taken and treated with a known excess of propylamine. The samples UV fluorescence is then measured and compared against a calibration curve.

The evaluated emission spectra then yields the actual molarity of the solution of reacted fluorescamine from which the amine content could be elucidated. Figure 5-10 shows the outcome from this. Predicted assay results were based on the predicted assay values expected.

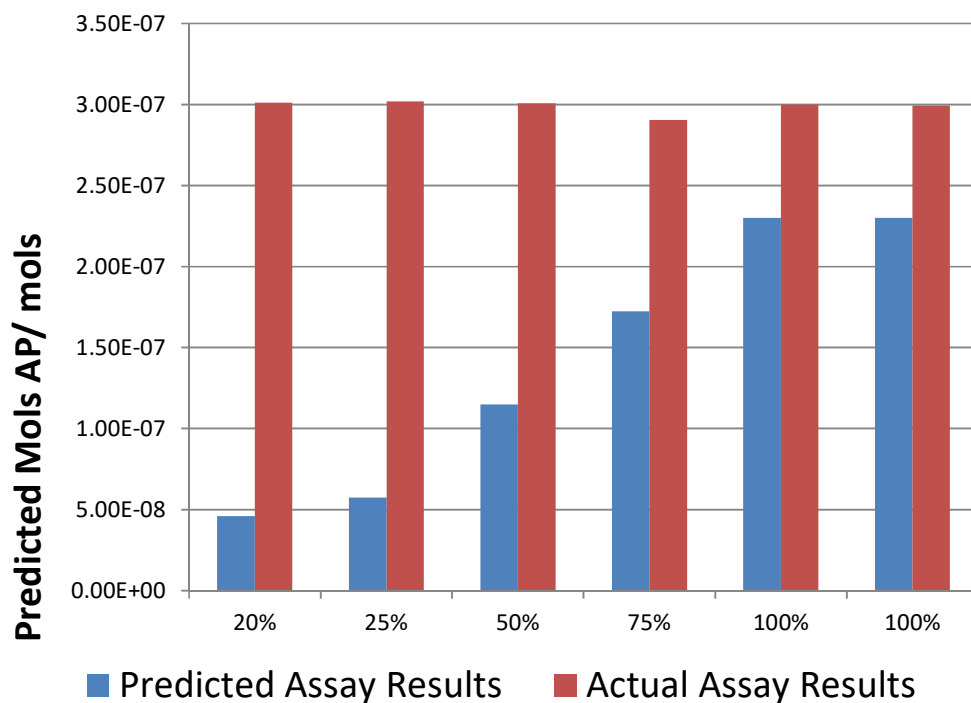


**Figure 5-10: Fluorescamine assay of organically modified silica. Predicted assay results are based on the predicted amine content assumed from the conditions used to create the OrMoSil in question, in this case this is linked to silica. This is discussed in greater detail in the section in Chapter 4 on Fluorescence Spectroscopy.**

The data shows that, rather than a lower quantity of amine consuming fluorescamine at the surface there appears to be an increase to consistently to  $3 \times 10^{-7}$  mols of AP detected; as this value coincides with the overall quantity of fluorescamine in total it is likely this means that absorption of the fluorescamine compound onto the silica particle as a whole has taken place resulting in relatively little fluorescamine being available for consumption at the [P] phase. Quantitative analysis of amine-coating of silica via this assay method did not yield the necessary results.

#### 5.4 Characterisation of IrCp\*-tethered AP-SiPs

Iridium Cyclopentadienyl (IrCp\*) catalyst species was attached to silica particles via 2 routes:

- A. triflation of the IrCp\* catalyst followed by condensation to the pre-prepared AP-SiP

B. IrCp\* triflation and addition to the APTES species then addition to the silica.

Both aimed at 20% AP coverage (condensation of the IrCp\*-APTES was prepared at the necessary ratio equivalent to the 20% AP-SiP prepared before).

SEM characterization showed route B results in silica material distinct from the original spherical particles used, dispersed amongst the silica particles; this could of arisen as a result of APTES condensing on itself in the presence of triflic acid.

Route A silica showed clean silica particles and SEM-EDX spectra indicated trace Iridium was bound to the particle.

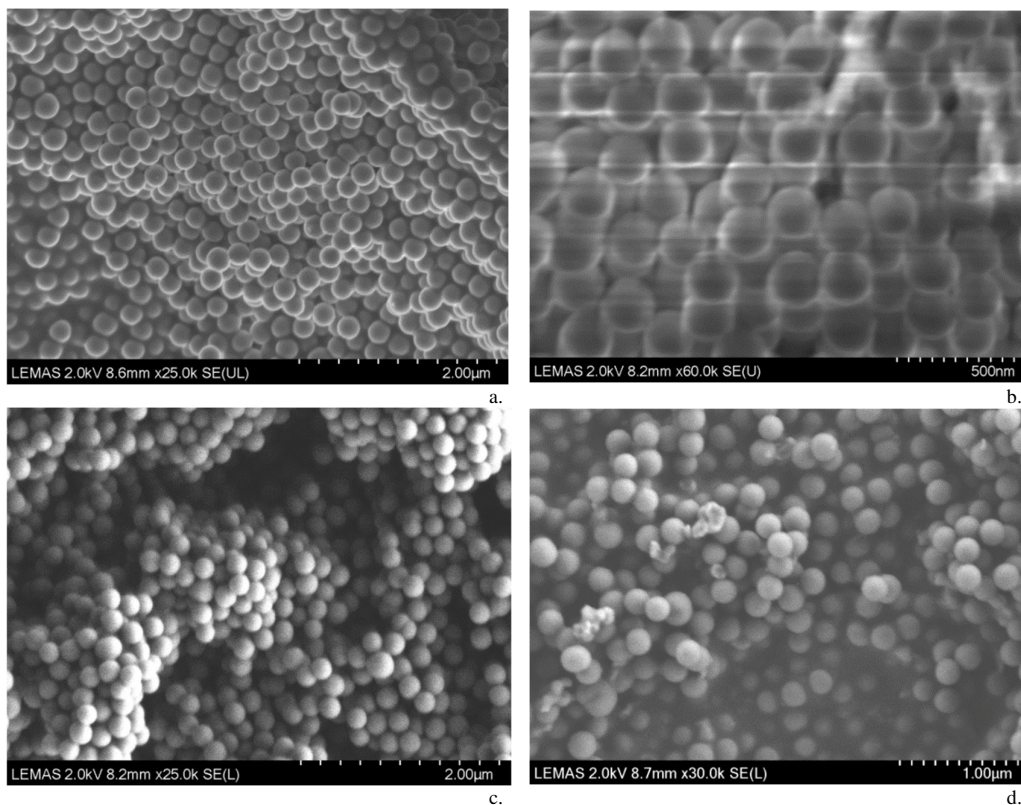


**Figure 5-11: SEM Images comprising: a. 250nm silica (untreated); b. Silica from the 20% APTES regimen; c. Silica post-route A to IrCp\*-APTES-Silica (copper mount); d. Silica post-route B to IrCp\*-APTES-Silica.**

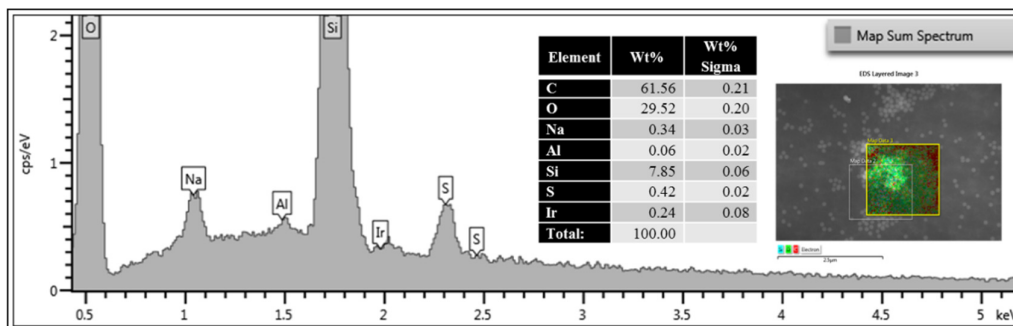


**Figure 5-12: SEM-EDX cross section of route A silica (AP-silica + IrCp\*) and iridium scanning**

#### 5.4.1 Benzaldehyde assay

In the presence of catalytically-active amounts of the IrCp-complex, benzaldehyde is converted into benzyl alcohol through transfer hydrogenation (as discussed in Chapter 1 and 2). Benzaldehyde assays were run on the silica particles created in A & B and unattached catalyst over 10 hours to confirm if there was any catalytic activity, output chemical moieties were analyzed using gas chromatography (GC) against samples of benzaldehyde and benzyl alcohol. (Figure 5-13).

No evidence of benzaldehyde conversion was evident in either silica; this compounded the evidence that the iridium content was too low to catalyze the reaction. Trace aldol condensation is seen across all samples as this is a consequence of a trace amount of benzaldehyde reacting to produce the aldol from 2 benzaldehyde molecules and is not indicative of reaction with the catalyst, as indicated by its appearance in all samples, including the test mixture of benzaldehyde and benzyl alcohol.

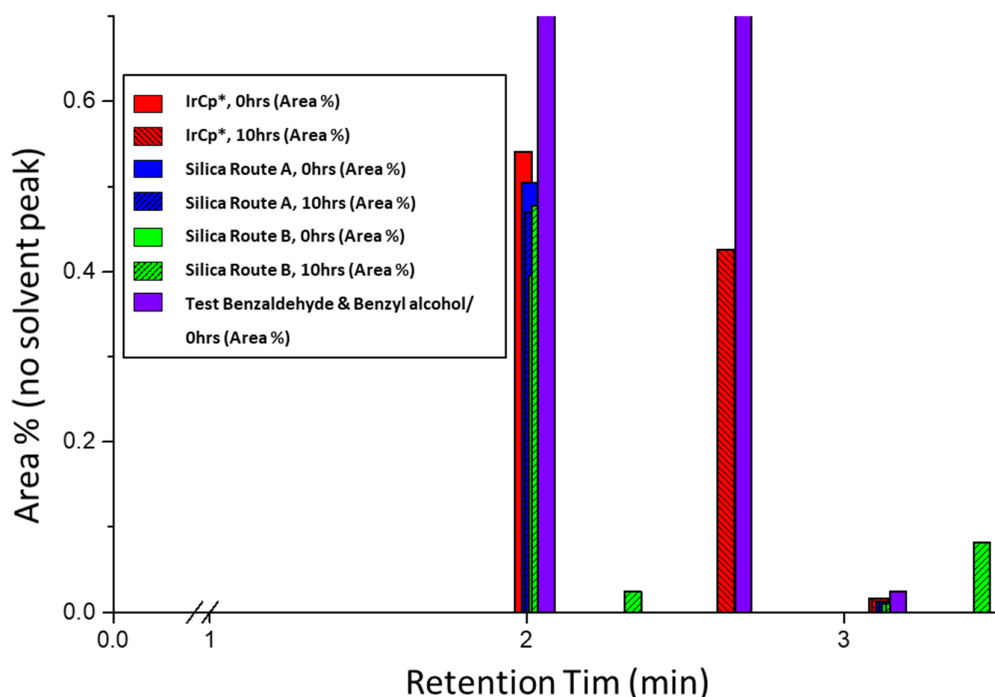


**Figure 5-13: Benzaldehyde assay of Routes A & B IrCp\*-SiPs vs. unattached IrCP\*.** Key: **Purple:** Test benzaldehyde and benzyl alcohol; **Red:** free Iridium cyclopentadienyl complex synthesised and utilised in the silica particles; **Blue:** IrCp-treated silica particles via route A; **Green:** IrCp-treated silica particles via route B.

### 5.5 Concluding Remarks

There are several examples of OrMoSils being used as catalysts but alternative solutions to the issue of organic material cohesion to the silica were sought and probed as well as changes made at others stages, from modification of the silica to improvements in how we encourage cohesion; some of these elements are discussed in the literature review (Chapter 2); however, the path chosen at this was upward; namely, growth of the organic component by the novel use of Brush Polymers attached at the surface of the silica particle using more advanced routes to this end.

## 6 Results: Creating Brush Polymers via Growth of pGMA on silica

In this chapter, the possibility of growing brush polymers, of poly-glycidyl methacrylate (pGMA) from the surface of discrete silica particle is explored as a platform for catalyst loading. The potential of this method for increasing the density of chemical moieties capable of attachment of a high number of catalyst species on the particle surface was thought to be a solution to the limited catalyst loading shown in the previous chapter when using a small molecular species such as APTES on the surface of the particles.

The chapter describes the steps taken to produce a dense layer of polymer chains on the particle surface and the associated characterization to quantify the polymer growth.

### 6.1 Thermogravimetric Analysis

A method for quantitatively measuring added organic content will ultimately be necessary to ascertain the nominal load capacity for my functionalized particles. Whilst chemistry is important in terms of functional groups presented, frequency and reproducibility, direct measurement of these factors is problematic for a number of reasons:

1. Surface chemistry of the functionalized SiP usually only accounts for a small fraction of the total measurable elements of a particle.
2. In the previous chapter we attempted to quantitatively determine amine-content using a fluorescamine assay, which was hoped would show that amine content as determined by electrophoretic data was correct; however, complete absorption of fluorescamine to the silica surface was suspected to have occurred. Fluorescamine selectivity of moiety is potentially a factor, particularly when in the presence of others, i.e. silylic acid surface groups, themselves present in the bulk.

We measured mass change of our samples as temperature increased, with static (held at a specific temperature for a defined period of time) and dynamic (temperature was increased at a specific rate between 2 temperatures) stages, which we refer to as the heating protocol. With careful consideration of this

heating protocol, identification of specific events in the decomposition of the OrMoSil is possible; there are events in decomposition for both silica and organic compounds (Zhuravlev, 2000) which we can observe within our materials and the extent of chemical change taking place; specifically:

1. Loss of loosely bound water (occurring around 100-120°C)
2. Loss of “secondary” water more intimately bound to the silica (occurring around 200°C).
3. The decomposition of organic content (occurring between 400-600°C).
4. Sintering (dehydration of silanol groups on the silica surface, occurring above 400°)

Blank silica, 20% AP-SiP, 100% AP-SiP and 1000% AP-SiP organically modified silicas (OrMoSils), were analyzed using thermogravimetric analysis (TGA) over a temperature range of 50-1000°C with the following TGA protocol utilized: under a nitrogen atmosphere, dynamic and static elements for the heating protocol were as follows:

1. Heated from 50-200°C at 10°C min<sup>-1</sup>, then held for 60 minutes.
2. 200-500°C at 5°C min<sup>-1</sup>.
3. 500-1100°C at 10°C min<sup>-1</sup>, before being cooled to room temperature at 10°C min<sup>-1</sup>.

This TGA protocol was determined by using a slow ramp on our blank silicas to determine points of interest over which we could hold. Table 6-1 shows the mass difference between the AP-SiP and the silica particle for an array of samples.

**Table 6-1: Sample Cohorts of AP-SiPs, with the %-weight loss range given as the difference between untreated silica and the AP-SiP. Average  $\text{mmols}_{\text{AP}} \text{g}_{\text{SiP}}^{-1}$  values given based on the average %-weight loss range.**

Sample Cohort	Total Weight/ $\text{mg}^4$	Average % Wgt Loss range	Average $\text{mmols}_{\text{AP}}/\text{g}_{\text{SiP}}$
AP-SiP20%	<b>57.04, 42.52, 49.86, 45.62</b>	<b>2.89-2.99%</b>	<b>0.341</b>
AP-SiP100%	<b>51.39, 44.92, 56.87</b>	<b>2.98-3.02%</b>	<b>0.348</b>
AP-SiP1000%	<b>29.88, 28.84, 32.80, 35.51</b>	<b>3.21-3.25%</b>	<b>0.374</b>

The average number of moles of 3-aminopropyl moiety on silica exhibits limited increase in samples with increasing ratios of APTES:Silica; for AP-SiP20%, the predicted maximum AP-content we would expect to observe can be seen below in Equation 6.1:

$$0.341 \times 10^{-3} \text{mols}_{\text{AP}} \text{g}_{\text{SiP}}^{-1} \times 83.17 \times 10^3 \text{mg mol}^{-1} = \mathbf{28.36 \text{mg}_{\text{AP}} \text{g}_{\text{SiP}}^{-1}} \quad (6.1)$$

Where  $83.17 \times 10^3 \text{mg mol}^{-1}$  is the mass of the AP-moiety in isolation from the silane backbone of either APTES or attached to silica.

(Predicted mass of AP based on EM results in Ch5:  **$19.41 \text{mg}_{\text{AP}} \text{g}_{\text{SiP}}^{-1}$** )

<sup>4</sup> Examples highlighted in red were excluded from the overall average as they produce aberrant results out of range of the others, potentially due to contamination.

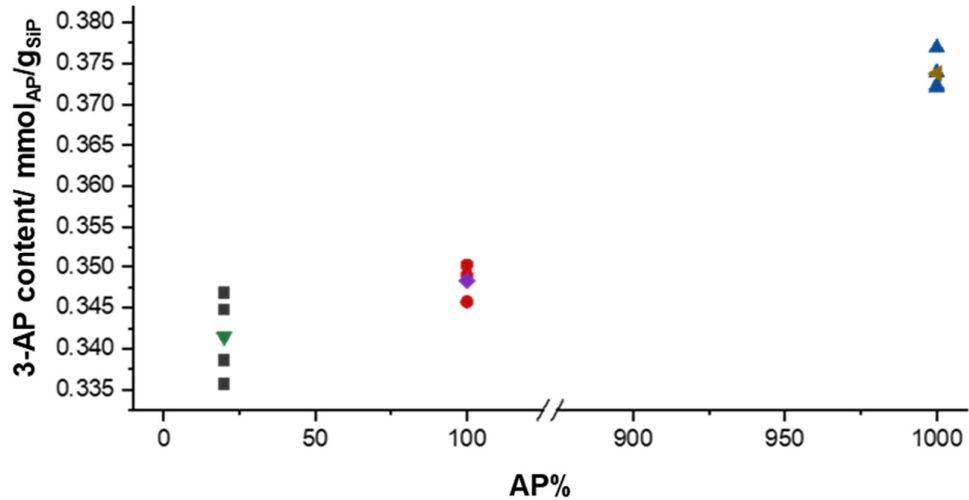


**Figure 6-1: Average AP-SiP TGA values for each AP-SiP sample in Table 6-1 vs AP% ratio to silica (assuming 1 APTES molecule per 3 Si-OH moieties. ▼, ◆, and ◀ are averaged values for the 3-aminopropyl excluding the values in Table 1.**

Results show limited increases in mass loss in spite of increasing APTES exposure for the silica, even in excess of the available Si-OH sites (

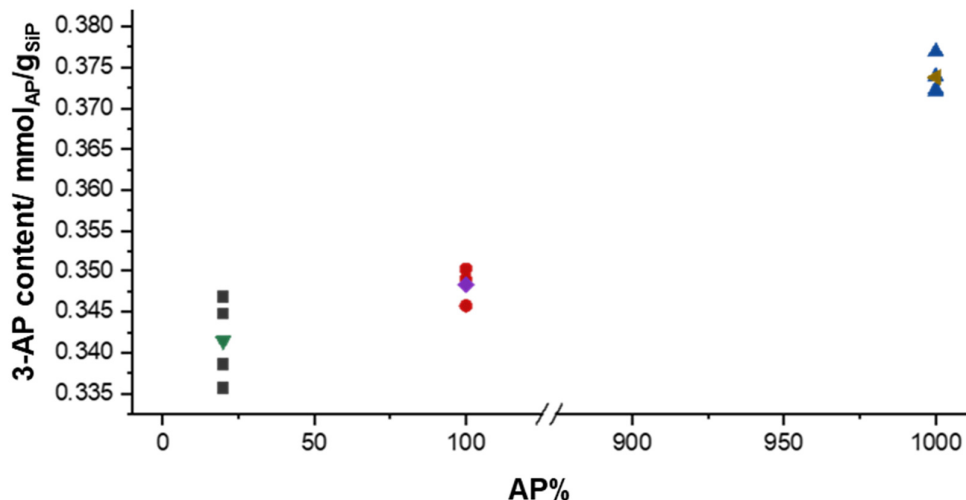


Figure 6-1); adding more APTES than 20% of the available silica Si-OH sites did not increase the total mass loss detected from TGA mass loss measurements in a significant amount.

Equation 6.1 gives us the mass of the AP-moiety ( $\text{mg}_{\text{AP}} \text{g}_{\text{SiP}}^{-1}$ ) per gram of silica; we can predict this to be  $19.41 \text{ mg}_{\text{AP}} \text{g}_{\text{SiP}}^{-1}$  for the 20%AP-SiP. The TGA result shows a mass loss of  $28.36 \text{ mg}_{\text{AP}} \text{g}_{\text{SiP}}^{-1}$ ; what this means is that the heating protocol and identification of the region associated with the organic moiety needs to be better isolated so that we can consistently identify the region associated with the loss of the 3-aminopropyl moiety.

The low quantity of available sites for binding iridium-cyclopentadienyl ( $\text{IrCp}^*$ ) catalyst to the silica surface direct resulted in us looking at increasing the number of available sites, namely, by growing upwards, i.e. by growing polymer from the surface with functional groups capable of attaching catalyst.

## 6.2 Addition of Glycidyl Methacrylate into an AP-SiP shell

3-Aminopropyl-coated silica particles (AP-SiP), with quantifiable and consistent levels of aminopropyl-surface coatings on their surface (Chapter 5), are reacted with glycidyl methacrylate (GMA) with the aim of creating a coating of methacryloxy-1- $\beta$ -hydroxy-3-aminopropyl trimethoxyl siloxane moieties at the surface (MAG-AP-SiP). Once the reaction was complete, the resultant solid was dispersed in a reaction medium for reversible addition–fragmentation chain-transfer (RAFT) polymerization with a chain transfer agent (CTA), additional GMA and initiator to produce free polymer both in the bulk and on the surface from the protruding methacryloxy-moiety (Figure 6-2).

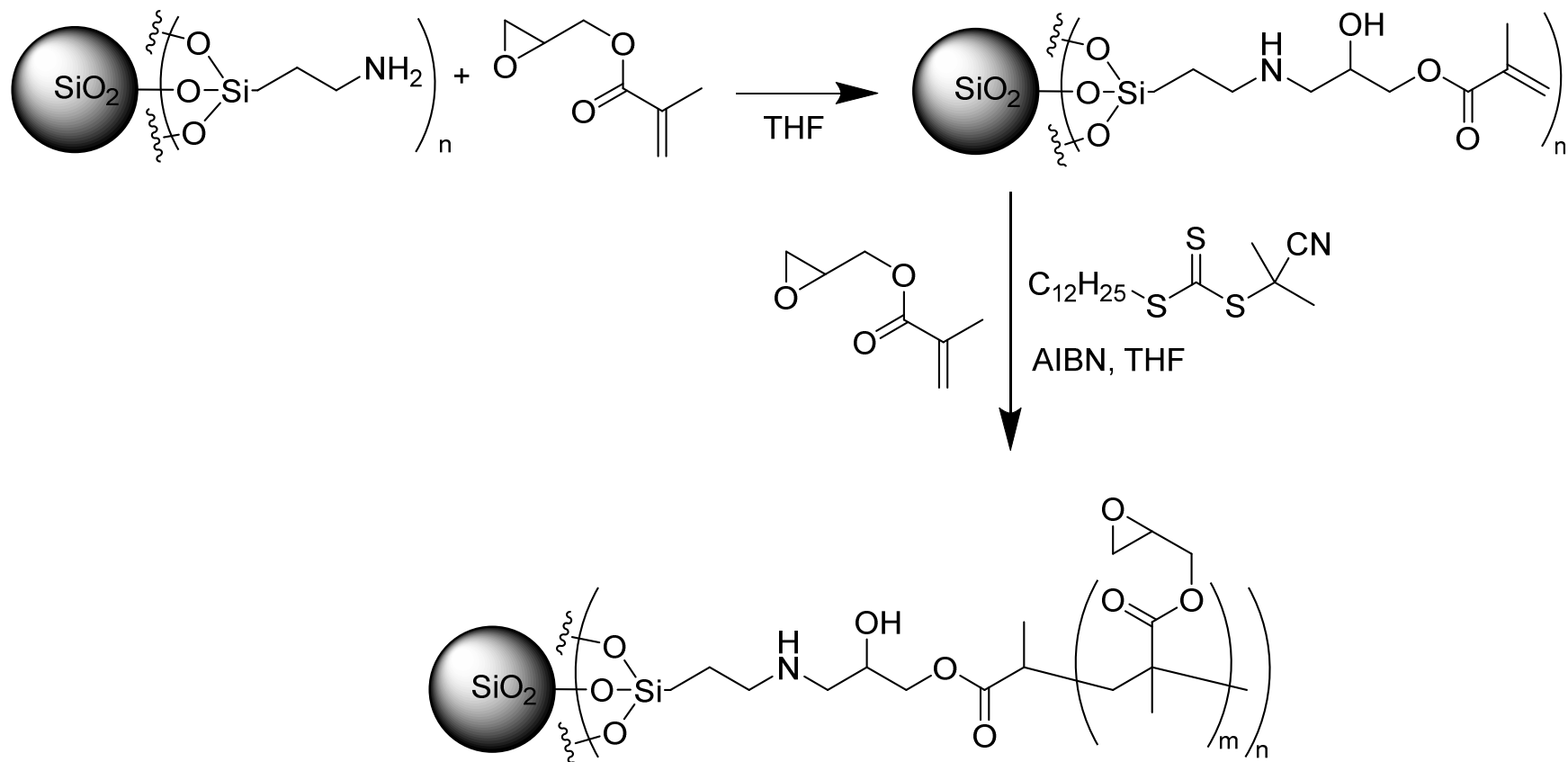
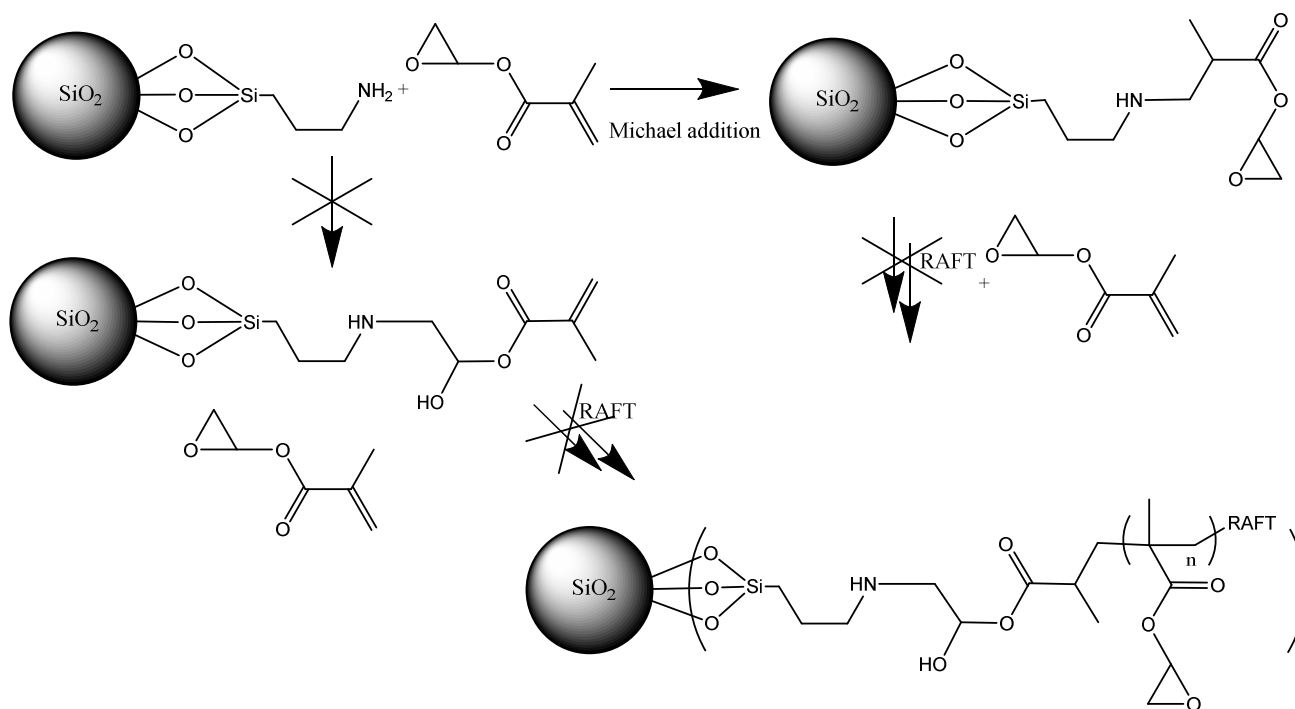


Figure 6-2: Mechanism of GMA coating onto the surface of APTES-modified silica particles via a methacryloxy-1- $\beta$ -hydroxy-3-aminopropyl trimethoxysilane. Proposed growth pathway of pGMA is then moderated via RAFT polymerization from the surface AP-GMA moiety whilst growing as a free polymer in solution.

However, after multiple unsuccessful attempts at trying to get particles of the MAG-AP-SiP to grow pGMA, guided by particle sizing which revealed no discernable change in particle size during preparation it was determined that Michael addition of the amine to the alkene bond had occurred (Figure 6-3).



**Figure 6-3: Michael addition of glycidyl methacrylate (GMA) to the aminopropyl-moiety of the silica particle (AP-SiP). Reaction is via the double bond with the amine resulting in deactivation for further polymerization from the double bond.**

An alternative solution was sought along the same approach, growing polymer from the surface via a CTA agent connected to the silica nanoparticle and its aminopropyl coating as demonstrated in the next section.

### **6.3 Creation of Brush Polymers via the formation of Chain-transfer Agent-coated Silicas (CTA-SiPs).**

In the presence of reversible addition–fragmentation chain-transfer (RAFT) chain-transfer agents (CTA) it is possible to grow polymers with well-defined polydispersity and structure as discussed in Chapter 3.3.1. The nature of RAFT polymerization means that CTAs act as moderating, and crucially, as directing agents for polymer growth; therefore, attaching a RAFT CTA to the surface of the silica particle (RAFT-SiP) should enable us to direct and control polymer growth from the silica surface.

Growing free polymer growth through RAFT polymerization in a dispersion of RAFT-SiPs results in growth in the free medium and at the particle surface; however, a combination of steric hindrance and a critical third dimension of travel compared to free CTA in solution, polymer growth is retarded at the silica surface. Due to the nature of CTA-controlled polymerization the ratio in size of free polymer to bound is usually consistent (Moraes et al., 2013), usually to a size proportional to the overall free polymer length with a similar degree of polydispersity (C. Li et al., 2006).

#### **6.3.1 *Synthesis of a CTA-functionalised silane coupling agent (SCA)***

Synthesis of the SCA-CTA is depicted in Figure 6-4 and is achieved by using 1-Ethyl-3-(3-dimethylaminopropyl)carbodiimide (EDCI) as an amide-coupling agent.

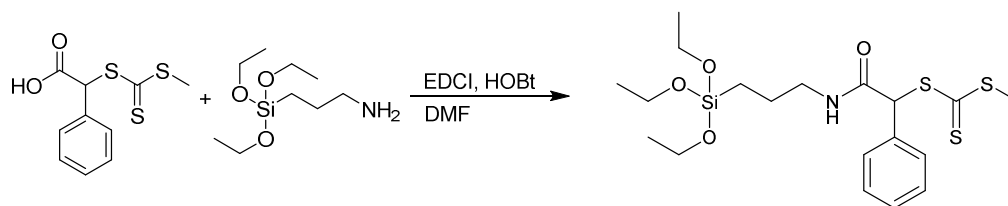


**Figure 6-4: Synthesis of mono-methyl trithio-2-phenylacetic acid (MMPAA) with 3-aminopropyl triethoxysilane (APTES) using amide-coupling agents to create the CTA-functionalised silane coupling agent (SCA). HOBt: Hydroxybenzotriazole; DMF: dimethyl formamide.**

The exact structure of the output SCA-CTA is difficult to characterize as extraction into ethyl acetate, repeated aqueous washing and subsequent drying, yielded a yellow oily substance in all instances. Evaluation of the  $^1\text{H}$ -NMR results shows that the peaks associated with the ethoxy-silane moieties do not correspond to their expected proportionality, but other components of the molecule align quite well with one another (Figure 6-5). This indicates that the CTA-SCA may be partially hydrolysed at the silane end or potentially in a state of flux and reconfiguration as anticipated in Figure 6-6, the main compound forming a heterocycle or potentially oligomers.

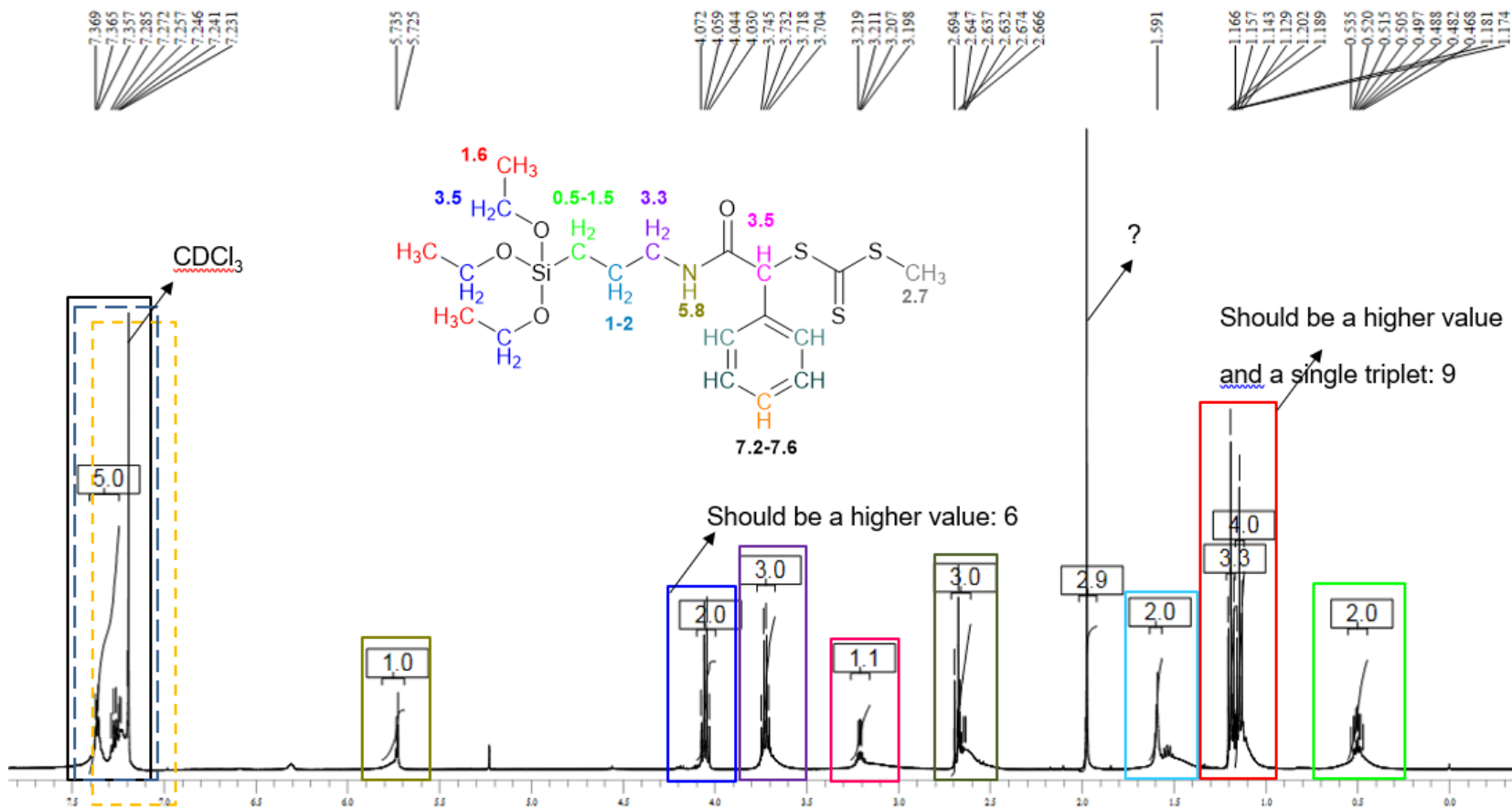


Figure 6-5: <sup>1</sup>H-NMR of the SCA-CTA recovered oil. Samples were dissolved in CDCl<sub>3</sub>. Proton-signal attribution did not correspond directly to the intended compound but key signals did and are colour-coded.

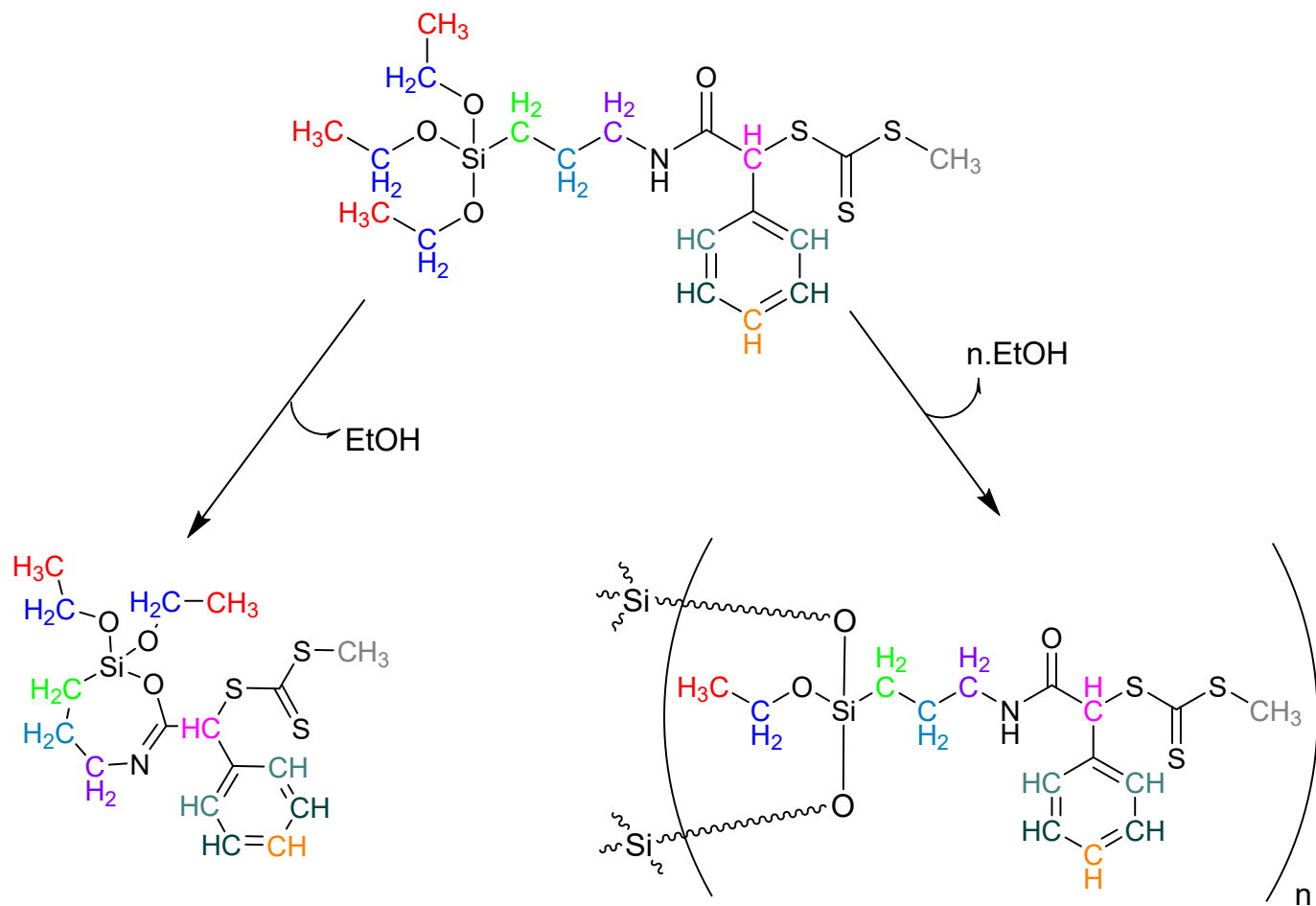
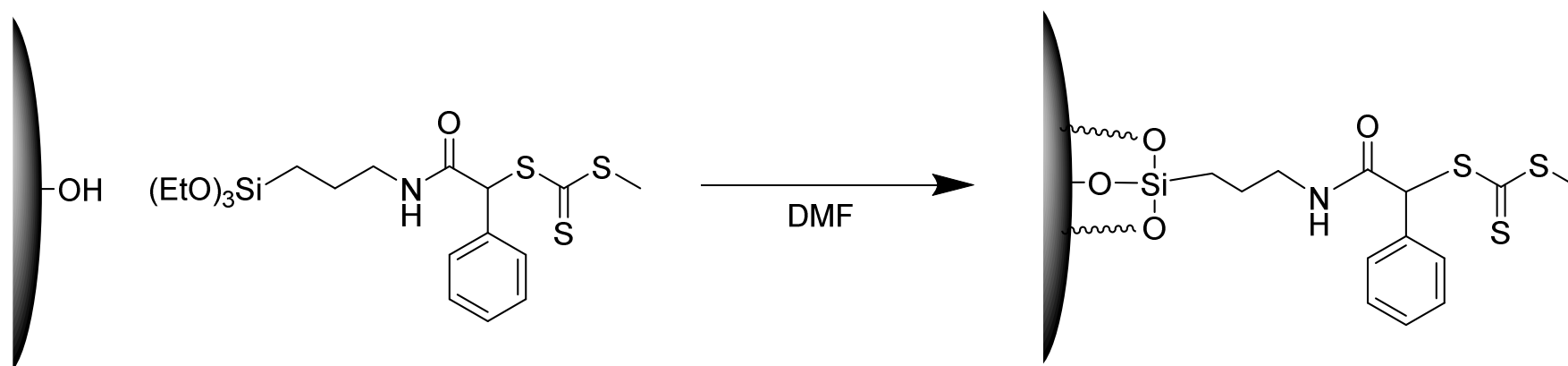


Figure 6-6: Proposed chemical reorganisation of the SCA-CTA compound. The lower left indicates a proposed mechanism for the formation of a heterocycle, the right, the formation of an oligomerised SCA-CTA.

The suggested structural reorganisations based on the NMR results does not suggest that the silane-coupling moiety was inactive, it is only predicted to be in flux but likely still available to react further with the catalyst for immobilisation. Reaction with the SCA was confirmed using thin-film chromatography, with the disappearance of the CTA compound being used to confirm readiness for the next step (3 hours). The SCA-CTA compound was combined with well-dispersed silica particles in multiple iterations and an array of conditions are tested as indicated in Chapter 4 to the silica to ensure complete coating (Figure 6-7).



**Figure 6-7: Simplified anticipated reaction scheme of the SCA-CTA compound with silica surface.**

The table below represents the various conditions that were used in attempts to conduct the reaction between the CTA-SCA and the silica surface.

**Table 6-2: Conditions for CTA-SCA condensation to silica particles. EDCI coupling of the chain-transfer agent (CTA) to the silane coupling agent (SCA) is as per Figure 6-4 in all instances.**

Iteration	Conditions
1	CTA-SCA oil extracted in an ethyl acetate/aqueous wash before drying then dissolving into toluene with dispersed silica particles and refluxed at 90°C in a 3:1 molar excess for 18 hours.
2	CTA-SCA solution is added in-situ to dispersed silica particles in DMF at 120°C at a ratio of 3:1 for 18 hours.
3	CTA-SCA oil extracted in an ethyl acetate/aqueous wash before drying is purified through a silica column. Resultant oil is dissolved in DMF with dispersed silica particles and refluxed at 120°C at a ratio of 3:1 for 18 hours.
4	Reiteration of 2: CTA-SCA solution is added in-situ to dispersed silica particles in DMF at 120°C at a ratio of 3:1 for 18 hours.

In all cases the dispersed solid is then diluted in acetone before repeated centrifugations at 10,000 rpm for 5 minutes, repeated with replacement acetone (x3) followed by water (x3), and subsequent drying in a vacuum oven overnight to produces an indelibly yellow solid. (Figure 6-8).

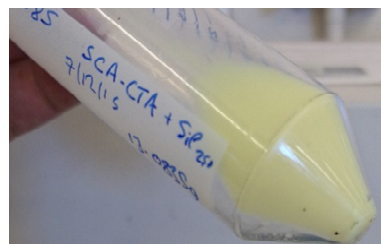


**Figure 6-8: Recovered CTA-SiP from iteration 1 following multiple washes in toluene (x3) and water (x3) before drying in a vacuum oven overnight.**

### 6.3.2 Discussion of TGAs of iterations 1-4

When characterizing the results of these experiments, the changes to the particle surface chemistry was monitored using Fourier-transform Infrared Spectroscopy. Thermogravimetric analysis was used to determine added organic mass to the silica and can be found in the appendices (Figure A-5 and A-6).

**Table 6-3: %-organic mass loss, taken as the difference in mass loss between the untreated silica (mass loss due to water, silica-surface dehydration and calcination) and the organically treated silica.**

Iteration	%-organic mass loss	
1	3.34	Mass increases were seen in all 4 iterations beyond the untreated silica, with the highest mass increase being associated with the purified CTA-SCA (iteration 3), but increases are seen in in-situ addition of the CTA-SCA (iteration 2 and 4). Limited conclusions can be drawn without a qualitative analysis of the chemical composition; FTIR was employed to determine the degree of chemical change.
2	5.36	
3	9.44	
4	4.39	

### 6.3.3 Discussion of FTIR results of iterations 1-4

Attenuated total reflectance (ATR) Fourier-transform infrared (FTIR) spectroscopy was used on all samples to determine the infrared spectra. Comparatives of untreated silica, an amine-treated chain-transfer agent (CTA), and the uncoupled CTA used in the synthesis of the CTA-SCA, and ultimately the CTA-SiP, can be seen in Figure A-7.

Figure A-8 shows comparative FTIR spectra versus iterations of the CTA-SiPs with iteration 4 given in Figure A-8ii.

All iterations of the CTA-SiP showed peaks around 3250 and 1650cm<sup>-1</sup> indicative of a carbonyl and amide bond respectively (Figures A-9 to A-12.) Iterations 1-3 showed minute, multiple peaks around the 1900-2100 region, potentially linked to the trithio-carbonate moiety at the silica surface. Whilst indicative of chemical change, the overwhelming signal peaks associated with Si-O-Si and Si-OH bends make it difficult to interpret. Polymerization at the silica surface was attempted in any case.

### 6.3.4 Polymerization at the surface

Samples of our functional silica particles, CTA-SiPs, are dispersed in an array of solvents in which methyl or glycidyl methacrylate monomer, free CTA (MMTPAA) and VASO64 initiator are dissolved at variable ratios. The mixture is sealed before being sparged for 5 minutes with nitrogen gas and subjected

to heating for 24 hours in an oil bath before being removed from the heat. The reaction mixture is added to a centrifuge tube an excess of THF before being dispersed, centrifuged, the solution removed and solid reserved, before being re-dispersed several more times in fresh THF. "Free" polymer could be extracted from the THF solution for analysis using  $^1\text{H-NMR}$  to determine chemical composition. Molecular weight and polydispersity was measured using several high performance liquid chromatograph (HPLC) techniques including size-exclusion chromatography (SEC-HPLC) and advanced polymer chromatography (APC). The extent to, if any, organic mass was added to the silica particle surface, is measured using thermogravimetric analysis (TGA), changes to its surface composition is ascertained using Fourier-transform infrared spectroscopy.

The range of experimental conditions are laid out in Table 6-4.

**Table 6-4: Polymerisation conditions; standard conditions throughout: Temperature hold: 64°C, Total volume: less than 6mL; hold time: 24 hours. CTA-SiP mass: 40mg; nitrogen sparge time: 5 minutes prior to temperature bath. Molar ratio of CTA to initiator,  $n_{\text{CTA}}/n_{\text{initiator}}$  ratio = 10.**

Experiment #	CTA-SiP iteration # in Table 6-2	Conditions	Degree of Polymerisation  DP = $[M]/[CTA]$
1. pMMA-SiP <sub>1</sub>	Table 6-2.1	Monomer ([M]): MMA; [CTA]: MMTPAA; solvent: DMF	50
2. pMMA-SiP <sub>2</sub>	Table 6-2.1	Monomer ([M]): MMA; [CTA]: MMTPAA; solvent: DMF	100
3. pMMA-SiP <sub>3</sub>	Table 6-2.2	Monomer ([M]): MMA; [CTA]: MMTPAA; solvent: DMF	50
4. pMMA-SiP <sub>4</sub>	Table 6-2.2	Monomer ([M]): MMA; [CTA]: MMTPAA; solvent: DMF	100
5. pMMA-SiP <sub>5</sub>	Table 6-2.3	Monomer ([M]): MMA; [CTA]: MMTPAA; solvent: DMF	50
6. pMMA-SiP <sub>6</sub>	Table 6-2.3	Monomer ([M]): MMA; [CTA]: MMTPAA; solvent: DMF	100
7. pMMA-SiP <sub>7</sub>	Table 6-2.4	Monomer ([M]): MMA; [CTA]: MMTPAA; solvent: toluene.	100
8. pGMA-SiP <sub>1</sub>	Table 6-2.4	Monomer ([M]): MMA; [CTA]: MMTPAA; solvent: toluene.	100

#### 6.3.4.1 Experiments 1 & 2: Iteration 1 CTA-SiP with MMA at DPs 50 and 100.

FTIR results for both pMMA-SiPs 1 and 2 displayed no material difference in their FTIR spectra (Figures A-5 and A-6 in the appendices), despite evidence of free polymerization based on SEC-HPLC results (Table 6-5). Observed free polymer was significantly higher than predicted in all cases but this process would be independent of polymerization at the silica particle surface. The expectation was to see bound-polymer at the surface and free polymer produced, depending on the efficacy with which the RAFT agent behaved there would be a proportional relationship between the 2.

TGA results for both pMMA-SiP<sub>1</sub> and pMMA-SiP<sub>2</sub> produced from CTA-SiP<sub>1</sub> showed a small reduction in mass in pMMA-SiP<sub>1</sub> and a large reduction in mass in pMMA-SiP<sub>2</sub> (Figure A-14 in the appendices); however, pMMA-SiP<sub>2</sub> appears to have a marked increase in mass during the 200°C hold period<sup>5</sup>

**Table 6-5: SEC-HPLC results for Molecular weight of the free pMMA polymer produced in-situ CTA-SiP<sub>1</sub>**

Experiment	Degree of Polymerisation DP = [M]/[CTA]	Predicted molecular weight of pMMA/ g mol <sup>-1</sup>	Mw	Mn	Poly-dispersity
pMMA-SiP <sub>1</sub>	50	5006	20,801	17,872	1.16
pMMA-SiP <sub>2</sub>	100	10,012	40,438	38,038	1.06

#### 6.3.4.2 Experiments 3 & 4: Iteration 2 CTA-SiP<sub>2</sub> with MMA at DPs 50 and 100.

Like iterations 1 and 2, iterations 3 and 4 showed no evidence of changes in their overall FTIR structure from the CTA-SiP experiments from the underlying CTA-SiP (Figure A-15 and Figure A-16), indicating no change in surface chemistry.

Comparison of the infrared spectra of oPETTC-SiP<sub>3</sub> with the attendant pHPMA-SiP<sub>3</sub> samples created show marked changes in the spectra pattern of the

<sup>5</sup> Small quantities of each pMMA-SiP were produced and the project had moved on before it was decided to repeat

pHPMA-SiPs, with the defined peaks between 3000-2700 disappearing (Figure A-36 in the appendices). This is consistent with what was seen in Figure A-30 with the pHPMA-SiP<sub>2a</sub> (the equivalent here being A-36iii), and the free polymer extracted from this in Figure A-31 from iteration 2.

SEC-HPLC showed free polymer in pMMA-SiP<sub>3</sub>, but repeated attempts to gather results for pMMA-SiP<sub>4</sub> showed aberrant values with the statistical molecular weight of 1288, below that of pMMA-SiP<sub>3</sub> (DP = 50) despite its higher predicted degree of polymerization (DP = 100) (Table 6-6).

**Table 6-6: SEC-HPLC results for Molecular weight of the free polymer produced in-situ CTA-SiP<sub>2</sub>**

Experiment	Degree of Polymerisation / DP = [M]/[CTA]	Predicted molecular weight of pMMA/ g mol <sup>-1</sup>	Mw	Mn	Poly-dispersity
pMMA-SiP <sub>3</sub>	50	5006	25,350	23,571	1.08
pMMA-SiP <sub>4</sub>	100	10,012	30,893	26,324	1.17

Similar to iterations 1 and 2, TGA analysis of 3 and 4 showed a marked reduction in organic mass compared to the CTA-SiP<sub>2</sub> used to create them (Figure A-17). The resultant mass loss in both cases was over 4% for both iterations with similar profiles to the CTA-SiP<sub>2</sub> TGA profile.

#### **6.3.4.3 Experiments 5 & 6: Iteration 3 CTA-SiP<sub>3</sub> with MMA at DPs 50 and 100.**

It appeared that polymerization at the surface had not been successful in any of the iterations of the CTA-SiP (Figure A-18 and Figure A-19); pMMA was present in all cases as a free polymer but FTIR showed that no discernible change in chemical structure at the surface could be seen, in spite of free polymer being detected using SEC-HPLC (Table 6-7).

**Table 6-7: SEC-HPLC results for Molecular weight of the free polymer produced in-situ with CTA-SiP<sub>3</sub>**

Experiment	Degree of Polymerisation/ DP = [M]/[CTA]	Predicted molecular weight/ g mol <sup>-1</sup>	Mw	Mn	Poly-dispersity/ (Mw/Mn)
pMMA-SiP <sub>5</sub>	50	5006	22,345	18923	1.18
pMMA-SiP <sub>6</sub>	100	10,012	33,440	28969	1.15

pMMA from this pMMA-SiP<sub>6</sub> was extracted by precipitating into methanol, re-dissolving in THF before drying out the sample in a vacuum oven overnight. FTIR revealed peaks in the 2900-3000cm<sup>-1</sup> region as well as sharp peaks in the 1680-1730cm<sup>-1</sup> region, which are both highly indicative of C-H and C=O bond stretches respectively. Peaks below 1500cm<sup>-1</sup> are highly indicative of pMMA when compared to commercial spectra for pMMAs of a similar chain length (Figure 6-9).

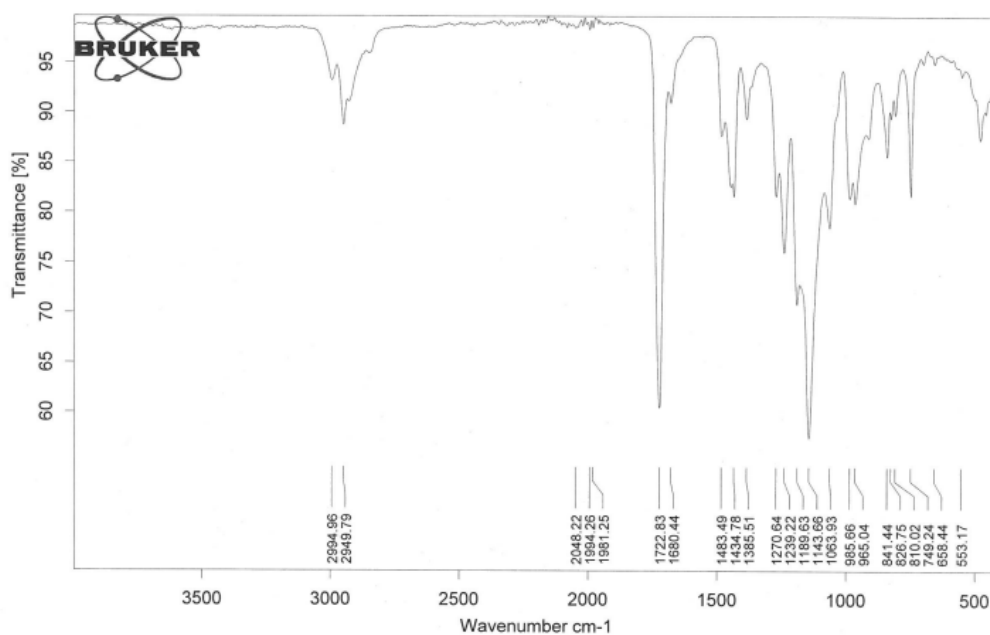


**Figure 6-9: FTIR spectra from the isolated free pMMA from pMMA-SiP<sub>6</sub> utilising CTA-SiP<sub>3</sub>.**

All evidence points to the added organic material at the surface not being active, with regards to having active chain-transfer moieties from which to grow polymer in-situ with free polymer in solution.

#### 6.3.4.4 Experiments 7 & 8: Iteration 4 CTA-SiP<sub>4</sub> with MMA and GMA at DP = 100.

The FTIR spectra of pMMA-SiP<sub>7</sub>, as with previous iterations, does not suggest pMMA has been grown from the silica surface (Figure 6-10). SEC-HPLC was not done on the free polymer.

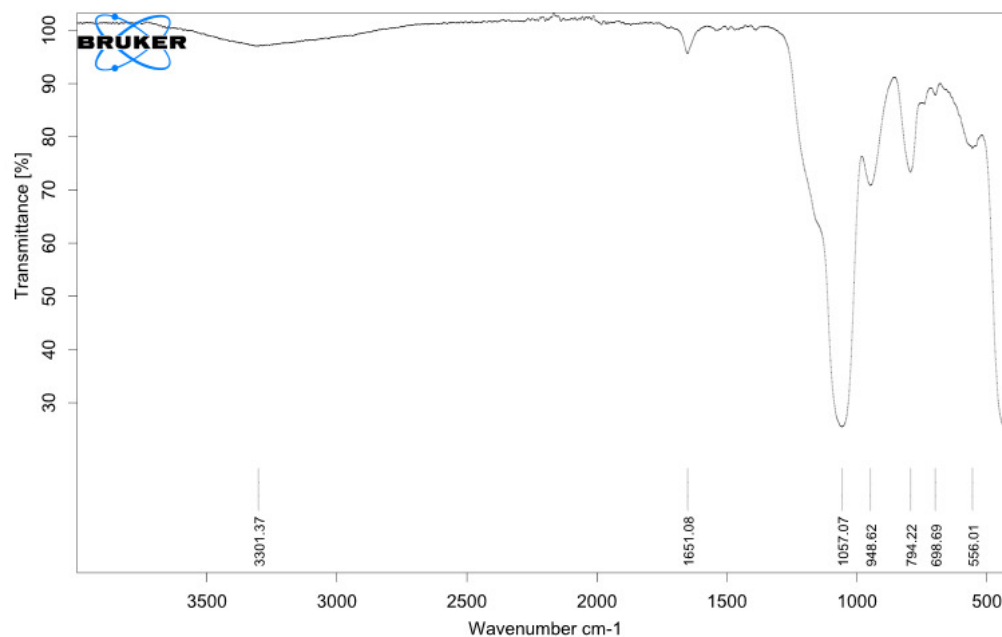


**Figure 6-10: FTIR spectra of pMMA-SiP<sub>7</sub> utilising CTA-SiP<sub>4</sub> at DP = 100.**

The reaction medium for pGMA-SiP created a gel which proved impossible to dissolve and retrieve the solid; SEC-HPLC on the extracted free polymer into dichloromethane revealed a highly disperse polymer; multiple runs showed a maximal peak that never accounted for more than 80% of the total detectable signal<sup>6</sup>.

<sup>6</sup> Previous SEC-HPLC results were all in excess of 98% for their maximal peak.

**Table 6-8: SEC-HPLC results for Molecular weight of the free poly(glycidyle methacrylate) polymer produced in-situ with CTA-SiP<sub>4</sub>. Chart includes details of the Peak Molecular Weight Report for %Area of the peak, with main weights being shown. All remaining individually detected at a maximum account for less than 3% of the peak area respectively.**

Experiment (SEC-HPLC run #)	Degree of Polymerisation/ DP = [M]/[CTA]	Predicted molecular weight/ g mol <sup>-1</sup>	Mw/ g mol <sup>-1</sup>	Mn/ g mol <sup>-1</sup>	Poly-dispersity/ (Mw/Mn)	%Area of main peak
pGMA-SiP (run 1)			62912, 409	42024, 375	1.50, 1.09	74.53%, 16.58%
pGMA-SiP (run 2)	100	14215	11446, 410	8501, 373	1.35, 1.10	65.833%, 21.51%
pGMA-SiP (run 3)			19695, 410	13280, 376	1.48, 1.09	76.93%, 13.94%

85

The likely source of this broad variance in polymer weight is likely due to epoxy-polymerisation, likely promoted by the presence of silylic acid moieties at the silica surface engaging in ring opening of the epoxy group of the glycidyl methacrylate, resulting in cross-linked polymerization. As SEC-HPLC analysis looks at the comparative exclusionary behaviours of similar polymers to a set of polymer similar enough in chemistry to be illustrative, it is likely the departure from similar poly-methyl methacrylate free polymers produced is as a result of cross-linkage and subsequent gelation. Organoclays have been shown to initiate epoxy self-polymerization (Chan et al., 2010) so this is possible.

### 6.3.5 *Kinetic Studies of pGMA*

Attempts to get polymers to grow from the silica surface via a surface-bound chain-transfer agent, were unsuccessful; free polymerization was occurring in the presence of free chain-transfer agent, indicating the likely source of something had occurred during attachment of the CTA-SCA to the silica surface, forming the CTA-SiP; likely this was down to deactivation of the RAFT group, disabling polymer growth at the silica surface whilst free polymer could be produced.

Another potential problem could be the mismatch in chain-transfer agent to the monomer family studied; the impact of RAFT agents on polymerization behavior is discussed in Chapters 2 and 3 but Figure 6-11 models what the idealized kinetic behavior of our polymerization would look like in 3 different situations:

- Conventional (no CTA, just monomer and initiator): no moderation of the kinetics of polymerization; entirely down to the availability of monomer, resulting in an initially rapid rate of polymerization, tailing off as monomer was consumed, likely resulting in polymers with high polydispersity.
- Retardation (good match between CTA and monomer): the initial rate of polymerization was retarded, resulting in moderation of the polymerization process and incorporation of chain-transfer agents into the polymer. Moderating the rate of polymerization should lead to the predictable control of polymer chain length based on the CTA content with relation to monomer and highly controlled polydispersity.
- Induction (poor match between CTA and monomer): the stability of the CTA when it becomes incorporated into the growing polymer chain is so high that the rate of polymerization is reduced significantly; as CTA begins to disassociate from the polymer chains the rate of reaction increases to and the rate of reaction begins to look comparable to the conventional rate, mean no to low moderation and likely poor control of the chain length but moderate control of polydispersity.

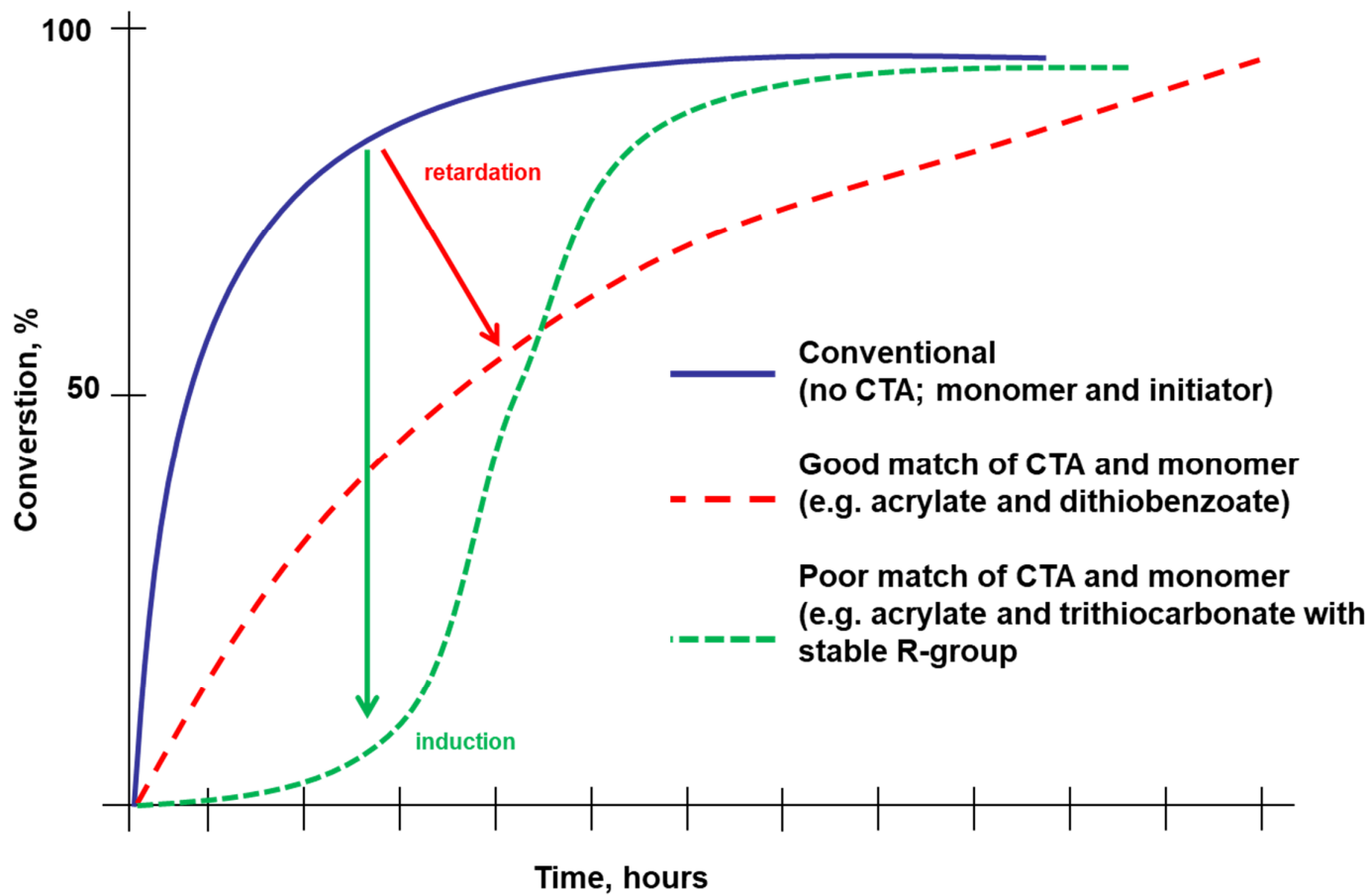
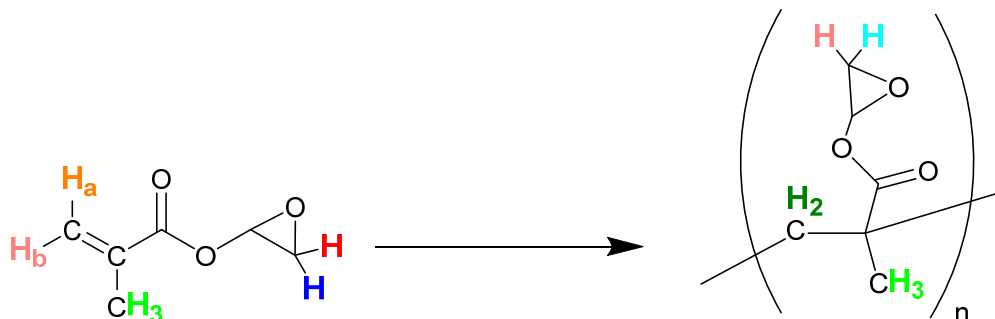


Figure 6-11: Scheme for kinetic behavior for the 3 potential scenarios of polymerization with or without a chain-transfer agent.

The kinetics of glycidyl methacrylate were investigated in order to determine if there was a problem associated with CTA moderation at the silica surface or within the free polymer synthesis itself; 3 scenarios are investigated and the conditions are in Table 6-9. The extent of the reaction is determined using  $^1\text{H-NMR}$ : polymerisation of GMA causes the NMR signals of the 2 geminal hydrogens on the epoxy group to shift, the ratio of the 2 new geminal peak seats to all peaks giving the extent of consumption (Figure 6-12).



**Figure 6-12: Schema for determining the extent of polymerization of pGMA. Red and blue geminal hydrogens on the epoxy ring have NMR signals that shift with polymerization. The alkene geminal hydrogens become indistinguishable from the methyl peak.**

**Table 6-9: Kinetic study scenarios for GMA polymerization: all studies were conducted with the same amount of monomer and molar equivalents of CTA when used and initiator. Reactions are sparged with N<sub>2</sub> for 5 minutes before being heated to 70°C, aliquots taken on an hourly basis are immediately cooled in an ice bath and <sup>1</sup>H-NMR is used to determine the extent of the reaction.**

Scenario	Detail	
Free-radical polymerization	CTA-free Polymerization in DMF with initiator only.	
MMTPAA-moderated polymerization		MMTPAA used as chain-transfer agent in DMF with initiator.
PETTC-moderated polymerization		PETTC used as chain-transfer agent in DMF with initiator

In the presence of both chain-transfer agents the reaction nears 70% conversion at 3 hours; however, only the PETTC-moderated polymerization continues to near completion at 6 hours (93%) in line with that expected for a good matching RAFT agent to monomer; the initiator-only polymerization and MMTPAA-moderated reaction's appearing to enter a period of induction before proceeding to 93% and 72% respectively at 8 hours.

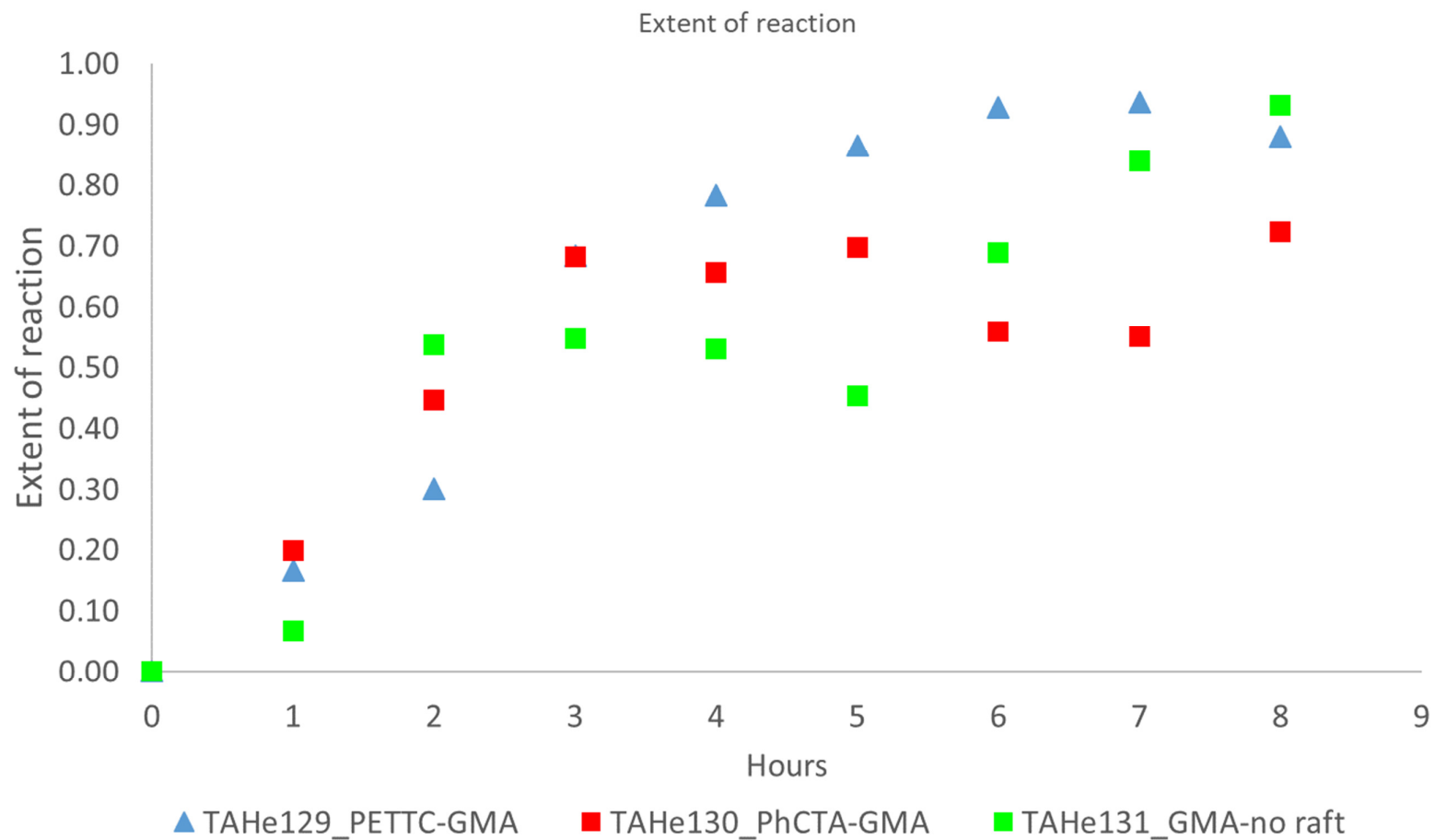


Figure 6-13: Kinetic studies of pGMA in 3 scenarios; ▲: PETTC as CTA; ◆: MTPAA; ■: no CTA, initiator only.

## 6.4 Concluding Remarks

Despite encouraging early stages suggesting a route to polymer growth at the silica surface ultimately it was unsuccessful; the likely reason for this was that the RAFT moiety had degraded when attached to the silica surface at some point at the condensation stage as the evidence suggested it was still present during the amine-coupling step.

More importantly though these studies indicated that glycidyl methacrylate would not be a suitable scaffold for iridium catalyst as it was consistently gelling in the presence of silica; even if solid, silica-attached pGMA could be isolated it would likely be impractical to extract and exploit for catalyst purposes.

Kinetic studies of pGMA in isolation did however suggest we could use more mild procedures in building our polymer backbone, particularly in the growth of material on the surface if we could improve on the silica condensation step. Efforts were then directed at using a more effective RAFT/CTA agent and milder conditions in order to create a CTA-active silica.

## **7 Results: Creating Brush Polymers via oligomerization of MAPTMS, subsequent growth of pHPMA polymers; observed attachment of iridium catalyst.**

In Chapter 6 we described the attachment of a chain-transfer agent (CTA),  $\alpha$ -(monomethyl trithiocarbonyl) phenyl acetic acid (MMTPAA) with a silane coupling agent (SCA), 3-aminopropyl triethoxysilane (APTES). We then described our attempts to attach this functionalized CTA-SCA to a 250nm silica particle (SiP) and subsequently grow free & bound-polymers of methyl methacrylate (MMA) and glycidyl methacrylate (GMA) using free CTA and bound CTA-moiety.

Free growth of polymer was achieved in solution, albeit polymer growth was poorly controlled by MMTPAA; however, no noticeable growth was observed of polymers at the surface, with neither the TGA result showing appreciable changes in lost organic mass or surface chemical change in its FTIR spectra. The reasons for this are unclear, but initial limited content of the CTA-SCA added to the SiP, or decomposition of the trithiocarbonate-group during reflux would likely figure into the reasons. Improved methods for addition and improvements in the behaviour of the CTA-SCA must be sought.

Additionally, attempts to polymerize glycidyl methacrylate in the presence of the CTA-Silica particles resulted in gelation and an inability to recover the silica particles; there is evidence this could be caused by the epoxy ring-opening reactions catalyzed by the silica surface causing cross-chain linkages (Chan et al., 2010).

Improvements in the way brush polymers were made and the polymers attached were sought.

## 7.1 Improved Brush Polymers.

The outcomes in Chapter 6 pointed to 2 major issues to overcome:

1. Improved resilience in the CTA-SiP when condensing onto the silica particle.
2. An alternative polymer system that won't gel in the presence of organically modified silicas (OrMoSils).

Ring-opening of glycidyl methacrylate polymers has been shown to occur in the presence of amine-treated organoclays (Chan et al., 2010); thus, given the issues experienced working with GMA avoiding amines and their analogues is ideal. Equally, chain-transfer agents in the reversible addition-fragmentation chain-transfer (RAFT) family of compounds can, post-polymerization, retain the CTA-moiety at the end of a polymer chain (Chapter 3); if you grow a polymer of one composition using a RAFT agent a second polymer of different composition can potentially grow from the "live" CTA end.

With this in mind, we generated oligomers of methacryloxypropyl trimethoxysilane (MAPTMS) using 4-cyano-4-(2-phenylethane sulfanylthiocarbonyl) sulfanylpentanoic acid (PETTC) chain-transfer agent to generate short-chain polymers, or oligomers, of around 5 monomers in length. The relatively high concentrations of CTA agent to monomer should make it likely the oligomer retains the active CTA agent through the polymerization stage and onto the silica surface once condensed to it (Figure 7-1). When a secondary polymerization reaction is initiated in the presence of the CTA-enabled silica particle, *o*CTA-SiP, should then participate in a second block-polymer growing from the silica surface (Figure 7-2).

Glycidyl methacrylate (GMA) was believed to gel in the presence of the silica surface (Chan et al., 2010); it also posed a non-ideal solution to linking to the iridium cyclopentadienyl (IrCp\*) compound, as the linking hydroxyl group would need to be changed to an amine to initiate the necessary epoxide ring-opening stage. Hydroxypropyl methacrylate (HPMA) was investigated instead to build the second portion of the block co-polymer, with a view that HPMA could be utilized for attachment of the original IrCp\* complex.

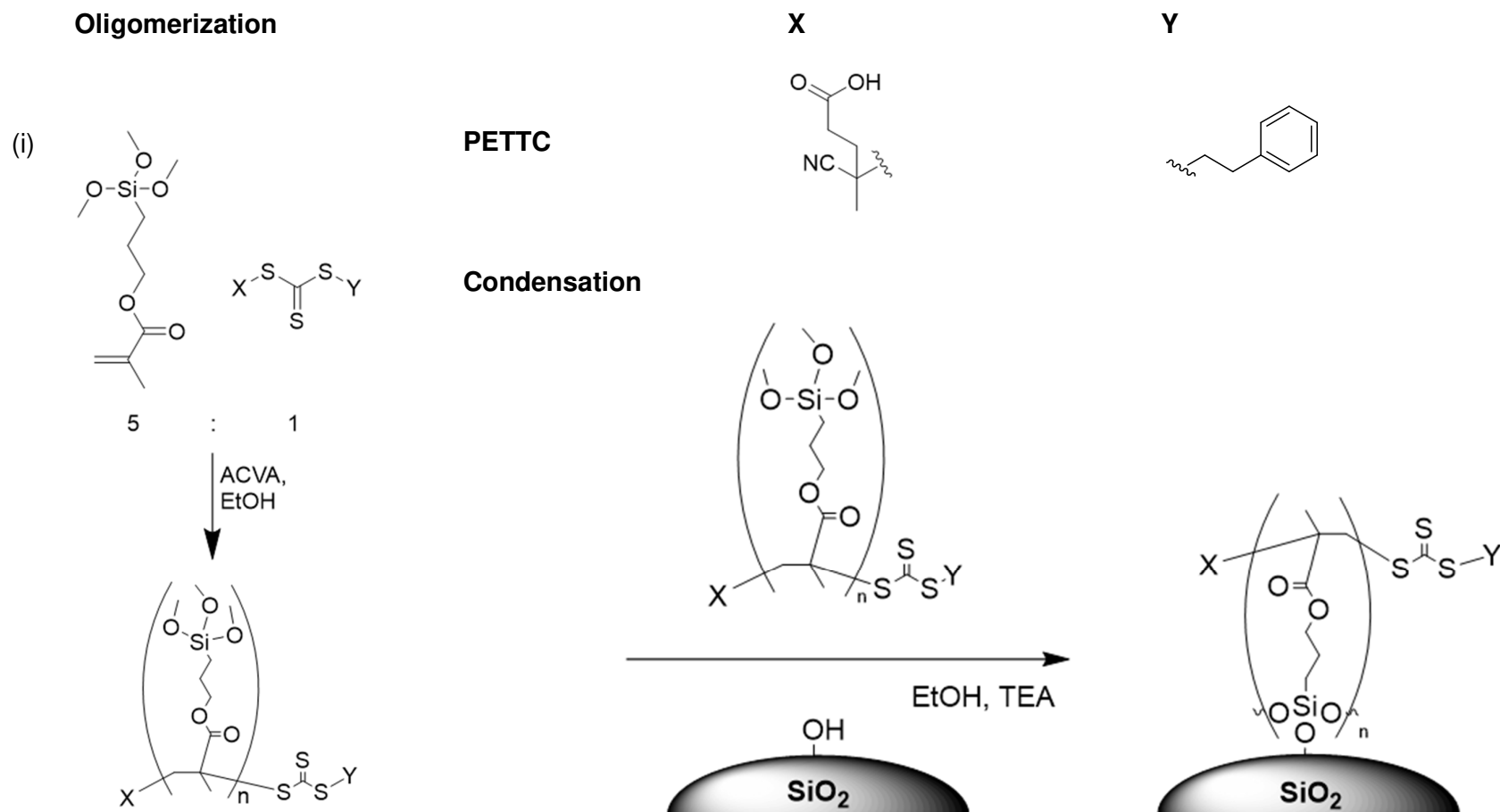


**Figure 7-1: (i) Synthesis of oligomers (5:1) of MAPTMS with PETTC to create oligo-CTA-SCAs (oCTA-SCAs); (ii) Condensation of oCTA-SCA to silica to create oCTA-SiPs. X and Y groups are as indicated above. The MAPTMS chain number, n, is indicated as aiming for a 5:1 molar ratio of MAPTMS:PETTC in in this initial stage.**

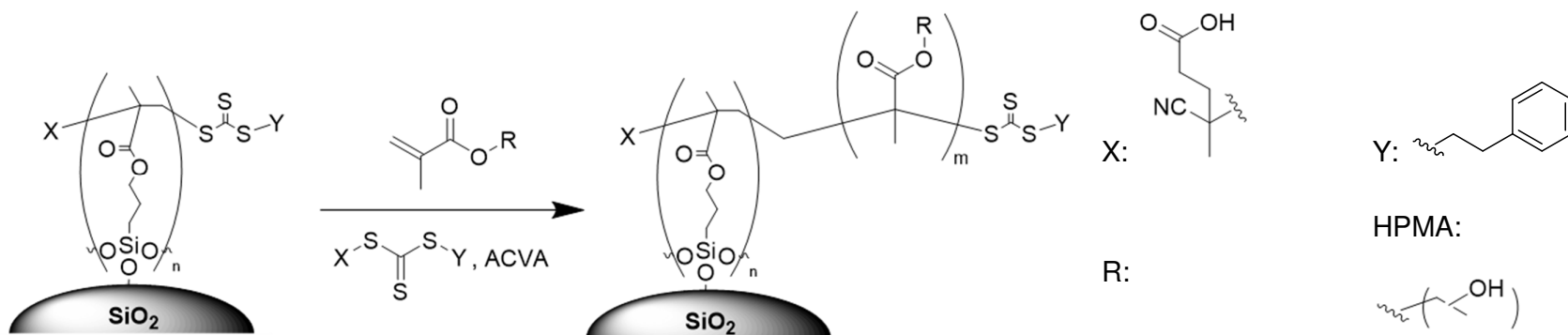


Figure 7-2: Polymer growth from an oligomer-treated silica particle,  $\alpha$ CTA-SiP. Hydroxypropyl methacrylate (HPMA) were used in the block-polymerization step. The HPMA polymer chain number,  $m$ , is given by the free monomer molar ratio to free CTA.

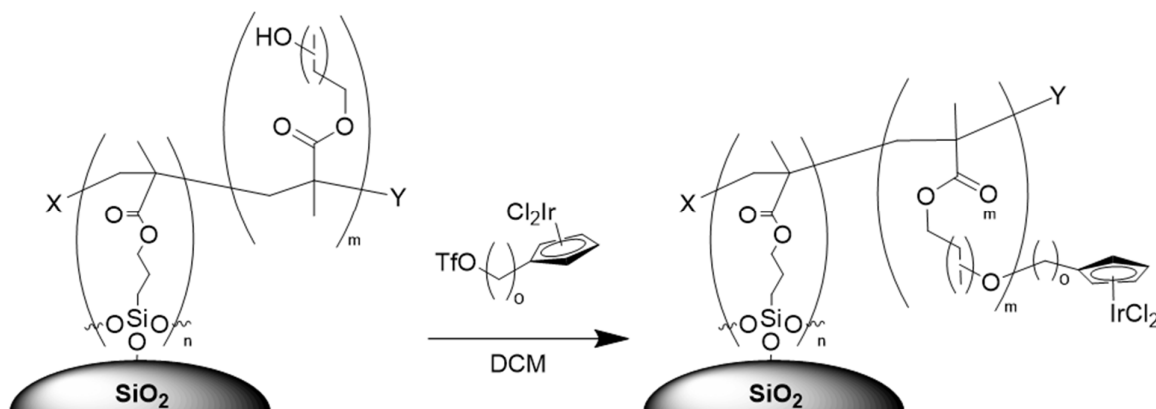


Figure 7-3: Functionalisation of the pHPMA-SiP with Iridium Cyclopentadienyl complex functionalised with a hydroxyl group. The carbon chain length of the  $\text{IrCp}^*$  complex,  $o$ , represents the number of carbons in the linking chain and was synthesised with a 5- and 12-carbon chain backbone; however, only the 5-carbon chain was investigated at this stage.

## 7.2 oPETTC-SiP synthesis and polymerization

The steps preceding the synthesis of pHPMA-SiPs and the variations were subject to multiple iterations to determine the best conditions but followed a basic plan throughout:

1. Oligomerization of oPETTC-SCA: synthesis of the oligomeric sub-unit with an active CTA unit, used to condense to silica.
2. Condensation of oPETTC-SCA to silica to form oPETTC-SiPs: this was usually done at a 1:1 weight-to-weight basis and thus in excess.
3. Polymerization of oPETTC-SiPs with methyl methacrylate (MMA) and hydroxypropyl methacrylate (HPMA) monomers to create pMMA-SiPs and pHPMA-SiPs respectively.

All iterations centred on this theme with adjustments in each to account for observed phenomena.

## 7.3 Synthesis of oPETTC-SCA

Several iterations of the oligo-MAPTMS-PETTC compound (oPETTC-SCA) were attempted with small variations to the following procedure: methacryloxypropyl-trimethoxysilane (MAPTMS) was dissolved in ethanol with 4-cyano-4-(2-phenylethane sulfanylthiocarbonyl) sulfanylpentanoic acid (PETTC), and initiator 4,4'-Azobis(4-cyanopentanoic acid) (ACVA) before the solution was sparged with nitrogen gas. The mixture was then heated and after a pre-requisite number of hours quenched in an ice bath before being used further (Figure 7-4).

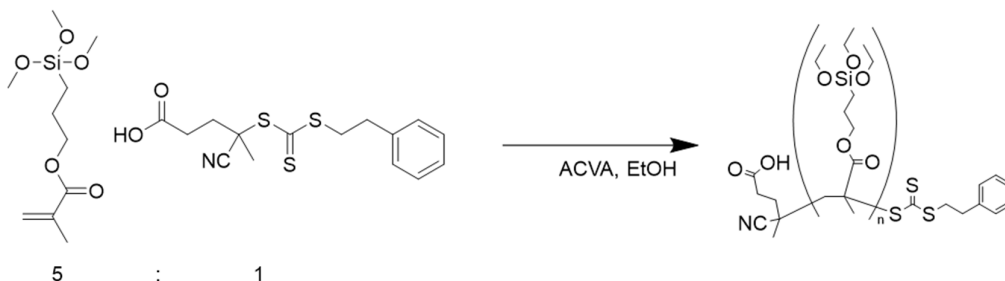


**Figure 7-4: MAPTMS was dissolved in DMF at a molar ratio of 5:1 to PETTC before polymerization is initiated with AIBN at 70°C for 3 hours.**

### 7.3.1 Condensation of *o*PETTC-SCA onto Silica.

Condensation of *o*PETTC-SCA to the 250nm-diameter silica particle to form *o*PETTC-SiP is illustrated in Figure 7-5:

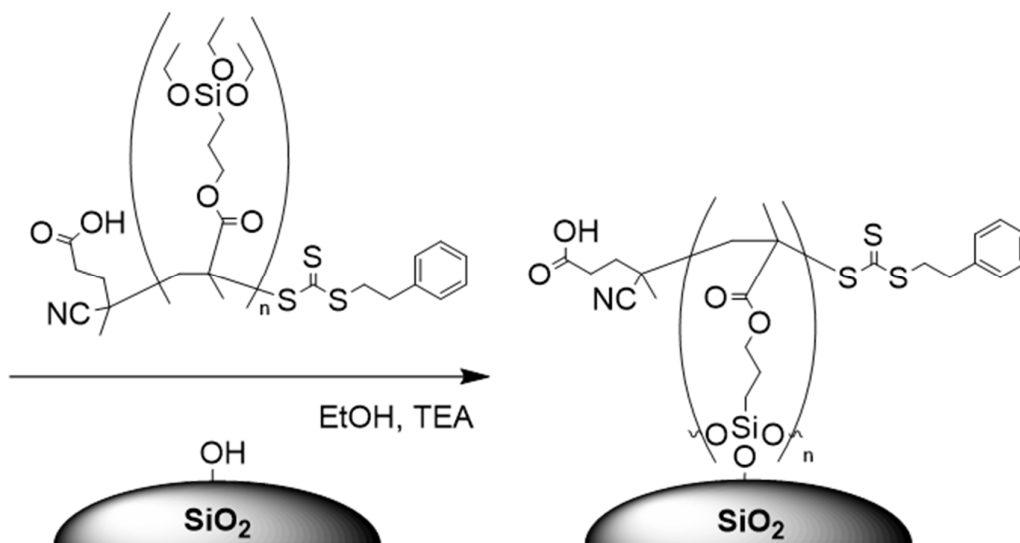


**Figure 7-5: Schematic showing the condensation of *o*PETTC-SCA to silica particles used throughout; individual conditions described in each section for each iteration.**

*o*PETTC-SCA synthesis was repeated in multiple iterations with modifications to the condensation step to silica particles and the specifics are described for each.

### 7.3.2 Polymerization to the modified surface of oPETTC-SiP

Polymer growth onto the oPETTC-SiP is illustrated in Figure 7-6:

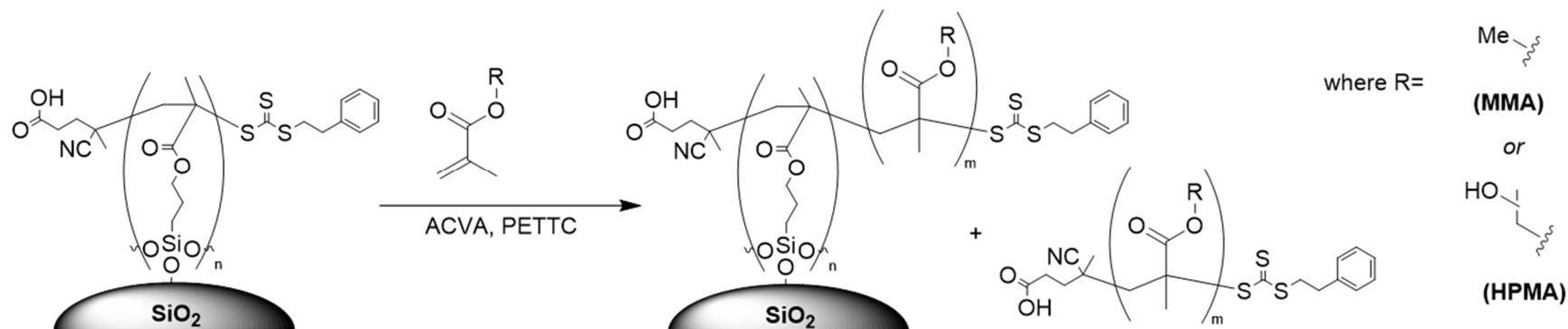


**Figure 7-6: Polymer growth from the oligomer-coated active-silica, utilizing free-polymerization of monomer in the presence of ACVA initiator and free chain-transfer agent. Specific conditions are discussed for each iteration, as is the monomer used.**

Free polymerization of methyl methacrylate (MMA) or hydroxypropyl methacrylate (HPMA) with PETTC RAFT agent was attempted with an array of conditions and molar ratios tried, with the different iterations detailed below.

#### 7.4 Iteration 1: 3-hour hold, purification testing, 18-hour condensation, and Polymerization of methyl methacrylate at DP = 100.

*o*PETTC-SCA was prepared using the above procedure and quench-cooled. The *o*PETTC-SCA was then split in 2:

- a) The sample was used as was, with no purification, made up to 50mL with toluene (*o*PETTC-SiP<sub>1a</sub>).
- b) A sample lot was purified through a silica plug in ethyl acetate, then washed in brine, the ethyl acetate layer dried, evaporated to an oil before being made up to 50mL with toluene (*o*PETTC-SiP<sub>1b</sub>).

Dispersed 250nm silica particles in ethanol (1g in 10mL, sonicated using a sonic probe at 40% amplitude for 2.5 minutes) was then added to both samples along with trace triethyl amine (TEA, 5 $\mu$ L) acting as catalyst before being refluxed at 100°C for 16 hours, before being centrifuged at 8000rpm for 10 minutes, decanted and repeated with fresh ethanol and re-dispersed 3 times, before being dried in a vacuum oven.

##### 7.4.1 FTIR comparison of PETTC, *o*PETTC-SiP<sub>1a</sub>, and *o*PETTC-SiP<sub>1b</sub>.

Iteration 1 of the *o*PETTC-SiP was prepared along 2 different routes: a). purified, b). and prepared and used as-is; both exhibited similar infrared spectra to each other and to the precursor PETTC chain-transfer agent the coating oligomer was based on (Figure A-20). This indicates a qualitative amount of active oligomer coating on the surface in both cases<sup>7</sup>.

---

<sup>7</sup> Appendices A-4 is the FTIR for blank silica used for comparison.

#### **7.4.2 Thermogravimetric analysis comparison of *o*PETTC-SiP<sub>1a</sub>, *o*PETTC-SiP<sub>1b</sub>, and untreated silica particles.**

The TGA heating protocol method was updated in line with Mueller et al (2003) to the following protocol to capture the major compositional changes: under a nitrogen atmosphere, dynamic and static elements for the heating protocol were as follows:

1. Heated from 50-125°C at 10°C min<sup>-1</sup>, then held for 10 minutes.
2. 125-280°C at 10°C min<sup>-1</sup>, then held for 10 minutes.
3. 280-540°C at 10°C min<sup>-1</sup>, then held for 10 minutes.
4. 540-800°C at 10°C min<sup>-1</sup>, then held for 10 minutes.
5. The material is then heated to 1100°C at 10°C min<sup>-1</sup> before being cooled to room temperature at 10°C min<sup>-1</sup>.

The dynamic and static elements can be seen in the Appendices for silica nanoparticles (Figure A-21), this technique is used from Chapter 7 onwards for all TGA samples unless explicitly stated otherwise.

Appendices Figure A-22 gives the TGA profiles for both *o*PETTC-SiPs *1a* and *1b* in comparison to one another. Figure A-23 shows the calculated breakdown of both.

In comparison to the blank, untreated silica *o*PETTC-SiPs *1a* and *1b* showed an additional mass content of 9.04% and 2.93% respectively; the purified silica showing a smaller quantity of additional mass content is in line with the procedures used to remove the extra mass; comparisons between *1a* and *1b* in terms of their FTIR spectra show that there is little difference in the surface chemistry; however, it would be difficult to determine if this translates into additional activity in terms of the ability to grow polymer from the surface so trialing the growth of methyl methacrylate (MMA) with it.

#### **7.4.3 Polymerization of methyl methacrylate using *o*PETTC-SiP<sub>1a</sub> and *o*PETTC-SiP<sub>1b</sub>, unpurified and purified oligomer-coated silica.**

Samples containing *1a* and *1b* *o*PETTC-SiP were prepared for polymerization using the following method: MMA and PETTC, at a molar ratio of 100:1, and the *o*PETTC-SiP were dispersed in tetrahydrofuran (THF) with ACVA initiator.

The solution was sparged with N<sub>2</sub> before being subjected to an atmosphere of N<sub>2</sub> and heated and stirred at 70°C for 3 hours. The mixture was then rapidly cooled in an ice bath, before being dispersed in ethanol, centrifuged at 8000rpm for 10 minutes, decanted and repeated with fresh ethanol and re-dispersion 3 times, before being dried in a vacuum oven. FTIR and TGA were utilized to get an indication of surface chemistry and organic content and HPLC was used to determine the approximate chain length of the free polymer, with several studies indicating bound-polymer growing at a proportional level of between 50-70% that of the free polymer (Li and Brian C Benicewicz, 2005; Gao et al., 2013).

FTIR of the particles from both feature can be seen in Figure A-24 in the appendices. Both have features common with silica but only *o*PETTC-SiP<sub>1a</sub> (ii) retains features expected of a silica particle coated with organic material. Peaks around 1725 and 1440cm<sup>-1</sup> were similar to those of extracted free polymers of pMMA from previous experiments (Figure A-25). The FTIR spectra of 12(i) suggests that there was not sufficient polymer on the silica surface and potentially decomposition of the underlying active CTA compound. Further analysis was discontinued.

TGA analysis of *o*PETTC-SiP<sub>1a</sub> can be seen in Figure A-26 in the appendices and shows a significant increase in mass within the organic region (125-540°C) with a mass loss in this region of 47.87%, an increase in the amount of observable mass from the original *o*PETTC-SiP<sub>1a</sub> of 38.83%.

Free polymer weight for both *1a* and *1b* samples obtained using SEC-HPLC can be seen in Table A-1 in the appendices. This shows a free polymer weight around 3-4000 daltons below the theoretical molecular weight likely due to an incomplete degree of polymerization given the hold time, strengthened given the wide polydispersity exhibited in both samples.

TGA analysis of pMMA-SiP<sub>1b</sub> was also done (Figure A-27). The mass loss in the equivalent 125-540°C region for pMMA-SiP<sub>1b</sub> was considerably lower at 7.02%, accounting for a 0.1% increase in mass over the *o*PETTC-SiP<sub>1b</sub> it was based on. This corresponds to the qualitative differences in FTIR spectra

between *1a* and *1b*, the latter missing reference peaks for the active CTA component and pMMA have disappeared.

Purification for future iterations were shelved; with the apparent success in adding additional CTA and subsequent polymer content to the silica particle seen in pMMA-SiP<sub>1a</sub>, a second iteration using the target monomer, hydroxypropyl methacrylate (HPMA), was trialled.

### **7.5 Iteration 2: 3-hour hold oligomerization, 18 hours condensation, polymerization of hydropropyl methacrylate at multiple degrees of polymerization of 50, 100, 200 and 500, and hold times.**

New samples of the oligo-CTA SCA, and subsequent steps from oPETTC-SiP<sub>2</sub> to polymerization with HPMA (pHPMA-SiP<sub>2</sub>) were carried out using the methods as laid out in 1.1 for each step, albeit with the modifications to the used monomer, from MMA to HPMA, and trialing multiple molar ratios of monomer to CTA (thought to be a good indicator of the eventual degree of polymerization, or DP) as laid out in Table A-2 in the appendices with the same oPETTC-SiP<sub>2</sub>.

#### **7.5.1 FTIR Comparisons of PETTC and oPETTC-SiP<sub>2</sub>.**

The FTIR spectra, in comparison the PETTC starting material, can be seen in Figure A-28 in the appendices. In spite of identical conditions and materials the FTIR spectra appears different to the neat oPETTC-SiP<sub>1a</sub> created in iteration 1. There are several more defined peaks at 2983, 2916 and 2849cm<sup>-1</sup> along with a broad Si-OH peaks around 3379cm<sup>-1</sup>.

#### **7.5.2 Thermogravimetric analysis of oPETTC-SiP<sub>2</sub>**

The TGA for oPETTC-SiP<sub>2</sub> can be seen in Figure A-29 in the appendices and shows significantly smaller quantities of oPETTC-SCA<sub>2</sub> condensed to the surface, with a mass loss of 5.64%; applying the previous assumptions of up to 4.04% being attributable to the silica surface chemistry; this gives us a total attributable organic content of at least 1.60%; however, given the qualitative nature of the FTIR spectra it seems likely the answer lies somewhere between 5.64 and 1.60%, with the difference in mass from the changing surface chemistry of untreated silica being the upper-most limit on organic content.

### 7.5.3 Polymerization of *o*PETTC-SiP<sub>2</sub>

Free-polymerization of hydroxyl-propyl methacrylate (HPMA) was attempted in the presence of free-PETTC RAFT agent and the *o*PETTC-SiP<sub>2</sub> to cause polymer growth from the CTA-active oligomer. This was done with an 18-hour hold with a molar ratio of monomer to free-CTA of 100, and following this at 4 different molar ratios of monomer to CTA (degrees of polymerization): 50, 100, 200 and 500 with a 5-hour hold. The longer hold time for both tranches of experiments was adopted as the free polymer produced in the presence of iteration 1 was smaller than predicted so a longer hold time was tried.

The FTIR spectra for the dried and cleaned pHPMA-SiP<sub>2a</sub> can be seen in Figure A-30 in the appendices. It shows peaks in the place suggestive of organic components synonymous with pHPMA; broad peaks at 3260cm<sup>-1</sup> could be attributable to either Si-OH or C-OH peaks, but peaks at 2980cm<sup>-1</sup> are strongly indicative of alkane bonding profiles and the strong peaks around 1750-1620cm<sup>-1</sup> is indicative of the ester backbones present in the methacrylate, either from oligomer or the pHPMA backbone. Free pHPMA was recovered from the polymerization media by sampling and dropping into excess dichloromethane to precipitate the pHPMA and its SEC-GPC profile can be seen in

Table A-3 and its FTIR spectra can be seen in Figure A-31, both in the appendices. The actual molecular weight indicates a degree of polymerization around 158, higher than expected.

Thermogravimetric analysis (TGA) of pHPMA-SiP<sub>2a</sub> suggests a small but quantitative change from the *o*PETTC-SiP<sub>2</sub> and can be seen in Figure A-32. A mass loss of 7.93% equates to an additional mass added of 7.93 - 5.64 = 2.29%; such a small quantity of polymer added to the surface content is in line with the qualitative change in nature of the infrared spectra of the polymer-functionalized silica particles; however a repeat of this iteration was warranted to see if improvements in organic content could be achieved.

Figure A-33 in the appendices shows the FTIR spectra of an array of silica particles collected from HPMA polymerization runs with a 5-hour hold time using the same *o*PETTC-SiP<sub>2</sub> used in pHPMA-SiP<sub>2a</sub>. They were cleaned and

extracted as discussed in previous sections. Samples with higher initial amounts of monomer appear to have look more like pHPMA-SiP<sub>2a</sub>, suggesting more polymer at the surface, whilst the equivalent example of 2a at hour-5 of its polymerization, pHPMA-SiP<sub>2c</sub>, has none of the peaks associated with oPETTC-SiP<sub>2</sub> but only weak broad peaks and structure we see in 2a.

5-hour holds do not appear to be long enough for complete growth of bound-polymers so thermogravimetric analysis was not carried out on these samples; dynamic light scattering (DLS) studies on all 5 pHPMA-SiP samples and their constituent parts can be seen in Table A-4 and Table A-5.

The increase in particle diameter appears to be consistent across the pHPMA-SiP<sub>2</sub> with DPs higher than 100; if growth is cut off during the induction phase of free polymer growth we would expect to see particle size be unchanged. This is likely due to chain transfer agent at its highest concentration retarding chain growth, which is desired for regulating the chain length at the end of a reaction, but if that reaction is cut off before it can proceed with the growth phase, both in the free media and grown from the silica surface, we would expect these chains to all be at the same length. A third iteration was needed with longer hold-times to proceed to the end of the reaction and total monomer consumption; however, time constraints meant that adding organometallic iridium complex to a functional organically-modified silica particle could not wait, so pHPMA-SiP<sub>2a</sub> was used as the candidate particle; this synthesis and analysis of these are covered in Chapter 4.

### **7.6 Iteration 3: 3-hour hold oligomerization, 18 hours condensation, polymerization of hydroxypropyl methacrylate at multiple degrees of polymerization of 50, 100, 200 and 500, with 18-hour hold times.**

Polymerization of free HPMA with PETTC acting as free CTA agent, at molar ratios of 50, 100, 200 and 500:1, was achieved in the presence of freshly prepared oPETTC-SiP<sub>3</sub>, prepared using the well-established method from previous iterations. The hold-time was increased to 18-hours so we could see the effects of as close to 100% completion of the polymerization phase as was possible.

Compared to *o*PETTC-SiP<sub>1a</sub> (the equivalent material from iteration set 1) both iterations 2 and 3 *o*PETTC-SCAs differed from it in that they were prepared and used as produced after 3 hours of oligomerization, dispersed in ethanol, rather than toluene, and refluxed at 90°C with trace trimethylamine acting as catalyst.

#### **7.6.1 FTIR Comparisons of *o*PETTC-SiP<sub>2</sub> with *o*PETTC-SiP<sub>3</sub>**

The oligomer-coated active silica particle *o*PETTC-SiP<sub>3</sub> produced was analyzed and can be seen in Figure A-34 in comparison to *o*PETTC-SiP<sub>2</sub>. Peaks trace well to the previous iteration. The interpretation from this spectra is that qualitative amounts of organic material have been added in similar amounts as with iteration 2.

#### **7.6.2 Thermogravimetric analysis of *o*PETTC-SiP<sub>3</sub>**

The TGA for *o*PETTC-SiP<sub>3</sub> showed an added organic component of 6.26% (Figure A-35); as with the second iteration, this is likely representative of a total added level of organic content between that value and the underlying value of 4.04%.

This is in line with iteration 2 which had a total mass in that region of 5.64%, and felt would be a useful comparison at the polymerization stage to build upon the 5-hour hold studies.

#### **7.6.3 Polymerization of *o*PETTC-SiP<sub>3</sub>**

Free-polymerization of hydroxyl-propyl methacrylate (HPMA) was attempted in the presence of free-PETTC RAFT agent and the *o*PETTC-SiP<sub>3</sub> to cause polymer growth from the CTA-active oligomer at 4 different molar ratios of monomer to CTA (degrees of polymerization): 50, 100, 200 and 500. An 18-hour hold was also adopted to ensure that polymerization would have arrived at the near complete consumption of monomer in both free and bound polymer construction. Particulate pHPMA-SiP<sub>3</sub> samples a-d were prepared as described in previous iterations for analysis. Free polymer SEC-GPC analysis can be seen in Table A-6.

Whilst the polymer chain length appears to vary from the theoretical chain length, based on calculations from the molar ratio between monomer and chain-transfer agent, they are reasonably well controlled in terms of polydispersity

(Pdl) up till you get to *3d* with a Pdl of 1.50; likely the larger chain length with such a small amount of chain-transfer agent meant tight control was difficult. Dynamic light scattering Z-average values for pHPMA-SiP<sub>3</sub> samples a-c can be seen in Table A-7. The pattern was similar to that in Table A-5 for samples in iteration 2, albeit particles produced with higher ratios of M:CTA (or DP) appear to be considerably more pronounced in their difference than with Table A-5 and a 5-hour hold; this suggests different mechanisms are dominant at higher concentrations of free CTA (PETTC) with respect to monomer than observed in the lower concentration samples above; if higher retardation of polymer growth is observed with more chain-transfer agent this could enable growth to proceed at a slower rate overall, leading to bound-polymer growth to begin at an earlier stage.

Thermogravimetric analysis was carried out to determine the impact on how much additional organic growth the particle size changes in Table A-7 represent and can be seen in Figure A-37 and Figure A-38 in the appendices and the mass loss associated with the constituent organic component and its comparison to the original constituent components in the form of the untreated silica particles, SiP<sub>250nm</sub>, and the subsequent oligomer-coated silica particle, oPETTC-SiP<sub>3</sub> can be seen in Table A-8. Table A-8 shows concomitant mass additions of both the oPETTC-SiP<sub>3</sub> and pHPMA-SiP<sub>3</sub> samples from the original silica particle used; however, aside from pHPMA-SiP<sub>3a</sub>, each of the iterations of pHPMA-SiP<sub>3</sub> appears to record a mass loss from the oligomer-coated silica it was hoped polymer could be grown from. Given both the FTIR and DLS data indicate that there has been a material change at the surface, in chemistry and physical size respectively, TGA has difficulty as a technique for quantitatively analyzing the addition of desirable chemical moieties.

#### **7.7 Iteration 4: 7-hour hold oligomerization & UV-Vis study of 2 weight ratios, 20 hours condensation, followed by polymerization of hydroxypropyl methacrylate with 18-hour hold times.**

In this iteration we hoped to determine if the reason for the observed low levels of add mass was attributable mass was linked to the degradation of the active CTA attached to the surface at the oligomerization stage.

To this end we started by going back to the oligomerization of MAPTMS to see if the trithiocarbonate moiety, at the centre of PETTC's chain-transfer capability, was being lost during the oligomerization of MAPTMS and also to look at seeing if changing the weight-to-weight ratio of *o*PETTC-SCA to silica would have any impact. A summary of the conditions observed are on Table 7-1.

**Table 7-1: Summary of the production of *o*PETTC-SiP<sub>4</sub> and *p*HPMA-SiP<sub>4</sub> particles.**

<b>Iteration name</b>	<b>Degree of polymerization (molar ratio of monomer, M, to CTA PETTC), hold time and details.</b>
<b><i>o</i>PETTC-SCA<sub>4a</sub></b>	DP: 5, 7-hour hold time. Used for UV-Vis studies in Section 0.
<b><i>o</i>PETTC-SCA<sub>4b</sub></b>	DP: 5, 7-hour hold time.
<b><i>o</i>PETTC-SiP<sub>4a</sub></b>	<i>o</i> PETTC-SCA was condensed at a w/w ratio of 1:2 grams oligomer:SiP.
<b><i>o</i>PETTC-SiP<sub>4b</sub></b>	<i>o</i> PETTC-SCA was condensed at a w/w ratio of 1:1 grams oligomer:SiP.
<b><i>p</i>HPMA-SiP<sub>4a</sub></b>	Synthesized from <i>o</i> PETTC-SiP <sub>4a</sub> , DP: 100, 18-hour hold.
<b><i>p</i>HPMA-SiP<sub>4b</sub></b>	Synthesized from <i>o</i> PETTC-SiP <sub>4b</sub> , DP: 100, 18-hour hold.

In an effort to understand the mechanism for oligomerization, and to see if we were losing active-CTA in the process, a longer hold time for the oligomerization was adopted with identical conditions and material weights as for previous iterations, but the oligomerization process was observed on an hourly basis using UV-Vis spectroscopy.

### **7.7.1 UV-Vis Spectroscopy monitoring monomer consumption of MAPTMS.**

Whilst preparing *o*-PETTC-SCA<sub>4a</sub> Benzene and ethene moieties absorb in the 210nm region whilst the trithiocarbonate moiety absorb in the 300nm range (Figure 7-7). We would expect to see the gradual disappearance of the 210nm and the 300nm signal to remain steady throughout; Working on the assumption that molar ratio of the benzene and the trithiocarbonate group would not change we could determine what component of the UV-Vis signal at 210nm belongs to the MAPTMS monomer by discounting the component belonging to the PETTC-benzene moiety based on the absorbance at 300nm for which the monomer does not absorb. This would eliminate issues over absorbance variability from other factors (solvent loss, error, etc).

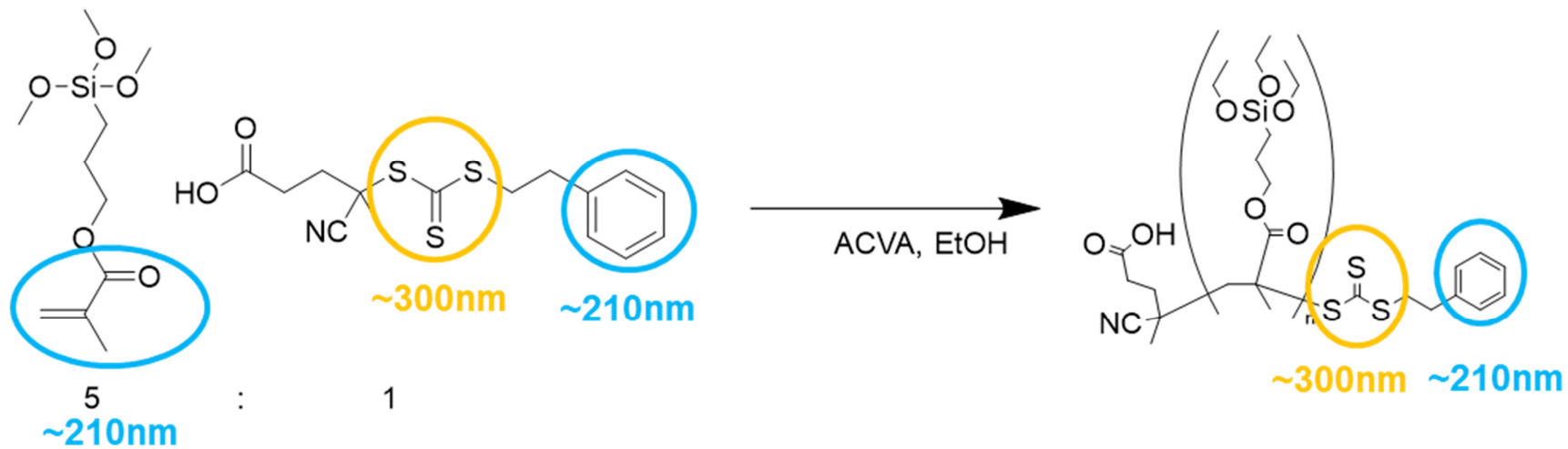


Figure 7-7: Schematic showing the oligomerization process and highlighting the chemical moieties and absorbance regions observable using UV-Visible Spectroscopy.

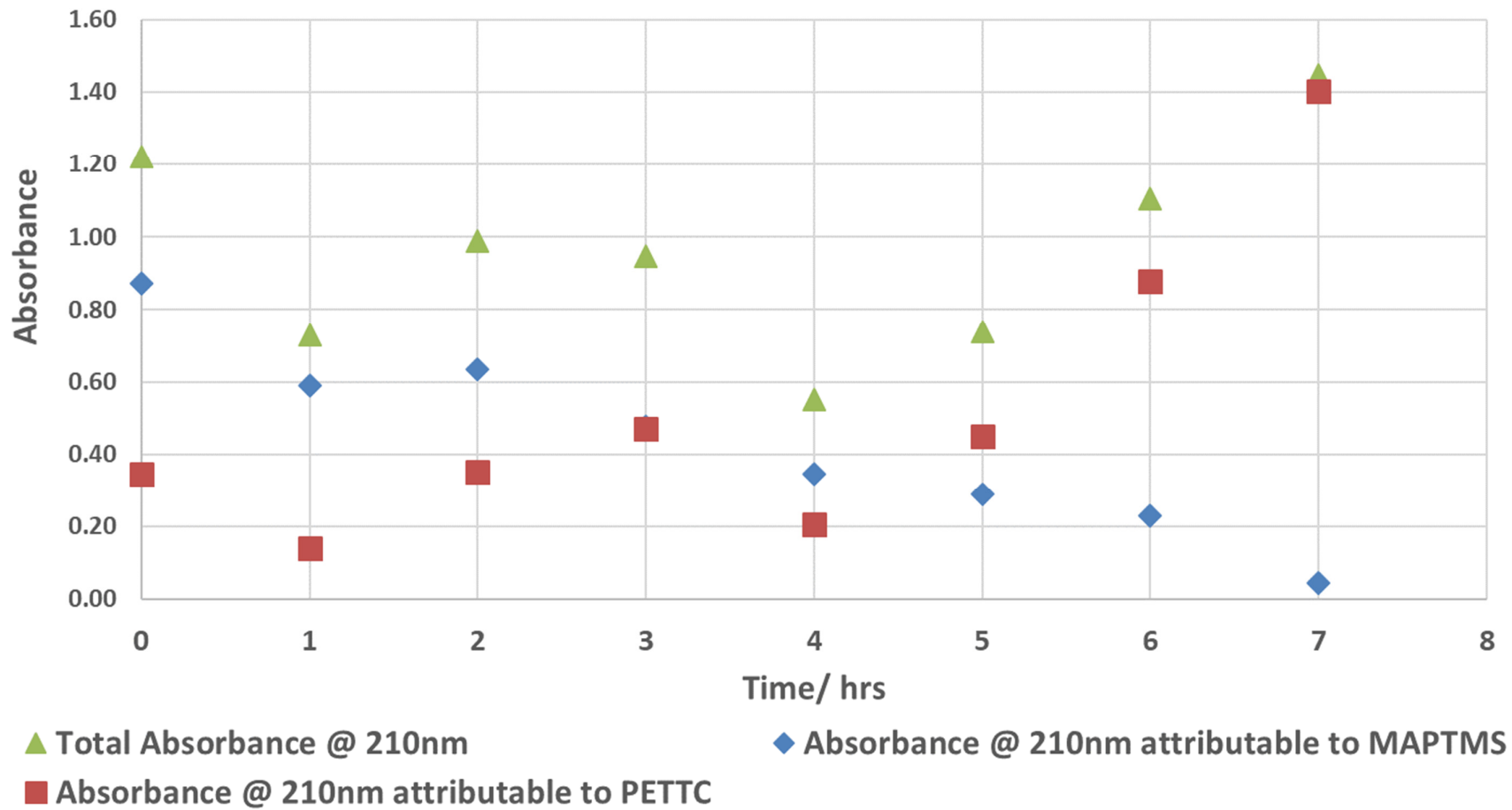
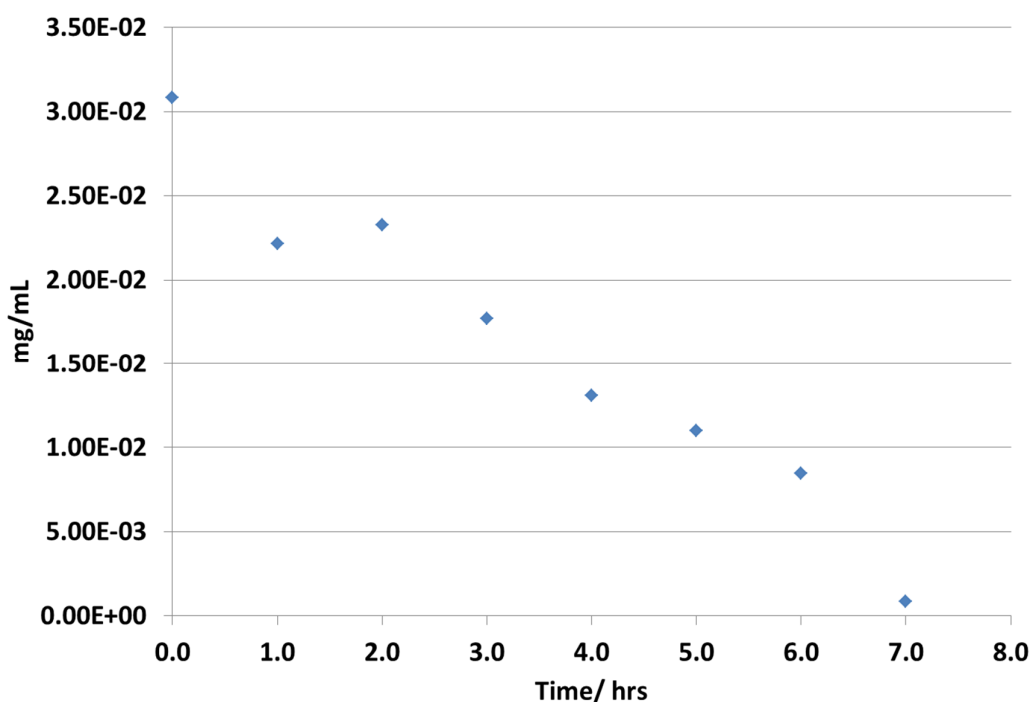


Figure 7-8: UV-Vis absorbance at 210nm. The value for MAPTMS absorbance attribution was determined by discounting the PETTC signal in comparison to its absorbance at 300nm and can be seen in the legend.

Based on the absorbance spectra in Figure 7-8 we can determine the absorbance of MAPTMS specifically, and on that basis compare it to calibration curve to determine concentration over time; this can be seen in Figure 7-9. There is a gradual drop of monomer content over time with a marked drop at 7 hours; likely, this is a result of continued sampling of the mix and/or evaporation of ethanol during reflux, but overall the pattern of monomer consumption is clear.



**Figure 7-9: MAPTMS monomer content over time during oligomerization. Values are derived from the absorbance spectra in Figure 7-8 and compared to the calibration curve for MAPTMS.**

However, whilst we can be confident of oligomerization of MAPTMS, we cannot confirm that the chain-transfer agent was incorporated into it; we would require conventional methods of condensation to silica and polymerization with HPMA.

### 7.7.2 FTIR comparison of *o*PETTC-SiP<sub>4a</sub> and *o*PETTC-SiP<sub>4b</sub>

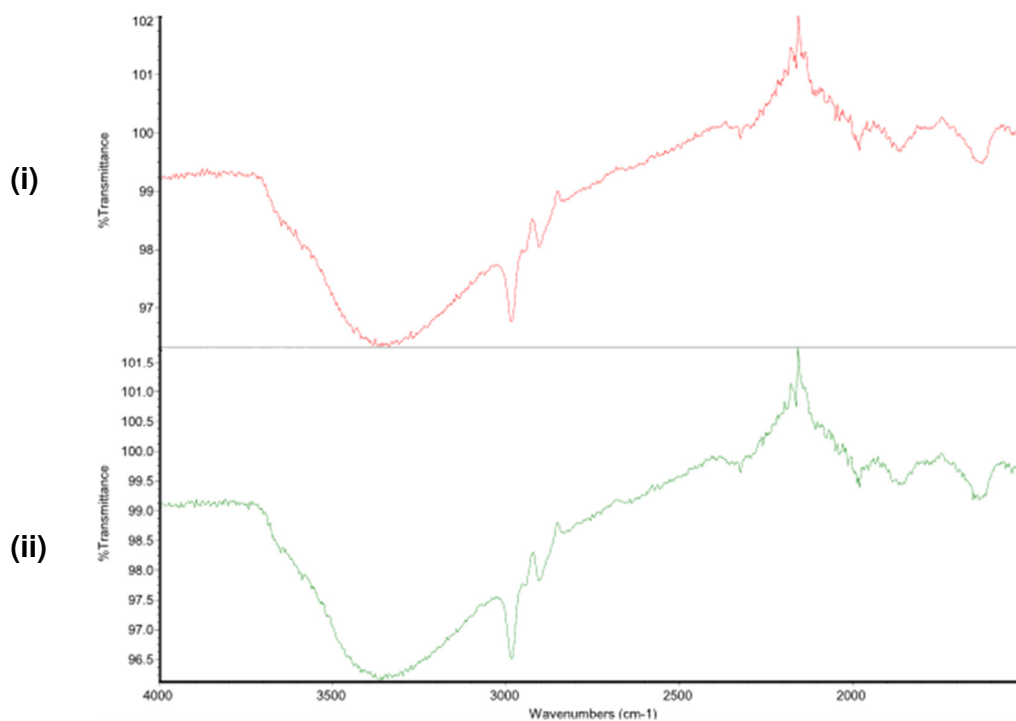


**Figure 7-10: Infrared spectra of the *o*PETTC-SiP<sub>4</sub> samples. Legend: (i): *o*PETTC-SiP<sub>4a</sub>; (ii): *o*PETTC-SiP<sub>4b</sub>.**

Following the condensation period, cleaning and drying as per previous iterations of the *o*PETTC-SiPs, FTIR spectra were taken for both *o*PETTC-SiPs and can be seen in Figure 7-10. Both particles showed remarkable comparability to each other and previous iterations suggesting that a 1:1 weight ratio of *o*PETTC-SCA to silica was excessive with the same outcome being present at lower concentrations.

### 7.7.3 Thermogravimetric analysis of $oPETTC-SiP_{4a}$ and $oPETTC-SiP_{4b}$

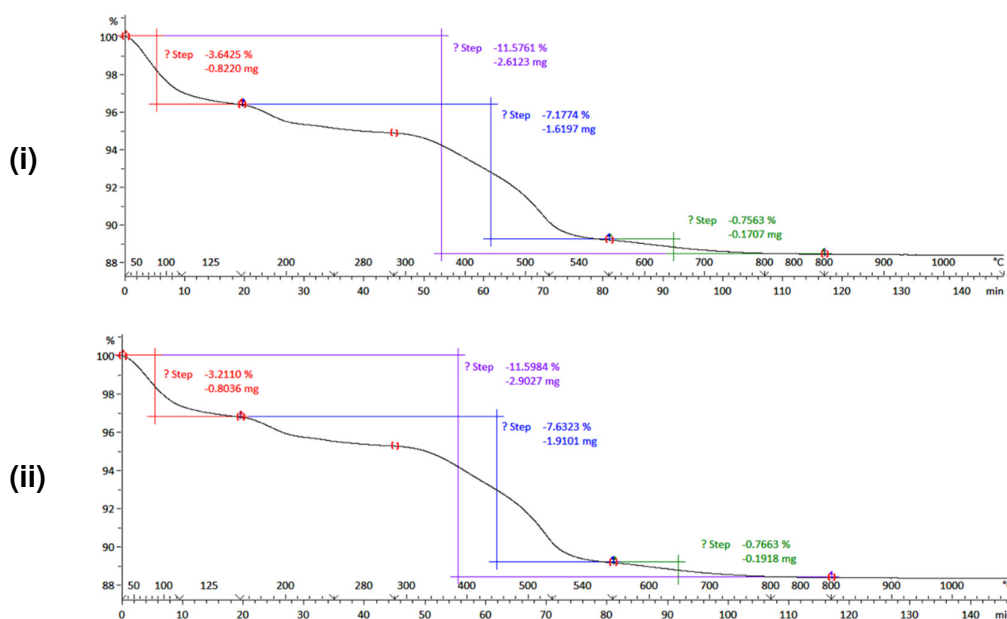


**Figure 7-11: Thermogravimetric analysis of  $oPETTC-SiP_4$  samples. Legend: (i):  $oPETTC-SiP_{4a}$ ; (ii):  $oPETTC-SiP_{4b}$ .**

Both oligomer-coated silica particles showed mass losses between the 125-540°C region of 7.18 and 7.63% respectively. This represents an increase in mass over previous iterations.

### 7.7.4 Polymerization of $oPETTC-SiP_4$ particles.

As per previous iterations oligomer-coated silica particles of  $oPETTC-SiP_{4a}$  and  $oPETTC-SiP_{4b}$  were dispersed in ethanol with HPMA monomer, ACVA initiator and PETTC for polymerization under nitrogen at 70°C. The molar ratio of monomer to PETTC was set at 100:1 and the reaction hold-time was set to 18 hours before the reaction media was cooled and the particulate matter recovered through subsequent washings in fresh ethanol before being vacuum-dried. A technique was created for cleaving bound polymer: trace organically modified silica (OrMoSils) is dispersed in caustic solution (10% aqueous NaOH) for 72 hours before neutralization with aqueous HCL (33% w/v) dissolution into the SEC-GPC media (dimethyl formamide/DMF, with 1wt% lithium bromide).

**Table 7-2: polymer SEC-GPC profiles for each pHPMA-SiP<sub>4</sub> created. Bound polymer values in parenthesis shows the actual DP values for the free polymer and the %-equivalent of that for the bound polymer in bold). Molar Ratio, M:CTA = 100; Theoretical Mn: 14,756.**

Sample, pHPMA-SiP	Mn/ g mol <sup>-1</sup> (actual DP/ free-polymer %)	Mw/ g mol <sup>-1</sup>	Pdl
4a (free)	19,625 (DP: 136)	22,340	1.14
<b>4a (bound)</b>	<b>9899 (50.4%)</b>	<b>11,185</b>	<b>1.13</b>
4b (free)	19,577 (DP: 136)	22,198	1.13
<b>4b (bound)</b>	<b>10,224 (52.2%)</b>	<b>11,324</b>	<b>1.11</b>

A concern of the cleavage technique for bound polymer was that it is likely destructive to other aspects of the polymer, particularly to the active-CTA moiety, so an exact comparative measure to free polymer cannot be explicitly stated, but the bound polymers do display a consistency of polymer length and polydispersity with the free polymer that suggests the overall structure, length and dispersity distribution is maintained.

FTIR spectra of both pHPMA-SiP<sub>4a</sub> and pHPMA-SiP<sub>4b</sub> can be seen in Figure 7-12 and Figure 7-13 in comparison to their respective oligomer-coated particle they were grown from. It is hoped that the surface chemistry for both would be identical despite the decrease in oPETTC-SCA used in the production of oPETTC-SiP<sub>4b</sub>.

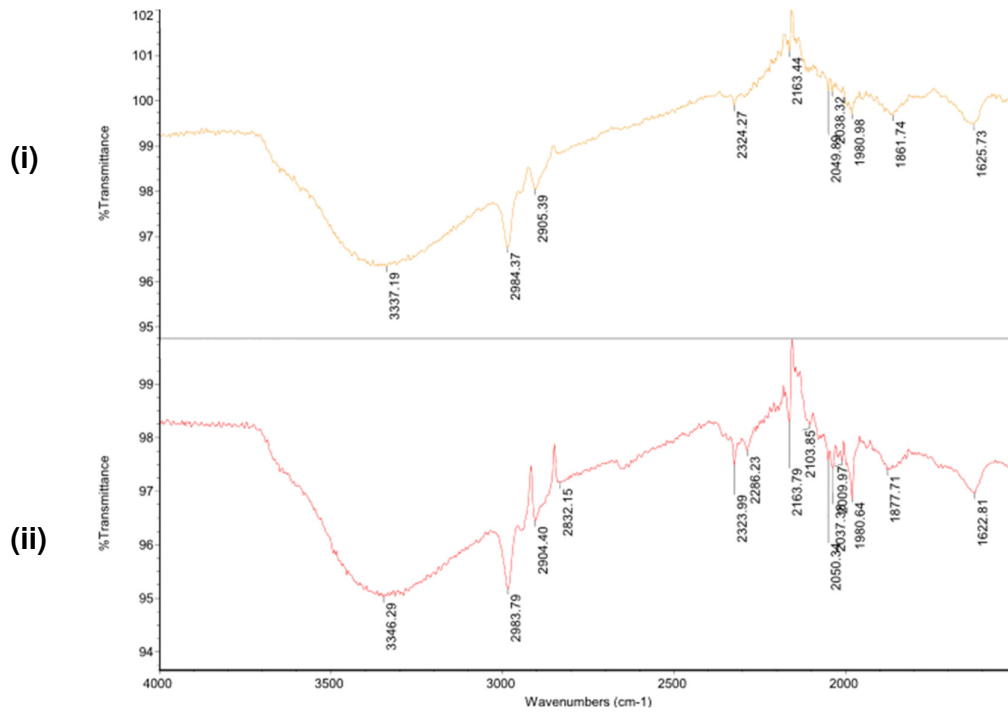


Figure 7-12: FTIR spectra comparison between (i) *o*PETTC-SiP<sub>4a</sub> and (ii) pHPMA-SiP<sub>4a</sub>. Peak region below 1500 omitted for clarity.

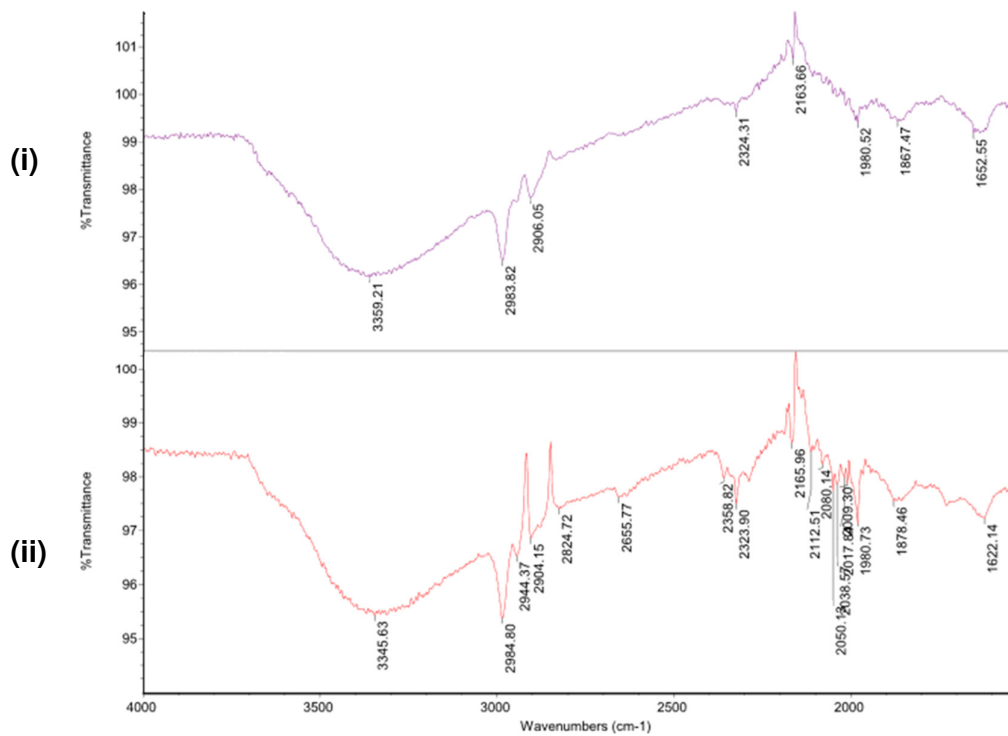


Figure 7-13: FTIR spectra comparison between (i) *o*PETTC-SiP<sub>4b</sub> and (ii) pHPMA-SiP<sub>4b</sub>. Peak region below 1500 omitted for clarity.

Both spectra show evidence of chemical change with more definite regions in line with added pHPMA content as per previous iterations. Dynamic light scattering of the polymer-coated silica particles was carried out and particle diameter values can be seen in

**Table 7-3: Dynamic Light Scattering (DLS) studies of oPETTC-SiP<sub>4a-b</sub> and pHPMA-SiP<sub>4a-b</sub> particles. Particles were dispersed in ethanol at <0.5 wt%. Legend: (i): oPETTC-SiP<sub>4a</sub>; (ii): oPETTC-SiP<sub>4b</sub>; (iii): pHPMA-SiP<sub>4a</sub>, DP = 100; (iv): pHPMA-SiP<sub>4b</sub>, DP = 100; (v): free polymer from pHPMA<sub>4a</sub>; (vi): free polymer from pHPMA<sub>4b</sub>. Particle diameter derived from size distribution by number values.**

	Particle diameter (d.nm)/ nm	PdI	Standard Deviation (d.nm)/ nm
(i)	277.1	0.06	5.1
(ii)	289.0	0.09	9.2
(iii)	627.7	0.18	97.1
(iv)	489.8	0.20	9.8
(v)	5.1	0.85	0.4
(vi)	5.2	0.76	0.3

Both paired sets for 4a (i, iii) prepared from a major excess of the oPETTC-SCA at a w/w average of 1:2, compared to 4b (ii, iv) with 1:1, shows a marked increase in size and polydispersity. The theoretical radius of gyration for polymer is given by the following equation:

$$R_{g,SAW} \approx l \left( \frac{N}{6} \right)^{3/5} \quad (7.1)$$

Where:  $R_{g,SAW}$  : radius of gyration, self-avoiding walk;  $l$ : approximate bond length of a HPMA bond ( $\approx 0.3\text{nm}$ );  $N$ : (theoretical) number of units.

Based on the free polymer weights given in Table 7-2, and the derived actual degree of polymerization of 136 in both cases, this would yield a value of:

$$R_{g,SAW} \approx 0.3 \left( \frac{136}{6} \right)^{3/5} \approx 3.2 \text{ nm} \quad (7.2)$$

Where:  $R_{g,SAW}$  : radius of gyration, self-avoiding walk

This is close to the observed diameter through DLS; however, the polydispersity suggests aggregated material of variable size and so DLS was not used elsewhere to calculate this.

Thermogravimetric analysis (TGA) was done on the cleaned pHPMA-SiP<sub>4</sub> samples using the TGA protocol for iteration 1 and beyond and can be seen in Figure 7-14. This was done to see if additional organic content had been added onto the oPETTC-SiP<sub>4a-b</sub> in comparison to previous iterations at this stage.

**Table 7-4: %-mass loss for the 125-540°C region determined through thermogravimetric analysis for pHPMA-SiP<sub>4</sub> samples and their constituent parts, collated from previous graphs. Legend: (i) Silica Particles, SiP<sub>250nm</sub> used in preparation of the rest; (ii) oPETTC-SiP<sub>4a</sub>; (iii): oPETTC-SiP<sub>4b</sub>, (iv): pHPMA-SiP<sub>4a</sub>, DP = 100; (v): pHPMA-SiP<sub>4b</sub>, DP = 100; (vi): pHPMA-SiP<sub>3d</sub>, DP = 500. Mass loss differences between the pHPMA-SiP<sub>4</sub> samples, the SiP<sub>250nm</sub> and their respective oPETTC-SiP<sub>4</sub> samples are shown in the second and third column respectively.**

	%-mass loss between 125-540°C/ %	Adjusted %-mass loss difference from untreated silica (i).	Adjusted %-mass loss difference from oPETTC-SiP <sub>4</sub> (referenced below).
(i)	4.04	0.00	-
(ii)	7.17	3.13	0.00
(iii)	7.63	3.59	0.00
(iv)	7.62	3.58	0.45 (ii)
(v)	8.67	4.63	1.04 (iii)

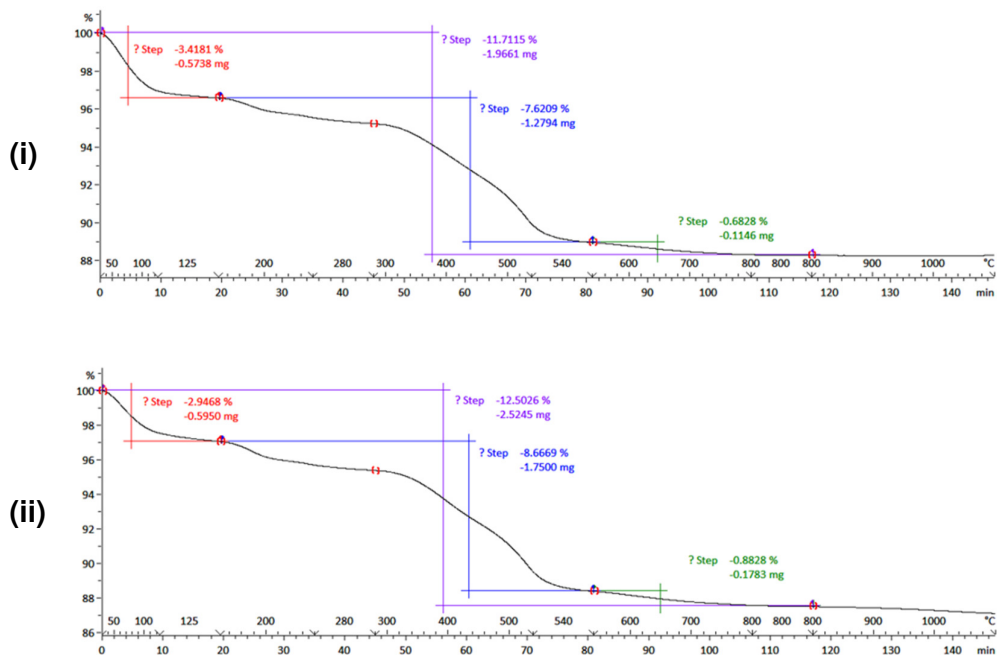


**Figure 7-14: Thermogravimetric analysis of pHMA-SiP<sub>4a-b</sub>. The TGA protocol used the new method as per that of the blank, untreated silica as in Figure A-21. Legend: (i) pHMA-SiP<sub>4a</sub>; (ii) pHMA-SiP<sub>4b</sub>.**

Compared to iteration 3 there appeared to be an ostensible increase in the organic content of the polymer-coated silica particle from their respective oligomer-coated silica particles, which combined with evidence of chemical and physical changes in the silica particle itself appears to show that polymer has indeed been grown, or at the very least made difficult to remove, to the silica surface.

## 7.8 Conclusions

The evidence presented by the consumption studies for iteration 4 polymer-coated silica, showing close to identical bound-polymer, is a good indicator that polymer growth not only proceeds from the silica surface, indicating active chain-transfer agent is transplanted onto it, but that its growth is consistent and controlled.

### 7.8.1 Polymer Chain Length and HPMA Molarity of

Time constraints meant performing additional consumption studies on previous iterations was not possible, and trials of adding organometallic iridium to the

first iteration of poly(hydroxypropyl methacrylate)-coated silica particles, pHPMA-SiP<sub>2a</sub>, were already underway. Based on the inferred values for pHPMA-SiP<sub>2a</sub>, with a free polymer weight of 22,734g mol<sup>-1</sup>, we would expect to a bound-polymer molecular weight of 11,663g mol<sup>-1</sup> (based on averaging of the %-bound polymer/free polymer weight of 51.3%).

We can calculate the number of moles of HPMA added to the silica particle via Equation 7.3:

$$\text{Molar mass}_{HPMA-on-silica} = \frac{m_{HPMA-on-silica}}{MW_{HPMA}} \quad (7.3)$$

Where:

**Molar mass<sub>HPMA-on-silica</sub>**: attributable moles of HPMA per gram of silica.

**m<sub>HPMA-on-silica</sub>**: mass of HPMA per gram of silica; derived from the %-difference in the attributable mass loss between the constituent oPETTC-SiP and its subsequent pHPMA-SiP divided by 100 (so that it is expressed as a mass of HPMA per mass of silica, not a percentage).

**MW<sub>HPMA</sub>**: molar mass of HPMA, measures in g mol<sup>-1</sup>.

We assume that all additional mass added to oPETTC-SiP<sub>2a</sub> during the HPMA-polymerization step, 2.29%, was down to additional units of monomer grown onto silica; on that basis 7.3 is calculated out as:

$$\left( \frac{0.0229g_{HPMA}}{144.17g\ mol_{HPMA}^{-1}} \right) g_{SiP}^{-1} = 0.16mmol_{HPMA}g_{SiP}^{-1} \quad (7.4)$$

Meaning for every gram of pHPMA-SiP<sub>2</sub> we have 0.16mmol of HPMA available as an upper limit for attachment of organometallic iridium.

To calculate the chain density Assuming the silica particle is a perfect sphere based on the specifications, a gram of silica would have a total surface area of 4.00x10<sup>18</sup> nm<sup>2</sup> g<sup>-1</sup>. Table A-3 gives the bound polymer weight and average number of monomer units as 14,756 g mol<sup>-1</sup> and 102 respectively, discounting

RAFT, which would be likely destroyed in the workup discussed in Section 7.7.4.

This gives the number of moles of bound pHPMA to the silica as  $0.16 \text{ mmol}_{\text{HPMA}}/102_{\text{HPMA/pHPMA}} = 1.57 \times 10^{-6} \text{ mol}_{\text{pHPMA}} \text{ g}^{-1}$ . Multiplied out by Avogadro's number we get  $9.45 \times 10^{17} \text{ chains g}^{-1}_{\text{silica}}$ . Meaning there are  $9.45 \times 10^{17} \text{ chains g}^{-1} / 4.00 \times 10^{18} \text{ nm}^2 \text{ g}^{-1} = \mathbf{0.24 \text{ chains nm}^{-2}}$

## 8 Addition of Iridium-Cyclopentadienyl to pHPMA-SiPs

Utilizing pHPMA-SiP<sub>2</sub>, the first available polymer-coated organically modified silica with the candidate polymer attached to the surface, attempts to attach organometallic iridium to the silica were made via the triflation exchange mechanism (Figure 8-1) and are described below.

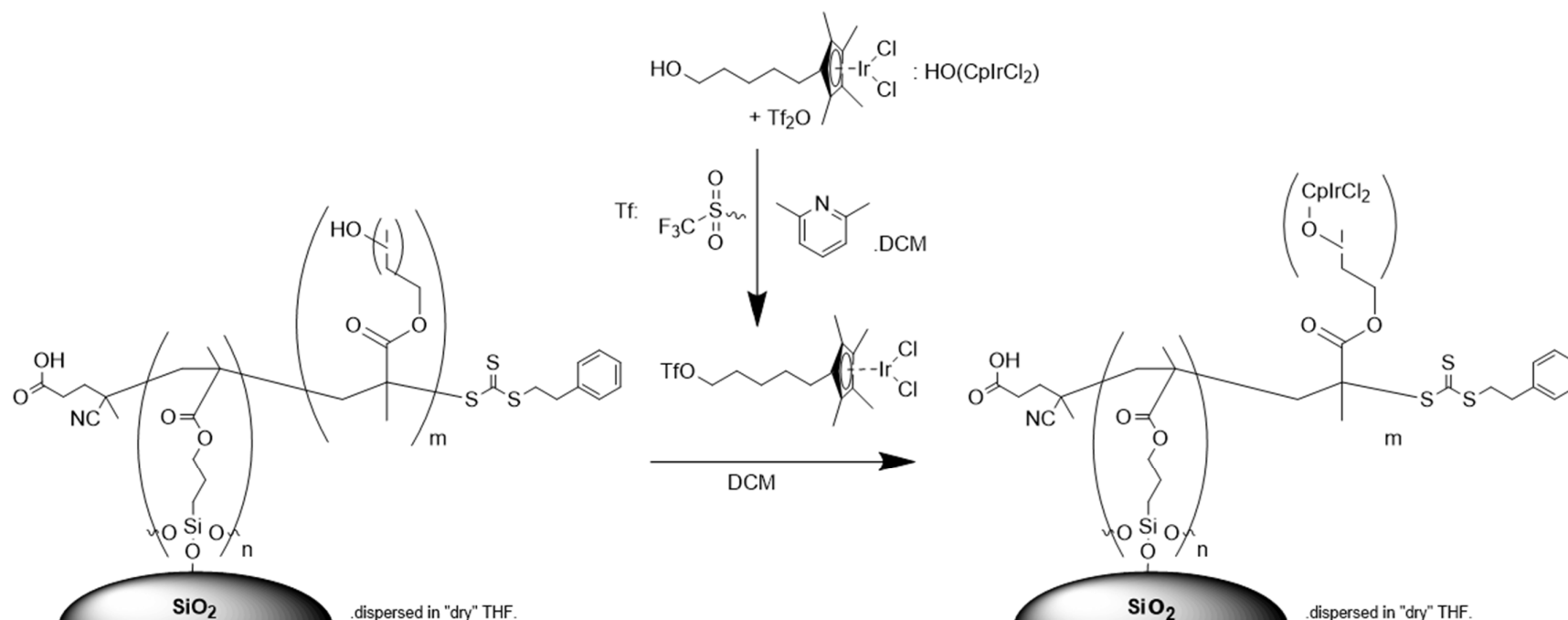


**Figure 8-1: Addition of Iridium-Cyclopentadienyl complex to pHPMA-SiP<sub>2a</sub> via triflation of the alkoxide-IrCP complex.**

## 8.1 Addition of Iridium-Cyclopentadienyl to pHPMA-SiPs

pHPMA-SiP<sub>2a</sub> is re-dispersed in THF and solvent-exchanged into fresh, anhydrous THF before re-dispersion; this was repeated 5 times to remove as much water from the silica as possible. Meanwhile the organometallic iridium complex (IrCp\*Cl<sub>2</sub>) was prepared for addition to pHPMA-SiP<sub>2a</sub>: 2,6-Lutidine, dissolved in anhydrous dichloromethane (DCM), was added to a solution of triflic anhydride in anhydrous DCM under a nitrogen atmosphere at -10°C. To this IrCp\*Cl<sub>2</sub>, dissolved in anhydrous DCM, was added slowly over 20 minutes, before the solution was evaporated to dryness and kept under a blanket of nitrogen. This was re-dissolved in fresh anhydrous DCM before being added to the nitrogen-sparged dispersion of pHPMA-SiP<sub>2a</sub> in anhydrous THF and left to stir at room temperature for 24 hours. The particulate material, designated IrCp\*-SiP from here onwards, was then cleaned with repeated solvent-exchanges into ethanol before vacuum drying.

### 8.1.1 FTIR comparisons of IrCp\*-SiP to its component parts.

FTIR spectra were taken for the free organometallic iridium catalyst, pHPMA-SiP<sub>2a</sub> and the recovered IrCp\*-SiP from the reaction scheme of these and can be seen in Figure 8-2.

All indications are that there is limited discernable change to the polymer-coating between the starter pHPMA-SiP<sub>2a</sub> particle and IrCp\*-SiP; however, several of the peaks associated with the iridium compound itself impinge on similar regions to the peaks for the polymer backbone and assuming a sub-optimal addition of iridium to the polymer-backbone it is entirely possible the peaks for it are masked by the signal for this backbone. With the addition of both a conceptual and literal new element, iridium, new methods for quantifying the degree of chemical change become available.

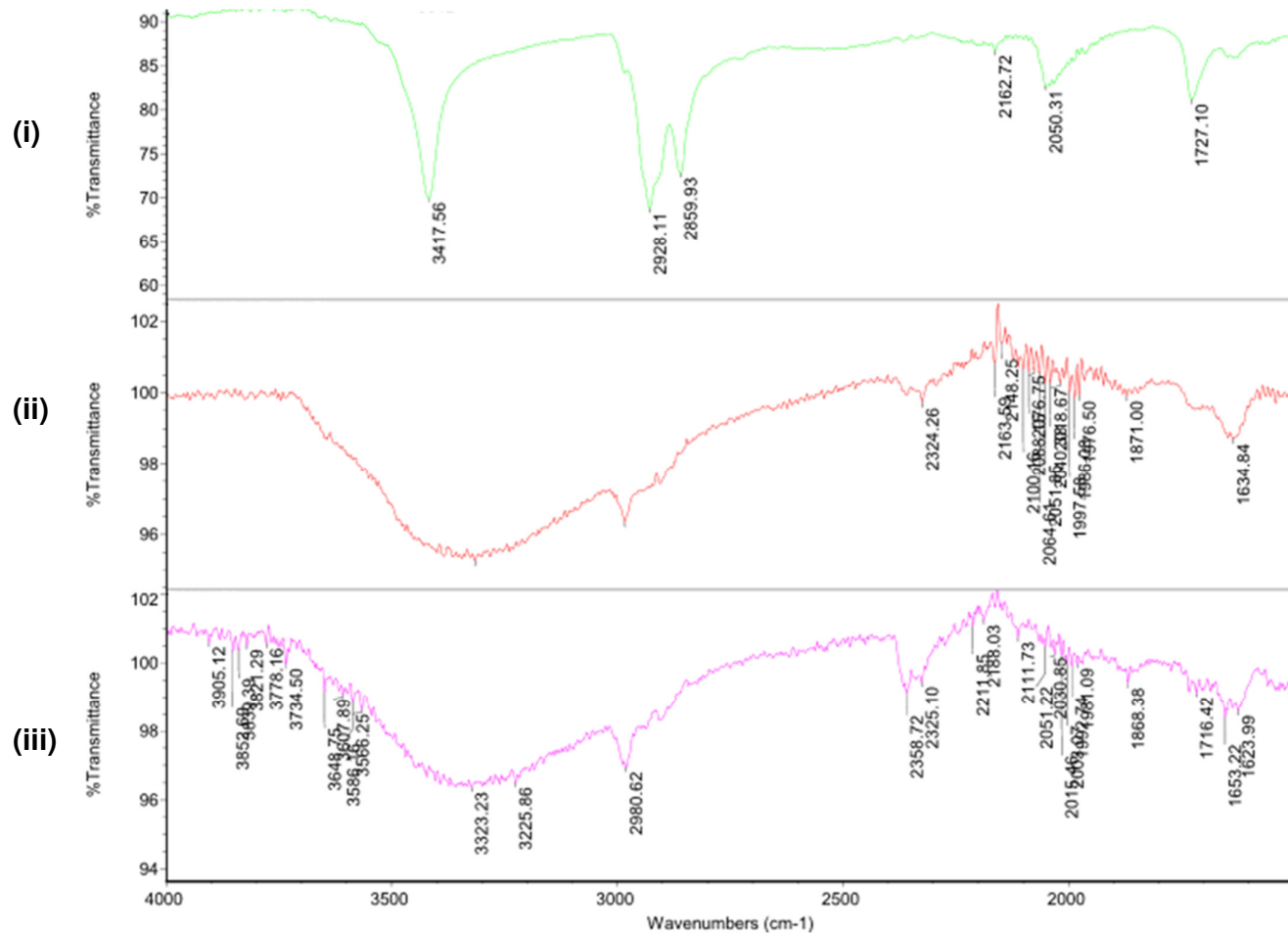


Figure 8-2: Comparison of FTIR spectra of IrCp\* free-catalyst; (ii) IrCp\*-SiP; (iii) pHPMA-SiP<sub>2a</sub>.

### 8.1.2 Inductively coupled plasma atomic emission spectroscopy

Inductively coupled plasma atomic emission spectroscopy (ICP-OES) analysis is a technique for quantitatively detecting specific chemical elements; it does this by subjecting a sample to a high-temperature, inductively-coupled plasma to produce excited atoms and ions, causing the sample to emit electromagnetic radiation characteristic of those specific elements proportional to the amount of that element within the sample. This was done by the same third party analysis company, Medac Limited, to give a direct comparison and is presented in Table 8-1.

**Table 8-1: ICP-OES analysis of IrCp\*-SiP in comparison to the original IrCp\*-wang**

Sample	Element	Result/ w/w%
IrCp*-SiP	Ir	0.22
IrCp*-wang	Ir	11.7

The presence of iridium is proof of concept, albeit limited. 0.22% Iridium-content is indicative of elemental content, not catalyst, which would include the organic component; a calculation showing the molar content of the catalyst in relation to the number of moles of HPMA should give us an indication of the attachment efficiency (number of molecules of IrCp\* for every HPMA molecule) and can be seen below in Equation 7.5 and 7.6.

$$\text{Molar mass}_{\text{Ir-on-silica}} = \frac{m_{\text{Ir-on-silica}}}{Mw_{\text{Ir}}} \quad (7.5)$$

Where:

**Molar mass<sub>Ir-on-silica</sub>**: attributable moles of Iridium per gram mols<sub>Ir</sub> g<sub>SiP</sub><sup>-1</sup>

**m<sub>Ir-on-silica</sub>**: mass of Iridium per gram of silica; 0.22% w/w = 0.22%/100% = 0.0022g<sub>Ir</sub> g<sub>SiP</sub><sup>-1</sup>

**Mw<sub>Ir</sub>**: Elemental mass, measured in g mol<sup>-1</sup> = 192.22g mol<sup>-1</sup>

Which gives the following value:

$$\frac{0.0022\text{g}_{\text{Ir}} \text{g}_{\text{SiP}}^{-1}}{192.22} = 0.011\text{mmol}_{\text{Ir}} \text{g}_{\text{SiP}}^{-1} \quad (7.6)$$

The attachment efficiency is then given by dividing the answer to Equation 7.6 by 7.4:

$$\frac{0.011\text{mmol}_{\text{Ir}} \text{g}^{-1}}{0.16\text{mmol}_{\text{HPMA}} \text{g}_{\text{SiP}}^{-1}} = 0.07 = 7\% \quad (7.7)$$

This value means that for every 100 molecules of HPMA in the bound-polymer attached to the silica surface 7 of them have organometallic iridium attached; applying the above equations to the Wang resin equivalent, using the molar loading value of 0.8mmol g<sup>-1</sup><sub>resin</sub> we get an attachment efficiency of 76%, an order of magnitude higher than the organically modified silica brush particles.

### 8.1.3 Transmission Electron Microscopy & Dynamic Light Scattering

Transmission electron microscopy (TEM) imaging was used to ascertain the polymer thickness of pHPMA-SiP<sub>2a</sub> and to observe any changes to the particle post-iridium functionalization for IrCp\*-SiP. These can be seen in Figure 8-3 and Figure 8-4 respectively.

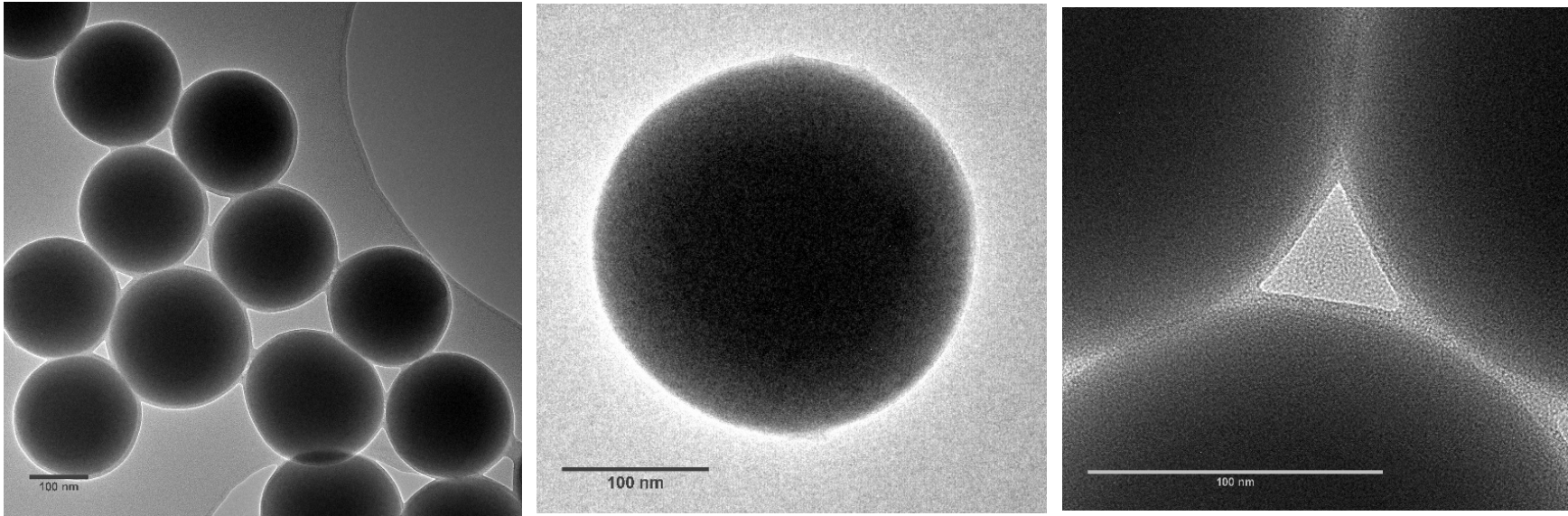


**Figure 8-3: TEM imaging of pHPMA-SiP<sub>2a</sub>.**

TEM imaging for pHPMA-SiP<sub>2a</sub> clearly shows a delineated layer from the core silica we can postulate is the polymer layer. Some of the particles are buttressed against one another with elongation of the polymer later visible; this could be evidence of aggregation of the coated silica particles or an artefact of the deposition process for imaging the particle.

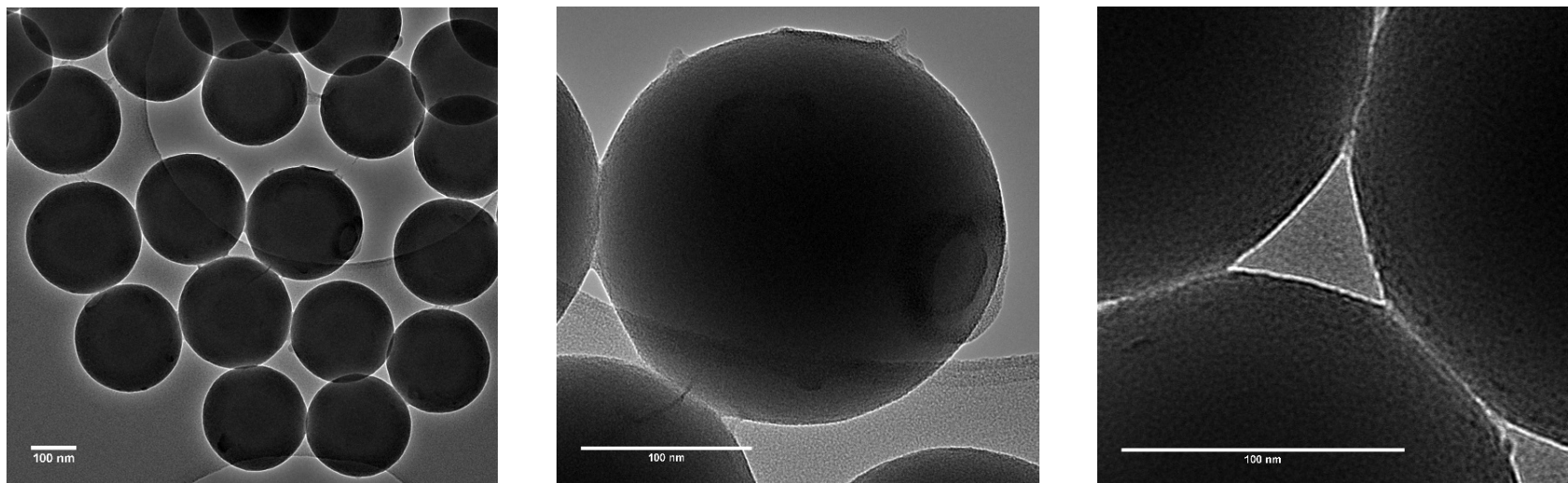


**Figure 8-4: TEM imaging of IrCp\*-SiPs**

TEM imaging for the IrCp\*-SiPs, which were created using pHPMA-SiP<sub>2a</sub>, shows similar layers of material delineated from the silica core, with some elongation where particles have coalesced as described above in Figure 8-3; however, the difference comes in that the uniformity observed for pHPMA-SiP<sub>2a</sub> particles appears to have been severely disrupted, with pitting and areas of discoloration suggesting pockmarking of the outer organic layer. The outer layer also appears much thinner near the buttressed regions between particles. Considering the nature of the treatment used to attach the IrCp\* moiety, which generates trifluoromethanesulfonic (triflic) acid during the process, there are several avenues for causing polymer-layer disruption at the surface and presumably chemical change.

dynamic light scattering studies of pHPMA-SiP<sub>2a</sub> (Table A-4iii) appear to indicate the size of the particle has increased on the oPETTC-SiP<sub>2</sub> (Table A-4ii) by nearly 56nm and its polydispersity has increased from 0.07 to 0.18, suggesting there is some aggregation present, either due to polymer aggregation between silica particles, or from facile aggregation between silica particles due to chemical change at the surface. DLS studies of IrCp\*-SiP can be seen in Table 8-2.

**Table 8-2: Dynamic Light Scattering Size Distribution by Number values for IrCp\*-SiP, with pHPMA-SiP<sub>2a</sub> shown for comparison. Both were dispersed in ethanol at <0.5%w/w in line with previous particle samples.**

	Particle Diameter (d.nm)/ nm	Pdl	Standard Deviation (d.nm)/ nm
IrCp*-SiP	1112.0	0.20	277.8
pHPMA-SiP <sub>2a</sub>	317.8	0.18	139.5

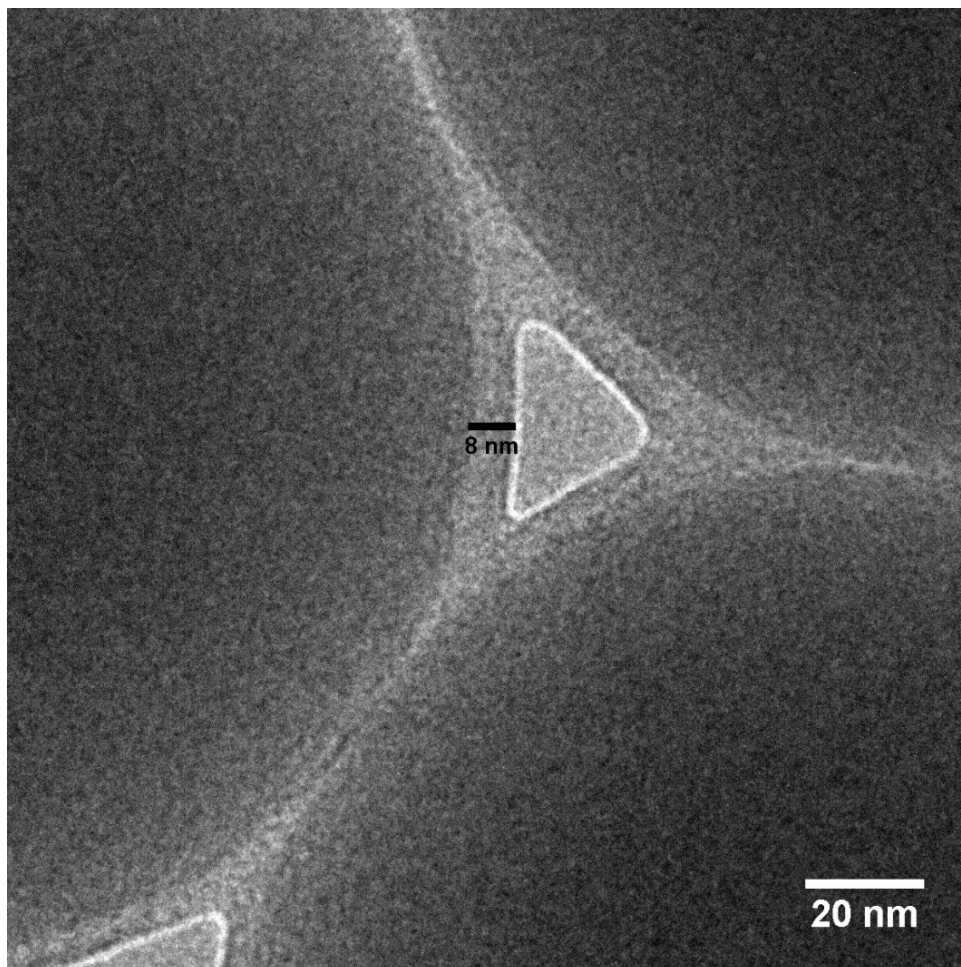
The particle diameter is multiples of the original particle, with the standard deviation and limited polydispersity being consistent with the original starting material suggesting small, consistent agglomerations. The DLS studies appear to support the supposition arrived at from the TEM imaging: pockmarking and polymer uniformity disruption resulting in limited periods of aggregation to other particles.

Image capture of the polymer coating suggests a layer-thickness of 8nm (Figure 8-5); whilst this represents the polymer layer in a vacuum in which solvent has been removed, this is roughly in line with the DLS diameters seen in

Table 7-3 (vi, v) for free polymers produced for iteration 4 polymer-coated silica. However, bound-polymer weight estimates put the molecular weight at 11,662g mol<sup>-1</sup> which would give it a DP of 81; computing this into the radius of gyration measurement gives the following:

$$R_{g,SAW} \approx l \left( \frac{N}{6} \right)^{3/5} \approx 0.3 \left( \frac{81}{6} \right)^{3/5} \approx 1.4nm \quad (7.8)$$

Where:  $R_{g,SAW}$  : radius of gyration, self-avoiding walk;  $l$ : approximate bond length of a HPMA bond ( $\approx 0.3\text{nm}$ );  $N$ : (theoretical) number of units.



**Figure 8-5: pHPMA-SiP<sub>2a</sub> TEM image showing polymer layer thickness at the uniform regions.**

This difference is a little over a third of the estimated size. Whilst this is in line with the DLS measurements for free polymer, which itself would have a larger radius of gyration, bound polymer at the surface doesn't appear to conform to the rules for the radius of gyration of a free, self-avoiding walk polymer.

### 8.1.4 Conclusions

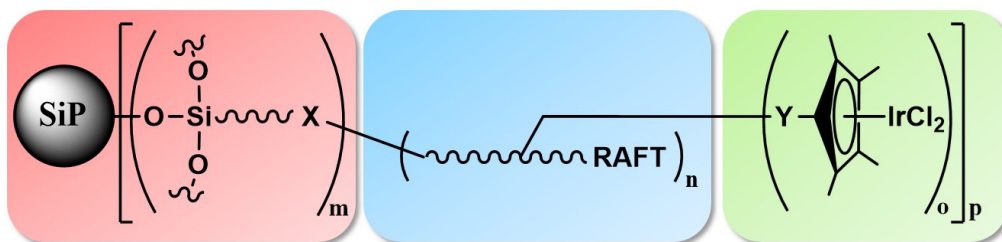


**Figure 8-6: Schematic describing the overall Polymer Brush approach that forms the basis of this thesis.**

The principle utility of Wang resins is to attach and grow peptides, and are therefore specifically built with the goal of attaching organic molecules in mind. The principle goal of my thesis was to investigate and find an alternative to the Wang resin that would display utility as a scaffold for organometallic iridium demonstrating this utility by displaying attached iridium and showing it working as a catalyst.

My thesis was partially successful in that we demonstrated a novel organically-modified silica particle to form brush-polymers with functional polymer capable of binding and retaining organometallic iridium moieties. However, there was not enough time in the process to ascertain its efficacy as a catalyst if at all, notwithstanding the low levels of iridium we ultimately bound to the surface.

For pHPMA-SiP<sub>2a</sub> we calculated the chain density in Section 7.8.1 to get a value of 0.24 chains nm<sup>-2</sup>. Compared to the available Si-OH content at the surface, given by the Zhuravlev model (Zhuravlev, 2000), of 4.9 OH nm<sup>-2</sup> we have an attachment efficiency of 4.8%. Notwithstanding other factors that could potentially lower the attachment efficiency, such as steric hindrance, there could be additional scope for improving polymer content here.

However, in the process of looking at direct functionalization of silica, to trying to functionalize silica with RAFT agents to creating the brush-polymers which ultimately demonstrated iridium-attachment we had disaggregated the steps at each stage and illustrated the issues with quantitatively analysing what was happening and how we could overcome the design impediment, enabling us to get an iridium-containing materials.

This material and the route we chose to get to it means that future materials that use this route would be able to manipulate the scaffold at multiple stages and manipulate components and procedures accordingly; for instance:

1. The core silica could be made much smaller, increase its surface area and available silylic acid surface content, enabling more active oligomeric coating to be inculcated onto the surface.
2. Oligomer chain-length could be decreased below the molar ratio of 5 monomer units of methacryloxypropyl trimethoxysilane (MAPTMS) to every one chain-transfer agent decreases, enabling more active-moiety per unit oligomer.
3. The chain-transfer agent (CTA) used to create the oligomer and used in the free-polymerization step beyond could be changed for a more copacetic agent so that molar ratios of monomer to CTA.

Whilst we did not demonstrate catalytic activity using our particles we did demonstrate a simple route to RAFT-functionalised silica, from which we demonstrated polymer growth and subsequent attachment of the organometallic iridium complex, albeit at low quantities compared to the commercial scaffold Wang resin. Further work would be necessary to demonstrate improvements in the loading capacity but as a proof of concept this shows a potential alternative to using Resin-based architecture for loading and a route towards truly quasi-homogenous catalyst species.

## References

- Alvaro, M., Corma, A., Das, D., Fornés, V. and García, H. 2004. Single-step preparation and catalytic activity of mesoporous MCM-41 and SBA-15 silicas functionalized with perfluoroalkylsulfonic acid groups analogous to Nafion. *Chemical Communications*. **4**(8), pp.956–957.
- Ambhaikar, N. and Krishnamurthy, D. 2014. Process research as a tool to attain Green Chemistry in the Pharmaceutical Industry *In: Chimica Oggi - Chemistry Today.*, pp.17–21.
- Anastas, P. and Eghbali, N. 2010. Green Chemistry: Principles and Practice. *Chemical Society Reviews*. **39**(1), pp.301–312.
- Andersson, P.G. 2011. *Iridium catalysis*. Springer.
- Argyle, M.D. and Bartholomew, C.H. 2015. Heterogeneous catalyst deactivation and regeneration: A review. *Catalysts*. **5**(1), pp.145–269.
- Astruc, D. 2007. *Nanoparticles and Catalysis* [Online] (D. Astruc, ed.). Wiley. [Accessed 28 March 2021]. Available from: <https://onlinelibrary.wiley.com/doi/book/10.1002/9783527621323>.
- Astruc, D., Lu, F. and Aranzaes, J.R. 2005. Nanoparticles as Recyclable Catalysts: The Frontier between Homogeneous and Heterogeneous Catalysis. *Angewandte Chemie International Edition*. **44**(48), pp.7852–7872.

- Ayyadurai, S., Novakovic, G.V., Freed, L.E., Langer, R.S. and Cooney, C.L. 1988. A workstation for visualization of fluid and particle motion in an enzymatic fluidized bed reactor for blood deheparinization *In: Proceedings of the Annual International Conference of the IEEE Engineering in Medicine and Biology Society* [Online]. IEEE, pp.1451–1452 vol.3. [Accessed 28 March 2021]. Available from: <http://ieeexplore.ieee.org/document/95310/>.
- Bautista, F.M., Caballero, V., Campelo, J.M., Luna, D., Marinas, J.M., Romero, A.A., Romero, I., Serrano, I. and Llobet, A. 2006. Heterogeneization of a new Ru(II) homogeneous asymmetric hydrogenation catalyst containing BINAP and the N-tridentate bpea ligand, through covalent attachment on amorphous AlPO<sub>4</sub> support *In: Topics in Catalysis* [Online]. Springer, pp.193–205. [Accessed 29 March 2021]. Available from: <https://link.springer.com/article/10.1007/s11244-006-0121-7>.
- Becker, L. 2002. Repeated blows. *Scientific American*. **286**(3), pp.76–83.
- Blacker, A.J., Brown, S., Clique, B., Gourlay, B., Headley, C.E., Ingham, S., Ritson, D., Screen, T., Stirling, M.J., Taylor, D. and Thompson, G. 2009. A low-waste process to sertraline by diastereomeric crystal resolution and waste isomer racemisation. *Organic Process Research and Development*. **13**(6), pp.1370–1378.
- Blacker, J. and Williams, M.T. 2011. *Pharmaceutical process development: current chemical and engineering challenges*. Royal Society of Chemistry.
- Bligaard, T., Bullock, R.M., Campbell, C.T., Chen, J.G., Gates, B.C., Gorte, R.J., Jones, C.W., Jones, W.D., Kitchin, J.R. and Scott, S.L. 2016. Toward Benchmarking in Catalysis Science: Best Practices, Challenges, and Opportunities. *ACS Catalysis*. **6**(4), pp.2590–2602.
- Brunel, D., Cauvel, A., Di Renzo, F., Fajula, F., Fubini, B., Onida, B. and Garrone, E. 2000. Preferential grafting of alkoxy silane coupling agents on the hydrophobic portion of the surface of micelle-templated silica. *New Journal of Chemistry*. **24**(10), pp.807–813.

- Brunelli, N.A., Didas, S.A., Venkatasubbaiah, K. and Jones, C.W. 2012. Tuning cooperativity by controlling the linker length of silica-supported amines in catalysis and CO<sub>2</sub> capture. *Journal of the American Chemical Society*. **134**(34), pp.13950–13953.
- Brunelli, N.A., Venkatasubbaiah, K. and Jones, C.W. 2012. Cooperative catalysis with acid-base bifunctional mesoporous silica: Impact of grafting and Co-condensation synthesis methods on material structure and catalytic properties. *Chemistry of Materials*. **24**(13), pp.2433–2442.
- Busacca, C.A., Fandrick, D.R., Song, J.J. and Senanayake, C.H. 2011. The Growing Impact of Catalysis in the Pharmaceutical Industry. *Advanced Synthesis & Catalysis*. **353**(11–12), pp.1825–1864.
- Butters, M., Catterick, D., Craig, A., Curzons, A., Dale, D., Gillmore, A., Green, S.P., Marziano, I., Sherlock, J.P. and White, W. 2006. Critical assessment of pharmaceutical processes - A rationale for changing the synthetic route. *Chemical Reviews*. **106**(7), pp.3002–3027.
- Campos, J., Hintermair, U., Brewster, T.P., Takase, M.K. and Crabtree, R.H. 2014. Catalyst activation by loss of cyclopentadienyl ligands in hydrogen transfer catalysis with Cp\*IrIII complexes. *ACS Catalysis*. **4**(3), pp.973–985.
- Carette, N., Engelkamp, H., Akpa, E., Pierre, S.J., Cameron, N.R., Christianen, P.C.M., Maan, J.C., Thies, J.C., Weberskirch, R., Rowan, A.E., Nolte, R.J.M., Michon, T. and Van Hest, J.C.M. 2007. A virus-based biocatalyst. *Nature Nanotechnology*. **2**(4), pp.226–229.
- Carmona, D., Lamata, M.P., Viguri, F., Rodríguez, R., Lahoz, F.J. and Oro, L.A. 2007. Half-Sandwich Rhodium (and Iridium) Complexes as Enantioselective Catalysts for the 1, 3-Dipolar Cycloaddition of 3, 4-Dihydroisoquinoline N-Oxide to Methacrylonitrile. *Chemistry—A European Journal*. **13**(35), pp.9746–9756.

- Castell, J. V., Cervera, M. and Marco, R. 1979. A convenient micromethod for the assay of primary amines and proteins with fluorescamine. A reexamination of the conditions of reaction. *Analytical Biochemistry*. **99**(2), pp.379–391.
- Chan, Y.N., Hsu, R.S. and Lin, J.J. 2010. Mechanism of silicate platelet self-organization during clay-initiated epoxy polymerization. *Journal of Physical Chemistry C*. **114**(23), pp.10373–10378.
- Chiefari, J., Chong, Y.K., Ercole, F., Krstina, J., Jeffery, J., Le, T.P.T., Mayadunne, R.T.A., Meijs, G.F., Moad, C.L., Moad, G., Rizzardo, E. and Thang, S.H. 1998. Living free-radical polymerization by reversible addition - Fragmentation chain transfer: The RAFT process. *Macromolecules*. **31**(16), pp.5559–5562.
- Ciriminna, R., Carà, P.D., Sciortino, M. and Pagliaro, M. 2011. Catalysis with Doped Sol-Gel Silicates. *Advanced Synthesis & Catalysis*. **353**(5), pp.677–687.
- Ciriminna, R., Fidalgo, A., Pandarus, V., Béland, F., Ilharco, L.M. and Pagliaro, M. 2013. The sol-gel route to advanced silica-based materials and recent applications. *Chemical Reviews*. **113**(8), pp.6592–6620.
- Ciriminna, R. and Pagliaro, M. 2003. Tailoring the Catalytic Performance of Sol-Gel-Encapsulated Tetra-n-propylammonium Perruthenate (TPAP) in Aerobic Oxidation of Alcohols. *Chemistry - A European Journal*. **9**(20), pp.5067–5073.
- Corma, A. and Garci, H. 2008. Supported gold nanoparticles as catalysts for organic reactions. *Chemical Society Reviews*. **37**(9), pp.2096–2126.
- Crabtree, R. 1979. Iridium compounds in catalysis. *Accounts of Chemical Research*. **12**(9), pp.331–337.
- Daniel, M.-C. and Astruc, D. 2004. Gold Nanoparticles: Assembly, Supramolecular Chemistry, Quantum-Size-Related Properties, and Applications toward Biology, Catalysis, and Nanotechnology.

- Dickerson, T.J., Reed, N.N. and Janda, K.D. 2002. Soluble polymers as scaffolds for recoverable catalysts and reagents. *Chemical Reviews*. **102**(10), pp.3325–3344.
- Engelmark Cassimjee, K., Kadow, M., Wikmark, Y., Svedendahl Humble, M., Rothstein, M.L., Rothstein, D.M. and Bäckvall, J.E. 2014. A general protein purification and immobilization method on controlled porosity glass: biocatalytic applications. *Chemical Communications*. **50**(65), pp.9134–9137.
- Feng, H., Zhang, R. and Yang, X. 2013. Synthesis of P(MBA-co-MAA) microsphere-grafted PAMAM dendrimers and their application as supporters for gold nanoparticles. *Colloid and Polymer Science*. **291**(6), pp.1329–1339.
- Ganeva, D.E., Sprong, E., de Bruyn, H., Warr, G.G., Such, C.H. and Hawket, B.S. 2007. Particle Formation in ab Initio RAFT Mediated Emulsion Polymerization Systems. *Macromolecules*. **40**(17), pp.6181–6189.
- Gao, J., Li, J., Benicewicz, B.C., Zhao, S., Hillborg, H. and Schadler, L.S. 2012. The mechanical properties of epoxy composites filled with rubbery copolymer grafted SiO<sub>2</sub>. *Polymers*. **4**(1), pp.187–210.
- Gao, J., Li, J., Zhao, S., Benicewicz, B.C., Hillborg, H. and Schadler, L.S. 2013. Effect of graft density and molecular weight on mechanical properties of rubbery block copolymer grafted SiO<sub>2</sub> nanoparticle toughened epoxy. *Polymer*. **54**(15), pp.3961–3973.
- Goeppert, A., Czaun, M., Jones, J.P., Surya Prakash, G.K. and Olah, G.A. 2014. Recycling of carbon dioxide to methanol and derived products-closing the loop. *Chemical Society Reviews*. **43**(23), pp.7995–8048.
- Gotthardt, H., Huss, O.M. and Weissuhn, C.M. 1979. Synthese und Cycloadditionen neuer Dimerer aus mesoionischen 1,3-Dithiolonen. *Chemische Berichte*. **112**(5), pp.1650–1659.

- Gregory, A. and Stenzel, M.H. 2012. Complex polymer architectures via RAFT polymerization: From fundamental process to extending the scope using click chemistry and nature's building blocks. *Progress in Polymer Science (Oxford)*. **37**(1), pp.38–105.
- Huang, Y., Liu, Q., Zhou, X., Perrier, S. and Zhao, Y. 2009. Synthesis of silica particles grafted with well-defined living polymeric chains by combination of RAFT polymerization and coupling reaction. *Macromolecules*. **42**(15), pp.5509–5517.
- Hunter, S.J. and Armes, S.P. 2020. Pickering Emulsifiers Based on Block Copolymer Nanoparticles Prepared by Polymerization-Induced Self-Assembly. *Langmuir*. **36**(51), pp.15463–15484.
- John R. Rumble, E. 2021. No Title. 'Abundance of Elements in the Earth's Crust and in the Sea' in *CRC Handbook of Chemistry and Physics, 102nd Edition (Internet Version 2021)*. CRC Press/Taylor & Francis, Boca Raton, FL. [Online]. Available from: [https://hbcpc.chemnetbase.com/faces/documents/14\\_10/14\\_10\\_0001.xhtml](https://hbcpc.chemnetbase.com/faces/documents/14_10/14_10_0001.xhtml).
- Jones, E.R., Semsarilar, M., Blanz, A. and Armes, S.P. 2012. Efficient Synthesis of Amine-Functional Diblock Copolymer Nanoparticles via RAFT Dispersion Polymerization of Benzyl Methacrylate in Alcoholic Media. *Macromolecules*. **45**(12), pp.5091–5098.
- Kang, S., Hong, S. Il, Choe, C.R., Park, M., Rim, S. and Kim, J. 2001. Preparation and characterization of epoxy composites filled with functionalized nanosilica particles obtained via sol–gel process. *Polymer*. **42**(3), pp.879–887.
- Keen, P.H.R., Slater, N.K.H. and Routh, A.F. 2014. Encapsulation of amylase in colloidosomes. *Langmuir*. **30**(8), pp.1939–1948.
- Kluwer, A.M., Simons, C., Knijnenburg, Q., Van Der Vlugt, J.I., De Bruin, B. and Reek, J.N.H. 2013. Catalyst recycling via specific non-covalent adsorption on modified silicas. *Journal of the Chemical Society. Dalton Transactions*. **42**(2), pp.3609–3616.

- Kolb, H.C., Finn, M.G. and Sharpless, K.B. 2001. Click Chemistry: Diverse Chemical Function from a Few Good Reactions. *Angewandte Chemie International Edition*. **40**(11), pp.2004–2021.
- Kuschel, A., Drescher, M., Kuschel, T. and Polarz, S. 2010. Bifunctional mesoporous organosilica materials and their application in catalysis: Cooperative effects or not? *Chemistry of Materials*. **22**(4), pp.1472–1482.
- Levenspiel, O. 1999. Chemical reaction engineering. *Industrial and Engineering Chemistry Research*. **38**(11), pp.4140–4143.
- Li, C. and Benicewicz, Brian C. 2005. Synthesis of well-defined polymer brushes grafted onto silica nanoparticles via surface reversible addition-fragmentation chain transfer polymerization. *Macromolecules*. **38**(14), pp.5929–5936.
- Li, C. and Benicewicz, Brian C 2005. Synthesis of Well-Defined Polymer Brushes Grafted onto Silica Nanoparticles via Surface Reversible Addition–Fragmentation Chain Transfer Polymerization. *Macromolecules*. **38**(14), pp.5929–5936.
- Li, C., Han, J., Ryu, C.Y. and Benicewicz, B.C. 2006. A versatile method to prepare RAFT agent anchored substrates and the preparation of PMMA grafted-nanoparticles. *Macromolecules*. **39**(9), pp.3175–3183.
- Li, Hui, Xu, L., Wei, W. and Li, Hexing 2014. Combination of enzyme and Ru-B amorphous alloy encapsulated in yolk-shell silica for one-pot dextrin conversion to sorbitol. *ACS Catalysis*. **4**(1), pp.251–258.
- Li, X., Blacker, J., Houson, I., Wu, X. and Xiao, J. 2006. An Efficient Ir(III) Catalyst for the Asymmetric Transfer Hydrogenation of Ketones in Neat Water. *Synlett*. (8), pp.1155–1160.

- Liu, L. and Corma, A. 2018. Metal Catalysts for Heterogeneous Catalysis: From Single Atoms to Nanoclusters and Nanoparticles. *Chemical Reviews*. **118**(10), pp.4981–5079.
- Lu, A. and O'Reilly, R.K. 2013. Advances in nanoreactor technology using polymeric nanostructures. *Current Opinion in Biotechnology*. **24**(4), pp.639–645.
- Lucas, S.J., Crossley, B.D., Pettman, A.J., Vassileiou, A.D., Screen, T.E.O., John Blacker, A. and Mc Gowan, P.C. 2013. A robust method to heterogenise and recycle group 9 catalysts. *Chemical Communications*. **49**(49), pp.5562–5564.
- Luo, S., Peng, Y., Zhang, B., Wang, P.G. and Cheng, J.-P. 2004. Some New Trends and Recent Progress Towards Environmentally Benign Synthesis. *ChemInform*. **35**(51), no-no.
- Ma, J.-Z., Hu, J. and Zhang, Z.-J. 2007. Polyacrylate/silica nanocomposite materials prepared by sol–gel process. *European Polymer Journal*. **43**(10), pp.4169–4177.
- Macquarrie, D.J., Jackson, D.B., King, B.L. and Watson, A. 2002. Preparation of novel organic-inorganic hybrid Micelle Templated Silicas. Comparison of different routes for materials preparation *In: Studies in Surface Science and Catalysis*. Elsevier Inc., pp.1125–1132.
- Madrahimov, S.T., Markovic, D. and Hartwig, J.F. 2009. The Allyl Intermediate in Regioselective and Enantioselective Iridium-Catalyzed Asymmetric Allylic Substitution Reactions. *Journal of the American Chemical Society*. **131**(21), pp.7228–7229.
- McNaught, A.D. and Wilkinson, A. 1997. *Compendium of chemical terminology on 'Catalyst'* [Online] 2nd editio. (A. D. McNaught & A. Wilkinson, eds.). Blackwell Science Oxford. Available from: <https://goldbook.iupac.org/terms/view/C00876>.

- Michaud, A., Gingras, G., Morin, M., Béland, F., Ciriminna, R., Avnir, D. and Pagliaro, M. 2007. SiliaCat TEMPO: An effective and useful oxidizing catalyst. *Organic Process Research and Development*. **11**(4), pp.766–768.
- Mizuno, N. and Misono, M. 1998. Heterogeneous catalysis. *Chemical Reviews*. **98**(1), pp.199–217.
- Moad, G., Chiefari, J., Chong, Y.K., Krstina, J., Mayadunne, R.T.A., Postma, A., Rizzardo, E. and Thang, S.H. 2000. Living free radical polymerization with reversible addition–fragmentation chain transfer (the life of RAFT). *Polymer International*. **49**(9), pp.993–1001.
- Moore, B.L., Lu, A., Longbottom, D.A. and O'Reilly, R.K. 2013. Immobilization of MacMillan catalyst via controlled radical polymerization: Catalytic activity and reuse. *Polymer Chemistry*. **4**(7), pp.2304–2312.
- Moore, B.L., Moatsou, D., Lu, A. and O'Reilly, R.K. 2014. Studying the activity of the MacMillan catalyst embedded within hydrophobic cross-linked polymeric nanostructures. *Polymer Chemistry*. **5**(10), pp.3487–3494.
- Moraes, J., Ohno, K., Maschmeyer, T. and Perrier, S. 2013. Synthesis of silica–polymer core–shell nanoparticles by reversible addition–fragmentation chain transfer polymerization. *Chemical Communications*. **49**(80), pp.9077–9088.
- Mori, K., Kondo, Y., Morimoto, S. and Yamashita, H. 2008. Synthesis and multifunctional properties of superparamagnetic iron oxide nanoparticles coated with mesoporous silica involving single-site Ti-oxide moiety. *Journal of Physical Chemistry C*. **112**(2), pp.397–404.
- Mori, K. and Yamashita, H. 2011. Design of Colloidal and Supported Metal Nanoparticles: Their Synthesis, Characterization, and Catalytic Application. *Journal of the Japan Petroleum Institute*. **54**(1), pp.1–14.

- Mori, K. and Yamashita, H. 2010. Progress in design and architecture of metal nanoparticles for catalytic applications. *Physical Chemistry Chemical Physics*. **12**(43), pp.14420–14432.
- Moshfegh, A.Z. 2009. Nanoparticle catalysts. *Journal of Physics D: Applied Physics*. **42**(23).
- Mueller, R., Kammler, H.K., Wegner, K. and Pratsinis, S.E. 2003. OH surface density of SiO<sub>2</sub> and TiO<sub>2</sub> by thermogravimetric analysis. *Langmuir*. **19**(1), pp.160–165.
- Muller, F.L. and Latimer, J.M. 2009. Anticipation of scale up issues in pharmaceutical development. *Computers and Chemical Engineering*. **33**(5), pp.1051–1055.
- Ng, L.V., Thompson, P., Sanchez, J., Macosko, C.W. and McCormick, A. V. 1995. Formation of Cagelike Intermediates from Nonrandom Cyclization during Acid-Catalyzed Sol-Gel Polymerization of Tetraethyl Orthosilicate. *Macromolecules*. **28**(19), pp.6471–6476.
- Ohno, K., Akashi, T., Tsujii, Y., Yamamoto, M. and Tabata, Y. 2012. Blood clearance and biodistribution of polymer brush-afforded silica particles prepared by surface-initiated living radical polymerization. *Biomacromolecules*. **13**(3), pp.927–936.
- Ohno, K., Ma, Y., Huang, Y., Mori, C., Yahata, Y., Tsujii, Y., Maschmeyer, T., Moraes, J. and Perrier, S. 2011. Surface-Initiated Reversible Addition–Fragmentation Chain Transfer (RAFT) Polymerization from Fine Particles Functionalized with Trithiocarbonates. *Macromolecules*. **44**(22), pp.8944–8953.
- Ohtaka, A., Kono, Y., Inui, S., Yamamoto, S., Ushiyama, T., Shimomura, O. and Nomura, R. 2012. Linear polystyrene-stabilized Pt nanoparticles for aerobic alcohol oxidation and hydrogen-transfer reduction in aqueous media. *Journal of Molecular Catalysis A: Chemical*. **360**, pp.48–53.
- Page, Z.A., Narupai, B., Pester, C.W., Bou Zerdan, R., Sokolov, A., Laitar, D.S.,

- Mukhopadhyay, S., Sprague, S., McGrath, A.J., Kramer, J.W., Trefonas, P. and Hawker, C.J. 2017. Novel Strategy for Photopatterning Emissive Polymer Brushes for Organic Light Emitting Diode Applications. *ACS Central Science*. **3**(6), pp.654–661.
- Pagliari, M. 2009. *Silica-Based Materials for Advanced Chemical Applications*. By Mario Pagliaro. [Online]. Wiley. [Accessed 28 March 2021]. Available from: <http://doi.wiley.com/10.1002/anie.200904266>.
- Pagliari, M., Ciriminna, R., Palmisano, G., Sciortino, M., Beland, F., Pandarus, V. and Tremblay, L. 2009. Recent advances in sol-gel catalysis for fine chemicals production. *Chimica oggi*. **27**(3), pp.13–16.
- Pandarus, V., Ciriminna, R., Béland, F., Gingras, G., Drobot, M., Jina, O. and Pagliaro, M. 2013. Greening heterogeneous catalysis for fine chemicals. *Tetrahedron Letters*. **54**(9), pp.1129–1132.
- Penfold, N.J.W., Lovett, J.R., Verstraete, P., Smets, J. and Armes, S.P. 2017. Stimulus-responsive non-ionic diblock copolymers: protonation of a tertiary amine end-group induces vesicle-to-worm or vesicle-to-sphere transitions. *Polymer Chemistry*. **8**(1), pp.272–282.
- Perrier, S., Takolpuckdee, P. and Mars, C.A. 2005. Reversible addition-fragmentation chain transfer polymerization mediated by a solid supported chain transfer agent. *Macromolecules*. **38**(16), pp.6770–6774.
- Perrier, S., Takolpuckdee, P., Westwood, J. and Lewis, D.M. 2004. Versatile Chain Transfer Agents for Reversible Addition Fragmentation Chain Transfer (RAFT) Polymerization to Synthesize Functional Polymeric Architectures. *Macromolecules*. **37**(8), pp.2709–2717.

- Piccialli, V. 2014. Ruthenium tetroxide and perruthenate chemistry. Recent advances and related transformations mediated by other transition metal oxo-species. *Molecules*. **19**(5), pp.6534–6582.
- Ramarao, C., Ley, S. V., Smith, S.C., Shirley, I.M. and DeAlmeida, N. 2002. Encapsulation of palladium in polyurea microcapsules. *Chemical Communications*. **10**, pp.1132–1133.
- Ranjan, R. and Brittain, W.J. 2007. Combination of living radical polymerization and click chemistry for surface modification. *Macromolecules*. **40**(17), pp.6217–6223.
- Satterfield and N, C. 1991. Heterogeneous catalysis in industrial practice. 2nd edition.
- Schmidt, H.K. 1992. Organically Modified Silicates as Inorganic-Organic Polymers *In: Inorganic and Organometallic Polymers with Special Properties* [Online]. Springer Netherlands, pp.297–317. [Accessed 28 March 2021]. Available from: [https://link.springer.com/chapter/10.1007/978-94-011-2612-0\\_20](https://link.springer.com/chapter/10.1007/978-94-011-2612-0_20).
- Schmidt, J., Kundu, D.S., Blechert, S. and Thomas, A. 2014. Tuning porosity and activity of microporous polymer network organocatalysts by co-polymerisation. *Chemical Communications*. **50**(25), pp.3347–3349.
- Semsarilar, M., Ladmiral, V., Blanzs, A. and Armes, S.P. 2014. Poly(methacrylic acid)-based AB and ABC block copolymer nano-objects prepared via RAFT alcoholic dispersion polymerization. *Polymer Chemistry*. **5**(10), pp.3466–3475.
- Sheehan, S.W., Thomsen, J.M., Hintermair, U., Crabtree, R.H., Brudvig, G.W. and Schmuttenmaer, C.A. 2015. A molecular catalyst for water oxidation that binds to metal oxide surfaces. *Nature Communications*. **6**.
- Sheldon, R.A. 1997. Catalysis and pollution prevention. *Chemistry and Industry*. (1), pp.12–15.

- Sherborne, G.J., Chapman, M.R., Blacker, A.J., Bourne, R.A., Chamberlain, T.W., Crossley, B.D., Lucas, S.J., McGowan, P.C., Newton, M.A., Screen, T.E.O., Thompson, P., Willans, C.E. and Nguyen, B.N. 2015. Activation and Deactivation of a Robust Immobilized Cp\*Ir-Transfer Hydrogenation Catalyst: A Multielement in Situ X-ray Absorption Spectroscopy Study. *Journal of the American Chemical Society*. **137**(12), pp.4151–4157.
- Singh, D., Pfromm, P.H. and Rezac, M.E. 2011. Overcoming mass-transfer limitations in partial hydrogenation of soybean oil using metal-decorated polymeric membranes. *AIChE Journal*. **57**(9), pp.2450–2457.
- Singh, R., Rozada-Sanchez, R., Dean, W., Perkins, J., Muller, F., Godfrey, A., Gernaey, K. V., Gani, R. and Woodley, J.M. 2012. A generic process template for continuous pharmaceutical production *In: Computer Aided Chemical Engineering*. Elsevier B.V., pp.715–719.
- Soleimani Dorcheh, A. and Abbasi, M.H. 2008. Silica aerogel; synthesis, properties and characterization. *Journal of Materials Processing Technology*. **199**(1), pp.10–26.
- Somorjai, G.A. and Li, Y. 2010. *Introduction to surface chemistry and catalysis*. John Wiley & Sons.
- Stasiak, M., Röben, C., Rosenberger, N., Schleth, F., Studer, A., Greiner, A. and Wendorff, J.H. 2007. Design of polymer nanofiber systems for the immobilization of homogeneous catalysts - Preparation and leaching studies. *Polymer*. **48**(18), pp.5208–5218.
- Stasiak, M., Studer, A., Greiner, A. and Wendorff, J.H. 2007. Polymer Fibers as Carriers for Homogeneous Catalysts. *Chemistry - A European Journal*. **13**(21), pp.6150–6156.
- Stöber, W., Fink, A. and Bohn, E. 1968. Controlled growth of monodisperse silica spheres in the micron size range. *Journal of Colloid And Interface Science*. **26**(1), pp.62–69.

- Talwar, D., Salguero, N.P., Robertson, C.M. and Xiao, J. 2014. Primary amines by transfer hydrogenative reductive amination of ketones by using cyclometalated Ir(III) catalysts. *Chemistry - A European Journal*. **20**(1), pp.245–252.
- Tang, W., Lau, C., Wu, X. and Xiao, J. 2014. Complexes as Highly Active Catalysts for the Hydrogenation of Imines. *Synlett*. (25), pp.0081–0084.
- Terashima, T., Ouchi, M., Ando, T., Kamigaito, M. and Sawamoto, M. 2007. Amphiphilic, thermosensitive ruthenium(II)-bearing star polymer catalysts: One-pot synthesis of PEG armed star polymers with ruthenium(II)-enclosed microgel cores via metal-catalyzed living radical polymerization. *Macromolecules*. **40**(10), pp.3581–3588.
- Terashima, T., Ouchi, M., Ando, T. and Sawamoto, M. 2011. Oxidation of sec-alcohols with Ru(II)-bearing microgel star polymer catalysts via hydrogen transfer reaction: Unique microgel-core catalysis. *Journal of Polymer Science Part A: Polymer Chemistry*. **49**(5), pp.1061–1069.
- Tsujii, Y., Ejaz, M., Sato, K., Goto, A. and Fukuda, T. 2001. Mechanism and kinetics of RAFT-mediated graft polymerization of styrene on a solid surface. 1. Experimental evidence of surface radical migration. *Macromolecules*. **34**(26), pp.8872–8878.
- Tudor, J. and O'Hare, D. 1997. Stereospecific propene polymerisation catalysis using an organometallic modified mesoporous silicate. *Chemical Communications*. (6), pp.603–604.
- Wang, S.-S. 1973. p-Alkoxybenzyl alcohol resin and p-alkoxybenzyloxycarbonylhydrazide resin for solid phase synthesis of protected peptide fragments. *Journal of the American Chemical Society*. **95**(4), pp.1328–1333.
- Werther, J., Hartge, E.-U. and Heinrich, S. 2014. Fluidized-Bed Reactors - Status and Some Development Perspectives. *Chemie Ingenieur Technik*. **86**(12), pp.2022–2038.

- Wesselbaum, S., vom Stein, T., Hintermair, U., Klankermayer, J. and Leitner, W. 2014. Continuous-Flow Hydrogenation of CO<sub>2</sub> Using Molecular Catalysts. *Chemie Ingenieur Technik*. **86**(9), pp.1428–1428.
- Wu, J., Barnard, J.H., Zhang, Y., Talwar, D., Robertson, C.M. and Xiao, J. 2013. Robust cyclometallated Ir(III) catalysts for the homogeneous hydrogenation of N-heterocycles under mild conditions. *Chemical Communications*. **49**(63), pp.7052–7054.
- Wu, L., He, Y.-M. and Fan, Q.-H. 2011. Controlled Reversible Anchoring of η<sup>6</sup>-Arene/TsDPEN- Ruthenium(II) Complex onto Magnetic Nanoparticles: A New Strategy for Catalyst Separation and Recycling. *Advanced Synthesis & Catalysis*. **353**(16), pp.2915–2919.
- Zhang, C., Hu, C., Zhao, Y., Möller, M., Yan, K. and Zhu, X. 2013. Encapsulation of laccase in silica colloidosomes for catalysis in organic media. *Langmuir*. **29**(49), pp.15457–15462.
- Zhuravlev, L.T. 2000. The surface chemistry of amorphous silica. Zhuravlev model. *Colloids and Surfaces A: Physicochemical and Engineering Aspects*. **173**(1–3), pp.1–38.

## Appendices

### i. List of Appendices Figures

Figure A-1: (i): low APTES content; (ii): high APTES content; Average diameter of modified 250nm silica nanoparticles with increasing %-APTES content as a function of pH; The suspension at original pH X was divided in half and concentrated HCl and NaOH solutions were added to gradually change the pH, decreasing and increasing it respectively.; Legend: ■ : 0.00x equivalents to silica (blank, untreated silica); legend: ■ : 0% equivalents to silica (blank, untreated silica); ● : 1%; ▲ : 10% ; ▼ : 20%; ◆ : 60%; ◀ : 100%; ▶ : 150%. .....	152
Figure A-2: Calibration curve for fluorescamine using propylamine (PrNH <sub>2</sub> ) solution. Multiple UV spectroscopy runs are carried out to produce an average which then has the zero point emission count subtracted to produce an adjusted emission count for each point on the curve. ....	153
Figure A-3: FTIR spectra for untreated, blank 250nm silica used in all iterations of organically modified silicas (OrMoSils). ....	153
Figure A-4: TGA analysis of the blank silica particle (SiP); TGA programme is as follows: dynamic temperature increase from 50-200°C; hold for 60 minutes; 200-500°C at a rate of 5°C/min dynamic then 500-1100°C at a rate of 10°C/min followed by a rapid decrease in temperature to 50°C. Total mass loss was recorded as 9.51%, attributable to the loss of free water and water molecules produced from surface calcination. ....	154
Figure A-5: Iterations 1 & 2 of CTA-SiP production from Table 6-2. With explanations for both to the right for each. ....	155
Figure A-6: Iterations 3 & 4 of CTA-SiP production from Table 6-2. With explanations for both to the right for each. ....	156
Figure A-7: FTIR spectra of pMMA-SiP1 utilising CTA-SiP1 polymerization in-site at DP = 50. ....	157
Figure A-8: FTIR spectra of: (i): Untreated, blank silica; (ii): benzylamine-couple CTA produced using the same method as the SCA-CTA used in the production of the CTA-SiP; (iii) Chain-transfer agent (CTA) used in the production of all iterations. ....	158

Figure A-9: FTIR spectra of iteration 1 of the CTA-SiP produced using the CTA-SCA <sub>1</sub> oil from Table 6-2. EDCI-coupled CTA-SCA was first purified in an aqueous ethyl acetate wash before being dissolved in toluene with dispersed silica and refluxed at 120°C. Once TLC determined loss of the CTA-SCA peak, the particulate material is collected and solvent exchanged into fresh toluene, then ethanol and washed with water before being dried in a vacuum oven.....	159
Figure A-10: FTIR spectra of iteration 2, produced using the CTA-SCA <sub>2</sub> oil from Table 6-2. EDCI-coupled CTA-SCA dissolved in DMF was added in-situ to silica dispersed in DMF and refluxed at 90°C. ....	160
Figure A-11: FTIR spectra of iteration 3 produced using the CTA-SCA <sub>3</sub> oil from Table 6-2. EDCI-coupled CTA-SCA was first purified in an aqueous ethyl acetate wash before purification through a silica column. The subsequent oil was dissolved in silica dispersed in DMF and refluxed at 90°C.....	161
Figure A-12: Iteration 4 of the CTA-SiP, produced using the CTA-SCA <sub>4</sub> oil from Table 6-2. EDCI-coupled CTA-SCA dissolved in DMF was added in-situ to silica dispersed in DMF and refluxed at 90°C. ....	162
Figure A-13: FTIR spectra of pMMA-SiP <sub>2</sub> utilising CTA-SiP <sub>1</sub> at DP = 100.....	163
Figure A-14: TGAs of pMMA-SiP <sub>1</sub> and pMMA-SiP <sub>2</sub> produced from CTA-SiP <sub>1</sub> with predicted degrees of polymerization (DP, based on a ratio of [MMA]:[CTA <sub>free</sub> ]. The CTA-SiP <sub>1</sub> used to make both pMMA-SiPs originally yielded a total mass loss of 12.85%, indicating a loss of mass at the particle surface. ....	164
Figure A-15: FTIR spectra of pMMA-SiP <sub>3</sub> utilising CTA-SiP <sub>2</sub> at DP = 50.....	165
Figure A-16: FTIR spectra of pMMA-SiP <sub>4</sub> utilising CTA-SiP <sub>2</sub> at DP = 100.....	166
Figure A-17: TGAs of pMMA-SiP <sub>3</sub> and pMMA-SiP <sub>4</sub> produced from CTA-SiP <sub>2</sub> with predicted degrees of polymerization (DP, based on a ratio of [MMA]:[CTA <sub>free</sub> ]. The CTA-SiP <sub>2</sub> used to make both pMMA-SiPs originally yielded a total mass loss of 14.87%, indicating a loss at the particle surface of mass in both cases of over 4%. ....	167
Figure A-18: FTIR spectra of pMMA-SiP <sub>5</sub> utilising CTA-SiP <sub>3</sub> at DP = 50. ....	168
Figure A-19: FTIR spectra of pMMA-SiP <sub>6</sub> utilising CTA-SiP <sub>3</sub> at DP = 100. ....	169

Figure A-20: (i) PETTC RAFT agent using the preparation of the oligo MAPTMS; (ii) oPETTC-SiP <sub>1b</sub> : the oligo-CTA-SiP prepared from purified oPETTC-SCA <sub>1</sub> using column chromatography; (iii) oPETTC-SiP <sub>1a</sub> prepared from non-purified oPETTC-SCA <sub>1</sub> .....	170
Figure A-21: TGA of 250nm silica nanoparticles using the new TGA protocol. The TGA protocol method was changed in line with Mueller et al. (2003) the new protocol to captures the major compositional changes associated with organic matter more effectively.....	171
Figure A-22: TGA Comparison between 1a ( <i>blue</i> ) and 1b ( <i>red</i> ), showing increases in organic content in the unpurified oPETTC-SiP <sub>1b</sub> over the purified oPETTC-SiP <sub>1a</sub> using the new TGA protocol described above in 7.4.2 and Figure 7-9.....	172
Figure A-23: TGA Comparison between 1a and 1b, showing the losses in organic content in the oPETTC-SiP <sub>1b</sub> and oPETTC-SiP <sub>1a</sub> using the new TGA protocol described above in Figure A-21.....	173
Figure A-24: FTIR of pMMA-SiPs from iteration 1 oPETTC-SiPs (i) 1b, produced with column-purified oPETTC-SCA; (ii) 1a, used as was, with no purification.....	174
Figure A-25: poly(methyl methacrylate), free polymer, produced by sampling the extracted media and dispersing into methanol to produce precipitate of pMMA, which was dried and analysed. ....	175
Figure A-26: pMMA-SiP <sub>1a</sub> made using the unpurified oligomer-coated, CTA-enabled silica. This uses the protocol as illustrated in Figure A-21. ....	176
Figure A-27: pMMA-SiP <sub>1b</sub> made using the purified oligomer-coated, CTA-enabled silica. This uses the protocol as illustrated in Figure A-21 .....	177
Figure A-28: (i) oPETTC-SiP <sub>2</sub> : the oligo-CTA-SiP prepared from oPETTC-SCA <sub>2</sub> and used as produced; (ii) PETTC RAFT agent using the preparation of the oligo-MAPTMS. For ease of view peaks below 1500cm <sup>-1</sup> , previously dwarfed by O-Si-O stretching have been omitted.....	179
Figure A-29: TGA of oPETTC-SiP <sub>2</sub> . Machine error during the procedure stopped the temperature increase after 620°C and limited amounts of the sample meant it could not be repeated.....	180
Figure A-30: FTIR spectra for the cleaned and dried sample of pHPMA-SiP <sub>2a</sub> (DP = 100). O-Si-O peaks below 1500cm <sup>-1</sup> omitted for clarity.....	181

Figure A-31: FTIR spectra of free pHPMA, precipitated in dichloromethane and vacuum oven-dried.....	182
Figure A-32: TGA of pHPMA-SiP <sub>2a</sub> . Protocol for TGA is as illustrated in Section 7.4.2. ....	183
Figure A-33: Iterations of pHPMA-SiP <sub>2b-e</sub> based on oPETTC-SiP <sub>2</sub> across multiple DPs all with 5-hour holds: (i) pHPMA-SiP <sub>2b</sub> , DP = 50; (ii) pHPMA-SiP <sub>2c</sub> , DP = 100; (iii) pHPMA-SiP <sub>2d</sub> , DP = 200; (iv) pHPMA-SiP <sub>2e</sub> , DP = 500. ....	184
Figure A-34: FTIR spectra for (i) oPETTC-SiP <sub>3</sub> ; (ii) oPETTC-SiP <sub>2</sub> . For ease of view peaks below 1500cm <sup>-1</sup> , previously dwarfed by O-Si-O stretching have been omitted. ....	187
Figure A-35: Thermogravimetric analysis of oPETTC-SiP <sub>3</sub> . The TGA protocol used the new method as per that of the blank, untreated silica as in Figure A-21.....	188
Figure A-36: FTIR spectra comparison between the oPETTC-SiP <sub>3</sub> and pHPMA-SiP <sub>3a-d</sub> . Legend: (i) oPETTC-SiP <sub>3</sub> ; (ii) pHPMA-SiP <sub>3a</sub> , DP = 50; (iii) pHPMA-SiP <sub>3b</sub> , DP = 100; (iv) pHPMA-SiP <sub>3c</sub> , DP = 200; (v) pHPMA-SiP <sub>3d</sub> , DP = 500. ....	189
Figure A-37: Thermogravimetric analysis of pHPMA-SiP <sub>3a-b</sub> . The TGA protocol used the new method as per that of the blank, untreated silica as in Figure A-21; Legend: (i): pHPMA-SiP <sub>3a</sub> , DP = 50; (ii): pHPMA-SiP <sub>3b</sub> , DP = 100. ....	191
Figure A-38: Thermogravimetric analysis of pHPMA-SiP <sub>3c-d</sub> . The TGA protocol used the new method as per that of the blank, untreated silica as in Figure A-21; Legend: (i): pHPMA-SiP <sub>3a</sub> , DP = 200; (ii): pHPMA-SiP <sub>3b</sub> , DP = 500. ....	192

## ii. List of Appendices Tables

Table A-1: Free polymer weight of pMMA for iteration 1 pMMA-SiPs.....	175
Table A-2: Iteration names for the 5 different pHPMA samples based on oPETTC-SiP <sub>2</sub> . ....	178
Table A-3: pHPMA free polymer weight for pHPMA-SiP <sub>2a</sub> . Number of monomer units in parenthesis (discounting RAFT moiety).....	178
Table A-4: Dynamic Light Scattering (DLS) studies of an array of particles analyzed in the production of iteration 2 particles. Legend: (i): Untreated 250nm silica; (ii): oPETTC-SiP <sub>2</sub> ;	

(iii): pHPMA-SiP <sub>2a</sub> , DP = 100, 18-hour hold. Samples are all dispersed in Ethanol at approximately 0.5%wt.....	185
Table A-5: Continuing Dynamic Light Scattering (DLS) studies of pHPMA-SiP <sub>2b-e</sub> particles. Legend: (iv): pHPMA-SiP <sub>2b</sub> , DP = 50; (v): pHPMA-SiP <sub>2c</sub> , DP = 100; (vi): pHPMA-SiP <sub>2d</sub> , DP = 200; (vii): pHPMA-SiP <sub>2e</sub> , DP = 500. Samples are all dispersed in Ethanol at approximately 0.5%wt.....	186
Table A-6: free polymer SEC-GPC profiles for each pHPMA-SiP <sub>3</sub> created. ....	187
Table A-7: Dynamic Light Scattering (DLS) studies of pHPMA-SiP <sub>3a-c</sub> particles from the 5-hour hold study. Particles were dispersed in ethanol at <0.5 wt%. Sampling was aggregated from several runs to give the average size. Legend: (i): pHPMA-SiP <sub>3a</sub> , DP = 50, (ii): pHPMA-SiP <sub>3b</sub> , DP = 100; (iii): pHPMA-SiP <sub>3c</sub> , DP = 200; (iv): pHPMA-SiP <sub>3d</sub> , DP = 500.....	190
Table A-8: %-mass loss for the 125-540°C region determined through thermogravimetric analysis for pHPMA-SiP <sub>3</sub> samples and their constituent parts, collated from previous graphs. Legend: (i) Silica Particles, SiP <sub>250nm</sub> used in preparation of the rest; (ii) oPETTC-SiP <sub>3</sub> ; (iii): pHPMA-SiP <sub>3a</sub> , DP = 50, (iv): pHPMA-SiP <sub>3b</sub> , DP = 100; (v): pHPMA-SiP <sub>3c</sub> , DP = 200; (vi): pHPMA-SiP <sub>3d</sub> , DP = 500. Mass loss differences between the pHPMA-SiP <sub>3</sub> samples and the SiP <sub>250nm</sub> and oPETTC-SiP <sub>3</sub> are shown in the second and third column respectively.....	193

A.1 Accompanying Figures and Tables to Chapter 5: Organically Modified Silicas (OrMoSils).

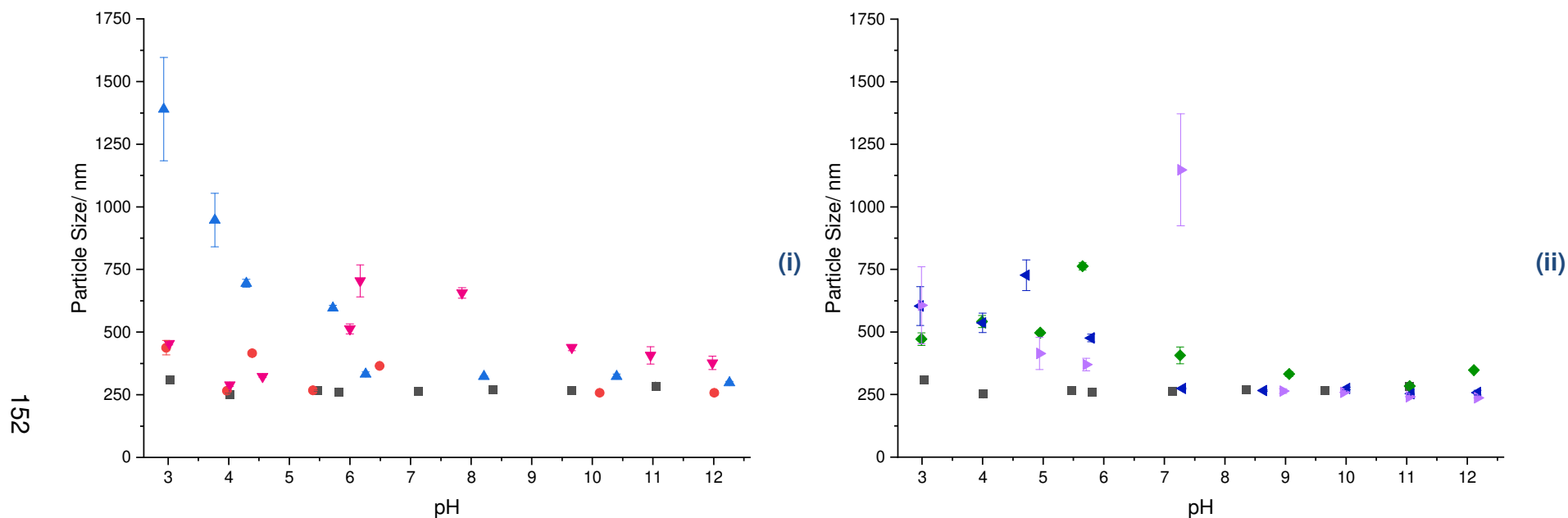
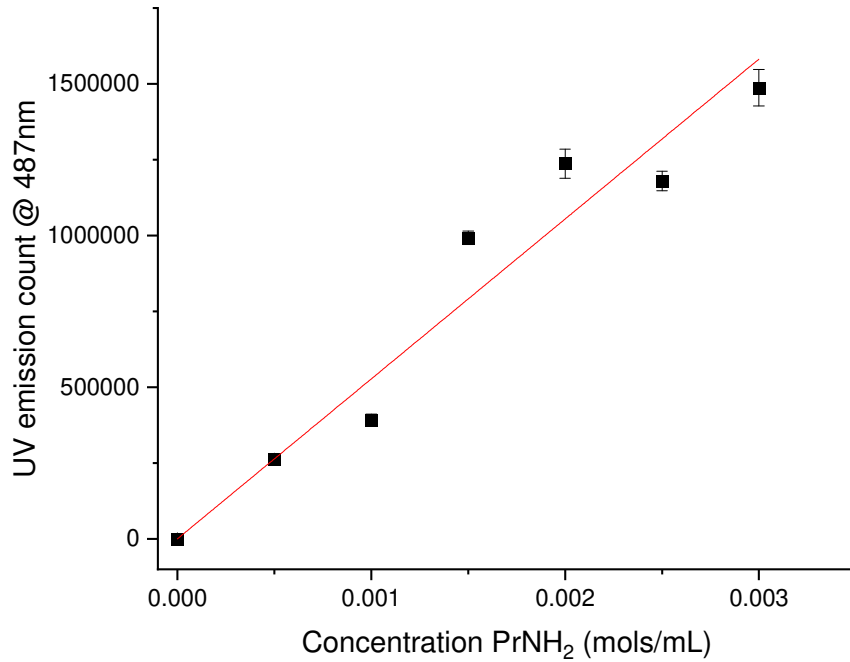
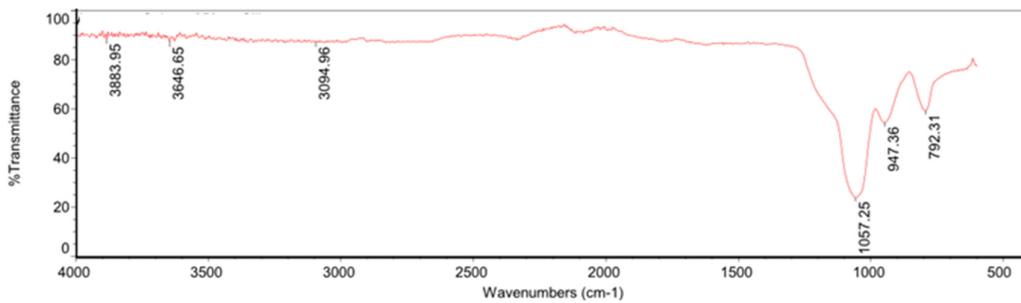


Figure A-1: (i): low APTES content; (ii): high APTES content; Average diameter of modified 250nm silica nanoparticles with increasing %-APTES content as a function of pH; The suspension at original pH X was divided in half and concentrated HCl and NaOH solutions were added to gradually change the pH, decreasing and increasing it respectively.; Legend: ■ : 0.00x equivalents to silica (blank, untreated silica); legend: ■ : 0% equivalents to silica (blank, untreated silica); ● : 1%; ▲ : 10%; ▼ : 20%; ◆ : 60%; ◀ : 100%; ▶ : 150%.



**Figure A-2: Calibration curve for fluorescamine using propylamine (PrNH<sub>2</sub>) solution. Multiple UV spectroscopy runs are carried out to produce an average which then has the zero point emission count subtracted to produce an adjusted emission count for each point on the curve.**



**Figure A-3: FTIR spectra for untreated, blank 250nm silica used in all iterations of organically modified silicas (OrMoSils).**

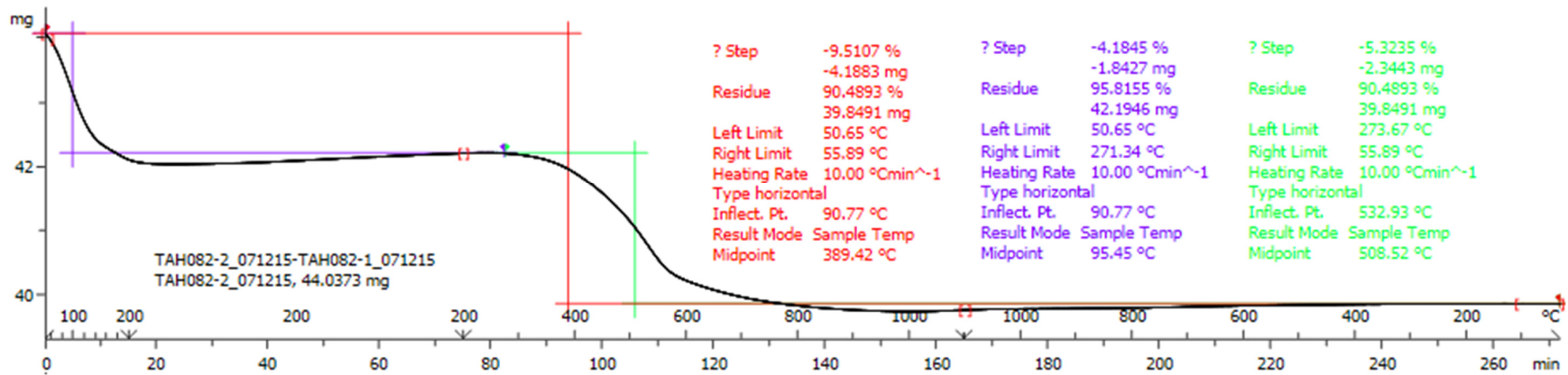
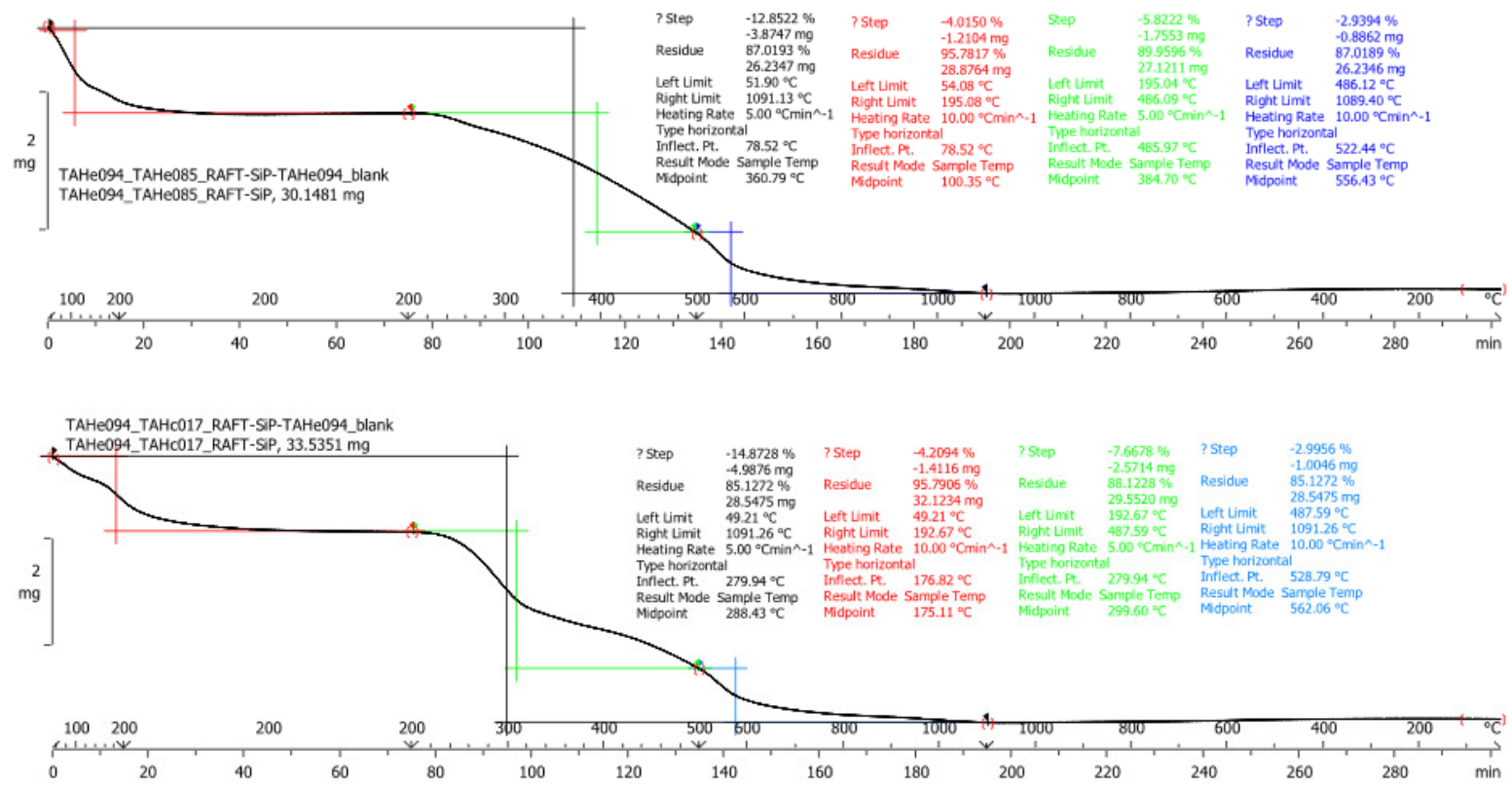


Figure A-4: TGA analysis of the blank silica particle (SiP); TGA programme is as follows: dynamic temperature increase from 50-200°C; hold for 60 minutes; 200-500°C at a rate of 5°C/min dynamic then 500-1100°C at a rate of 10°C/min followed by a rapid decrease in temperature to 50°C. Total mass loss was recorded as 9.51%, attributable to the loss of free water and water molecules produced from surface calcination.

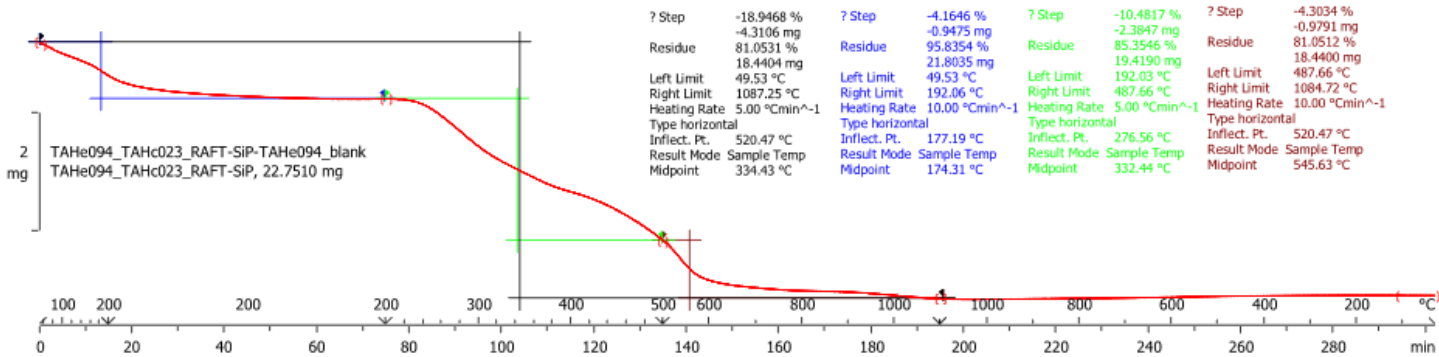
## A.2 Accompanying Figures and Tables to Chapter 6.3: Creation of Brush Polymers via the formation of Chain-transfer Agent-coated Silicas (CTA-SiPs).



Iteration 1. CTA-SCA oil used to make CTA-SiP<sub>1</sub>: oil extracted in an ethyl acetate/aqueous wash, then dissolved into toluene with dispersed silica particles, refluxed at 90°C in a 3:1 molar excess for 18 hours.

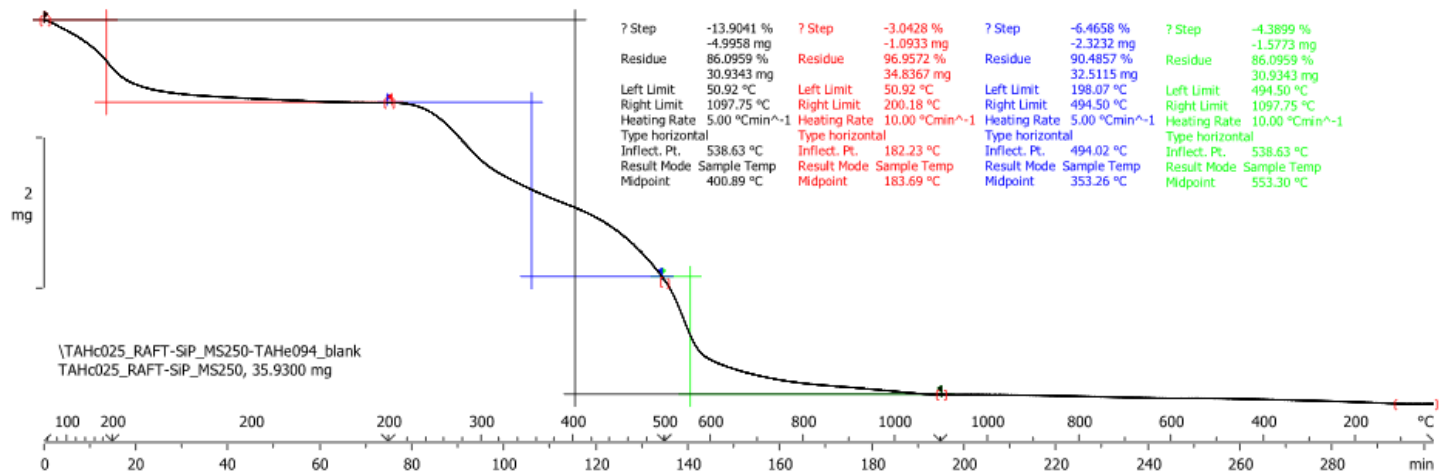
Iteration 2. CTA-SCA oil used to make CTA-SiP<sub>2</sub>: oil in reaction solution added in-situ to dispersed silica particles in DMF at 120°C at a ratio of 3:1 for 18 hours.

Figure A-5: Iterations 1 & 2 of CTA-SiP production from Table 6-2. With explanations for both to the right for each.



Iteration 3. CTA-SCA oil used to make CTA-SiP<sub>3</sub>: oil extracted in an ethyl acetate/aqueous wash, followed by purification through a silica column. Resultant oil is dissolved in DMF with dispersed silica particles and refluxed at 120°C at a ratio of 3:1 for 18 hours.

156



Iteration 4. CTA-SCA oil used to make CTA-SiP<sub>4</sub>: repetition of Iteration 2, oil in reaction solution added in-situ to dispersed silica particles in DMF at 120°C at a ratio of 3:1 for 18 hours.

Figure A-6: Iterations 3 & 4 of CTA-SiP production from Table 6-2. With explanations for both to the right for each.

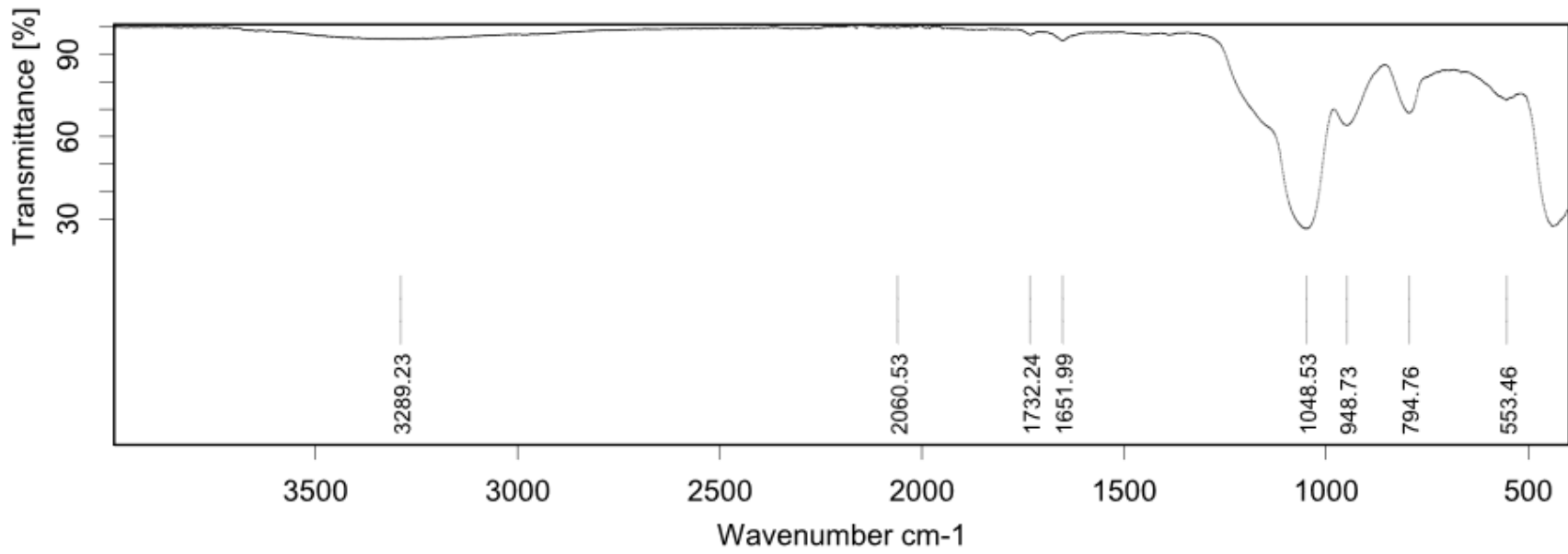
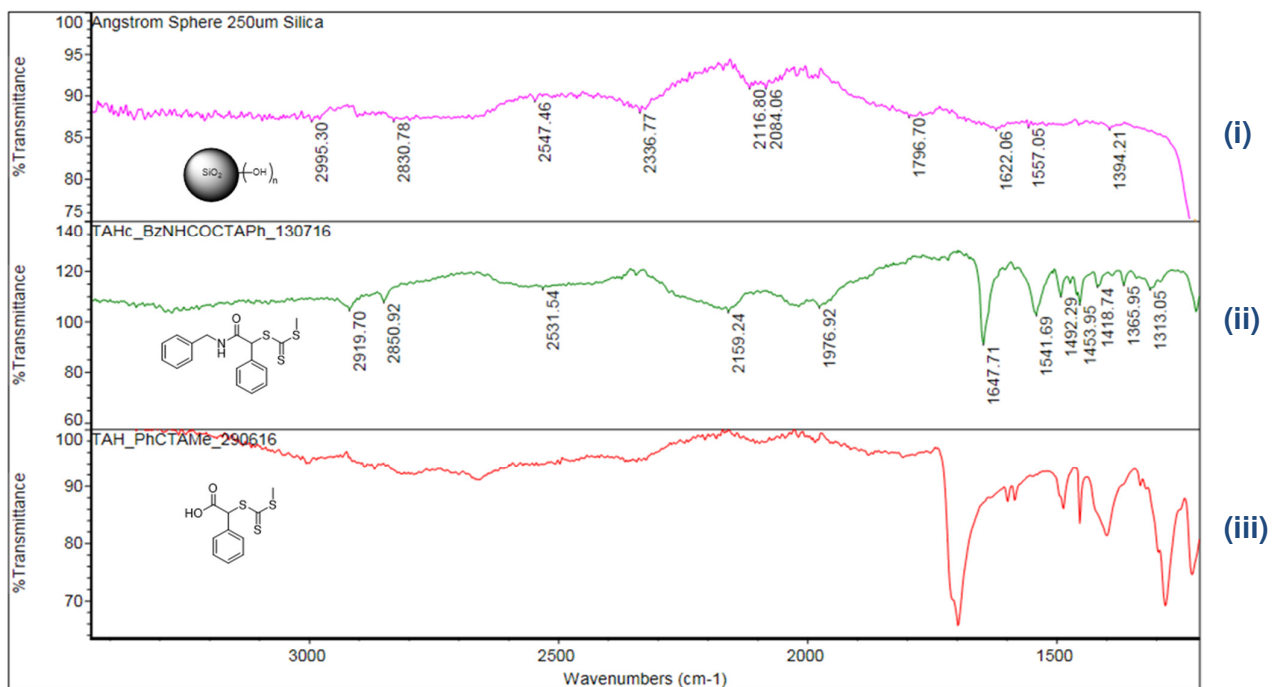
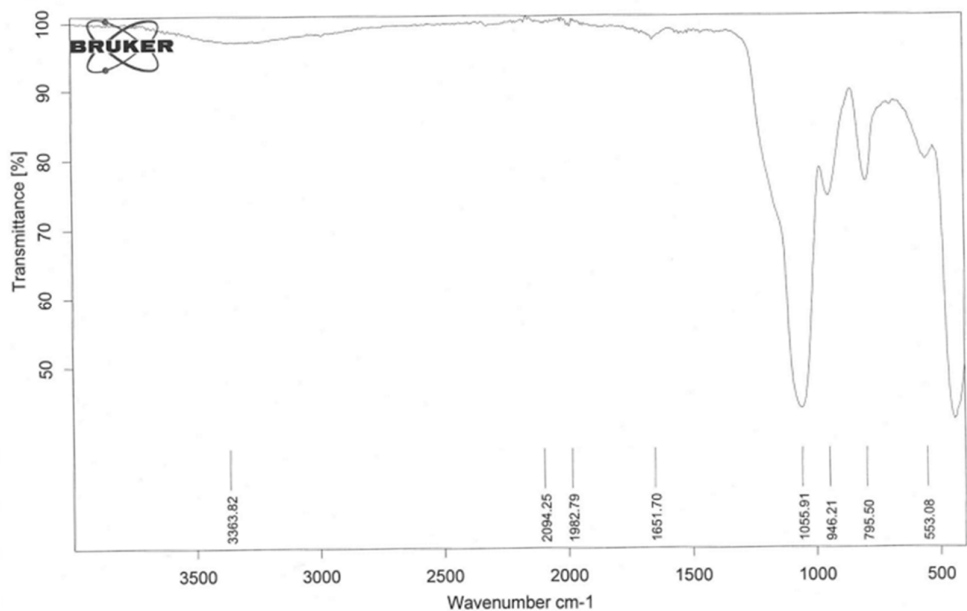


Figure A-7: FTIR spectra of pMMA-SiP1 utilising CTA-SiP1 polymerization in-site at DP = 50.



**Figure A-8: FTIR spectra of: (i): Untreated, blank silica; (ii): benzylamine-couple CTA produced using the same method as the SCA-CTA used in the production of the CTA-SiP; (iii) Chain-transfer agent (CTA) used in the production of all iterations.**



**Figure A-9: FTIR spectra of iteration 1 of the CTA-SiP produced using the CTA-SCA<sub>1</sub> oil from Table 6-2. EDCI-coupled CTA-SCA was first purified in an aqueous ethyl acetate wash before being dissolved in toluene with dispersed silica and refluxed at 120°C<sup>8</sup>. Once TLC determined loss of the CTA-SCA peak, the particulate material is collected and solvent exchanged into fresh toluene, then ethanol and washed with water before being dried in a vacuum oven.**

<sup>8</sup> Original file lost with only the scan available.

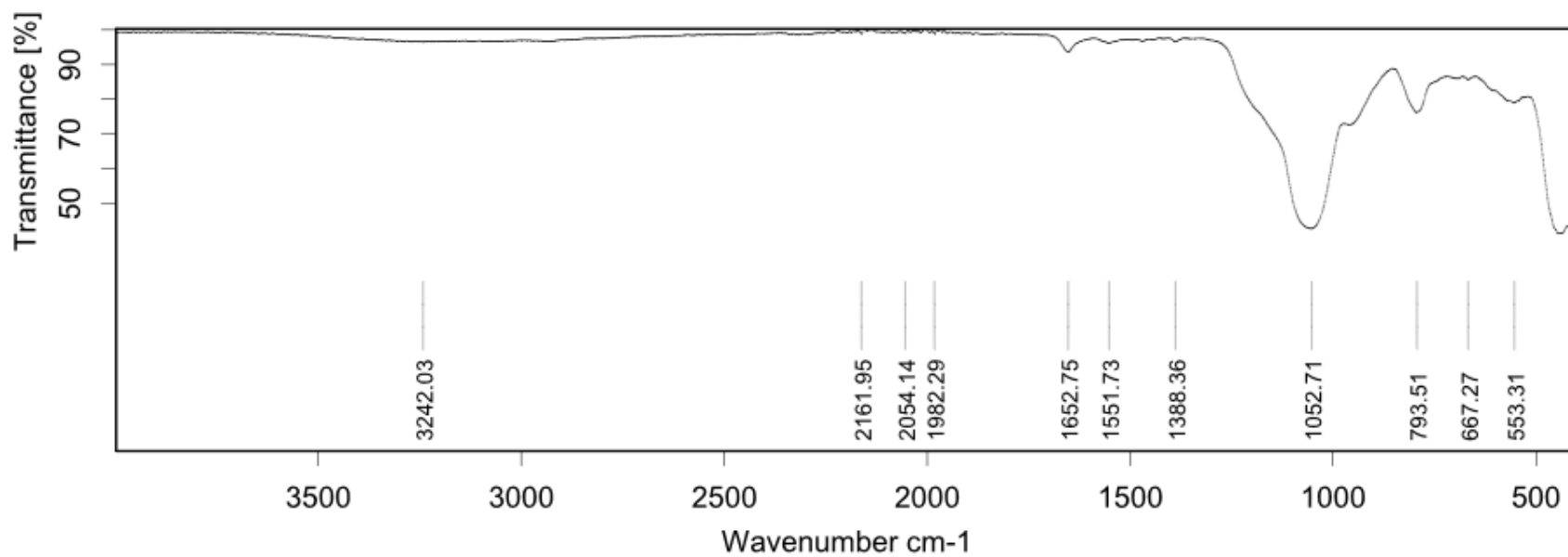
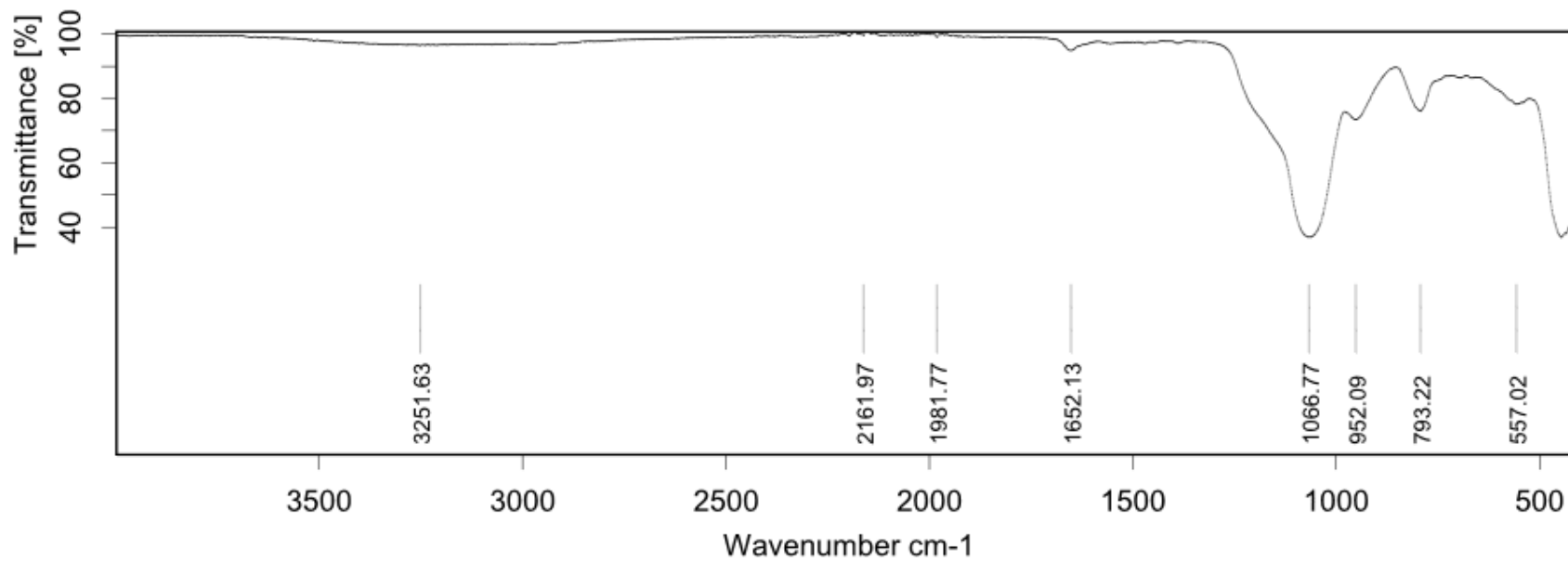


Figure A-10: FTIR spectra of iteration 2, produced using the CTA-SCA<sub>2</sub> oil from Table 6-2. EDCI-coupled CTA-SCA dissolved in DMF was added in-situ to silica dispersed in DMF and refluxed at 90°C.



**Figure A-11: FTIR spectra of iteration 3 produced using the CTA-SCA<sub>3</sub> oil from Table 6-2. EDCI-coupled CTA-SCA was first purified in an aqueous ethyl acetate wash before purification through a silica column. The subsequent oil was dissolved in silica dispersed in DMF and refluxed at 90°C**

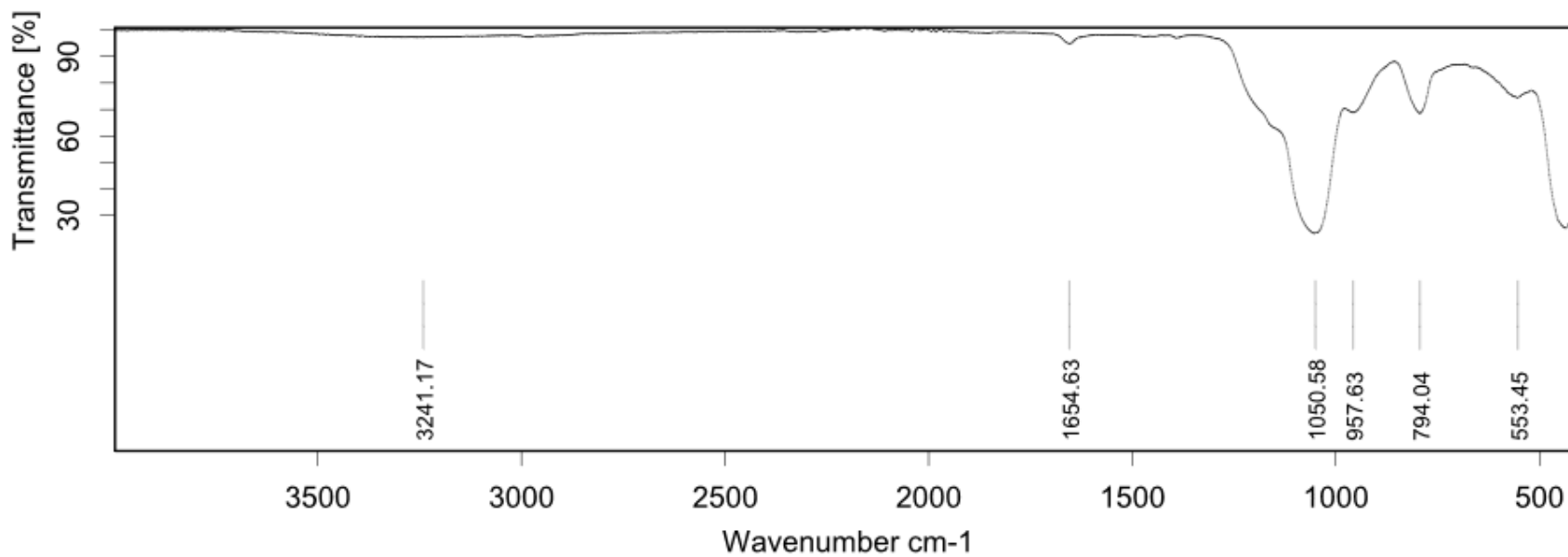


Figure A-12: Iteration 4 of the CTA-SiP, produced using the CTA-SCA<sub>4</sub> oil from Table 6-2. EDCI-coupled CTA-SCA dissolved in DMF was added in-situ to silica dispersed in DMF and refluxed at 90°C.

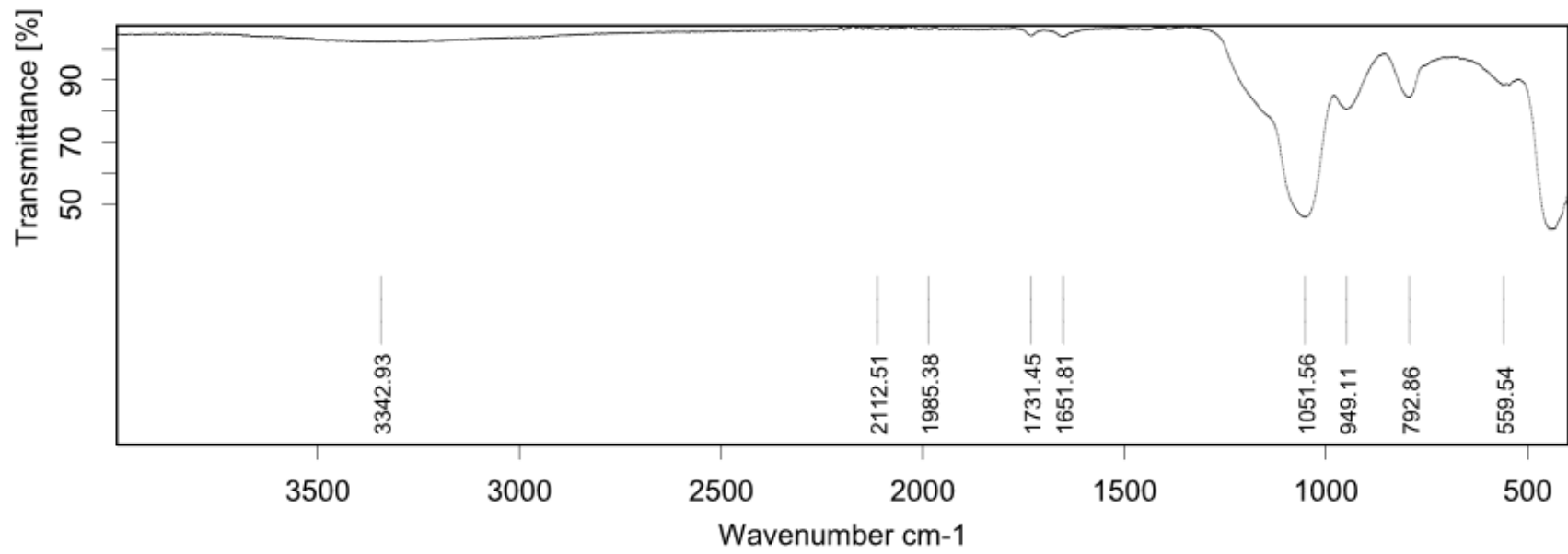
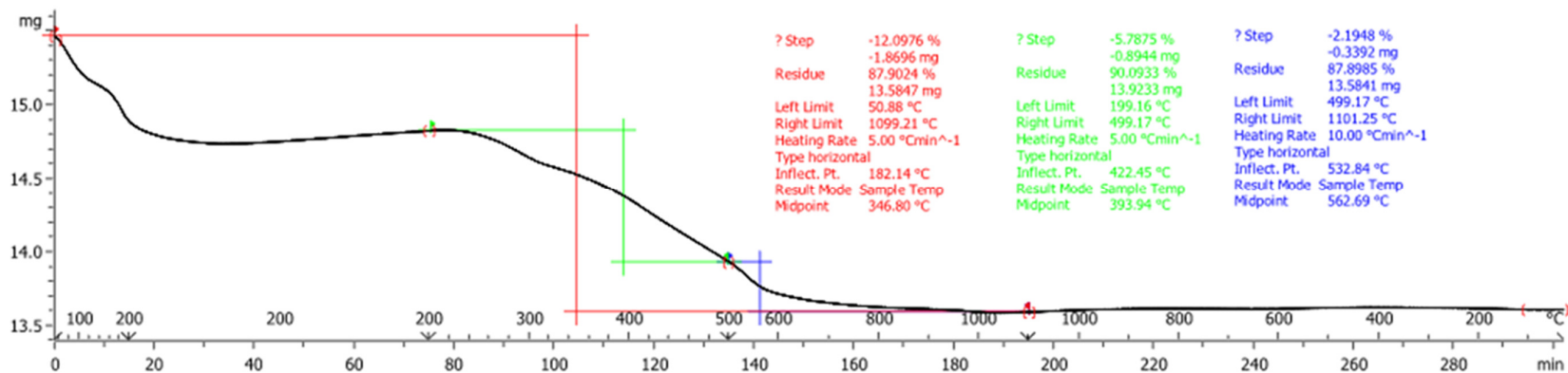
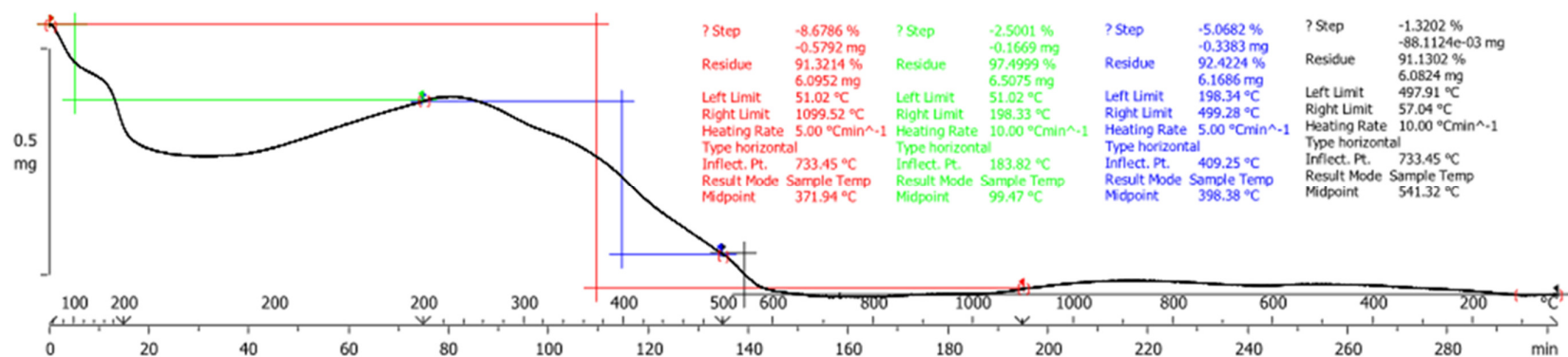


Figure A-13: FTIR spectra of pMMA-SiP2 utilising CTA-SiP1 at DP = 100.



(1)



(2)

Figure A-14: TGAs of pMMA-SiP<sub>1</sub> and pMMA-SiP<sub>2</sub> produced from CTA-SiP<sub>1</sub> with predicted degrees of polymerization (DP, based on a ratio of [MMA]:[CTA]<sub>free</sub>). The CTA-SiP<sub>1</sub> used to make both pMMA-SiPs originally yielded a total mass loss of 12.85%, indicating a loss of mass at the particle surface.

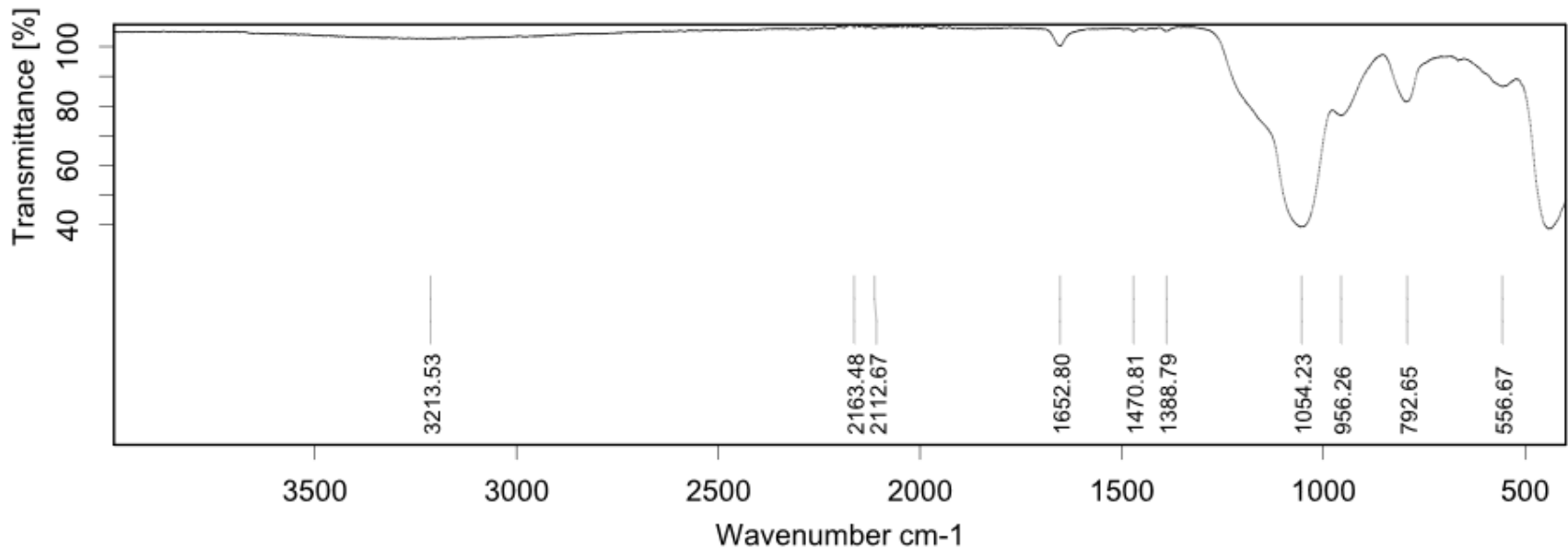


Figure A-15: FTIR spectra of pMMA-SiP3 utilising CTA-SiP2 at DP = 50.

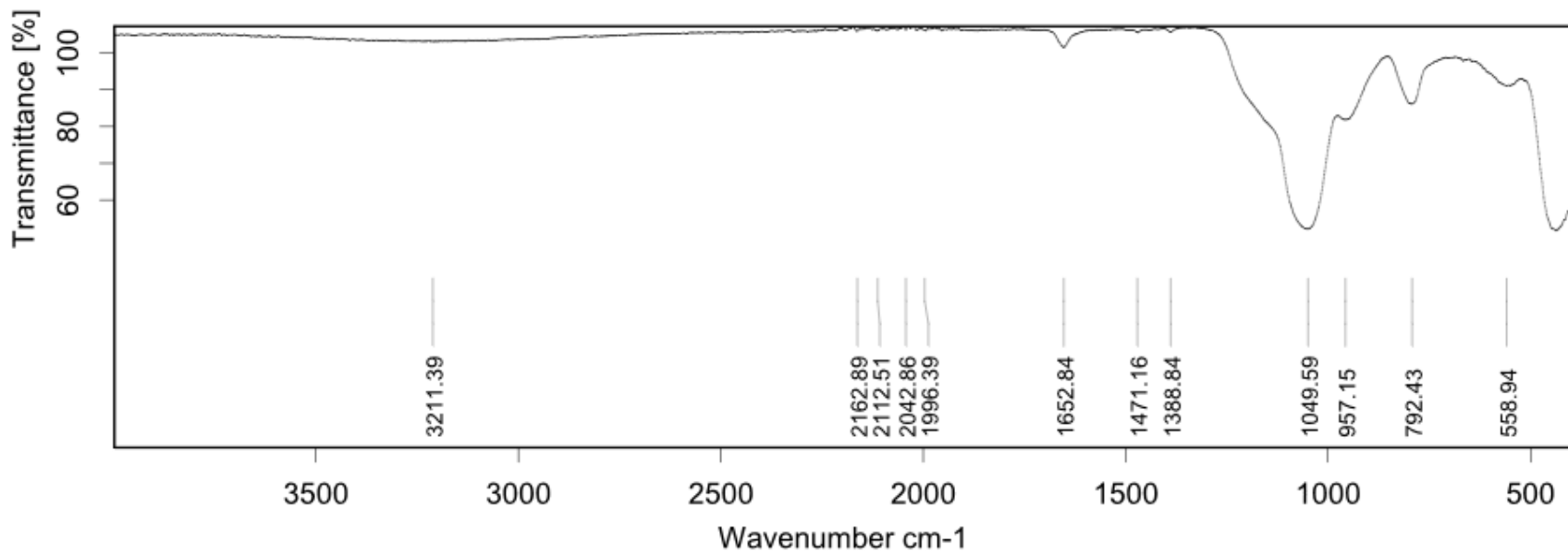


Figure A-16: FTIR spectra of pMMA-SiP<sub>4</sub> utilising CTA-SiP<sub>2</sub> at DP = 100.

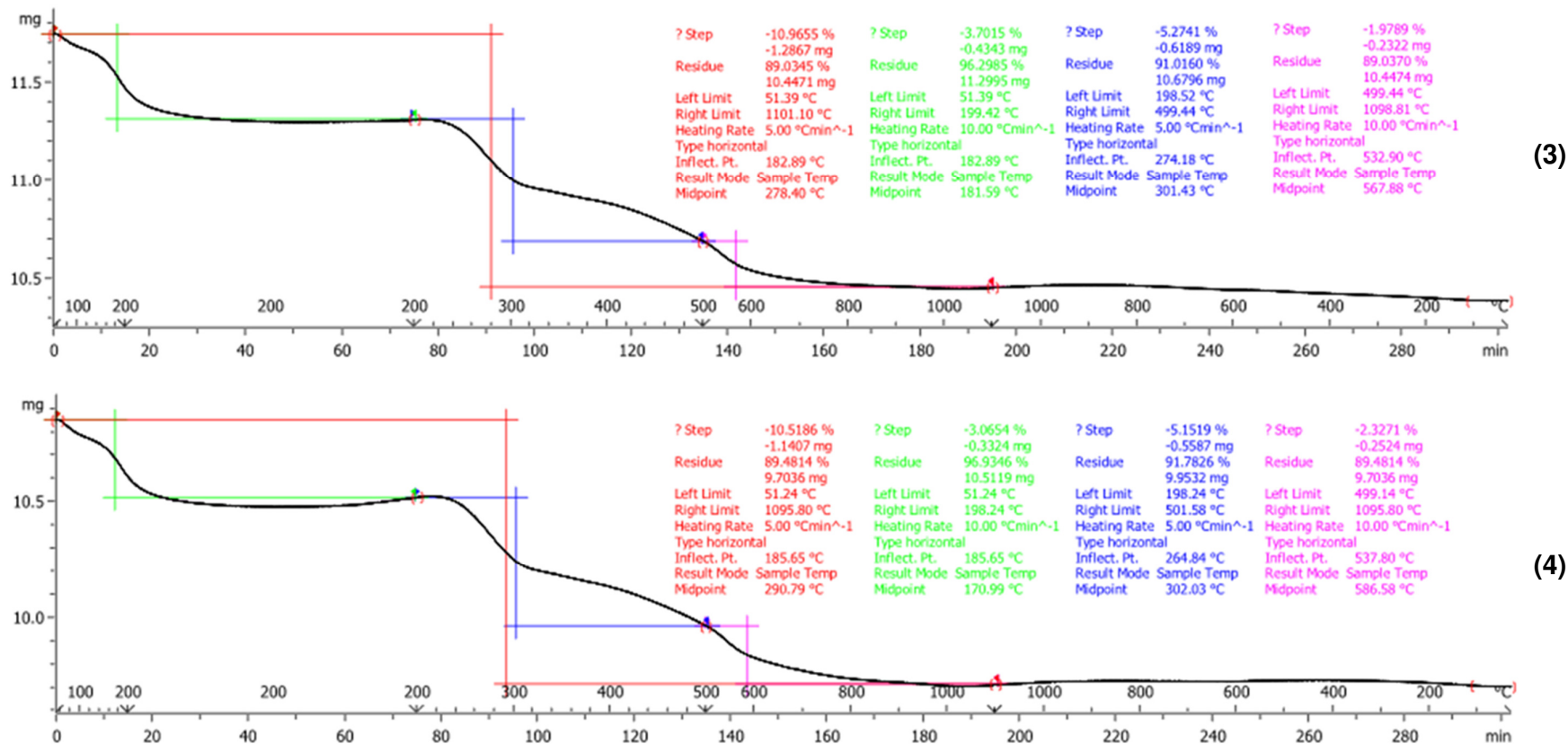


Figure A-17: TGAs of pMMA-SiP<sub>3</sub> and pMMA-SiP<sub>4</sub> produced from CTA-SiP<sub>2</sub> with predicted degrees of polymerization (DP, based on a ratio of [MMA]:[CTA<sub>free</sub>]). The CTA-SiP<sub>2</sub> used to make both pMMA-SiPs originally yielded a total mass loss of 14.87%, indicating a loss at the particle surface of mass in both cases of over 4%.

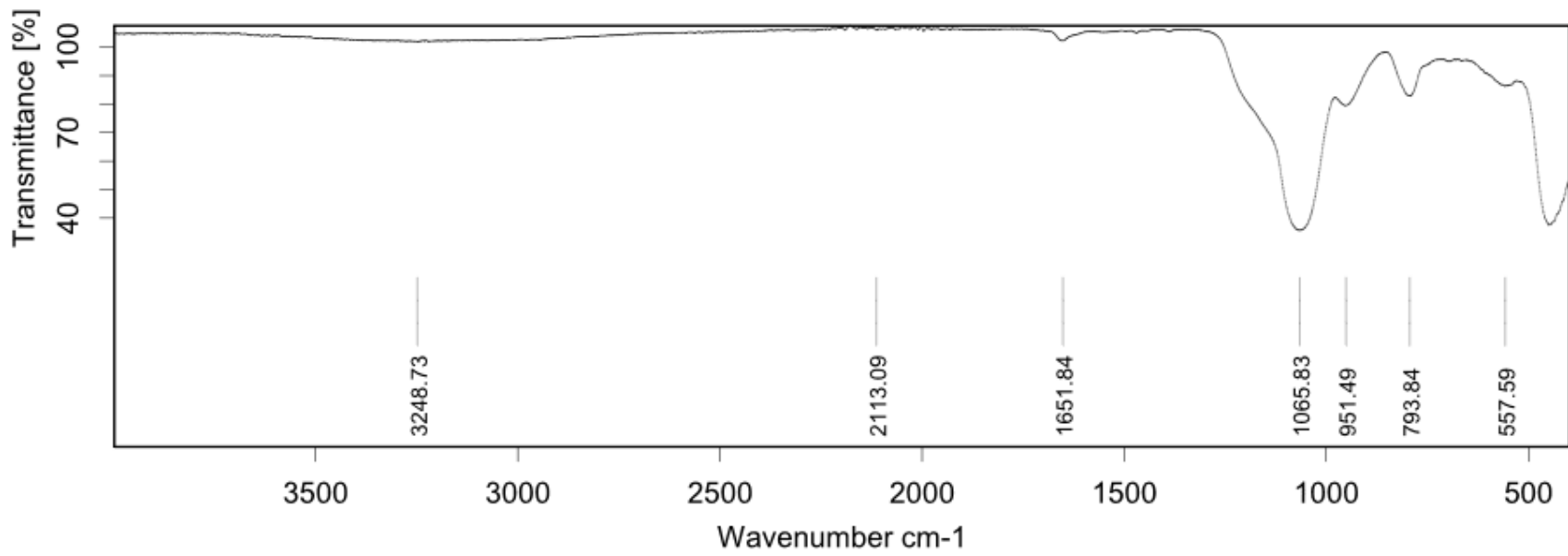


Figure A-18: FTIR spectra of pMMA-SiP<sub>5</sub> utilising CTA-SiP<sub>3</sub> at DP = 50.

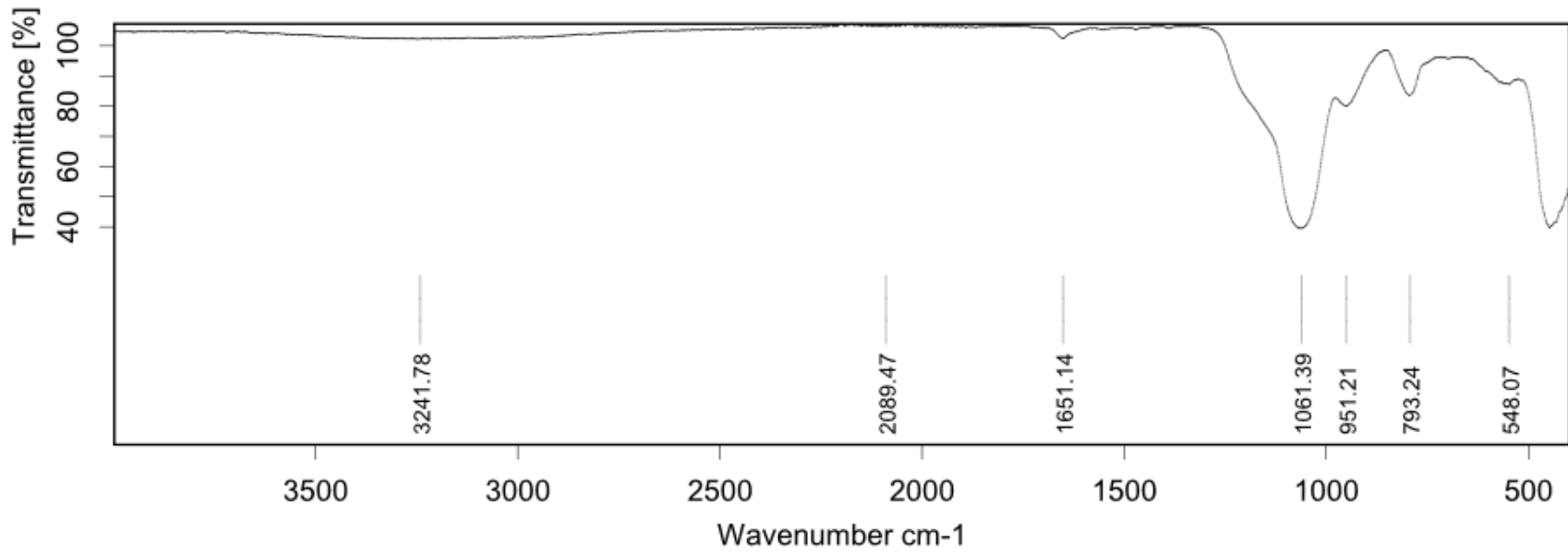
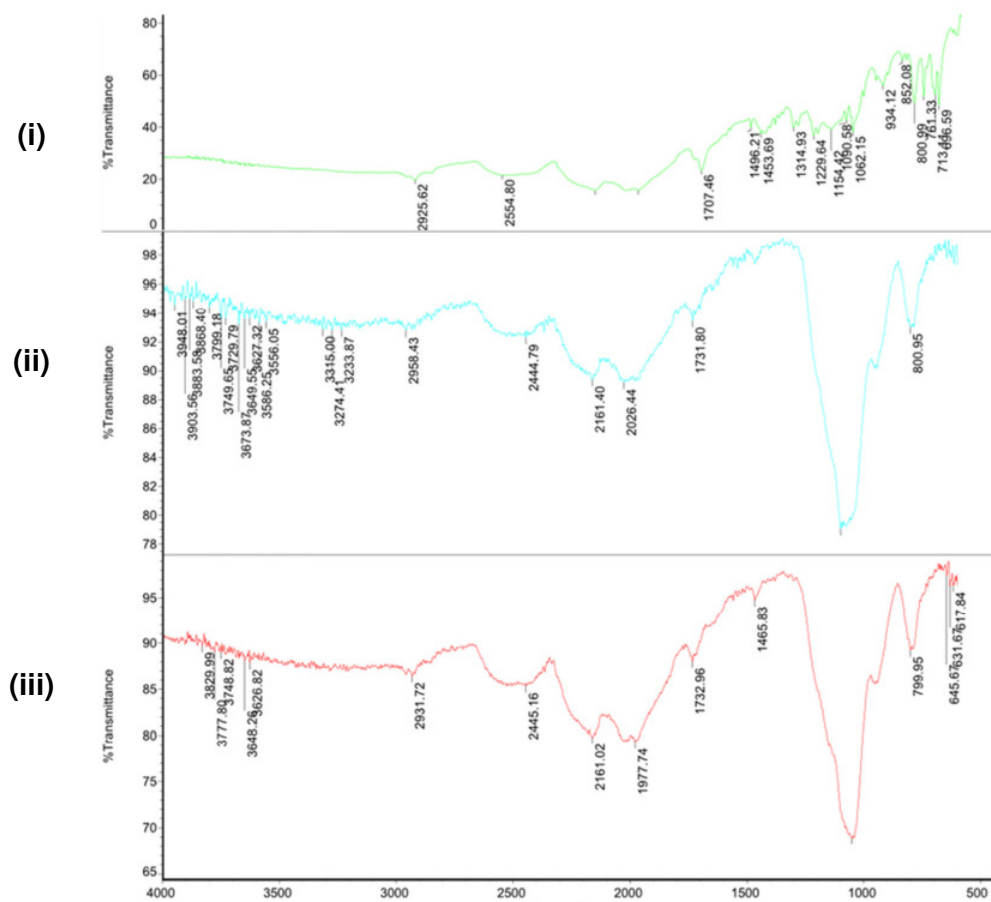


Figure A-19: FTIR spectra of pMMA-SiP<sub>6</sub> utilising CTA-SiP<sub>3</sub> at DP = 100.

**A.3 Accompanying Figures and Tables to Chapter 7.4. Iteration 1: 3-hour hold, purification testing, 18-hour condensation, and Polymerization of methyl methacrylate at DP = 100.**



**Figure A-20: (i) PETTC RAFT agent using the preparation of the oligo MAPTMS; (ii) oPETTC-SiP<sub>1b</sub>: the oligo-CTA-SiP prepared from purified oPETTC-SCA<sub>1</sub> using column chromatography; (iii) oPETTC-SiP<sub>1a</sub> prepared from non-purified oPETTC-SCA<sub>1</sub>**

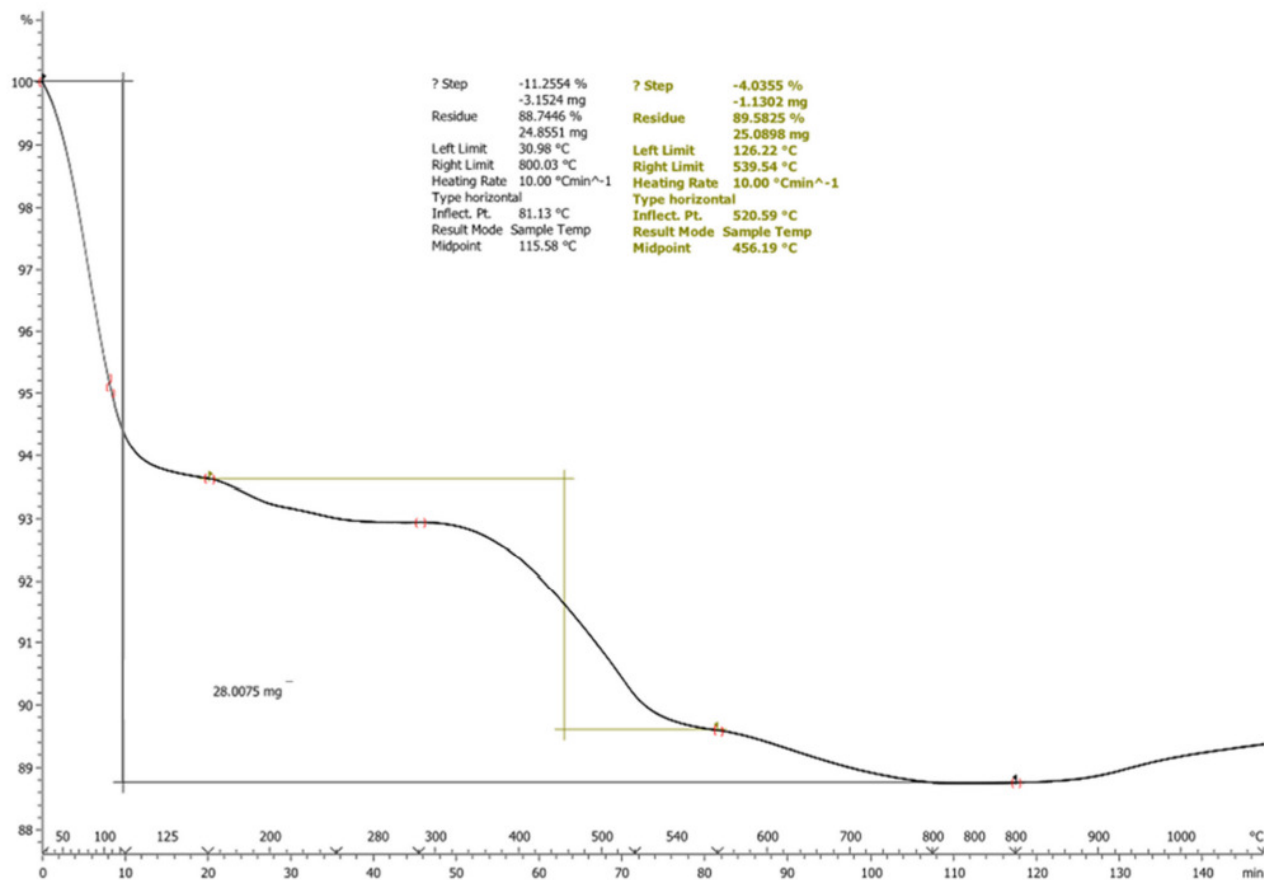


Figure A-21: TGA of 250nm silica nanoparticles using the new TGA protocol. The TGA protocol method was changed in line with Mueller et al. (2003) the new protocol to captures the major compositional changes associated with organic matter more effectively.

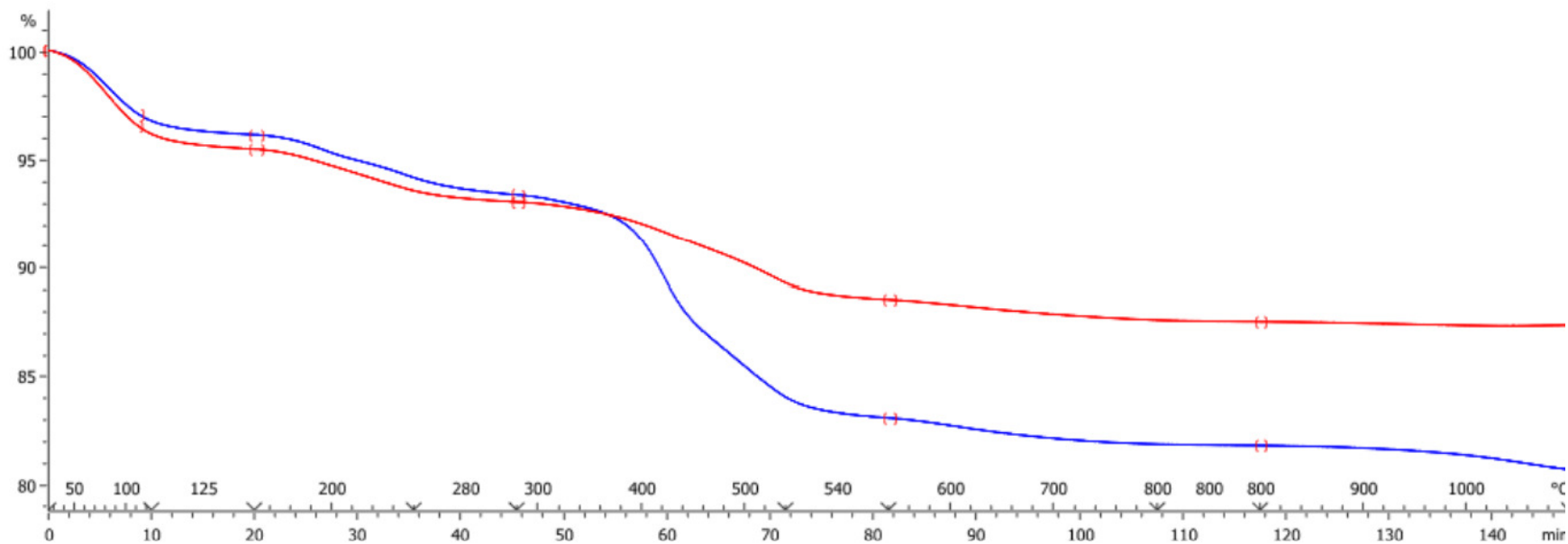
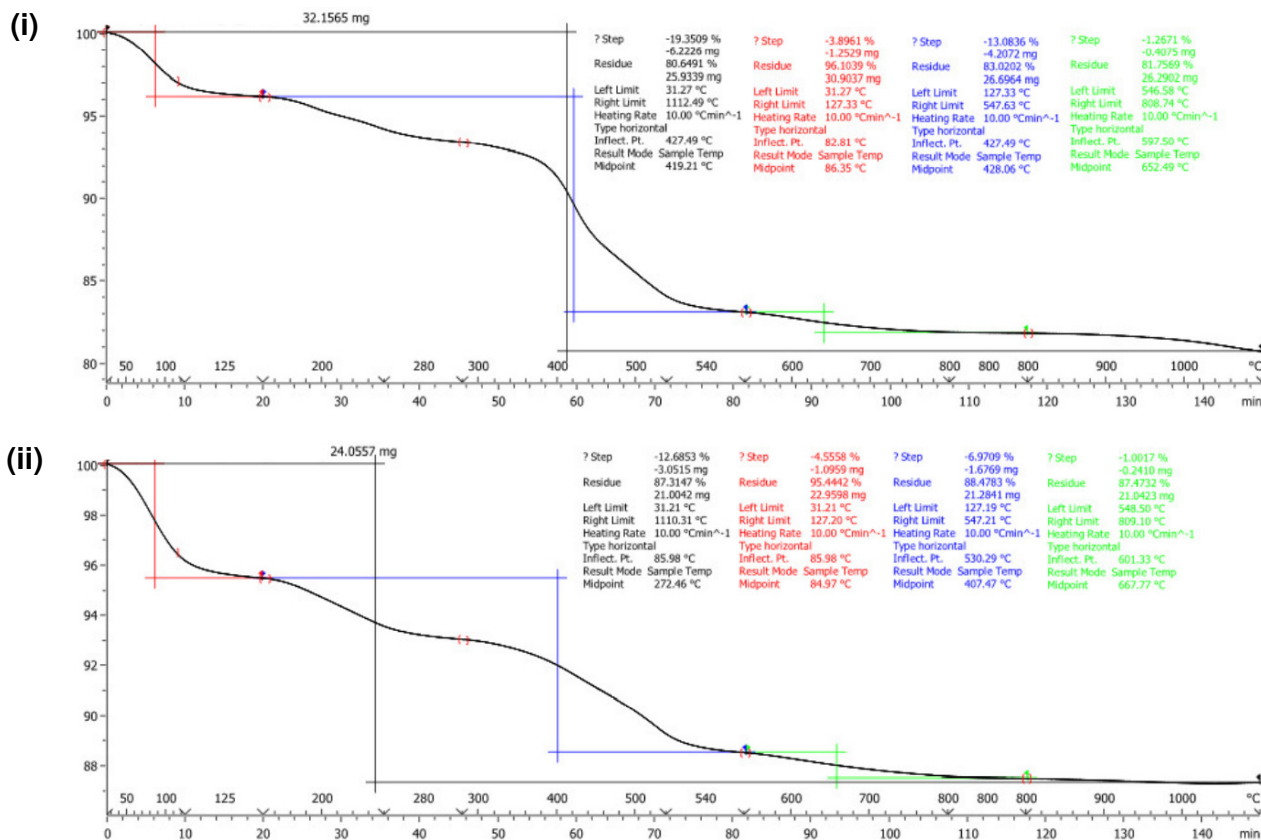


Figure A-22: TGA Comparison between 1a (*blue*) and 1b (*red*), showing increases in organic content in the unpurified oPETTC-SiP<sub>1b</sub> over the purified oPETTC-SiP<sub>1a</sub> using the new TGA protocol described above in 7.4.2 and Figure 7-9.



oPETTC-SiP<sub>1a</sub>, coated silica  
using the neat oPETTC-SCA as  
made.

Organic content as determined  
between 125 and 540 °C =  
13.08% (- 4.04% silica = **9.04%**).

oPETTC-SiP<sub>1b</sub>, coated silica  
using the purified oPETTC-SCA  
as described above.

Organic content as determined  
between 125 and 540 °C =  
6.97% (- 4.04% silica = 2.93%).

Figure A-23: TGA Comparison between 1a and 1b, showing the losses in organic content in the oPETTC-SiP<sub>1b</sub> and oPETTC-SiP<sub>1a</sub> using the new TGA protocol described above in Figure A-21.

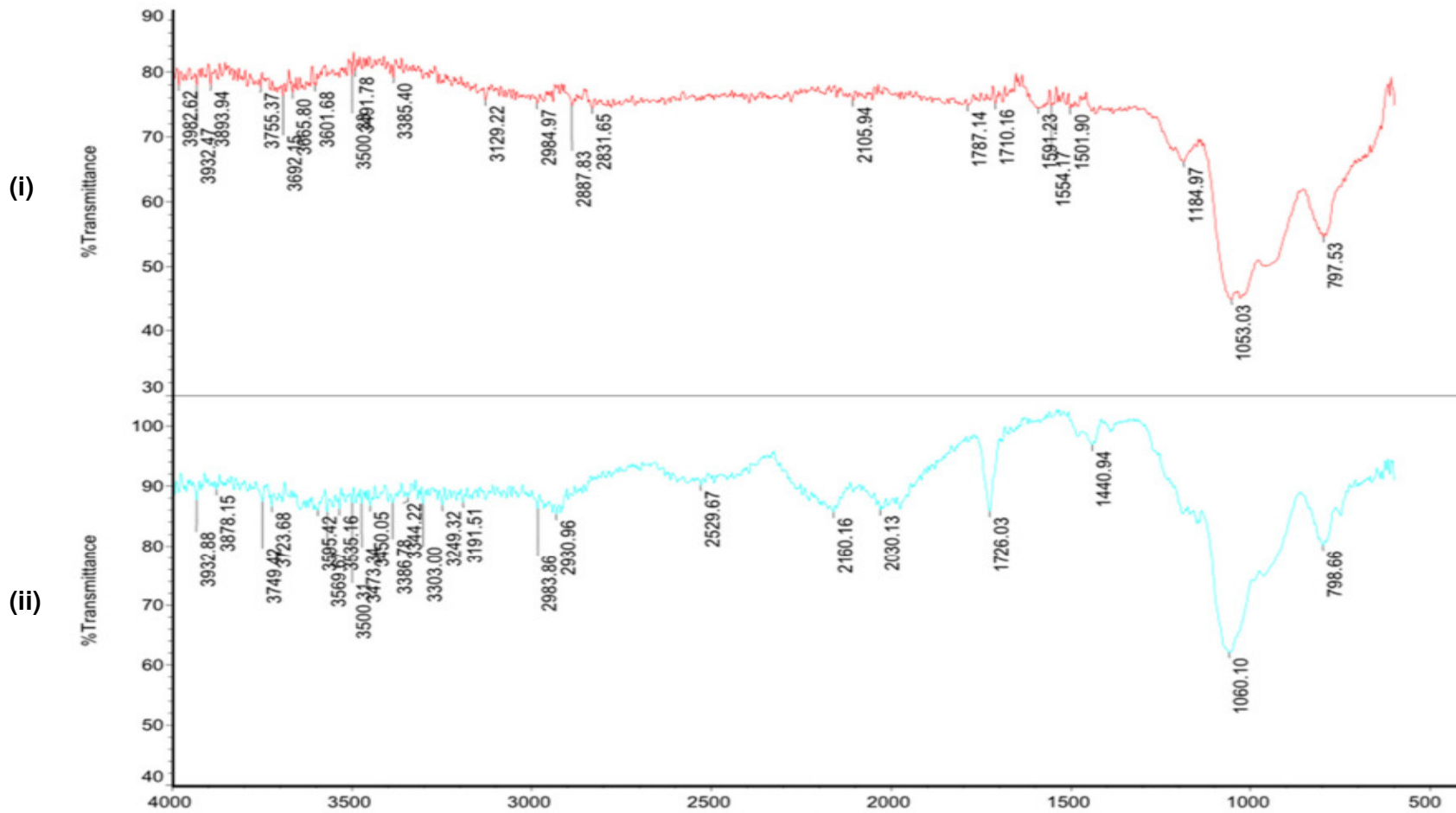
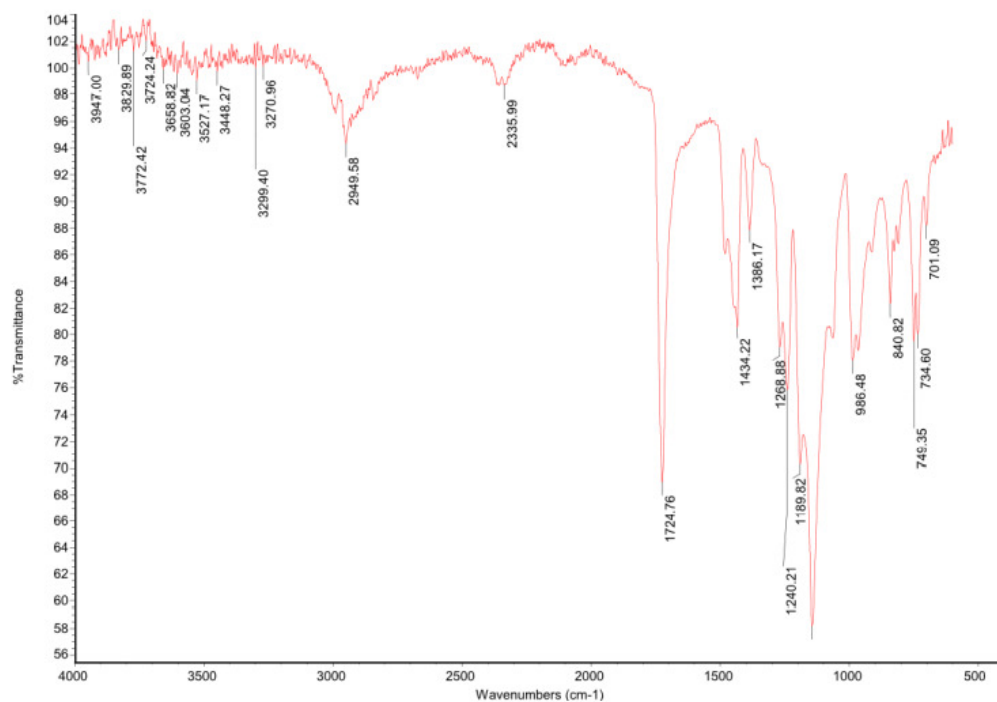


Figure A-24: FTIR of pMMA-SiPs from iteration 1 oPETTC-SiPs (i) 1b, produced with column-purified oPETTC-SCA; (ii) 1a, used as was, with no purification.



**Figure A-25: poly(methyl methacrylate), free polymer, produced by sampling the extracted media and dispersing into methanol to produce precipitate of pMMA, which was dried and analysed.**

**Table A-1: Free polymer weight of pMMA for iteration 1 pMMA-SiPs**

Name	Theoretical Mw/ g mol <sup>-1</sup>	Weight average/ Mw	Number average/ Mn	Polydispersity Mw/Mn
pMMA-SiP <sub>1a</sub>	10012	5982	4379	1.37
pMMA-SiP <sub>1b</sub>	10012	6353	5248	1.21

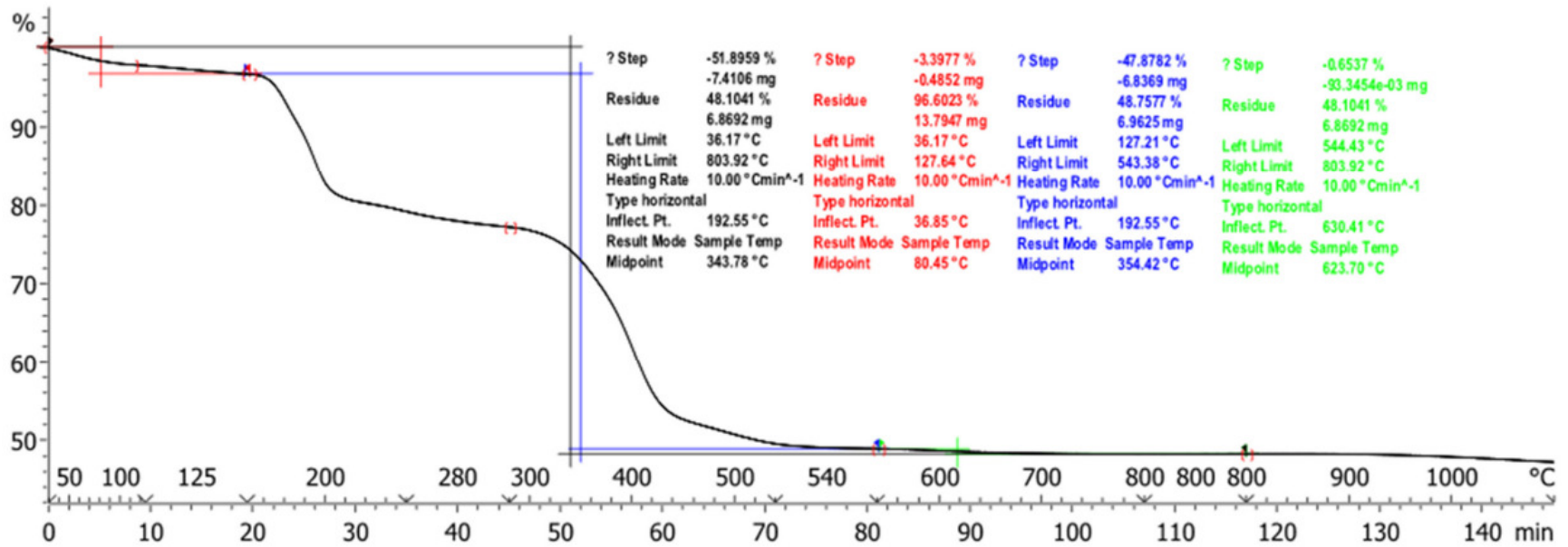


Figure A-26: pMMA-SiP<sub>1a</sub> made using the unpurified oligomer-coated, CTA-enabled silica. This uses the protocol as illustrated in Figure A-21.

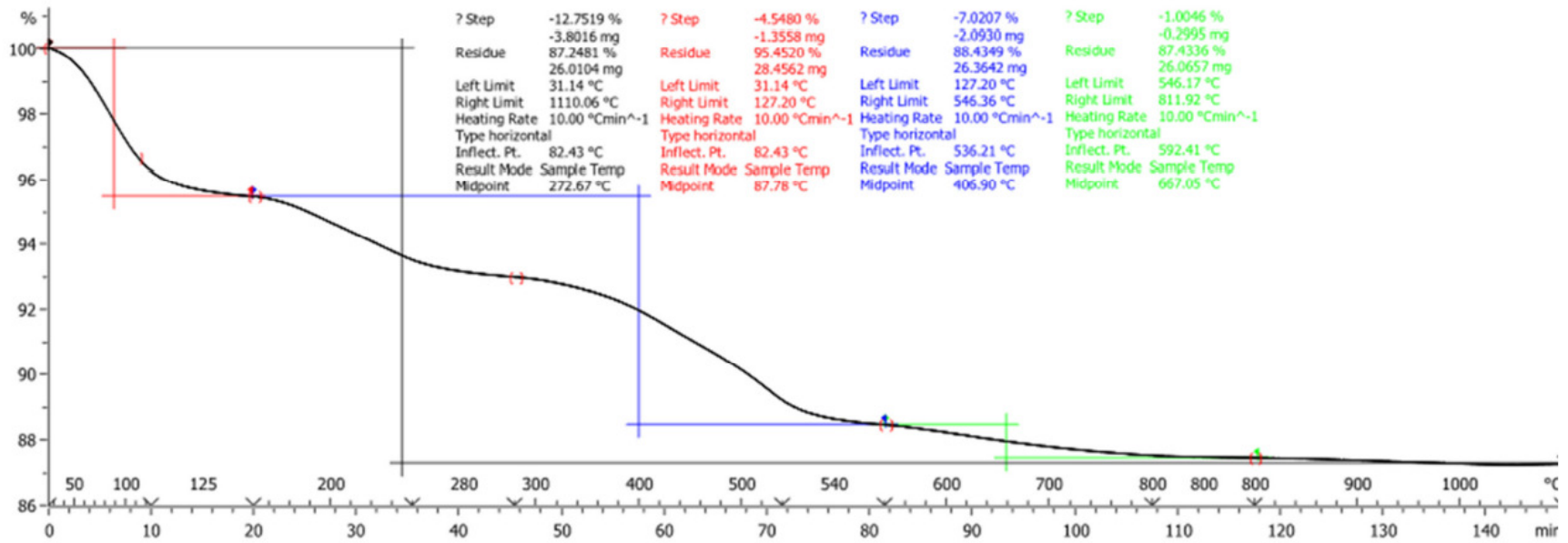


Figure A-27: pMMA-SiP<sub>1b</sub> made using the purified oligomer-coated, CTA-enabled silica. This uses the protocol as illustrated in Figure A-21

A.4 Accompanying Figures and Tables to Chapter 7.5. Iteration 2: 3-hour hold oligomerization, 18 hours condensation, polymerization of hydropropyl methacrylate at multiple degrees of polymerization of 50, 100, 200 and 500, and hold times.

Table A-2: Iteration names for the 5 different pHPMA samples based on oPETTC-SiP<sub>2</sub>.

Iteration name	Degree of polymerization (molar ratio of monomer, M, to CTA PETTC), and hold time.
pHPMA-SiP <sub>2a</sub>	100, 18-hour hold.
pHPMA-SiP <sub>2b</sub>	50, 5-hour hold.
pHPMA-SiP <sub>2c</sub>	100, 5-hour hold.
pHPMA-SiP <sub>2d</sub>	200, 5-hour hold.
pHPMA-SiP <sub>2e</sub>	500, 5-hour hold.

Table A-3: pHPMA free polymer weight for pHPMA-SiP<sub>2a</sub>. Number of monomer units in parenthesis (discounting RAFT moiety)

Molar ratio, M:CTA	Theoretical Bound-Polymer Mn/ g mol <sup>-1</sup>	Free Polymer Mn/ g mol <sup>-1</sup> (actual DP)	Mw/ g mol <sup>-1</sup>	PDI
100	14,756 (102)	22,734 (158)	24,928	1.097

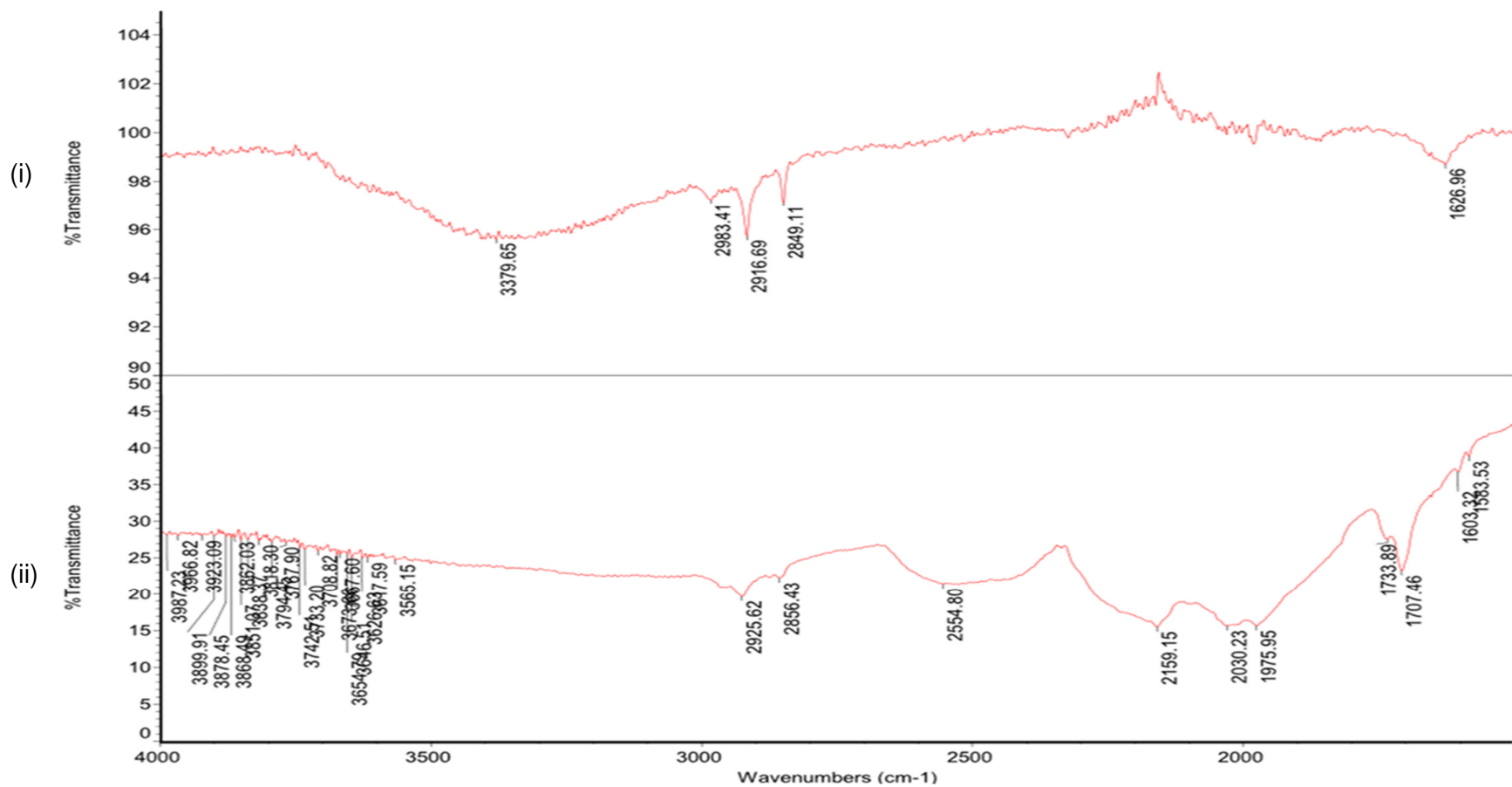


Figure A-28: (i) *o*PETTC-SiP<sub>2</sub>: the oligo-CTA-SiP prepared from *o*PETTC-SCA<sub>2</sub> and used as produced; (ii) PETTC RAFT agent using the preparation of the oligo-MAPTMS. For ease of view peaks below 1500cm<sup>-1</sup>, previously dwarfed by O-Si-O stretching have been omitted.

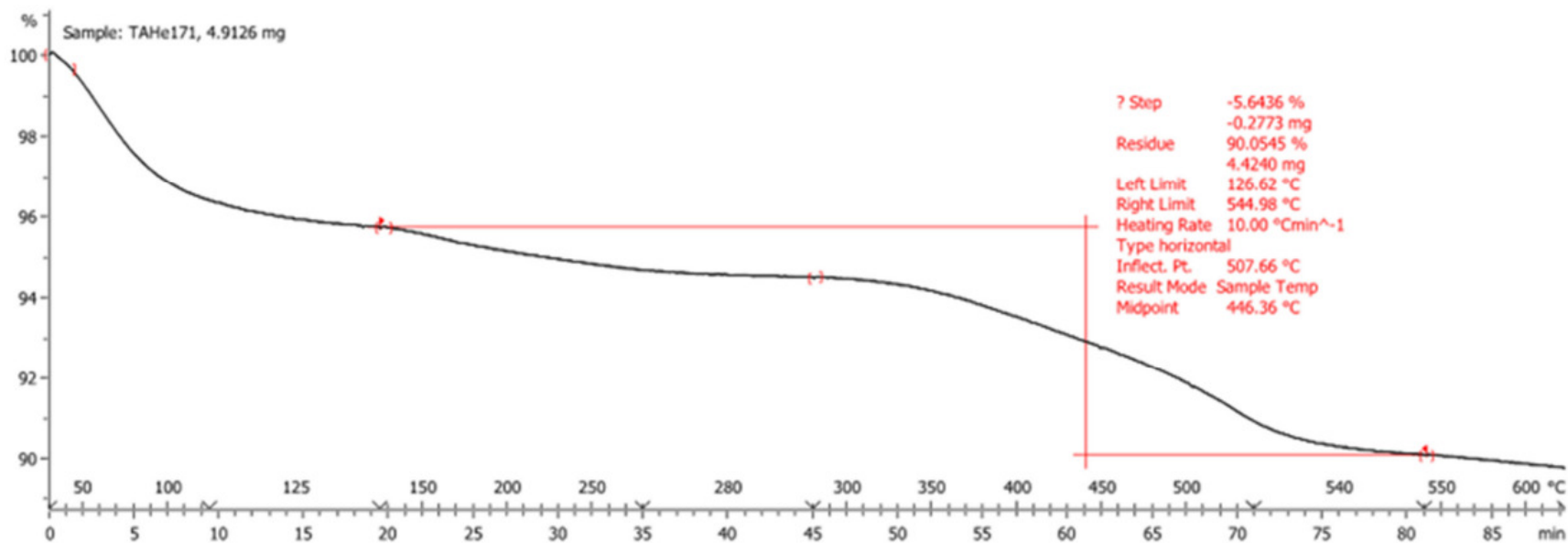


Figure A-29: TGA of oPETTC-SiP<sub>2</sub>. Machine error during the procedure stopped the temperature increase after 620°C and limited amounts of the sample meant it could not be repeated<sup>9</sup>.

<sup>9</sup> Iteration 3 followed this as a consequence, with larger quantities produced as well as trying alternative degrees of polymerization with HPMA.

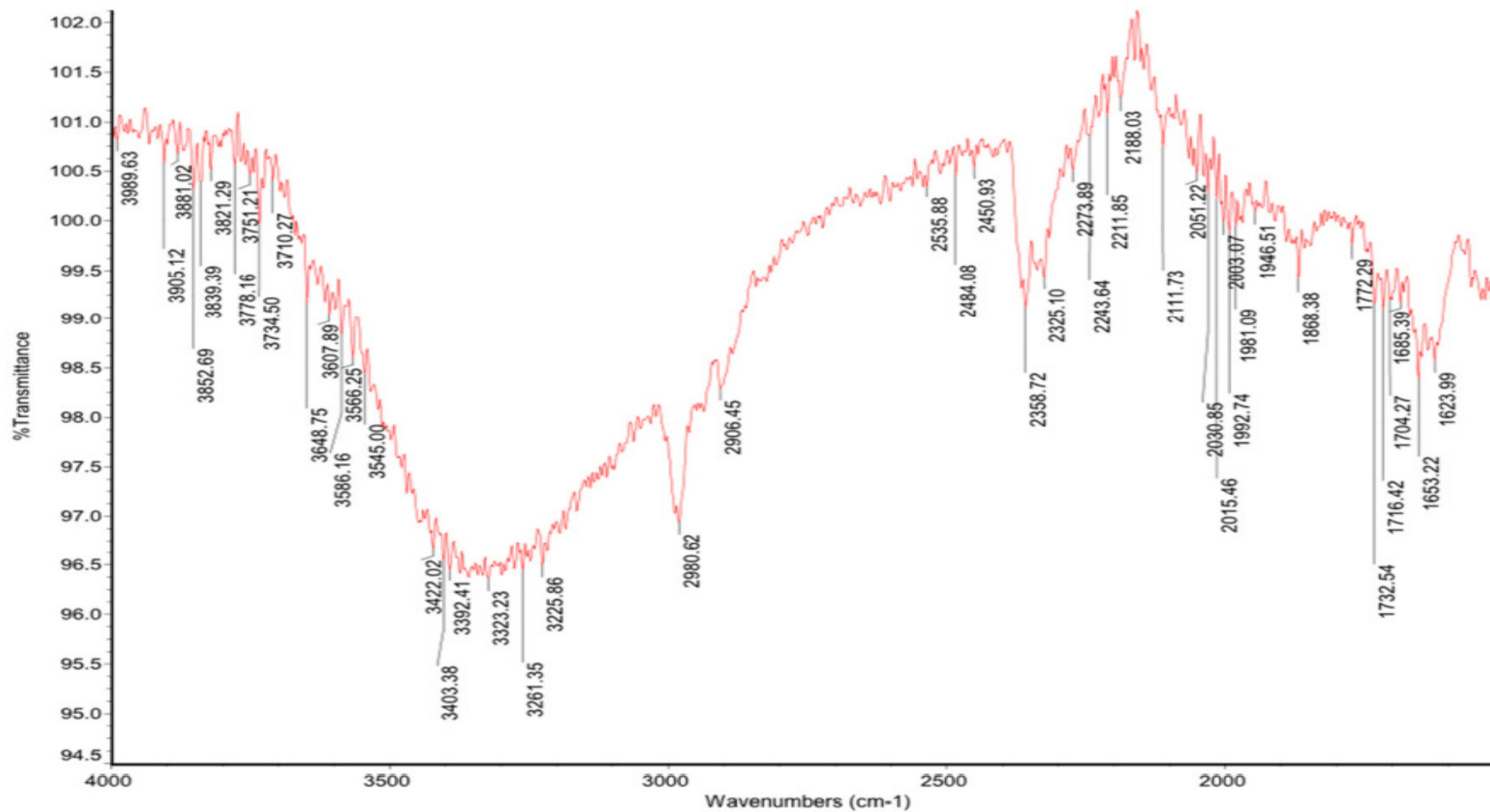


Figure A-30: FTIR spectra for the cleaned and dried sample of pHMA-SiP<sub>2a</sub> (DP = 100). O-Si-O peaks below 1500cm<sup>-1</sup> omitted for clarity.

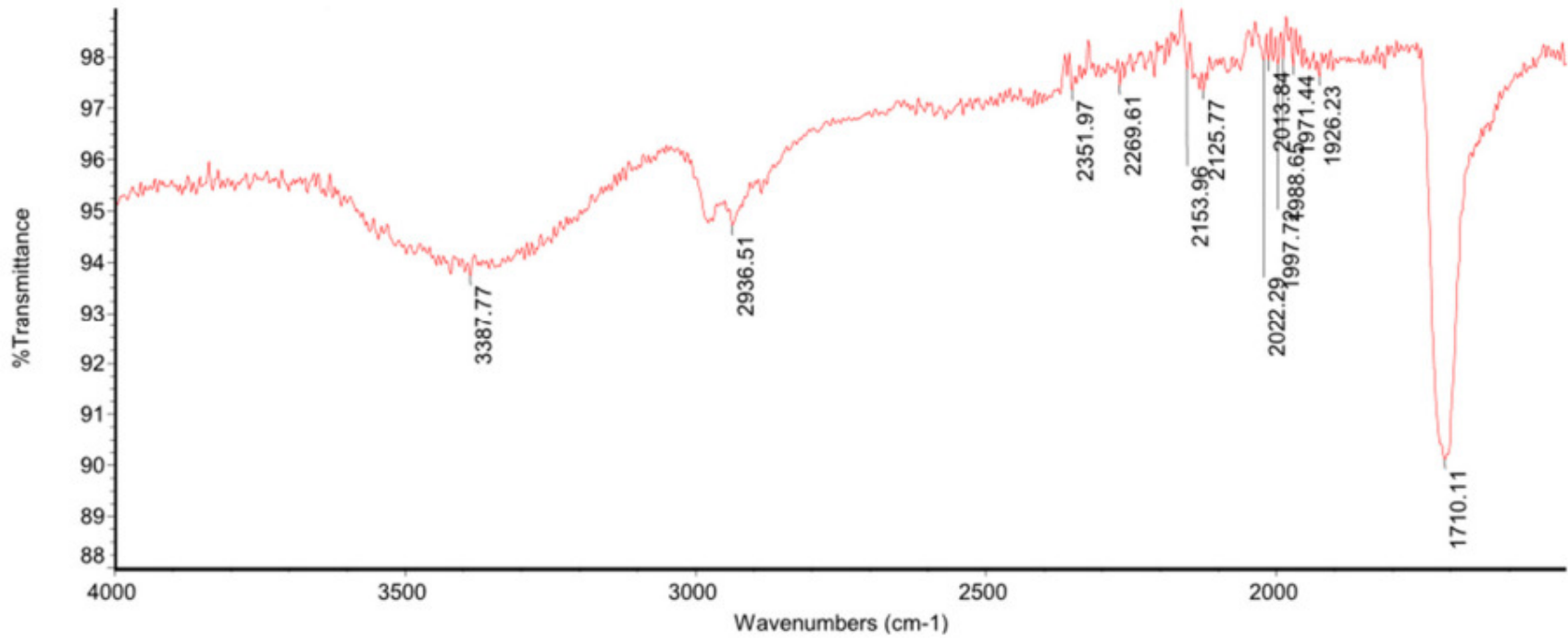


Figure A-31: FTIR spectra of free pHPMA, precipitated in dichloromethane and vacuum oven-dried.

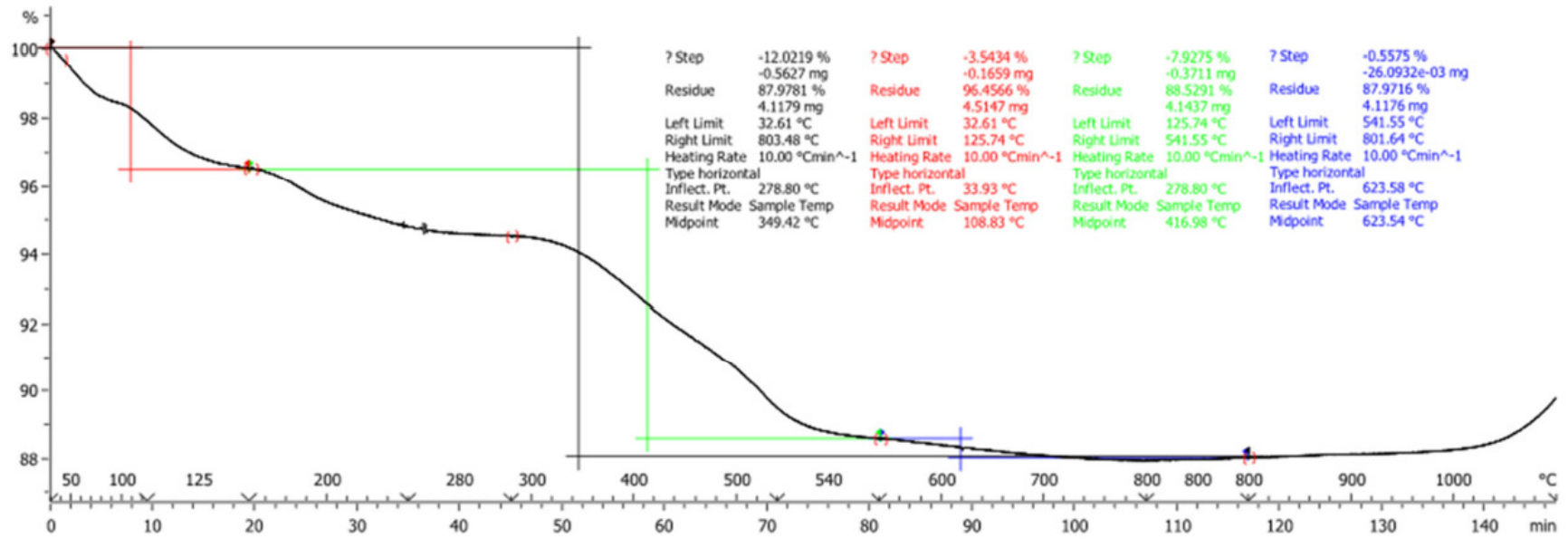
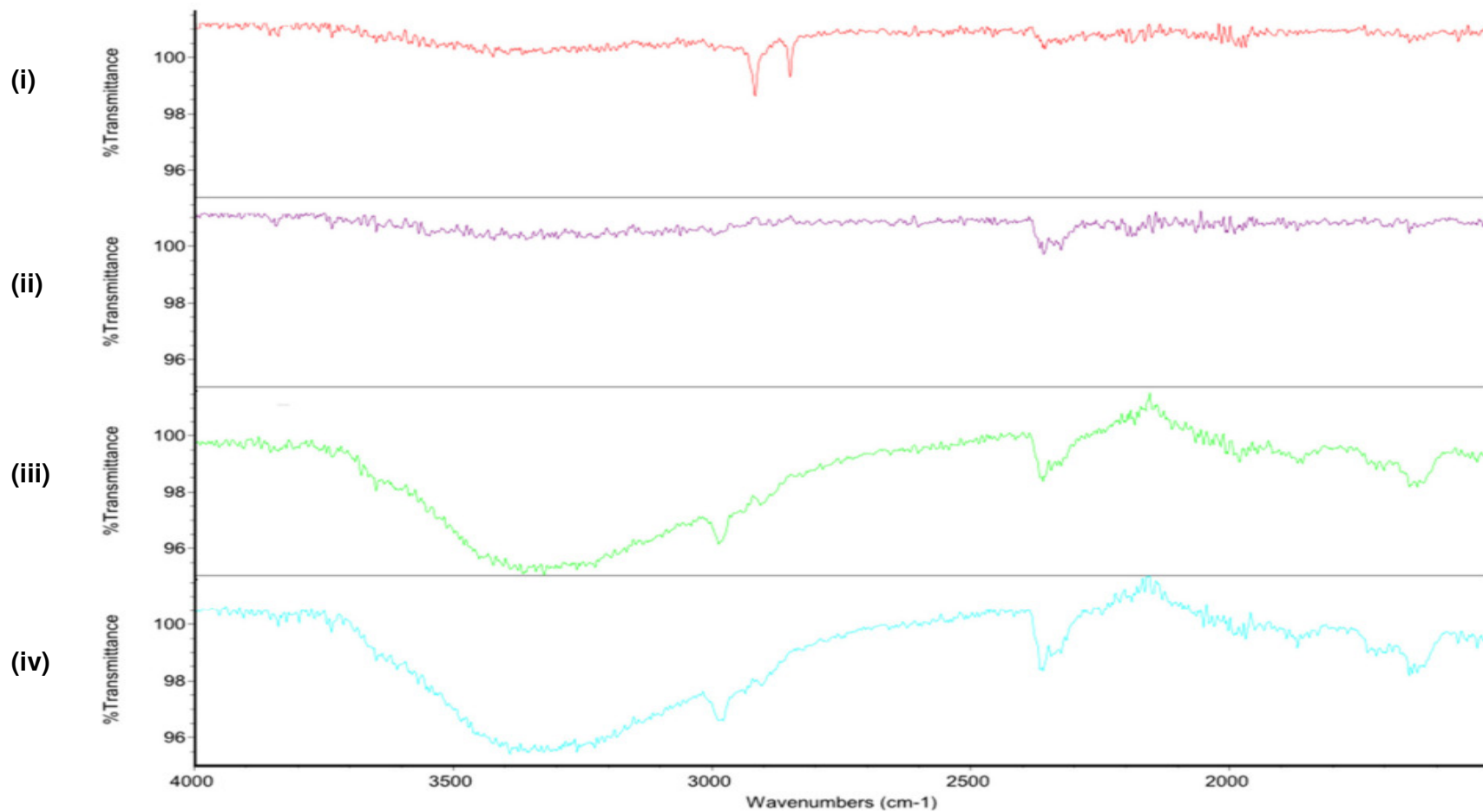
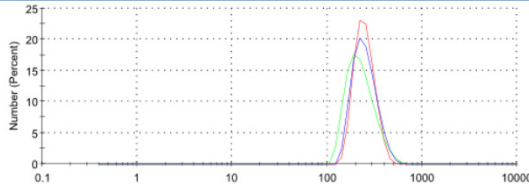
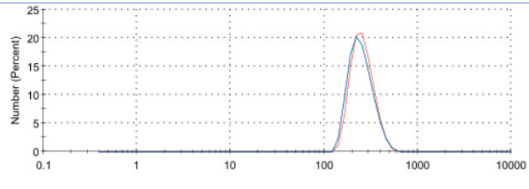
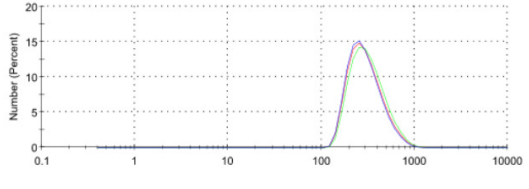


Figure A-32: TGA of pHMA-SiP<sub>2a</sub>. Protocol for TGA is as illustrated in Section 7.4.2.

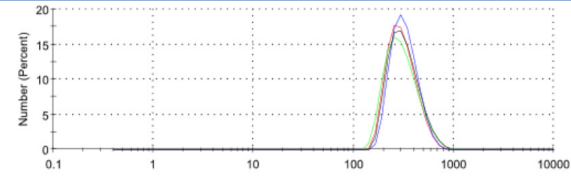
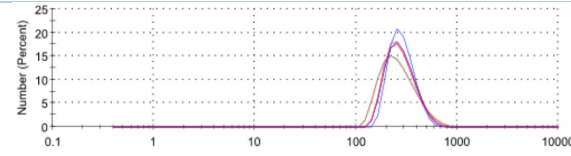
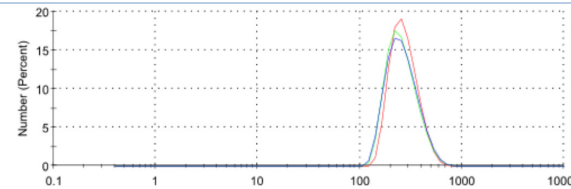
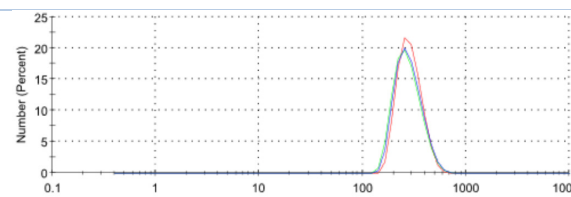


**Figure A-33: Iterations of pHPMA-SiP<sub>2b-e</sub> based on oPETTC-SiP<sub>2</sub> across multiple DPs all with 5-hour holds: (i) pHPMA-SiP<sub>2b</sub>, DP = 50; (ii) pHPMA-SiP<sub>2c</sub>, DP = 100; (iii) pHPMA-SiP<sub>2d</sub>, DP = 200; (iv) pHPMA-SiP<sub>2e</sub>, DP = 500.**

**Table A-4: Dynamic Light Scattering (DLS) studies of an array of particles analyzed in the production of iteration 2 particles. Legend: (i): Untreated 250nm silica; (ii): oPETTC-SiP<sub>2</sub>; (iii): pHPMA-SiP<sub>2a</sub>, DP = 100, 18-hour hold. Samples are all dispersed in Ethanol at approximately 0.5%wt**

	<b>Particle diameter, size distribution by number graph, Size (d.nm)/ nm</b>	Particle diameter, size distribution by number graph, Size (d.nm)/ nm	PdI	Standard Deviation (d.nm)/ nm
<b>(i)</b>		<b>251.4</b>	<b>0.01</b>	<b>61.5</b>
<b>(ii)</b>		<b>262.0</b>	<b>0.07</b>	<b>72.1</b>
<b>(iii)</b>		<b>317.8</b>	<b>0.18</b>	<b>139.5</b>

**Table A-5: Continuing Dynamic Light Scattering (DLS) studies of pHPMA-SiP<sub>2b-e</sub> particles. Legend: (iv): pHPMA-SiP<sub>2b</sub>, DP = 50; (v): pHPMA-SiP<sub>2c</sub>, DP = 100; (vi): pHPMA-SiP<sub>2d</sub>, DP = 200; (vii): pHPMA-SiP<sub>2e</sub>, DP = 500. Samples are all dispersed in Ethanol at approximately 0.5%wt**

	<b>Particle diameter, size distribution by number graph, Size (d.nm)/ nm</b>	Particle diameter, size distribution by number graph, Size (d.nm)/ nm	PdI	Standard Deviation (d.nm)/ nm
<b>(iv)</b>		<b>330.7</b>	<b>0.15</b>	<b>119.2</b>
<b>(v)</b>		<b>288.0</b>	<b>0.11</b>	<b>101.7</b>
<b>(vi)</b>		<b>279.4</b>	<b>0.13</b>	<b>87.9</b>
<b>(vii)</b>		<b>290.6</b>	<b>0.05</b>	<b>76.9</b>

**A.5 Accompanying Figures and Tables to Chapter 7.6. Iteration 3: 3-hour hold oligomerization, 18 hours condensation, polymerization of hydroxypropyl methacrylate at multiple degrees of polymerization of 50, 100, 200 and 500, with 18-hour hold times.**

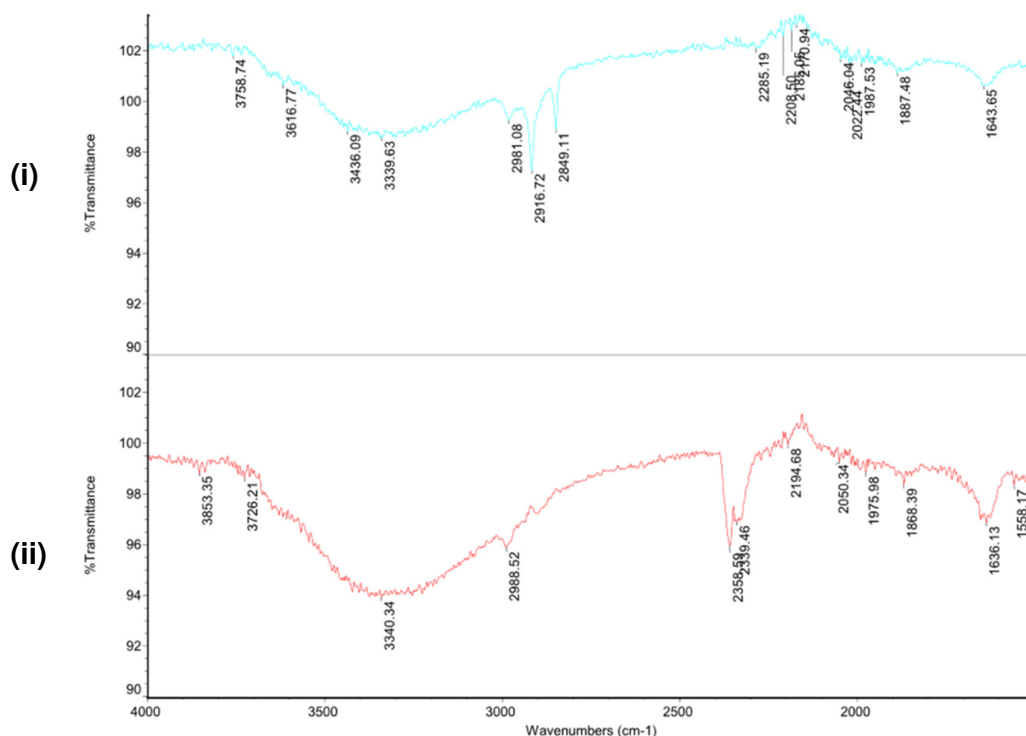


**Figure A-34: FTIR spectra for (i) oPETTC-SiP<sub>3</sub>; (ii) oPETTC-SiP<sub>2</sub>. For ease of view peaks below 1500cm<sup>-1</sup>, previously dwarfed by O-Si-O stretching have been omitted.**

**Table A-6: free polymer SEC-GPC profiles for each pHPMA-SiP<sub>3</sub> created.**

Sample, pHPMA-SiP	Molar ratio/DP, M:CTA	Theoretical Mn/ g mol <sup>-1</sup>	Mn/ g mol <sup>-1</sup> (actual DP)	Mw/ g mol <sup>-1</sup>	Pdl
3a	50	7548	13,311 (92)	15,618	1.17
3b	100	14,756	20,255 (140)	24,342	1.20
3c	200	29,173	32,305 (224)	39,521	1.22
3d	500	72,424	52,742 (366)	79,074	1.50

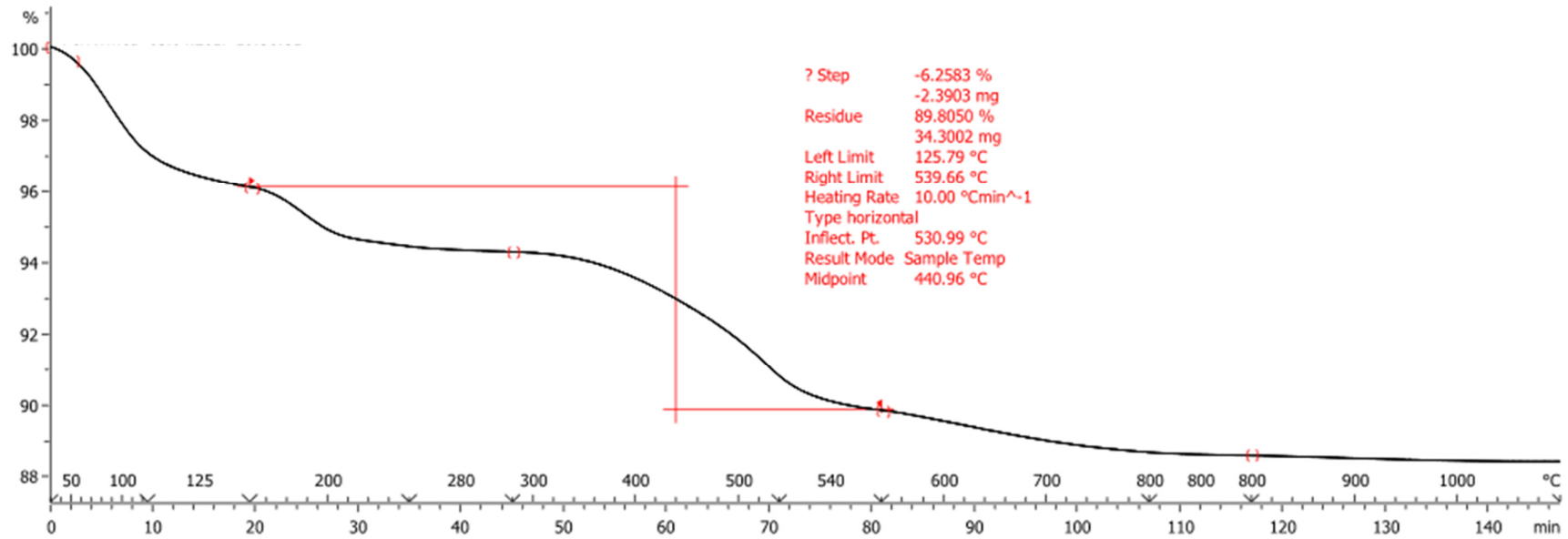
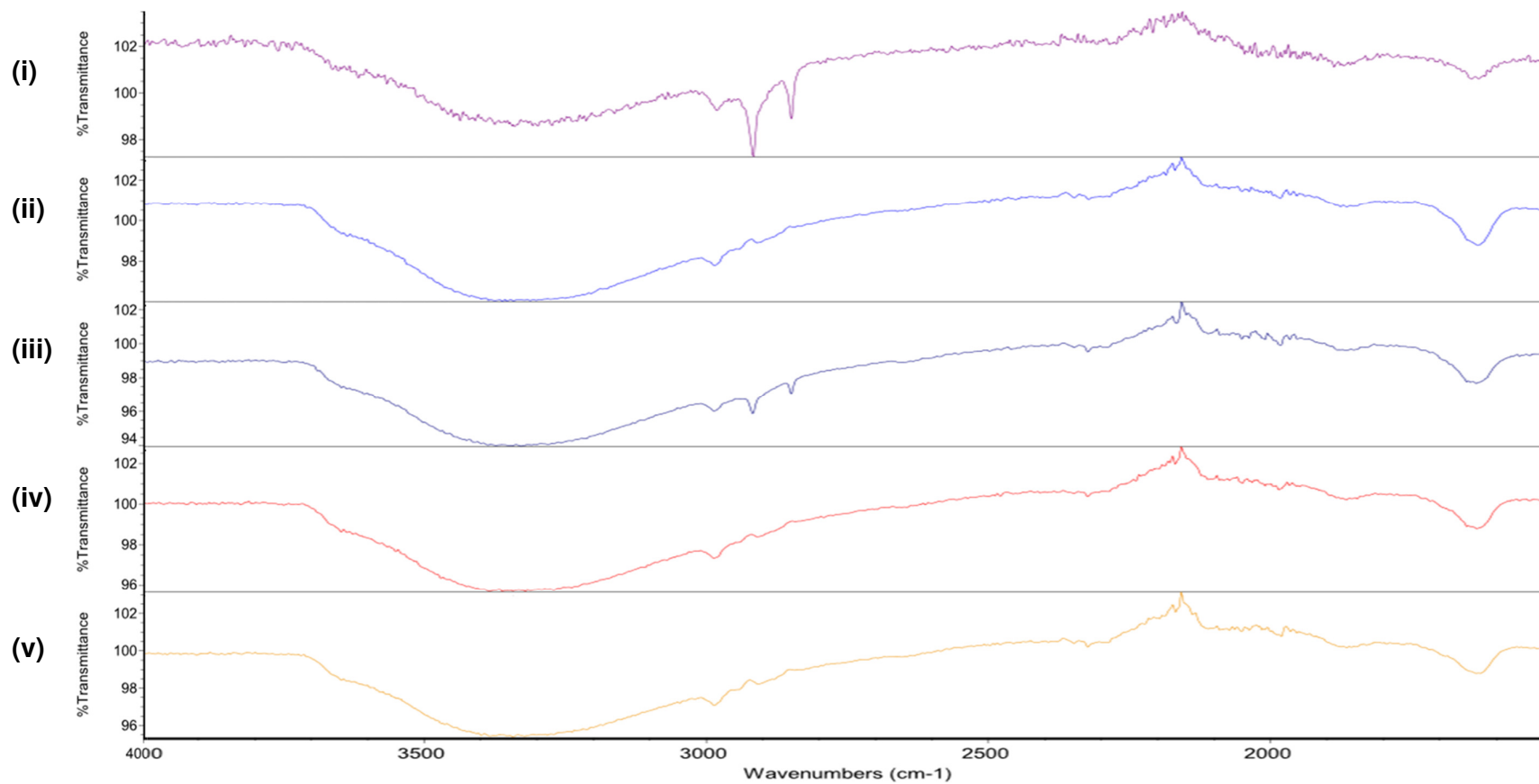


Figure A-35: Thermogravimetric analysis of oPETTC-SiP<sub>3</sub>. The TGA protocol used the new method as per that of the blank, untreated silica as in Figure A-21.



**Figure A-36: FTIR spectra comparison between the *o*PETTC-SiP<sub>3</sub> and pHPMA-SiP<sub>3a-d</sub>. Legend: (i) *o*PETTC-SiP<sub>3</sub>; (ii) pHPMA-SiP<sub>3a</sub>, DP = 50; (iii) pHPMA-SiP<sub>3b</sub>, DP = 100; (iv) pHPMA-SiP<sub>3c</sub>, DP = 200; (v) pHPMA-SiP<sub>3d</sub>, DP = 500.**

**Table A-7: Dynamic Light Scattering (DLS) studies of pHPMA-SiP<sub>3a-c</sub> particles from the 5-hour hold study. Particles were dispersed in ethanol at <0.5 wt%. Sampling was aggregated from several runs to give the average size. Legend: (i): pHPMA-SiP<sub>3a</sub>, DP = 50, (ii): pHPMA-SiP<sub>3b</sub>, DP = 100; (iii): pHPMA-SiP<sub>3c</sub>, DP = 200; (iv): pHPMA-SiP<sub>3d</sub>, DP = 500.**

	<b>Particle diameter, size distribution by number graph, Size (d.nm)/ nm</b>	<b>Pdl</b>	<b>Standard Deviation (d.nm)/ nm</b>
<b>(i)</b>	360	0.19	162
<b>(ii)</b>	285	0.12	87
<b>(iii)</b>	298	0.15	92
<b>(iv)</b>	330	0.18	90

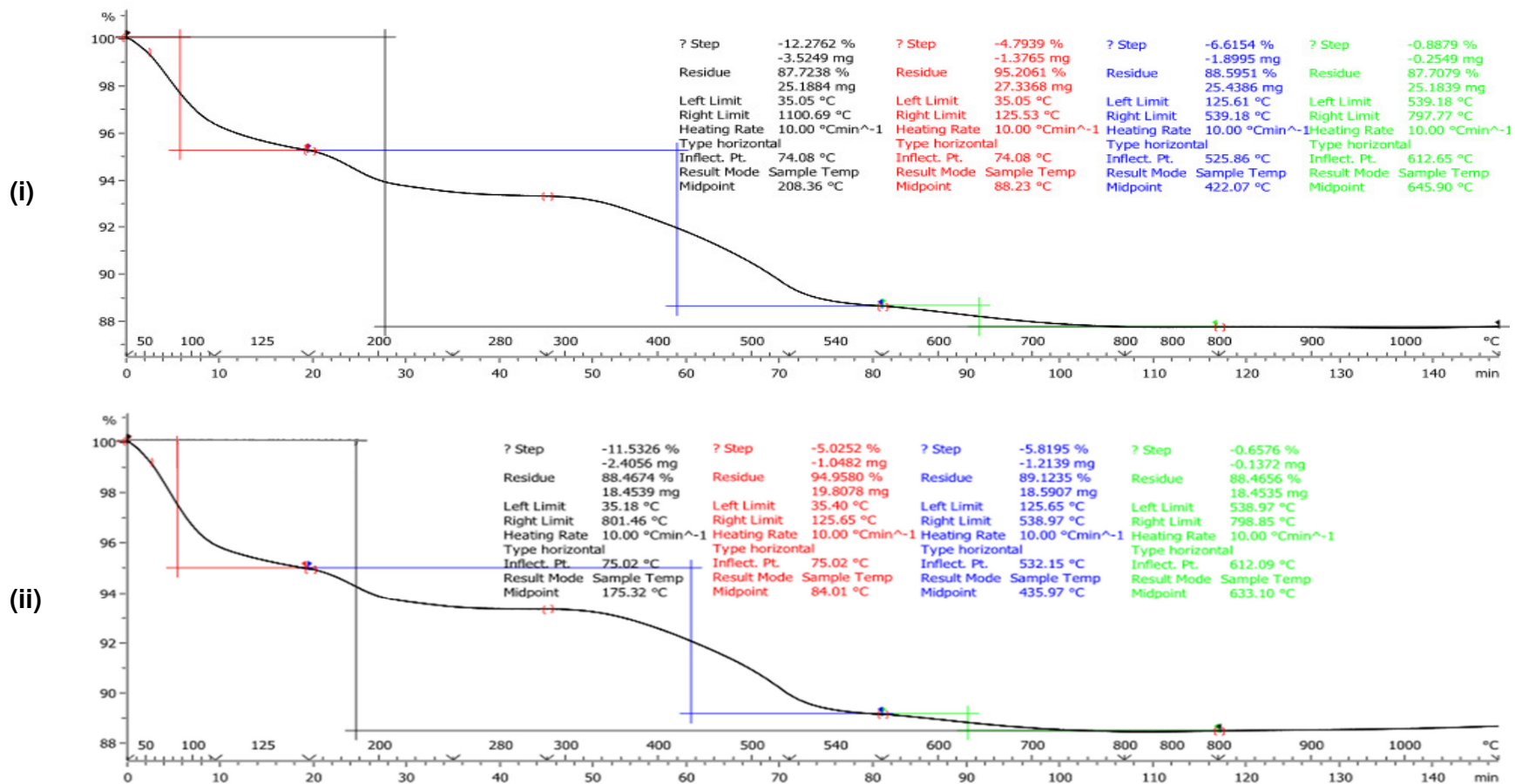


Figure A-37: Thermogravimetric analysis of pHPMA-SiP<sub>3a-b</sub>. The TGA protocol used the new method as per that of the blank, untreated silica as in Figure A-21; Legend: (i): pHPMA-SiP<sub>3a</sub>, DP = 50; (ii): pHPMA-SiP<sub>3b</sub>, DP = 100.

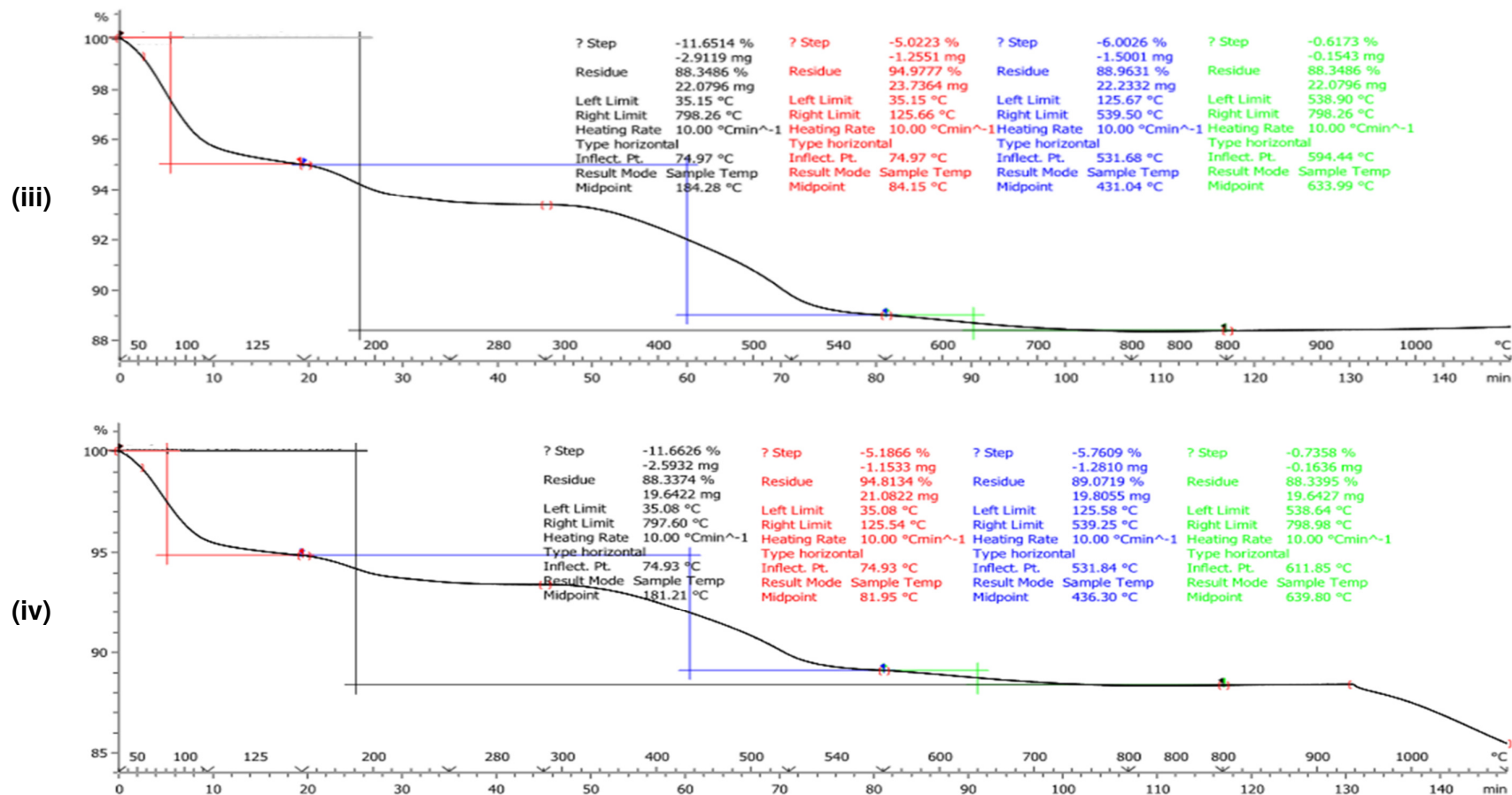


Figure A-38: Thermogravimetric analysis of pHPMA-SiP<sub>3c-d</sub>. The TGA protocol used the new method as per that of the blank, untreated silica as in Figure A-21; Legend: (i): pHPMA-SiP<sub>3a</sub>, DP = 200; (ii): pHPMA-SiP<sub>3b</sub>, DP = 500.

**Table A-8: %-mass loss for the 125-540°C region determined through thermogravimetric analysis for pHPMA-SiP<sub>3</sub> samples and their constituent parts, collated from previous graphs. Legend: (i) Silica Particles, SiP<sub>250nm</sub> used in preparation of the rest; (ii) oPETTC-SiP<sub>3</sub>; (iii): pHPMA-SiP<sub>3a</sub>, DP = 50, (iv): pHPMA-SiP<sub>3b</sub>, DP = 100; (v): pHPMA-SiP<sub>3c</sub>, DP = 200; (vi): pHPMA-SiP<sub>3d</sub>, DP = 500. Mass loss differences between the pHPMA-SiP<sub>3</sub> samples and the SiP<sub>250nm</sub> and oPETTC-SiP<sub>3</sub> are shown in the second and third column respectively.**

	<b>%-mass loss between 125-540°C/ %</b>	<b>Adjusted %-mass loss difference from untreated silica (i).</b>	<b>Adjusted %-mass loss difference from oPETTC-SiP<sub>3</sub> (ii).</b>
<b>(i)</b>	4.04	0.00	-
<b>(ii)</b>	6.26	2.22	0.00
<b>(iii)</b>	6.62	2.58	0.36
<b>(iv)</b>	5.82	1.78	-0.44
<b>(v)</b>	6.00	1.96	-0.26
<b>(vi)</b>	5.76	1.72	-0.50